ELECTRIC AND MAGNETIC PHENOMENA IN WATER AND LIVING SYSTEMS

BY

MOHAMMAD JABERANSARI

A thesis presented for the
Degree of Doctor of Philosophy
at the University of Salford

Department of Electronic and Electrical Engineering

University of Salford

1989

CONTENTS

		PAGE
Acknowledgements		i
Dedication		ii
Summary		iii
	PART ONE	
CHAPTER 1	Biological cells	
1.1	Introduction	1
1.2	Yeast cells	1
1.2.1	Growth rate	3
1.2.2	Pure culture	6
1.2.3	Logarithmic curve	7
1.2.3.1	Lag phase	8
1.2.3.2	Exponential phase	8
1.2.3.3	Stationary phase	9
1.2.3.4	Death phase	9
1.2.4	Synchronous growth	10
1.2.5	Cultivation and examination of *Saccharomyces cerevisiae*	10
1.2.5.1	Preparation of media	10
1.2.5.2	Pressure cooker (sterilizer)	11
1.2.5.3	Inoculating cabinets	11
1.2.5.4	Containers	11
1.3	Leishmania cells	12
1.3.1	*Leishmania major*	13
1.3.2	Physiology of Leishmania major cells	14
1.3.3	Nutrition and growth	15
1.3.4	The Leishmaniases in man	15
1.4	Water in biological system	16
REFERENCES		
CHAPTER 2	Dielectrophoresis, pearl chain formation and cellular rotation in biological systems	
2.1	Introduction	20
2.2	Dielectrophoresis	20
2.2.1	Basic theory of dielectrophoresis	22
2.2.2	Comparison of dielectrophoresis and electrophoresis	26
2.3	Pearl chain formation	27
2.3.1	Theoretical aspects of yield	29
2.3.2	Mechanism involved in the response of the living cells to non-uniform electric fields	33

2.4	Cellular rotation	34
2.4.1	AC and DC responses	41
2.4.2	Advantages and future application	43

REFERENCES

CHAPTER 3 Electron & Ion beam charging of surfaces

3.1	Introduction	45
3.2	The electronic beam as a technological process	45
3.2.1	Energy conversion at the point of action	47
3.2.2	X-ray production and shielding	48
3.2.3	Thermionic emission and emission of secondary electrons and electron back-scattering	49
3.2.4	Electron range	50
3.2.5	Charge and dose effect	51
3.3	Isotope separator	53
3.3.1	Basic data	53
3.3.1.1	Ion source	53
3.3.1.2	H.T. supply	54
3.3.1.3	Analysing magnet	54
3.3.1.4	Target chamber	55
3.3.2	General data	56
3.3.2.1	Special notes	59
3.4	Van de Graaff	61
3.4.1	The high voltage terminal	62
3.4.2	Magnetic analyser	64
3.4.3	Ion beam flight path	64
3.4.4	Target chamber	65
3.5	DC plasma ion bombardment	68
3.5.1	Gas discharge	70

REFERENCES

PART TWO

EXPERIMENTAL WORKS AND OBSERVATIONS

CHAPTER 4	Thin film electrodes	
4.1	Introduction	71
4.2	Wire electrodes and problems associated with wire electrodes	71
4.3	Preparation of electrodes by thin film vacuum	73
4.3.1	Preparation of mask	73
4.3.2	Pre-cleaning of the glass slide	75
4.3.3	Evaporation process	75
4.3.3.1	Evaporation method	76
4.3.4	Sputtering process	79
4.3.4.1	Sputtering method	80
4.3.4.2	Advantages	80
4.4	Electrode effect	81
4.5	Electrode cleaning	81
REFERENCES		
CHAPTER 5	Electronic circuit design and applications	
5.1	Introduction	83
5.2	Three-phase voltage generator circuit	83
5.2.1	Three-phase rotating electric field	85
5.3	Four-phase voltage generator	87
5.3.1	Four-phase rotating electric field	88
5.4	Fixed Voltage Regulator	90
5.5	Charge-sensitive amplifier	91
5.6	Ioniser	94
5.6.1	Circuit design of an ionizer	95
5.6.2	Testing	99
5.6.3	Measurements	99
5.7	Computer controlled oscillator	103
5.7.1	Using a D/A converter with a microcomputer	107
5.8	Class AB emitter follower	109
5.8.1	Class B and class AB push-pull operation	109
REFERENCES		

CHAPTER 6 Construction of the electron beam gun

6.1 Introduction 115

6.2 Requirements for constructing the electron gun 115

6.3 Electron optical system 119
6.3.1 Magnetic lens 119
6.3.2 Phosphor screen 120
6.3.2.1 Preparation of the phosphor screen 121

6.4 Experiments 122

6.5 Operation of the electron gun 125

6.6 Measurements on the electron gun 125
6.6.1 Beam current/Energy 125
6.6.2 Beam current vs Filament current 130
6.6.3 Filament current/Energy/Beam current 132

REFERENCES

CHAPTER 7 Charge Implantation Experimental: Equipment and procedure

7.1 Introduction 134

7.2 Electron bombardment and injection 134
7.2.1 Electron charge measurement 137
7.2.1.1 Decay time 137
7.2.1.2 Errors 138
7.2.1.3 Results 138
7.2.2 Dose calculation 140

7.3 Van de Graaff 141

7.4 Isotope separator 142

7.5 DC plasma ion bombardment system 144
7.5.1 Ion bombardment method by DC plasma ion 147
7.5.2 Infrared measurement 147

REFERENCES

CHAPTER 8 Experiments with cell oscillation and rotation

8.1 Introduction 151

8.2 Action of non-uniform electric fields on Leishmania and yeast cells in H_2 and Sub-H_2 ranges 153

8.2.1 Observation of pearl chains at sub-audio frequencies 154

8.3	Experiments involving cell rotation	157
8.3.1	Procedure	159
8.3.2	Problems associated with CSR studies	160
8.3.3	Sources of error	162
8.3.4	Results	162
8.4	Discussion	169

REFERENCES

CHAPTER 9 Cellular Attachment

9.1	Introduction	173
9.2	Scratched plastic as a substrate for attachment	175
9.3	Surface of substratum	178
9.4	The physical implications of the attachment of L.major cells to electron bombarded surfaces	179
9.4.1	Electron bombardment	180
9.4.2	Ion implantation	184
9.5	Effect of ionisers on Leishmania cells	185
9.6	Charge distribution	188
9.7	U.V. sterilization effect	189
9.8	Advantages of "In vitro" attachment	189
9.9	Discussion	190

REFERENCES

CHAPTER 10 The effects of magnetic fields on water and ice formation.

10.1	Introduction	192
10.2	Experiments on ice formation	193
10.3	Ice crystals from frozen saline	199
10.3.1	Temperature	201
10.3.2	Exposure time	201
10.3.3	Current	201
10.3.4	Frequency	204
10.4	Ice crystals	208
10.4.1	Bragg's law	209
10.4.2	Scattering of X-rays	209
10.4.3	Diffraction of X-rays	211
10.4.4	Transmission of X-rays	217
10.5	Supercooling	223
10.6	Discussion	228

REFERENCES

CONCLUSION 232

APPENDIX 1 Savouraud Dextose Agar 235

APPENDIX 2 Electronc Data Sheets 237

APPENDIX 3 Three dimensional program 247

APPENDIX 4 Least square program 249

APPENDIX 5 Millipore letter 253

PUBLICATIONS 255

ACKNOWLEDGEMENT

The author would like to give his sincere thanks to Dr. C.W. Smith for his continuous encouragement and supervision during his eight years at Salford University as an undergraduate and graduate student.

Professor D. Molyneux and Dr. K Wallbank are thanked for their help during the biological work and informative discussions.

Many thanks are also conveyed to Mr. E. Brimble, Department of Electronic and Electrical Engineering; The Computer Laboratory and the Library Staff, and to Mrs. P Fleming who has given her time and assistance in typing this thesis.

DEDICATION

The Author's heartfelt thanks go to his beloved parents, his wife and his baby, for just about everything

SUMMARY

We are called organisms because our cells are organized into a co-operative assemblage of interacting elements. Human beings are more than simply bags of interacting chemicals walking around enclosed within 1.8 square metres of skin. It has long been known that biological organisms, including ourselves, use chemical communication systems. Internally from tissue-to-tissue, for example, there are hormones; and externally, between individual organisms, particularly insects, there are pheromones. For the most part, the regulation of biological processes has been assumed to take place by means of chemical communication systems from a transmitter molecule via diffusion or bulk transport as the transmission link to a receiver or receptor molecule. Multicellular organisms, and human beings, comprise at least (10^{14}) cells, a more rapid and efficient system of communication, other than a solely chemical means, is necessary to provide for the vast number of interactions essential for proper management of the whole system. In real time such a system might need to have a band width only obtainable with an optical carrier. Organisms are also dielectric resonators by virtue of their difference in dielectric constant from their environment, and, thus, are surrounded by an evanescent electromagnetic envelope which can act as a communication link to a similar field system [1]. Bioelectromagnetic fields are part and parcel of life, the study of which involves the study of the electric, magnetic and electromagnetic field patterns surrounding a living system.

The phenomena of bioelectromagnetic field interactions with water, and simple cells such as yeasts, Saccharomyces cerevisiae and parasites Leishmania major have been demonstrated by several experimental

approaches, namely:

i) Direct dielectric measurements on water [2].

ii) Dielectrophoresis experiments on yeast cells.

iii) Cellular spin resonance of yeast and parasite cells.

iv) Observation of attachment of parasite cells to negatively (electron beam) charged substrates.

v) Studies of ice crystals grown in the presence of a magnetic field.

Dielectrophoresis experiments carried out on living yeast cells during the course of the writer's MSc work [2] showed that there is an anomaly in the "pearl chain" formation of yeast cells as the geomagnetic field strength satisfies the resonance condition for H^1 (the yield of pearl chains drops in the region of 2.7 kHz for a geomagnetic field strength of 0.7 gauss). This corresponds to the proton nuclear magnetic resonance which results in a repulsion force between the cells in the pearl chain.

In the continued course of the work described in this thesis, the interaction of rotating electric fields has been studied in respect of the yeast and parasite cells. A cellular spin resonance of lone cells has been observed at critical values of the environmental magnetic fields, and the spectrum of the rotation speed of cells for different values of the applied frequency of rotating electric field is shown and discussed in Chapter (8). In this case the electrodes were made of thin films of platinum or gold prepared by vacuum sputtering. Thin film metal electrodes allow the microscope observations to be carried out at high optical magnification using short working distance objectives. The details of the preparation of these electrodes are given in Chapter (4).

The treatment of polystyrene petri dishes to produce a negative electrostatic charge on their surface was found to facilitate the attachment of Leishmania major cells thereby permitting their culture "in vitro". It may be that an electrostatic phenomenon provides the effective mechanism.

Attempts were made to elucidate these attachment systems by comparing the effects of charging polystyrene petri dishes either negatively by electron bombardment or possibly by the use of a positive ion beam. In Chapter (9) effects are described which were obtained when these experiments were carried out using Leishmania major cells. It became clear that these cells had a clear preference for the negative (electron charged) surfaces and regarded them as a good place to stick.

Chapter (3) explains the physical nature of the processes by which the polystyrene petri dishes may be negatively or positively charged. Since the electron-beam charging of the petri dishes resulted in the attachment of parasites to the surface of the substrate which had received the negative charge, presumably, in some important respect, this stimulated their normal habitat on cuticular surfaces in the gut of their sandfly host which is known to carry a negative charge. The polystyrene petri dishes were electron beam irradiated at a variety of charge doses. For the low doses (10^{16} e/m), a special low-energy electron gun had to be constructed, as described in Chapter (6).

Any living organism is approximately 80% water. Although the interaction of the weak geomagnetic field with water will cause proton precession at the frequency of magnetic resonance, the organism can survive the effect of a strong, steady magnetic field even though this may have an effect on the cell water as demonstrated by the formation

of ice crystals from water exposed to a magnetic field. Some hypersensitive patients react not only to certain chemicals in very small amounts, but may also react to magnetic field treated water, differently depending upon the specific frequencies [3]. For this reason also, possible effects of a magnetic field on water through the ice crystals formed by freezing water in a magnetic field were investigated by X-ray crystallography (Chapter (10)).

REFERENCES

1) RIVERA, H., POLLOCK, J.K. and POHL, H.A. "A.C. Field Patterns About Living Cells", Cell Biophysics, 1985, 7, p.43.

2) JABERANSARI, M. "Dielectrophoresis, Electrodynamic and Magnetic Resonance Phenomena in Yeast Cells", M.Sc. Thesis, Salford University, 1985.

3) SMITH, C.W., CHOY, R., MONRO, J. Environmental, Allergenic and Therapeutic Effect of Electromagnetic Field", 3rd Annual International Symposium on Man and His Environment in Health and Disease, Feb. 21-24, Dallas, Texas.

PART I

THEORETICAL WORK

CHAPTER (1)

BIOLOGICAL CELLS

1.1 INTRODUCTION

The experiments reported in this thesis were confined to two different kinds of biological systems: yeast cells (Saccharomyces cerevisiae) and parasites (Leishmania major). The following pages describe the basic physiology, and the nutrition and cultivation of these cells together with their importance to and effect on man and his environment. Because of the pathogenicity of Leishmania major cells, the number of experiments on these cells was limited; reliance had to be placed on information obtained from researchers having the necessary skills for results involving the handling of the live parasites.

1.2 Yeast cells

Yeasts have been defined as fungi whose usual and dominant growth form is unicellular, and great variations exist among them. Yeast cells may be spherical, ellipsoidal or cylindrical: the yeast cells used in this research were Saccharomyces cerevisiae and these are roughly spherical in shape. Cells of Saccharomyces cerevisiae are usually within the range 2 μm to 8 μm in diameter with 3 μm to 15 μm length for the major axis of the most ellipsoidal cells.

Figure (1.1) shows the yeast cell structure. The protoplasm of a yeast cell is enclosed by a cell wall and cytoplasmic membrane and contains a nucleus, a large vacuole, and numerous granules and fat globules. The cell wall is composed of an outer dense layer of about 0.05 μm thickness and a less dense layer of about 0.2 μm. The internal wall is composed of polymers of glucose and mannose with smaller amounts of protein, lipid and chitin. The nucleus is less than 1 μm diameter.

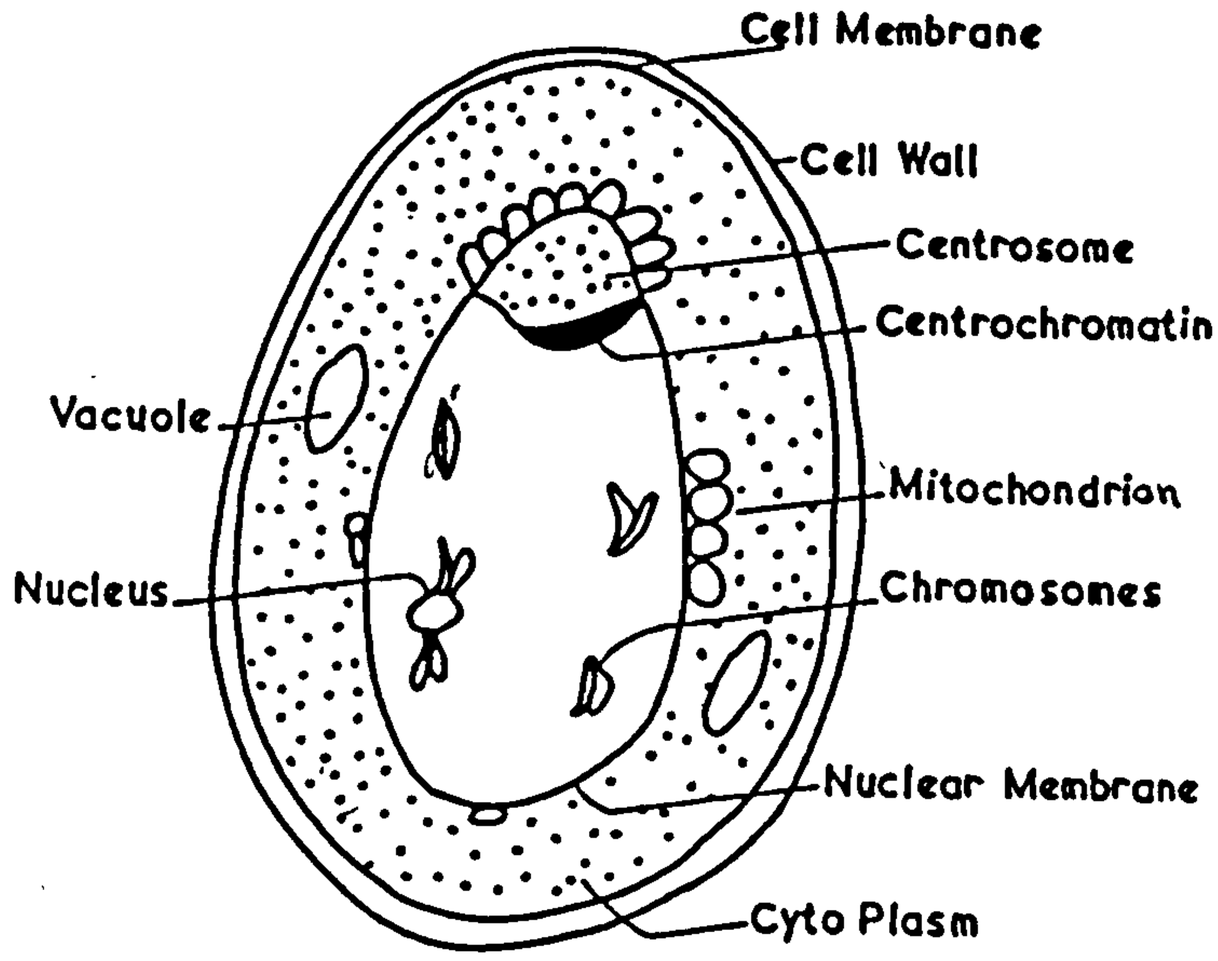

Fig.1.1 The structure of the yeast cell according to Lindegren (1952)

Yeasts require the same chemicals as other forms of life. These include carbon, hydrogen, oxygen, nitrogen, phosphorus, potassium, sodium chloride, sulphur, mangnesium, iron, zinc, manganese, copper and molybdenum. These are often present in sufficient amounts as impurities in the water or other ingredients of culture media.

Yeast cells were the first organisms to be shown to grow in the absence of atmospheric oxygen and also grow over a wide range of pH values. The optimum rate of growth usually occurring between pH 4.5 and 5.0.

Growth cannot be expected at temperatures much below freezing, nor does it occur above 47°C, the most favourable temperature is usually between 20°C and 30°C.

Cells of most species are killed within five to ten minutes at 52°C to

58°C, the medium in which the organisms are suspended affects the sterilization time and temperature.

1.2.1 Growth rate of yeast

Growth is defined as an increase in the number of microbial cells. Growth rate is expressed as the growth per unit time.

In the yeast micro-organism, growth usually involves an increase in cell numbers. A single cell will continually increase in size until it is double its original size. Then the cell division occurs, resulting in the formation of two cells the size of the original cell. The interval between the successive formations of two cells from one is called the generation time. Generation time is thus the time required for the cell population to double. It has been found to be more convenient to replace the generation time by mean generation time (M.G.T.). This is because not all the cells will produce even a single daughter cell, but also it is commonly observed that some cells develop two or more buds at the same time.

Under optimum conditions, one can easily determine the mean generation time by the equation (1.5) derived below. Experimentally, the mean generation time for yeast cells is determined by inoculating the medium with a known number of cells, allowing the yeast to grow under optimum conditions, and then determining the final cell population, now too large to be counted directly, by serial dilution and counting.

The experimental data required to calculate the MGT includes (a) the number of yeast cells present at the beginning, (b) the number of yeast cells present at the end of a given time interval, and (c) the time

interval.

The relationship of cell numbers and mean generation time can be expressed by the following equations where B is the number of yeast cells inoculated into medium or cell count at zero time. b is the number of cells at the end of the given time period t. G is the mean generation time (MGT) and n the number of generations each of time equal to MGT.

Starting with a single cell, the total population b at the end of a given time period would be expressed by

$$b = 1 \times 2^n \qquad 1.1$$

where 2^n is the cell population after the nth generation. However, under practical conditions, the number of cells B introduced into the medium at time zero is not one, but more likely, several thousand, so the formula now becomes

$$b = B \times 2^n \qquad 1.2$$

Solving Equation (1.2) for n,

$$\log_{10}^{b} = \log_{10}^{B} + n \log_{10}^{2}$$

$$n = \frac{\log_{10}^{b} - \log_{10}^{B}}{\log_{10}^{2}} \qquad 1.3$$

If one now substitutes the value for the $\log_{10}^{2}$, which is 0.301, in the above equation, then

$$n = 3.3 \log_{10} \frac{b}{B} \qquad 1.4$$

Thus, by use of equation (1.4) the number of mean generations that have taken place can be calculated provided initial population B and the population b after time t is known and the growth is only a single exponential.

The mean generation time G is equal to t (the time which elapsed between b and B) divided by the number of generations n, or

$$G = \frac{t}{n} = \frac{t}{3.3 \log_{10}(b/B)} \qquad 1.5$$

In equation (1.5) G is usually expressed in hours per cell division.

The mean generation time is strongly dependent upon the nutrient in the medium or prevailing physical conditions, like temperature, pH, etc.

Yeasts are almost universally present in soils and from this source they are widely disseminated by insects: they also travel on dust particles and water droplets in the air. In a dry state they are known to survive for at least four years. Hence, it is obvious that they may easily find access to substances capable of supporting their growth.

Yeasts have a particular predeliction for acid foods that contain sugar, from which they produce ethyl alcohol and a large quantity of carbon dioxide gas. Fruits are especially subject to this type of spoilage. Since yeasts, unlike moulds, can grow in the absence of

oxygen, sealing a food container does not prevent spoilage.

Yeasts are also very important in industry. Alcoholic fermentation has been practiced for thousands of years. Strains of Saccharomyces cerevisiae are used to make beers, ales, wines, CO_2 and industrial alcohol. This organism also produces the various fermented milks such as the Kafir' Koumiss' and Matzoon and participates in the production of certain cheeses. Compressed yeast is used not only in baking but also as a source of vitamins and of enzymes useful in the manufacture of syrups and confectionery products.

1.2.2 Pure culture

When yeasts grow in an artificial medium which is referred to as a "culture", different species of yeast growing on the same kind of culture medium may appear quite different. To determine the chracteristics of a particular species of mirco-organism, it is important that the organism be isolated and grown in the laboratory as a pure culture. There are a variety of techniques whereby the different species in a natural specimen can be isolated and grown as a pure culture [1]. However, only the Spread-Plate Technique is discussed here:

By means of a transfer loop a portion of the yeast specimen suspension is placed into a liquid medium (inoculum). In this present work, The medium used was Sabouraud Medium (See Appendix (1)). The inoculum is then incubated for eight hours. A few drops of the culture are transferred by spreading or streaking over the surface of a nutrient agar medium. The nutrient agar medium used was Sabouraud dextrose agar. Spread plates are usually streaked using a sterilised bent glass

rod. This manipulation distributes the yeast cells over the agar surface so that separated yeast colonies may develop from each individual yeast cell.

However, one of the limitations of this technique is that only a small amount of the specimen can be spread over the surface of the medium.

1.2.3 Logarithmic curve

The progressive doubling of yeast cell numbers results in a continually increasing rate of growth in the population. When a fresh medium is inoculated with a given number of cells, and the yeast cell population is determined intermittently during an incubation period of 48 hours and the logarithm of the number of cells versus time is plotted, the following phases of growth can be recognised; lag phase, exponential phase, stationary phase, and the death phase (Figure 1.2)

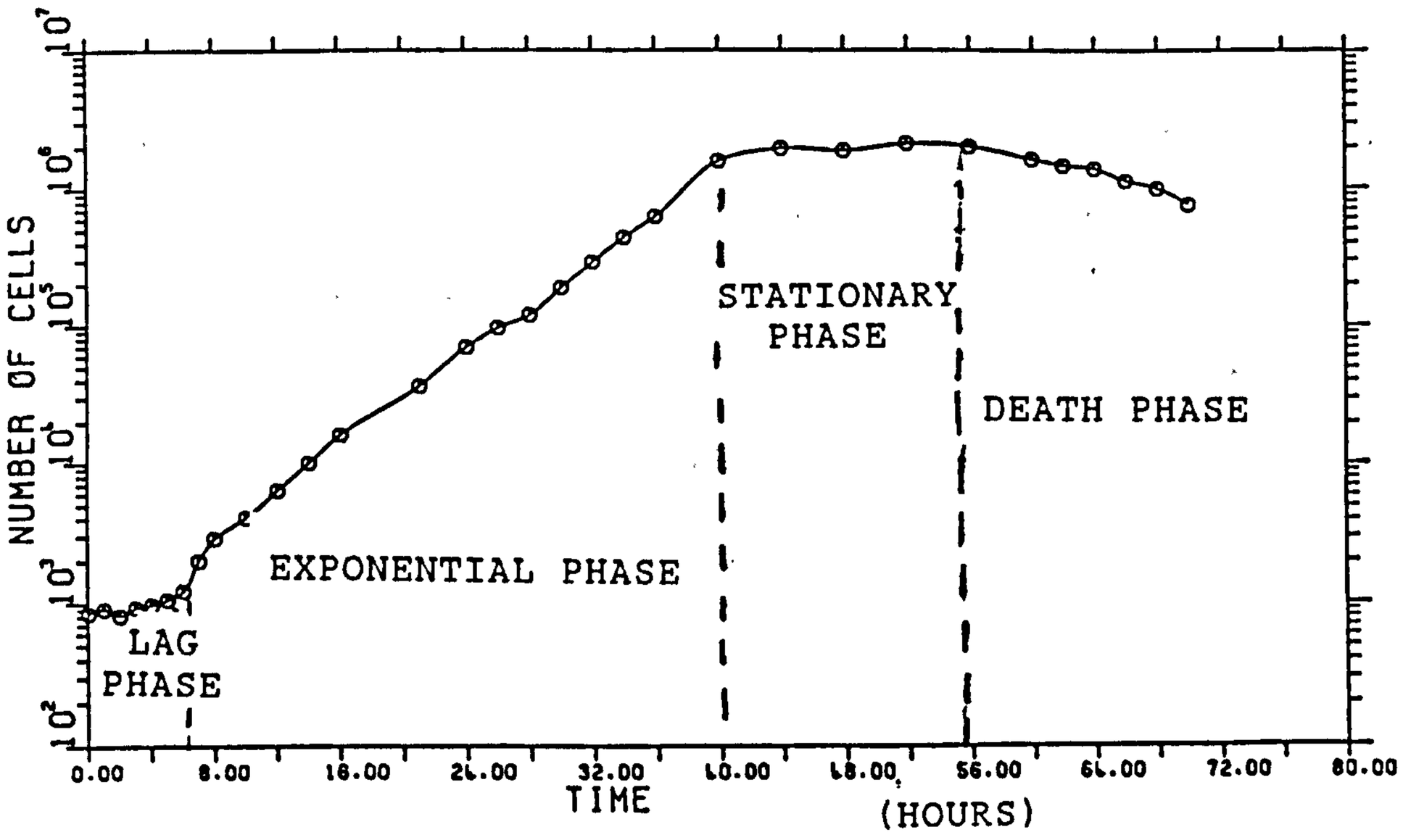

Fig. (1.2) Different phases of the growth of the yeast cells by Jaberansari [1]

1.2.3.1 Lag phase

When a yeast cell is inoculated into a fresh medium, growth usually does not begin immediately but only after a period of time. This interval is called the Lag phase and it may be brief or extended depending on the conditions. In this phase, each cell grows by increasing its cell mass. The cell enlarges, undergoing extensive macromolecule synthesis. This period is an adaption stage: growth without cell division. The lag also occurs because the cells must become adjusted to the new medium before growth can begin. A lag can be avoided if an exponentially growing culture is transferred to an identical culture medium at exactly the same temperature. In this case, no adjustment by the cells is needed, and growth can continue at the same rate. At the end of Lag phase, each organism divides. From experimental graph it can be seen that it takes about four hours from inoculation before cells start dividing.

1.2.3.2 Exponential phase

During this period the cells divide steadily at a constant rate. This is a consequence of the fact that each cell divides to form two or more cells, and so on. The growth rate of yeast is also greatly affected by the culture medium and environmental conditions, especially temperature. In practice, one usually tries to choose a culture medium and a temperature that are optimum for the organism.

Exponential growth cannot proceed indefinitely or else the world would be swamped with micro-organisms. Obviously, something must happen to limit growth long before this time. What generally happens is that an essential nutrient of the medium is used, waste products of the yeasts build up in the medium to an inhibitory level and the yeasts themselves

produce specific inhibitutory substances, the colicins. Thus exponential growth ceases and the population reaches the stationary phase.

1.2.3.3 Stationary phase

During the stationary phase the population remains the same, and the birth rate is balanced by the death rate. In this phase the slowing of the growth rate continues after 40 hours. Here there is also exhaustion of the nutritional factors of the medium and the accumulation of waste products. The population then remains constant for about 16 hours.

1.2.3.4 Death phase

Following the stationary phase, the cells may begin to die off faster than new cells are produced. Death occurs either because the yeast undergoes starvation or because some toxic products (colicins) are produced that accumulate and attenuate the growth or kill the yeast cells.

It is possible to maintain viable cultures and prevent the onset of the death phase by removing cultures from the incubator shortly before exponential growth is over and placing them at a lower temperature, where growth and function are slowed. Death often occurs less rapidly if the organism is grown on a culture medium that is not too rich, since in a rich medium a high population density occurs and hence, more waste and toxic products build up.

The only way a culture can be maintained is by periodic transfer to a fresh medium. The growth of the culture must be watched, and as soon

as the stationary phase is approached, a transfer to a fresh medium should be made.

1.2.4 Synchronous growth

The number of cells in a culture usually increases smoothly because at any time at least a few cells are dividing, in other words, cell division is not normally synchronized. However, a population in which all the cells are undergoing division at approximately the same time is sometimes desirable, particularly for growth studies of yeast cells. But the synchrony generally lasts for only a few generations since even the daughters of a single cell soon get out of step with one another. Synchronization is achieved by inoculating cells into a medium at a sub-optimal temperature, if they are kept in this condition for some time, they will metabolize slowly but will not divide. When the temperature is raised to the optimum, the cells begin to undergo synchronized division. They may also be given an osmotic change "shock" to trigger the division process. When these cells are observed by phase contrast microscope, they are all reasonably well synchronized with each other.

1.2.5 Cultivation and examination of Saccharomyces cerevisiae

The basic equipment and techniques needed for growing Sacchromyces cerevisiae involved the following:

1.2.5.1 Preparation of media

Sabouraud liquid media capable of supporting the growth of micro-organisms are now available in a ready-prepared dehydrated state (Oxoid Ltd and Difco). It is often convenient to dissolve the ingredients in water contained in a large beaker or flask, and then dispense the

resulting medium into appropriate containers ready for autoclaving.

1.2.5.2 Pressure cooker (steriliser)

This is needed to sterilise media and equipment such as glassware that will withstand a high temperature. When sterilising media in screw cap containers, enough room must be left inside the bottle for the medium to expand and the cap left partially unscrewed so that air can escape.

1.2.5.3 Inoculating cabinets

These are highly desirable for the transfer of microbes to culture media since they protect the operator from the microbes he is handling, and also minimise contamination of the cultures from air-borne particles. The cabinet consists of a "perspex" box with a sliding door to screen the operator from the TUV sterilizing lamp.

1.2.5.4 Containers

The containers employed in the experiments were those required to hold the culture medium and grow the yeast cells. They are listed below:

i) Petri dishes (diameter 9 cm): sterile plastic petri dishes are now readily available and these are very convenient for use in a microbiology laboratory. They are used to grow yeast cells on solid agar media and can then be disposed of. Glass petri dishes which can be re-used after sterilization are also available.

ii) Bacteriological tubes are used to hold 10-15 ml of solid or liquid media. They are glass tubes (25 ml) with a loose metal cap or cotton wool bung which can be removed with ease when tranferring an inoculum. Agar media may be prepared as a "deep" or as a "slope",

i.e. the agar poured in with the tube vertical, or inclined and then left to set.

iii) Screw cap glass bottle of 20-30 ml capacity.

iv) Medical flats are flat-bottomed glass containers; the 100 ml and 250 ml sizes are the most useful. The main function of these is to store large quantities of prepared sterile media. Such volumes of agar media take about an hour to melt in hot water or several minutes when using the microwave oven. However, they do save time when a large number of agar plates have to be poured.

v) Conical flask, preferably 100 and 250 ml are required for growing the yeast in liquid culture media.

1.3 LEISHMANIA CELLS

Life in the animal world consists of communities of organisms which live by eating each other. In a broad sense, all animals are parasites in that they are helpless without other organisms to produce food for them. Plants alone are able to build up their body substance out of sunlight, water and chemicals. But, animal and plants are preyed upon not only by larger forms which overpower and eat them, they also fall prey to successively smaller forms of life which attack and destroy small more-or-less replaceable portions of the host, or even more subtly, exploit the energies of the host by subsisting on the food on which a lot of time and energy has been expended in collecting. There are vast numbers of species of animals in the world and their common names differ in different parts of the world. Indeed, the same common name may refer to different organisms in different places. The only

feasible solution has been to give each organism a scientific name which does not vary. The genus used in this part of the work is the Leishmania parasite.

The word Leishmania, which is capitalized, is the genus name. This indicates the group to which this particular type of parasite belongs. Different names have also been given to the diseases produced by it, but infections with Leishmania species are technically called Leishmaniases. Leishmaniases are examples of zoonoses which reach man through insect vectors. Various rodents, dogs, and other carnivores especially, maintain the infection in nature ie. they are "reservoir hosts". Most mammalian Leishmania can infect man. We shall discuss one of the widely accepted groups and the exact species which have been used during this research programme. Later we shall describe the physiology of this species and its nutrition and growth, and the clinical danger of this Leishmania species to man.

1.3.1 Leishmania major

The Leishmanias are heteroxenous. Part of their life cycle is spent in the gut of a fly, where they assume the form of a promastigote; the remainder of their life cycle is completed in vertebrate tissues. The species of Leishmania used for investigating cellular attachment to the electrostatically charged petri dishes was the one causing cutaneous sores, "Leishmania major". The second word of "Leishmania major" (which is not capitalized), is the species name, and indicates the type of parasite itself. Leishmania major produces a cutaneous ulcer known as "cutaneous leishmaniasis". There are two varieties of cutaneous disease which are distinguished on pathological and epidemiological grounds, the urban type known as L.tropica, and the rural type L.major.

The urban type is found in more densely populated areas. By contrast, the rural type is found in sparsely inhabited regions. The variety of Leishmania chosen in this project was the L.major type (cutaneous leishmaniasis) because of low pathogenisity. These were obtained from a soldier in a prisoner of war camp (during the Iran-Iraq war) in the South-western province of Iran known as Khozestan, in middle east Asia.

1.3.2 Physiology of Leishmania major cells

Parasites in the genus Leishmania are unicellular and usually uniflagellate elongated organisms measuring 4 to 40 um in total length. They are either mobile and free-swimming or sedentary and attached to the cuticle of the invertebrate host's gut, the sandfly. They belong to the family Trypanosomatidae of the suborder Trypanosomatina, and order Kinetoplasticida. They are characterised by a single mitochondrion containing a small compact mass of DNA. This is the Kinetoplast which lies close to the base of the flagellum, the locomotory organelle, and usually stains intensely with Romanowsky stains such as Giemsa's.

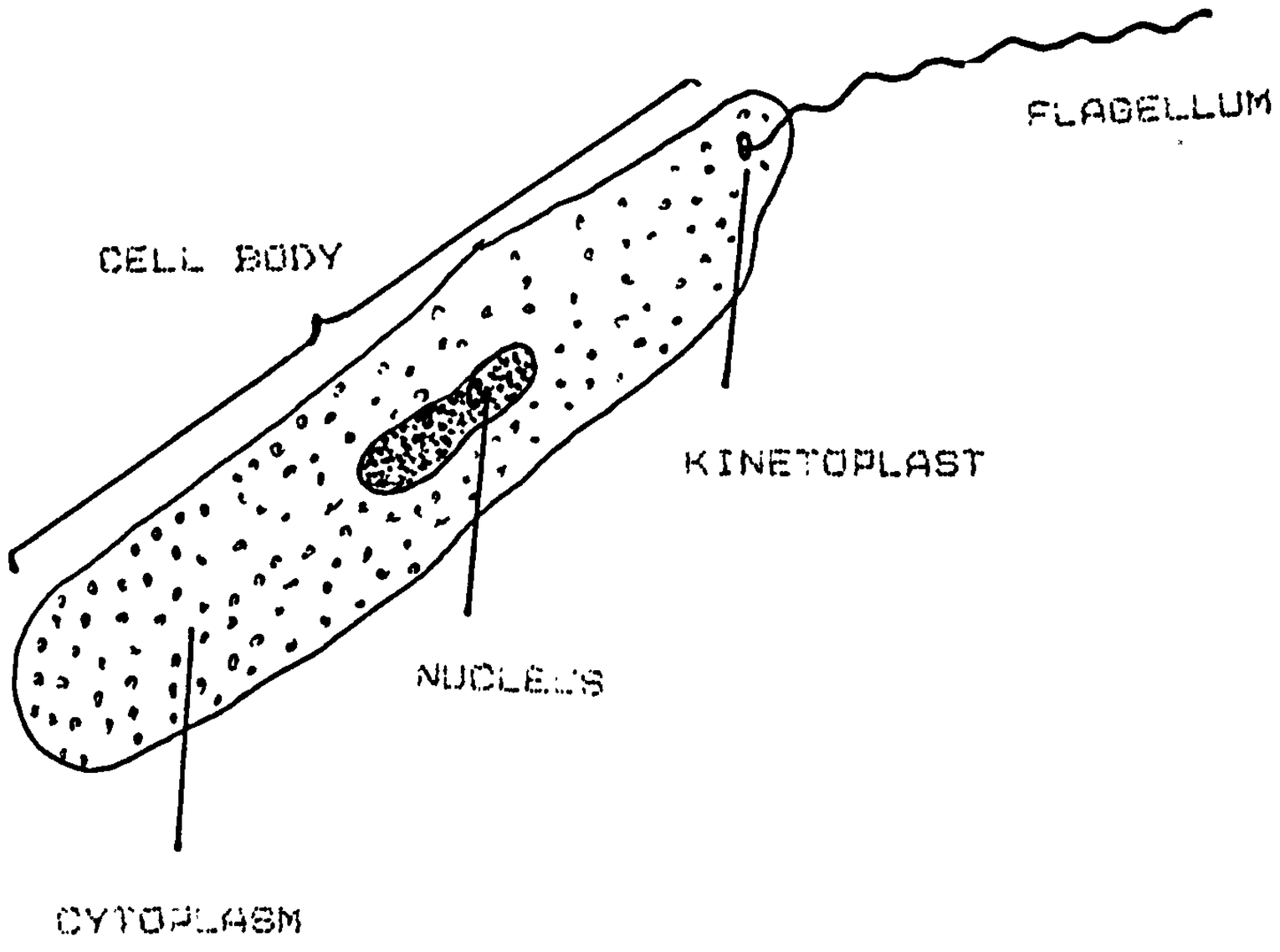

Fig. (1.3) Basic structure of "Leishmania major" cells

1.3.3 Nutrition and growth

Leishmania major cells were grown and suspended in a tissue culture medium 199 (GIBCO), Grace's insect tissue culture medium (GIBCO) or Schneiders Drosophila medium (GIBCO). The above media each supplemented with 20% foetal calf serum (FCS, Sera-Lab) formed the basis for the culture system investigated. For convenience, and to preclude contamination, each culture medium was stored in aliquots of 50 or 100 ml and the FCS was in 5 or 10 ml aliquots prior to use. All aliquots were incubated at 34°C. for 72 hours as a sterility check. Aliquots of tissue-culture medium were then stored at 4°C. and the sera at -10°C. until needed. Further mention of any of the media studied, i.e. Grace's, or medium 199, includes 20% FCS (V/V), unless otherwise indicated.

Leishmania promastigotes multiply by binary fission, doubling every 4-8 hours while in the lag phase of growth.

1.3.4 The Leishmaniases in Man

Although the leishmaniases give rise to important public health problems, current efforts to control these diseases are insufficient. The wide diversity of both the clinical forms of the diseases and the epidemiological situations mean that each focus requires specific control principles and methods. Moreover, Leishmaniasis control is usually hampered by ignorance of the true relevance of the diseases and underestimation of the human suffering and invalidity they cause.

There are a few clinical forms of Leishmaniases in man, but the species used in this project, L.major, is the least pathogenic, causing a self-

healing and limited antaneous sore (Fig. 1.4). Other species often cause fatalities.

The clinical features of cutaneous leishmaniasis (CL) tend to differ between and within regions, reflecting intraspecific variations in the parasite, and also, perhaps, in the genetically determined response of the patient.

A classical lesion starts as a nodule at the site of inoculation. A crust develops centrally which may fall away exposing an ulcer which then heals gradually leaving a depressed scar with altered pigment.

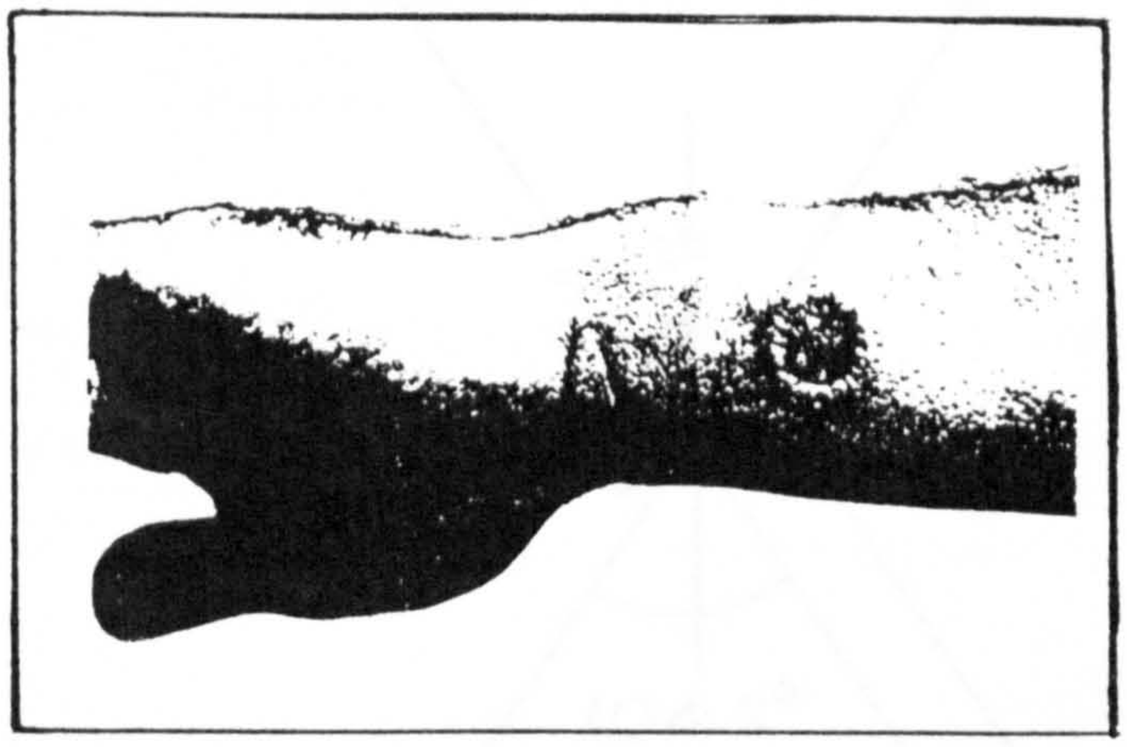

Figure (1.4) cutaneous leishmaniasis: the picture shows an ulcer due to Leishmania major lesions [2]

1.4 Water in a biological system

It is well known that water forms a necessary constituent of cells and life cannot exist, even for a limited period, in the absence of water. Desiccated spores can survive dryness and become viable when water is available, but do not exhibit the properties of life when dry. So, this naturally occurring inorganic liquid is essential for the maintenance of inorganic life. Apart from acting as a proton-exchange

medium, water permeates through living organisms and functions as a lubricant in the form of surface films and viscous juices. Water is the solvent which promotes biological hydrolysis in which proteins and carbohydrates are broken down; lipids, although not actually modified chemically, are solubilized in the aqueous medium. Thus, the energy required for biosynthesis derives partially from the energy of formation of water. Another important function of water is the thermal regulation of living organisms, its large heat capacity coupled with the high water content are responsible for maintaining isothermal conditions. The high thermal conductivity of water prevents serious local temperature fluctuations.

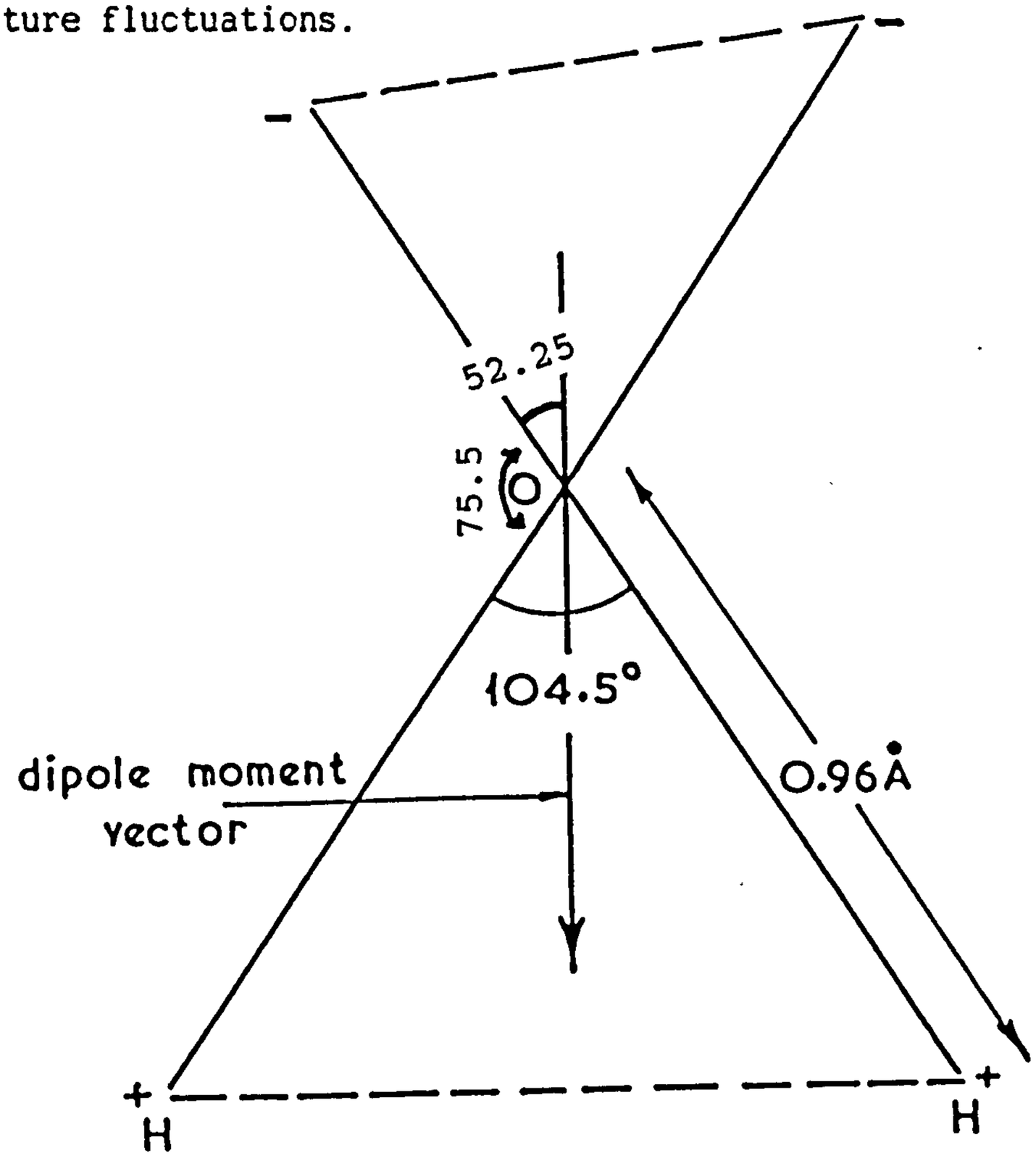

Fig. (1.5) Structure of water molecule (HASTED [4]). The oxygen atom is considered to be more electronegative than the hydrogen atom. When they are bonded, a dipole moment will exist with the oxygen negative and it appears probable that the dipole moment vector bisects the HOH angle and points from the negative oxygen atom to the positive region between the hydrogen atoms.

The physical state of water in cells is a subject of controversy [3]. According to the "classical theory" of membranes intracellular water is in the same form as liquid water and the interior of the cell can be considered as a compartment containing a solution of ions, small molecules and macromolecules bounded by a lipoprotein membrane. This membrane is responsible for maintaining the intercellular distributions of ions by means of critical pore size and ion "pump" located within the membrane walls. A small fraction of the water is "bound", i.e. in hydration layers of macromolecules or cellular membranes. The extent of these hydration layers is unspecified.

The electrical properties of the water molecules can be approximately represented by a resultant permanent dipole (Fig. 1.5). The angle HOH was taken as 104.5° , with a similar angle between the vectors from oxygen atom to the negative charge concentrations [4]. The linking of the oxygen atom is through the hydrogen and the called the hydrogen bond. Each hydrogen is closer to one oxygen than to the one at the other end of the linkage. Thus each water molecule preserves its identity.

However, the electrons are attached more strongly towards the heavier oxygen molecules and this leads to the slight negative charge in this region and a slight positive charge in the region of the hydrogen nuclei. This imbalance in charge gives the water molecule an electrical polarity; water is thus a polar molecule characterized by a relaxation time centred around 9.2 picoseconds at 20°C. The dielectric constant also changes from the low frequency value of about 80 to 5.5 over this dispersion region [4].

Although the water structure does not exist for any appreciable period of time, but it might well have a significance and a long range coherence on a time-scale of the order of picoseconds. According to Hasted [5], the lifetimes of any dipole ordering and the vibrational and rotational modes of any such structuring would be very sensitive to changes in pressure, temperature and to the presence of solutes.

Water accounts for between 80% and 90% of the weight of a micro-organism. According to Rose [5] the water requirements of micro-organisms can be expressed quantiatively in the form of the water activity (a_w) of the environment or substrate, this is equal to P/P_o, P being the vapour pressure of the solution and P_o the vapour pressure of water. Water has an a_w value of 1.00, this value decreases when solutes are dissolved in water.

Yeasts vary in the optimum a_w values required for growth, but the minimum values for these organisms (0.91 - 0.88) are lower than those of the majority of bacteria [5].

The general effect of lowering the a_w value of a medium below the optimum is to increase the length of the lag phase of growth and to decrease the growth rate and the size of the crop of the organism [6].

It must be concluded that from the different ways in which water is involved with the life processes indicates clearly that water, acting as a solvent, a dispersing and lubricating medium, a versatile reactant and that, morphologically and functionally - life as we know it and water are inseparable. It is therefore, hardly surprising that living organisms are sensitively attuned to the properties of their water.

REFERENCES

1) JABERANSARI, M. "Dielectrophoresis, electrodynamic and magnetic resonance phenomena in yeast cells", M.Sc. Thesis, University of Salford, 1985

2) The LEISHMANIASES, Report of a WHO expert committee. World Health Organization, Geneva, 1984.

3) CLEGG, J. Trans.far.soc.,1938,34,p.282.

4) HASTED, J.B. "Aqueous dielectrics", ed. A.D. Buckingham. London: Chapman and Hall, 1973.

5) ROSE, A.H. "Chemical microbiology", 3rd ed. London: Butterworth, 1976.

CHAPTER (2)

DIELECTROPHORESIS, PEARL CHAIN FORMATION AND CELLULAR ROTATION IN BIOLOGICAL SYSTEMS

2.1 INTRODUCTION

This chapter considers the subject of "Dielectrophoresis" in the context of "bunching effects" by which the cells are brought into close contact by means of an alternating electric field. The cells often form chain-like patterns, hence the commonly applied term "pearl chain" formation. This is described in the second part of this chapter.

It is not unusual to see several cells in a long "pearl chain" of cells spinning individually in their places as the frequency is changed. Several types of electric fields can be used to produce this phenomenon, including circularly rotating fields using a multiplicity of electrodes. Part C of this chapter presents a theory to explain the spin of cells by an applied electric field.

2.2 Dielectrophoresis

"Dielectrophoresis" is defined [1] as the motion of matter due to polarization effects in a non-uniform electric field in which the most polar matter moves towards the region of greatest field intensity. It is to be carefully distinguished from motion caused by the response to free charge on a body in an electric field (uniform or non-uniform), which is known as electrophoresis and is proportional to the field. In dielectrophoresis studies it is therefore important to use alternating fields because this effect depends on the square of the field and electrophoretic effects are thereby eliminated.

Dielectrophoresis has a relatively simple physical explanation. Any electric field, uniform or non-uniform, exerts a force upon a charged body. It is characteristic of non-uniform fields however, that they exert a force upon neutral bodies. A wide variety of interesting and

useful events take place as a result. The use of biological dielectrophoresis is generally restricted to the use of alternating electric fields rather than static fields as applied in electrophoresis. This is a major point of difference in the two techniques.

It is helpful, in considering the nature of the action of a non-uniform field upon neutral matter, to explain the various possible responses of yeast cells to non-uniform fields.

By comparison with uniform field effects, the deliberate study of non-uniform field phenomenon has been attempted by relatively few workers. Wrede [2] in the late 1920s studied the use of non-uniform electric fields to deflect molecular beams, and in 1938 Muller [3] presented theoretical evidence to show that non-uniform field effects would not be significant for molecular sized particles. More recently, this subject has gained fresh momentum, chiefly as a result of the considerable and significant work by Pethig, Zimmerman & Pohl. [1, 4, 5]. This work, together with that of Losche & Hultschig [6], has given both a theoretical and practical foundation for the study of dielectrophoresis. The effects are easily measurable for large neutral particles of solid, liquid, or gas. But, as the size of the electrically neutral particles approaches that of small yeast cells (approx. 5 μm), the random thermal processes of Brownian Motion begin to mask dielectrophoretic phenomena.

It is the purpose of this chapter to outline the physical principles of dielectrophoresis, and to indicate its relevance to the study of yeast cells.

2.2.1 Basic theory of dielectrophoresis

In understanding the action of non-uniform electric fields on electrically neutral particles, it will be helpful, first, to consider the action of electric fields on electrically charged particles. If a particle possessing a positive charge +Q is placed in a uniform electric field of intensity E volts/meter, it will experience a force F=Q.E, and will be pulled along the field lines towards the electrode of opposite polarity, in this case the cathode, as shown in Fig.(2.1). The behaviour of neutral particles is different.

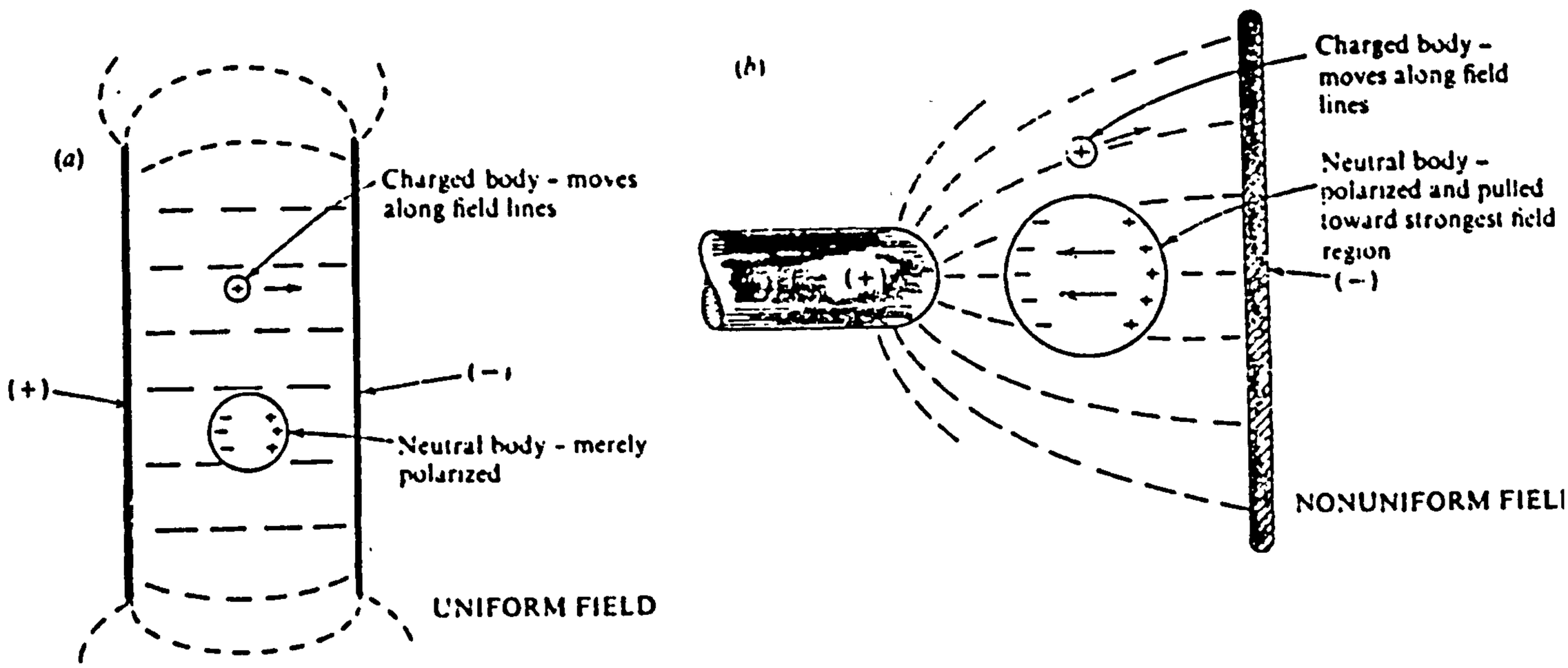

Fig. (2.1) Comparison of behaviour of neutral and charged bodies in (a) a uniform electric field; (b) a non-uniform electric field (7)

In a uniform field the neutral particle will merely become polarized, with a positive charge being induced on the side nearest the cathode, and a negative charge on the opposite side nearest the anode, as shown in Figure (2.1a). Since the particle is electrically neutral, then these two regions of induced charge will be of equal magnitude. The extent of the polarization will depend upon its total polarizability.

If the particle is composed of anisotropic material, or the particle is asymmetric in shape (e.g. elongated), then this polarization may produce a torque acting upon the particle to orientate or align it with the field direction. No such torque will result for a uniformly isotropic particle. Whether or not an induced torque results, no net force will act upon this neutral particle in a uniform field, and it will remain motionless unless subjected to forces arising from other effects.

In a non-uniform electric field, the behaviour of neutral particles is different. The neutral particle will again become polarized, but now a net force will act upon the particle so as to give it a translational motion towards the region of strongest electric field. This effect can be described with reference to Fig. (2.1), where it is seen that the field E_l to the left of the neutral particle is greater than the field E_r to the right.

The induced positive and negative charge δq on the sides of the particle will still have equal magnitudes so that the net force, proportional to $E_l \, \delta q$, pulling the particle towards the cathode will exceed that pulling it towards the low field direction of the anode. This net force producing the translational motion is termed the dielectrophoretic force.

If the polarity of the electrode arrangement shown in Fig. (2.1) were to be reversed, the neutral particle would still move towards the left, in other words, towards the region of greatest field intensity. This now indicates another fundamental difference between the behaviour of charged and neutral particles in electric fields. In an alternating

electric field, the charged particle will always tend to move towards the electrode having the opposite polarity to its own net charge; it appears, in fact, that a more detailed analysis shows that a gentle force acts upon a charged particle in an alternating field so as to force it away from the region of highest field intensity [7].

A neutral particle, on the other hand, will tend towards the field region of maximum intensity, no matter what is happening to the polarity of the electrode producing the region of maximum field intensity.

The theory for the force exerted by a non-uniform field on an electrically neutral body suspended in a fluid medium, will now be outlined. Provided certain assumptions are made, this theory can be reduced to a relatively simple analytical expression. The treatment given here is based on that given by Pethig [1].

In a static field, the net translational force on a neutral small body at equilibrium is given by

$$F = (\mu.\triangle)E \qquad (2.1)$$

where u is the dipole moment vector (induced or permanent), $\triangle$ is the del vector, and E the external electric field. For the case where the neutral dielectric body is homogeneously, linearly, and isotropically polarizable, then

$$\mu = \alpha VE \qquad (2.2)$$

where α is the polarizability, and V is the volume of the body.

This gives

$$F = \alpha V\ (E.\nabla)E \qquad (2.3)$$

$$= \alpha V \nabla (E^2)/2.$$

Now consider the body to be a sphere of radius a, composed of an ideal (zero conductivity) dielectric of permittivity K_2, suspended in an ideal dielectric fluid medium of infinite extent and permittivity K_1, then the field interior E_{in} to the small spherical body associated with an external field E is given by:

$$E_{in} = \left(\frac{3K_1}{K_2 + 2K_1}\right) E. \qquad (2.4)$$

The induced polarization per unit volume is:

$$H = K_2\ (K_2 - K_1)\ E_{in} \qquad (2.5)$$

and the induced dipole moment of polarizable sphere is given by:

$$\mu = VH = \alpha VE$$

the polarizability of per unit volume is therefore given (equations (2.4) and (2.5) as

$$\alpha = H/E = (K_2 - K_1)\ \frac{E_{in}}{E}$$

$$= 3K_1 \left(\frac{K_2 - K_1}{K_2 + 2K_1}\right) \qquad (2.6)$$

and from equation (2.3), the total dielectrophoretic force F acting on the small sphere of volume $V = 4/3\ a^3$ is given by

$$F = 2\pi a^3 \left(\frac{K_1(K_2-K_1)}{(K_2+2K_1}\right) \nabla (E^2). \qquad (2.7)$$

From this equation we see that the dielectrophoretic force depends directly upon the volume and polarizability of the body, and upon the square of the electric field intensity. This field square law dependence reminds us that dielectrophoresis is independent of the sign

of the field, and that it can take place in both an alternating and static field.

2.2.2 Comparison of dielectrophoresis and electrophoresis

An illustration of the contrast between electrophoresis and dielectrophoresis is given in Fig. (2.2). Here positive, negative and neutral particles are in a non-uniform field produced by two concentric spheres.

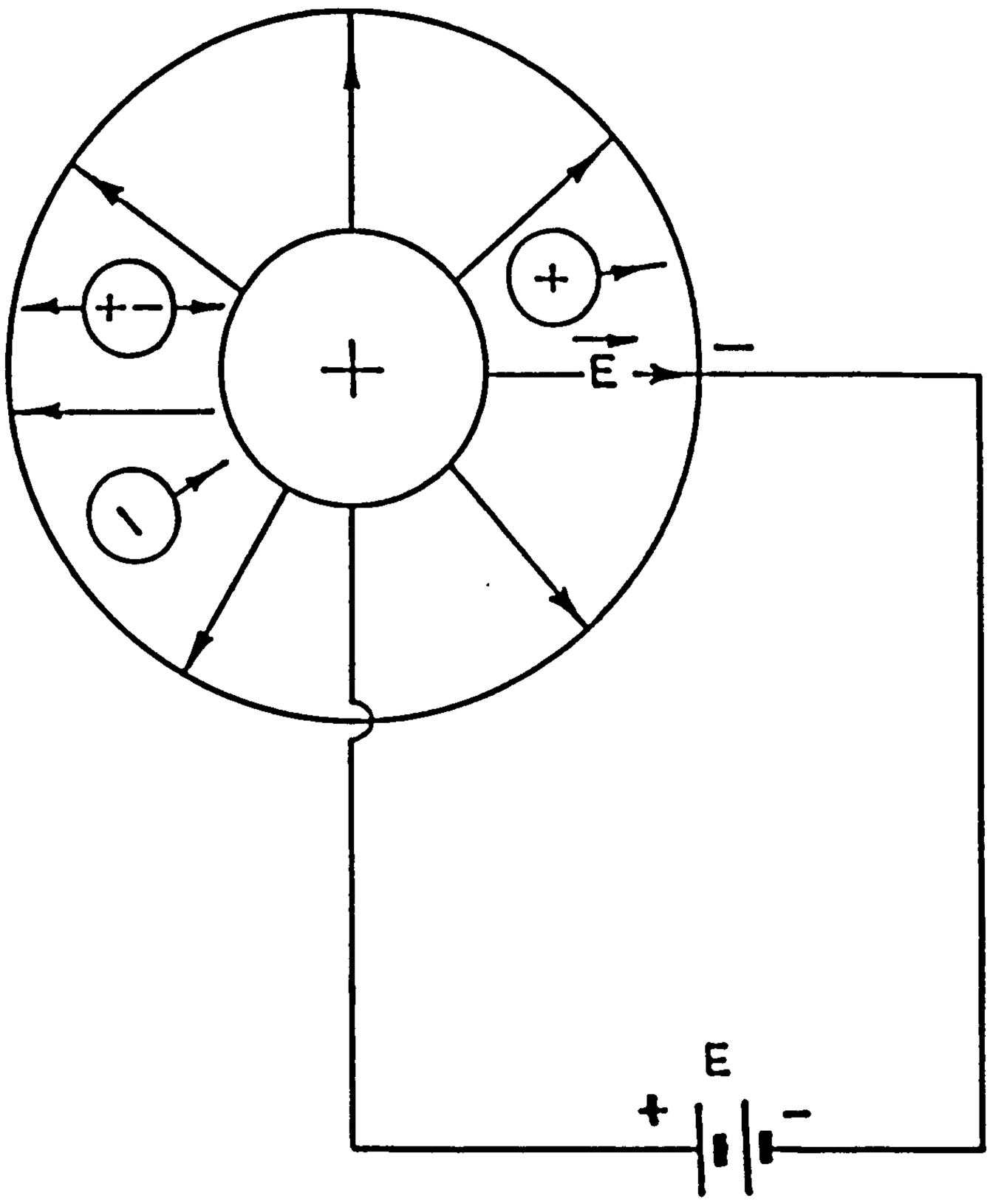

Fig. 2.2 Electrophoresis and dielectrophoresis

The charged particles obey the laws of electrostatics and move to the oppositely charged electrodes, the positive charge toward the outer wall and the negative charge toward the central sphere. The neutral particle is polarised by the field and its individual charges lie in a stronger field than the positive charges which experience a stronger force. The result is a net force on the particle in the direction of the central electrode. A change in polarity of the electrodes causes the charge particles to reverse their direction of motion. The neutral particle, however, continues to be pulled inward. An alternating electric field will cause the electrophoresis forces to average to zero, leaving only the dielectrophoresis effects. In dielectrophoretic studies it is, therefore, important to use alternating fields.

Dielectrophoresis deposits volumes of particles proportional to the applied voltage during equal times of deposition, provided a substantial difference exists in the relative permittivities of the particle and the surrounding medium [ie. $(K_2 - K_1) \gg 1$]. Electrophoresis can be appreciable even when the free charge per unit volume of the particle is quite small: it is unlike dielectrophoresis in that it does not depend upon the particle volume (and hence upon the total polarization available), but rather upon the free charge on the particle.

2.3 Pearl chain formation

The pearl chain formation arises in the following way. The particles which have a polarizibility greater than that of the surrounding medium, distort the field. Each particle then experiences a non-uniform field near the other. As each is already polarized by the external field, the particles are then attracted to the regions of

higher field intensity near each other, as shown in Figs. (2.3) and (2.4). The average length of the chains of cells collected after a specified time interval is reported as the "yield" or dielectrophoretic collection rate.

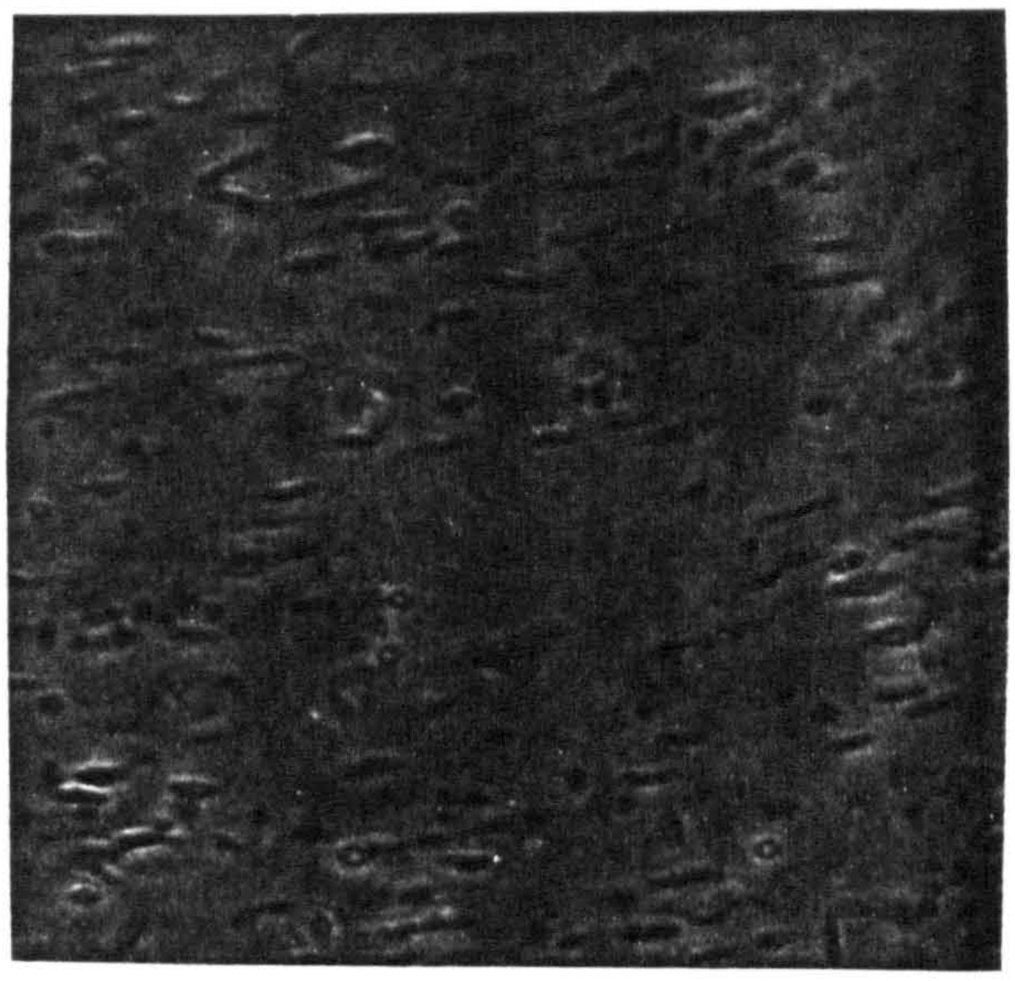

Fig. (2.3) Shows the action of a non-uniform electric field on L.major cells. The L.major parasites (neutral particle) have become polarized and the cells lie in alignment with the field lines produced by the electrodes (x 100).

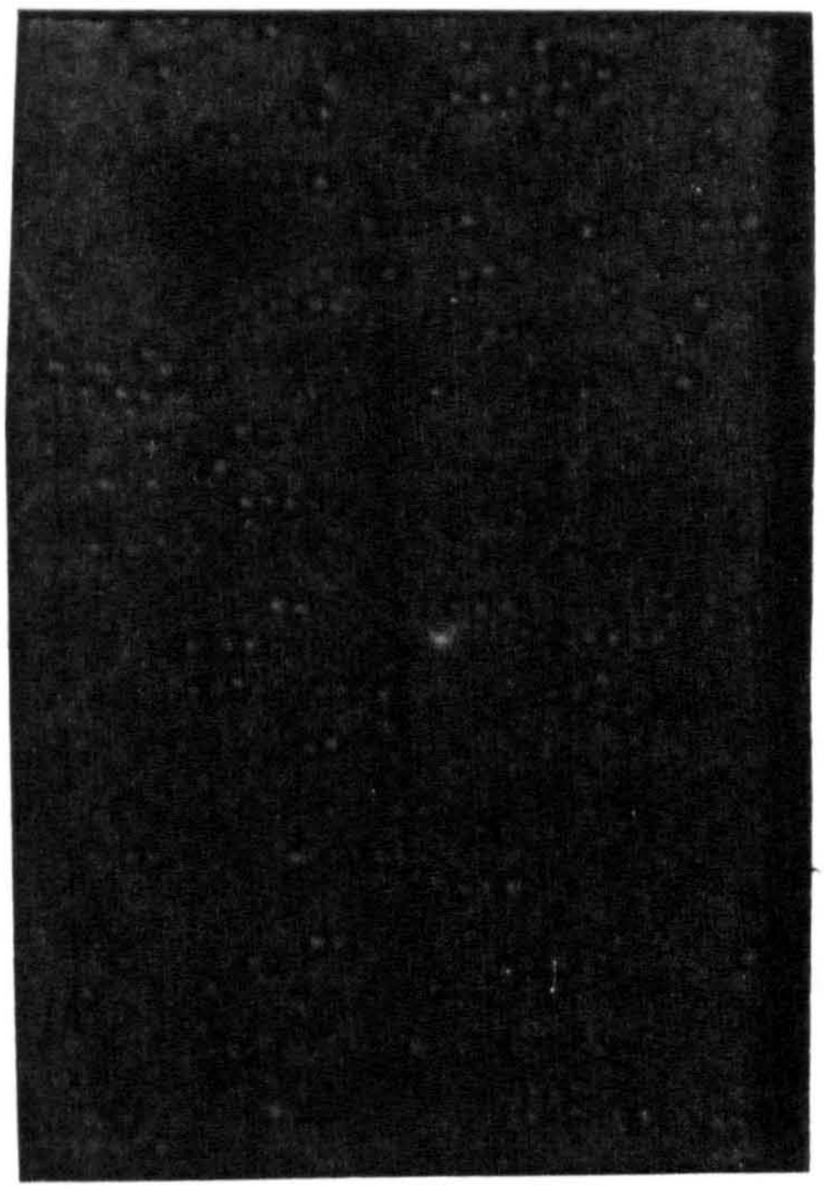

Fig. (2.4). This photograph shows how a net force (as a result of a non-uniform electric field on neutral particles) has acted upon the particles and has caused the pearl chain formation of yeast cells (S.C. x 100).

This rather unfortunate choice of terms is used, probably, to explain the fact that many biologists still do not know about the phenomenon of pearl chain formation in the presence of an alternating electric field. However, this technique has been used by a few investigators [2-5] in various laboratories for the separation and isolation of cells. The use of this procedure for cell separation presupposes that the cells differ considerably in their volume, since their dielectric properties and the frequency dependence of these properties for the same part of the cell division cycle are very similar. Such differences in volumes are rare in cell preparation of medical or biological interest, so that this technique will probably find only limited application to the detection of abnormalities in dielectric properties.

2.3.1 Theoretical aspects of yield

The dielectrophoresis force on a non-conducting sphere immersed in a non-conducting fluid and in a slightly non-uniform electric field has been shown [equation (2.7)] to be given by:

$$F = 2\pi a^3 \frac{K_1(K_2-K_1)}{(K_2+2K_1)} \nabla(E^2)$$

where a is the radius of the sphere, K1 and K2 are the permittivities of the fluid and the sphere respectively, and $\nabla(E^2)$ is the gradient that would be obtained at the location of particle if the particle were not there. It is convenient to combine the effect of the electrical characteristics of the materials into a single term and define the excess dielectric constant as

$$K_{clf} = \frac{K_1(K_2-K_1)}{K_2+2K_1} \qquad (2.8)$$

then

$$F = 2\pi a^3 K_{clf} \nabla(E^2) \qquad (2.9)$$

In the case of conducting media the effect is no longer given by equation (2.7) but it is possible to put all of the effects due to the materials into a single parameter and define an excess dielectric constant using equation (2.9). Since this excess dielectric constant will certainly not be a real constant for biological materials it is called the excess permittivity [1].

By specifying the electrode geometry, the resulting field and the corresponding force could be determined. The rate of the collection of a suspension of similar bodies can be found from the knowledge of the force on the body which results in the prediction of this motion. The force in a radial field can be derived following Pohl [7].

Mirrored symmetry exists between two rounded pin tips, and the electric field is essentially that between a round pin tip and a flat plate electrode. The field is approximately the same as that produced by concentric spherical electrodes near one of the spherical pin tips.

At some radius r the potential between two concentric spheres of radius r_1 and r_2 such that $r_1 \ll r_2$ is

$$V_o = \frac{V_1 r_1 (r_2 - r_1)}{(r_2 - r_1) r} \qquad (2.10)$$

where V_1 is the root-mean-square of the alternating potential of the inner spherical electrode, and $V_2 = 0$. Since

$$E_o = -\triangle V_o = \frac{V_1 r_1}{r^2} \left(\frac{r_2}{r_2 - r_1} \right) r_o \qquad (2.11)$$

$$(E_o)^2 = \frac{V_1^2 r_1^2 r_1^2}{r^4 (r_2 - r_1)^2} \qquad (2.12)$$

and

$$\triangle(E_o)^2 = -4\left[\frac{V_1 r_1 r_2}{r_2 - r_1}\right]\frac{2r_o}{r^3} \tag{2.13}$$

where r_o is the unit r-vector. From equation (2.9) the force on a spherical particle in this field is given by:

$$F = \frac{8\pi V_1^2 r_1^2 r_2^2 K_{mf} a^3}{r^3(r_2 - r_1)2}\, r_o \tag{2.14}$$

When p is positive and the negative sign indicates that the force is directed inwards towards the region of strongest field.

A spherical particle will experience a viscous drag force (Stokes' Law) opposing its motion when it moves under the action of the dielectrophoretic force equation (2.14).

$$F_d = -6\pi a \eta V \tag{2.15}$$

Where η and V are the viscosity of the suspended fluid and particle velocity through the medium respectively. Under dynamic equilibrium

$$F + F_d = 0 \tag{2.16}$$

By substituting equation (2.16) into equation (2.14) an equation for the velocity can be obtained.

$$V = -\frac{4}{3}\frac{V_1^2 r_1^2 r_1^2 K_{mf} a^2}{\sqrt{\eta}\, r^3(r_2 - r_1)^2}\, r_o \frac{dr}{dt}\, r_o \tag{2.17}$$

For a particle to travel from a radial distance r_o to the central

electrode the required time is given by:

$$t = \int_{o}^{t} dt = r_o \int_{r_o}^{r_1} \frac{dr}{V} \qquad (2.18)$$

From equation (2.17) into equation (2.18) and integrated gives:

$$t = \frac{\sqrt{(r_2-r_1)^2(r_o^6-r_1^6)}}{8a^2V_1^2r_1^2r_2^2K_{eff}} \qquad (2.19)$$

By taking $r_o \rangle 2r_1$ for most cases of interest, and then as $r_o^6 \rangle 64r_1^6$ equation (2.19) may be reduced to

$$t = \frac{\sqrt{(r_2-r_1)^2 ro^6}}{8a^2V_1^2r_1^2r_2^2K_{eff}} \qquad (2.20)$$

the particles collected, normally projecting outward from the inner electrode in the form of pearl chain formation and is approximately cylindrical in shape with an approximate volume V_c given as:

$$V_c = Yd\sigma = Y\, r_1^2\, d\theta \cdot d\theta \qquad (2.21)$$

Where y is the length of the chain (that is the yield) and do is the cross sectional area at which the point of attachment to the central electrode subtends a solid angle d0 generated at the centre of the electrode. If $r_o \rangle\rangle$ a, then the volume of suspension swept out to form the pearl chain during the time t is just the volume of a cone of solid angle $d\theta$ extending out to a distance of r_o. The volume V swept out in time is:

$$V_e = \frac{(r_o^3 - r_1^3)}{3} d\theta = \frac{r_o^3}{3} d\theta \quad (\text{for } r_1 \langle\langle r_o) \qquad (2.22)$$

The volume of particles contained in this cone is given by:

$$V_c = \frac{4\pi a^3}{3} \; C \; V_s \qquad (2.23)$$

Where C is the concntration of particles, by using equations (2.22) to (2.23) an equation for the yield can be obtained as

$$Y = \frac{4\pi a^3 C \; r_o^3}{9 r_1^2} \qquad (2.24)$$

r_o^3 can be obtained by solving equation (2.20) and then substituting in equation (2.24) gives

$$Y = \frac{8\pi C V_1 r_2 a^4}{9 r_1 (r_2 - r_1)} \left[\frac{2\zeta K_{eff}}{\sqrt{\quad}} \right]^{1/2} \qquad (2.25)$$

Application of equation (2.25) to a practical system (that is, to a real, but not on loss free dielectric) showed good agreement with the experiment in that there are linear responses of the yield with voltage over much of the range and the number of cells collected vary directly with the square root of the time. (Jaberansari [8]).

2.3.2 Mechanisms involved in the response of the living cells to non-uniform electric fields

The cells will be polarised by the application of an electric field. The resulting dipoles will be unequally acted upon in a non-uniform field and a net force will result.

For the cells to move to the region of highest field intensity, they must exhibit higher polarizability than the suspending medium, which is in this case aqueous. Water is a highly polar material and will itself be strongly pulled towards the region of the highest field intensity by the non-uniform field giving a pressure gradient. The cells, however,

can attain a higher polarizability in a number of ways. Firstly, the cell itself is largely water. Secondly, there are dissolved in the intra-cellular regions numerous polar molecules (proteins, DNA, RNA, etc.), all of which contribute to the polarization. Thirdly, there are structured regions which can act as capacitive regions, interfered, or interpoles. For example, there are the lipid membranes across which the electrolytes can act to produce observable charge distributions. Fourthly, there are structured areas at the cell surface where ionic double layers can produce quite enormous values of polarization ($k_{orr} > 10^6$).

However, when live cells are killed, their response to a non-uniform field is somewhat different. When our cells, both membrane and nucleus were damaged by prolonged (overnight) exposure to a TUV lamp (wavelength 254 nm); effectively, the cells were killed. The nucleus then appeared granular as observed under a phase contrast microscope; this exposure resulted in the cell being unable to reproduce. For these cells, dielectrophoresis does not reflect those polarization mechanisms which are sensitive to the physiological state as found with live cells.

2.4 Cellular rotation

Investigations into the behaviour of cells in high-frequency alternating electric fields frequently indicate that cells start to spin under defined conditions. Holzaptel et al [9] explains this phenomenon as resulting from the direct influence of the applied alternating field on the cells and, additionally, from interaction of dipoles generated in adjacent cells. Based on this theory, Arnold and Zimmerman [10] indicated that even single cells rotated if they were placed in a rotating high-frequency field. Therefore, a rotating

electric field was used to produce cellular rotation for the observations during this research programme. Such a field can be generated in a chamber consisting of three electrodes driven by sinusoidal voltage (Chapter (5)) with progressive 120° or four electrode with 90° phase shifts progressively between them.

In general, the rotational behaviour of biological particles can be interpreted as rotation of dielectric bodies in rotating electric fields. Particle rotation was found to be attributable to polarization phenomena resulting from charge separations on dielectric boundary layers. In Fig. (2.5) the principle of rotation is demonstrated on a homogenous sphere in an external medium (liquid).

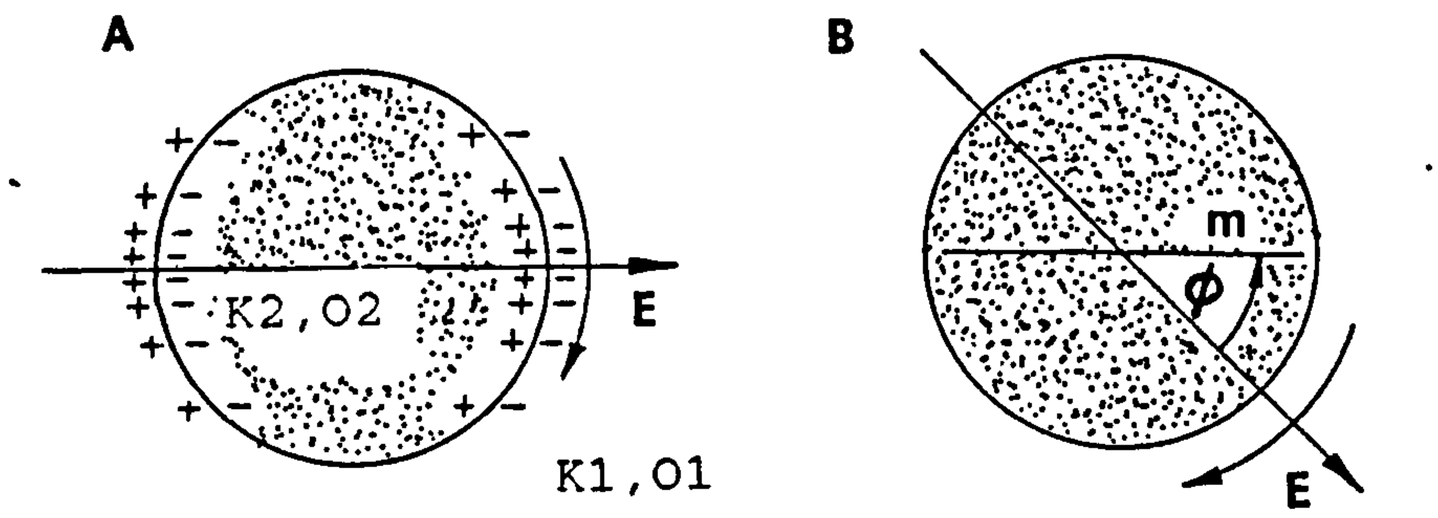

Fig. (2.5) Polarized dielectric sphere in an external medium K_1 K_2 - dielectric constants, O_1-O_2 - conductivities

Particle polarization can be described by the resulting electrical dipole (m). At low angular frequencies, the dipole (m) follows the field vector (E_o) without delay. Charge separation and charge dispersion, therefore, are much faster than the movement of the field vector. In other words, $w\tau \ll 1$ (where τ is the time constant of the

polarization process and w the angular frequency of the rotating field). With w increased, dipole orientation is slower and follows the field vector by a definite angle (ϕ) (Fig. (2.5)). In such cases the relaxation time of the polarization process close to the dielectric barriers cannot be neglected ($w\tau = 1$). A definite torque (N) will occur in this frequency range and lead to rotation of the particle. A maximum of angular velocity can be observed if $w\tau = 1$. Further increases in angular frequency are followed by drops in polarization, and at $w\tau \gg 1$ no torque acts at all.

Rotational behaviour is much more complicated when it comes to biological particles (yeast cells, Leishmania major cells). The principles and theoretical considerations of this phenomena are discussed by a number of researchers [11 & 12]. The origins of the observed cellular spin resonance are, as yet, not determined. There are, in theory, two distinct ways in which an applied rotating electric field could evoke cell spinning [13].

A - Cell-cell polarization

The theory given by Pohl [11] includes an expression for the spin rate, W_c, for a freely-spinning particle in a rotating electric field. But first, the following assumptions may be made for cellular spin resonance (CSR) of a spherical cell particle in a n electrode, n phase, voltage component rotating electric field generator.

Assumptions

1. A homogeneous dielectric sphere in a homogenous medium.

2. The rotating speed, W_c of cells is much less than that of the applied field, $W_E = 2\pi f = 2\pi/p$. (i.e. $W_c \ll W_E$).

3. The polarization of the sphere can be respented by a simple single time constant Debye type of relaxation time, τ.

4. The field is applied as a series of sine waves of magnitude E_o , each for a duration of θ sec., at intervals of s seconds during which the speed is ns=p sec., that is each phase begins 360°/n apart from the adjacent phase.

5. The cells rotate in near-equilibrium according to Stokes' Law for hydrodynamic drag.

With the above restrictions and assumptions,

$$W_c = \frac{3^{1/2} E_o K_{eff} E_o^2 (\tau/s)}{4\pi f (1-e^{-3\theta/\tau})} (1-e^{-\theta/\tau})3 \qquad (2.26)$$

Where $K_{eff} = Re\{K_1^*(K_2 - K_1)/K_2 + 2k_1\}$ and K_1^* is the complex conjugate of K_1.

τ is the relaxation time of the cell-water system.

E_o is the maximum field strength applied by each phase of the signal.

f is the duration of signal.

s is the time between the successive starts of the signals.

Spin rate

From the above equation the spin rate W_c, is proportional to E_o^2, τ, $1/f$, $1/\theta$, and to K_{eff}, the effective dielectric constant of the sphere, and is independent of the sphere radius.

B - Natural, intrinsic oscillating cellular dipoles

The interaction of such natural radio frequency dipolar fields with the external oscillating field is the most probable cause of CSR, but this needs further examination and study [14]. If the frequency of the applied rf field is f(E) and that of the natural cellular oscillating dipole field is f(D), then one can expect the frequency of the cellular rotation to be:

$$f(E) = f(D) \pm f(R) \qquad (2.27)$$

The present model is that the natural rf oscillating dipoles arise from oscillating chemical reactions coupling within the cells to physically mobile regions of ions so as to produce charge density waves. There are several well studied systems of oscillating reactions [15-17].

If, during the ionic phase, the outward speed of travel of the positive ions does not exactly match that of the negative ions, then a charge wave will develop (Fig.2.6). As these developing charge waves encounter structures within the cell that effect a parallelization of the wave development, collimation of the charge wave will ensue. The various charge waves travelling within these parallel regions will then develop a co-operative correlation [18] to form a coherent set of charge waves involving large regions of the cell as a co-operative oscillating giant dipole. The testable model suggests a number of experimental studies as to its energy source, its strength and cause. There are, of course, a number of structures known in cells which might be able to effect parallelization of such charge waves. These include the mitotic spindle apparatus, the walls of the endoplasmic reticulae

(ER), the grana of chloroplasts, and the laminae of the cristae in mitochondira. Oscillating systems in biology are well known. Excellent reviews of these are available [19].

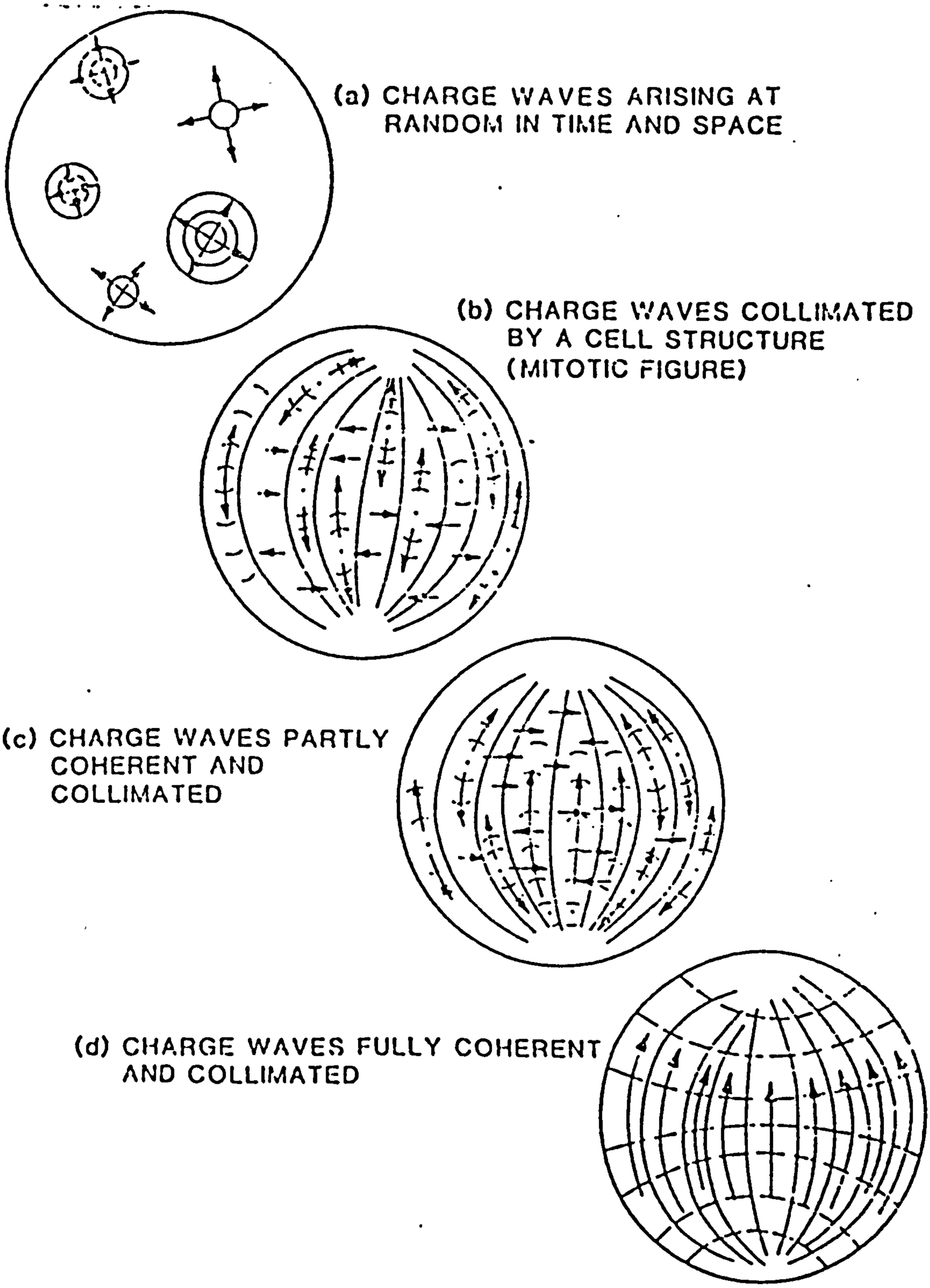

Fig. 2.6 A model for the production of natural rf electrical dipolar oscillations in cells.

(A) Charge waves from periodic reactions radiate out from various initiating sites in the cell. As shown, the waves from various sites are incoherent and uncollimated.

(B) If various possible structures are present in the cell, the individual charge waves can become collimated and parallelized. Although longitudinal waves are shown for ease of the graphic, presentation waves progressing at right angles to the intracellular surfaces are probably the more likely. As parallelizing structures one may have various cytoskeletal elements such as endoplasmic reticulum (ER) microtubules, actin microfilaments, various trabeculae, and membranes as in chloroplast granae and mitochondrial cristae. (28)

(C) Collimation and partial coherence of charge waves, providing an oscillating dipole.

(D) Charge waves collimated and almost completely coherent. It is expected that the resultant dipole oscillator will be evident outside the cell only when the charge waves are very close to the outer plasmalemma, because of the short range of electric fields in the conductive plasma of the cell interior.

Whether the proposed charge waves providing the source of the natural rf oscillations are due to reactions which proceed geometrically parallel to or at right angles to the laminar cell structures is not known, although kinetic data on the assumed charge waves imply that the charge waves proceed across, rather than along, the laminar regions, especially in the case of the high frequency oscillations. The study of oscillating reactions is in an increasingly active state. An interesting paper by Schmidt and Ortoleva [20] suggests how oscillating reactions might be coupled to waves of electrical charge.

Frohlich [21] showed that an assembly of randomly oscillating, but lightly coupled, similar dipoles would be driven to operate in a co-operatively condensed mode if the input power (chemical, electrical or mechanical) exceeded a certain minimum level. This, and a series of stimulating subsequent papers, opened a new avenue of cellular studies [10, 12, 13].

Whatever model is eventually found to be correct for the origins of the observed natural rf oscillations of cells, it will be of much interest to learn if they are cause or effect, necessity or frill in the living state.

We must conclude from this observation described in Chapter (8) that the CSR is due to natural rf oscillations as modified by the polarizability of the cell and medium, and acting in response to the applied field. This is a somewhat complex physical problem and needs quantitative treatment and resolution.

2.4.1 AC and DC Responses

If natural and internally driven dipoles are present, they can be expected to evoke a torque and a spinning of the cells if (Pohl [22]) the dipolar frequency, f_D , matches that of the external field, f_E , as seen during the cellular spinning at frequency f_R, i.e., Eq. (2.27) applies.

Thus, the frequency f_D will be slightly modifiable by the presence of the external field at f_E, ("motor-boating") and by the presence of its internal polarization $\propto (E, f_D)$. Such a response of a natural oscillating dipole, expressed in terms of the internal polarization of

the cell, can be expected to result in spinning whether the applied field sinusoidal (AC) or pulsed DC (rectified sinusoidal) of the same basal frequency. It is expected then to vary with the square of the applied field intensity.

On the other hand, if the cell subjected to an external field has no natural oscillating dipole, but has only that dipole induced by the presence of an external field, then such a cell would only librate but not spin synchronously. If a cell spins while in the presence of a high frequency AC field, and continues to spin when this field is smoothly altered to that of a pulsed DC field of the same frequency, we may be assured that it has a natural rf dipole. If, on the other hand, it does not spin but only librates in the pulsed DC field, then induced and not natural rf dipoles are indicated present.

It is interesting to note that rotation of deoxygenated sickled erythocytes in a rotating magnetic field was recently reported by Riberia et al [23]. The speed rotation was proportional to the square of magnetic field strength. In recent years the orientation of cells, organelles and tissues in a homogenous magnetic field has been reported on. For sickled erythrocytes, self-orientation is perpendicular to the magnetic field [24-27].

Smith, Aarholt and Jaffary [28] have also reported the effect of magnetic fields on several biological cells. They reported the existence of a proton NMR effect involving the geomagnetic field when they were examining the behaviour of cells under the influence of dielectrophoretic forces. However, the already reported effects of electric and magnetic fields on living cells were sufficient to merit

further investigations into this area of research.

2.4.2 Advantages and future application

Investigations on the behaviour of cells in high frequency alternating electric fields frequently find cells starting to spin under defined conditions, this has become known as "Electrotation". Electrotation is a new method and its application to various problems depends on its future technical development.

At present, the method of electrotation as observed under a microscope has been considered a useful tool for certain purposes of analysis. In particular, it permits a non-destructive analysis of selected single cells. A considerable advantage for many problems of cell biology and biotechnology. Biophysical properties of the membrane of cells such as their conductance, and the specific capacitance and the conductance of the cell plasma can be measured by this method [11, 13]. It allows a time saving selection for locating single cells in a contactless and non-destructive manner. For medical purposes the examination of single cells in cell suspensions is possible. This method may also be extended to computer-aided data recording and processing systems with special interfaces for electronic field generation and control devices, and special variable measuring chambers.

Electrorotation can further be applied for studying

(a) characterisation and the study of the influence of drugs and other agents on cells (in particular of such drugs as affect membrane permeability, e.g. diuretics, ionophores);

(b) characterisation of cells before and after artificially induced

fusion (intactness of membrane, detection of successful fusion);

(c) differentiation and classification of cells (e.g. vitality test);

(d) interaction of cells with artificial surfaces; (eg. Leishmania cells)

(e) separation of cells under special conditions

REFERENCES

1) PETHIG, R. "Dielectric and Electric Properties of Biological Materials", Wiley, Chichester, 1979.

2) WREDE, E. Z.Physik, 1927, 44, p.261.

3) MULLER, F., WISE, H. Veroffentl Siemens Worken, 1938, 17, 20.

4) ZIMMERMAN, U. "Electric Field Mediated Fusion and Related Electrical Phenomena", Biochemica. Biophys., 1982A, 694, p.227.

5) POHL, H.A. Dielectrophoresis, Cambridge University Press, Cambridge, 1978.

6) MÜLLER,F., AND WISE,H.,Verffentl, Siemens Werken,1986,17,p.2[illegible].

7) POHL, H.A. J. Theor. Biol., 1981A, 93, p.207.

8) JABERANSARI, M. Dielectrophoresis, Electrodynamics and Magnetic Resonance Phenomena in Yeast Cells, M.Sc. Thesis, Salford University, 1985.

9) HOLZAPFEL, C., VIENKEN, J., and ZIMMERMAN, U. "Rotation of Cells in An Alternating Electric Field", J. Membrane Biol., 1982, 67, p.13.

10) ARNOLD, W.M., WENDT, B., ZIMMERMAN, U. and KORENSTEIN, R. Biochem. Biophys. Acta, 1985, 813 (Act A), p.117.

11) POHL, H.A. "A New Method for Determining the Dielectric Properties of Living Cells", Int. Journal of Quantum Chemistry, 1983, 10, p.161.

12) HAAGEDORN, R., FUHR, G. "Calculation of Rotation of Biological Objects in the Electric Rotating Field", Studia Biophysica, 1984, 102(3), p.229.

13) GLASER, R., FUHR, G. "Electrorotation of Single Cells - A New Method for Assessment of Membrane Properties". Electrical Double Layers in Biology (Martin Blank eds.), Plenum Press, New York & London, 1986.

14) POHL, H.A. J. Biological Physics, 1983, 11, p.59.

15) NOYES, R.M. and FIELD, R.J. Ann. Rev. Phys. Chem., 1974, 25, p.95.

16) NOYES, R.M. Acc. Chem. Res., 1977, 10, p.214.

17) EPSTEIN, I.R., KUSTIN, K., DE KEEPER, P. and ORBAN, M. J.Am. Chem. Soc., 1981, 103, p.2133.

18) POHL, H.A. and CRANE, J.S. Biophysical Journal, 1971, 11, p.725.

19) TREHERNE, J.E., FOSTER, W.A., SCHOFIELD, P.K. "Cellular Oscillators", J. Exp. Biol. (Review Volume), 1979, 81.

20) SCHMIDT, S., ORTOLEVA, P. J. Chem. Phys., 1979, 71, p.1010.

21) FRÖHLICH, H. IEEE Trans. Microwave Theory Techniques, 1978, MTT-26, 613.

22) POHL, H.A. "Microdielectrophoresis of Living Cells" in Bioelectrochemistry (H. Keyzer and F Gutmann, eds.), Plenum Press, NY, 1980B.

23) RIBEIRO, P.C., DAVIDORICH, M.A., WAJNBERG, E., BERNSKI, G. and KISCHINEVSKY, M. Biophys. J., 1981, 36, p.443.

24) ARNOLD, W., STEELE, R. and MULLER, H. Proc. Nat. Acad. Sci., U.S.A., 1958, 44, p.1.

25) MURAYAMA, M. Nature, 1965, 206, p.420.

26) GEACINTOV, N.E., VAN NOSTRAND, F., BECKER, J.F. and TINKER, J.B. Biochem. Biophys., 1972A, 267, 65.

27) BERCKERS, J.F., GEACINTOV, N.E. and SWENBERG, C.E. Biochem. Biophys., 1978A, 503, 545.

28) AARHOLT, E., FLINN, E.A. and SMITH, C.W. Phys. Med. Biol., 1981, 26, p.613.

CHAPTER (3)

ELECTRON & ION BEAM CHARGING OF SURFACES

3.1 INTRODUCTION

This chapter will review theoretical aspects of electron bombardment processes and mechanisms and their relationship to X-ray production and shielding, secondary electrons, electron backscattering, electron range and the charge and dose effects. This is because Leishmania major cells tend to attach only to electron beam scored substrates.

Following this theoretical work on electron beam injection there are some basic results for ion implantation using isotope separators, Van de Graaff and D.C. plasma ion sources.

Finally, the theories presented in this chapter are very preliminary in nature.

3.2 The Electronic Beam as a Technological Process

Any electron bombardment (EB) processing technique utilising electron beams requires that in the work chamber the electron beam, as the energy carrier, be adequately matched to the properties of the target material so as to act in the most appropriate manner. Electron beam generation takes place in an electron gun which is described in Chapter (6). Such a gun is based on the thermionic emission of free electrons into a vacuum, followed by the acceleration and beam formation in electrostatic fields, and thus beam focussing and deflection through either magnetic or electric fields. The electron beam is guided into the work chamber through an aperture in the (high energy) electron gun chamber. The parts, or products, to be processed, which generally have to be moved in some appropriate manner, were arranged at the work site.

Since the general and unrestricted propogation of an electron beam is

only possible in a high vacuum, it is necessary to pump down the beam-generating and guidance spaces. In general, and this is also the case for the work chamber (Chapter (7)), vacuum systems are therefore among the most important components of an EB processing plant. The vacuum required in the beam-generating chamber of a gun is usually of the order of 10^{-2}-10^{-4} Pa, and that in the work chamber is generally around 10^{-2} Pa.

There were no gas-type pressures used in the chamber for electron bombardment of the target material and accelerating voltage, and beam current and exposure time are the principal parameters that determine the interaction between beam electrons and target material from the point of emission to the electron bombardment site.

When the beam impinges on the matter to be bombarded, the kinetic energy of the electrons is converted into various kinds of energy through interaction with the atoms of the target material.

In general, electron beams have many technological applications. For example, when the beam is utilised for melting, welding, evaporation, or thermal processing, it is the produced thermal energy that is used. With non-thermal processing and other radiation processes the collisions of the beam electrons excite or ionize the electron shells of the atoms and molecules, which as a follow-up process, initiates chemical reactions. Sterilization through electron beams is based on similar processes so that, as a result, biological systems are killed. Other actions of electron beams during impingement on matter are beyond the scope of this thesis.

3.2.1 Energy Conversion at the point of action

When an acceleration voltage Va is applied, electrons are accelerated in the electrostatic field of the beam source so that they attain a kinetic energy E, where kinetic energy E = e x Va and e is the electron charge. The accelerating voltages used in this project are in the range 500-20 x 10^{-3} volts. In this sort of energy range, the electron velocities are:

$$V_e = \sqrt{\frac{2E}{m}} \qquad (3.1)$$

where Ve is the electron velocity

m is the mass of an electron

E is the kinetic energy of electron

For the above energy range, the electron velocities are 0.04 - 0.3 of the velocity of light.

At the point of beam impact interactions with the atoms of the electron bombarded matter convert the kinetic energy of the electron beams into either heat or atomic or molecular excitation energy. A certain portion of the incident electrons will be back-scattered. In addition, secondary processes produce X-rays, secondary electrons, and possibly, thermionic electron emission at the point of beam incident. The generated heat results in a small rise in temperature at the work site (this is greater at higher electron energies), limited by heat conduction from the zone of energy conversion, to the environment. (Fig. (3.1))

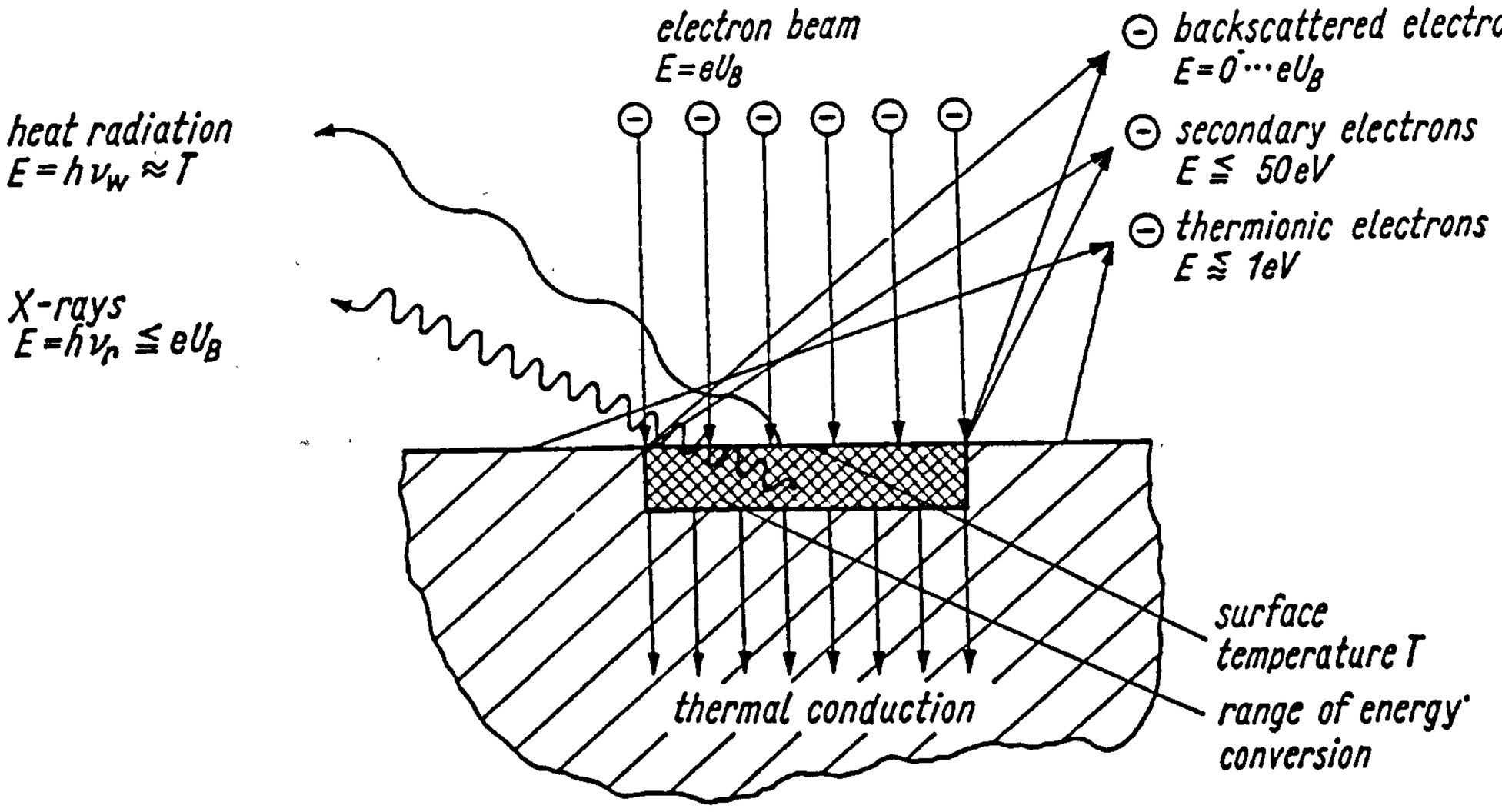

Figure (3.1) Beam action upon impingement on matter

3.2.2 X-ray Production and Shielding

As with other particle or wave radiations, X-radiation is biologically active and, if a particular intensity is exceeded, represents a health hazard. Because its occurence is inevitably linked to all EB processing techniques, suitable shielding is required for protection in the immediate vicinity of electron beam bombardment. Energy losses on the work site caused by x-radiation are of the order of 1% less [1]: they depend on the energy of the beam electrons and on the atomic number of the matter bombardment by the beam. The portion of the beam energy

converted into X-radiation is [1]

$$\eta_r \approx 10^{-9} V_a z \qquad (3.2)$$

where Va is expessed in volts.

In low energy ranges the resultant energy in the total X-ray emission can be neglected, but this emission cannot be neglected when working in high energy ranges. Because the penetrability of X-rays increases with quantum energy, and hence with the irradiant electron beam energy, shielding measures are determined mainly by the maximum accelerating voltages to be used in a particular EB bombardment application.

3.2.3 Thermionic Emission and Emission of Secondary electrons and electron back-scattering

The emission of secondary electrons at the point of beam action takes place with an energy lower than 50 eV. Being proportional to the impinging beam current, the emitted flow of secondary electrons depends on the target material - in particular, its surface as well as the angle of the incident beam and the electron energy.

With the commonly-used operating regime in zero-field space, the emission of secondary and thermal electrons is limited to low values because of space-charge formation. This is why their emission is practically meaningless as far as the energy balance of the EB bombardment is concerned. Their total dissipation amounts to about 1/1000 beam power.

Electron back-scattering causes emission of electrons within the range

of beam action, the X-ray energy spectrum of which goes up to the energy of the beam electrons is most intense at about 1/3 of this. Above all, the portion of back-scattered beam electrons and their energy spectrum and direction distribution are determined by the atomic number Z of the target material as well as by the angle of incidence, contrast to thermionic emission, it is independent of temperature. Obviously the lower the atomic number the lower back-scattering, but back-scattering increases with the angle between the direction of beam incidence and the normal to the surface. Because of energy loss, the emission of back-scattered electrons has a negative effect on the surface electron charge in electron bombardment processes.

3.2.4 Electron Range

The electrons in the beam impinging on the target material (polystyrene) are subjected to elastic and inelastic collisions with atoms or molecules upon matter penetration. The beam electron transfers energy to the particle struck and thereby departs from its initial trajectory. Since the mass of an electron is small (1/2000) compared to that of atoms or molecules, the striking electron loses only a very small fraction of its energy during each collision (about 30eV). Hence, a great many collisions are needed for the electron beam to give all its energy to the polystyrene petri dish.

The distance from a perpendicular target surface, within which the electrons give off practically all their energy, is called the electron range S. It is solely determined by the electron energy and the polystyrene density (ρ). Because the impact probability depends on the electron energy, there are diverse analytical relationships for the various energy ranges [2]. For energies up to 100 keV

$$S \simeq 2.1 \times 10^{-12} \frac{Va^2}{\rho} \qquad (3.3)$$

where S (cm) is the electron range in the polystyrene and Va (volts) is the acceleration voltage traversed by the beam electrons and ρ ($g.cm^{-3}$) is the density of polystyrene.

For an electron beam of energy Va = 20 kV onto polystyrene, this yields an electron penetration depth of 8μm (polystyrene ρ = 1.05 gm^{-3}). Hence the beam energy is converted within this very thin surface layer and the electrons are trapped in the polystyrene [3] because of its very low conductivity.

3.2.5 Charge and Dose Effect

There are a few recently published papers, for example those by Watson [4] on the transport of electrons in polystyrene, which observe that the surface potential of polystyrene will be changed as the electrons get trapped within the polystyrene. The decay is characterised by an initial discharge; the rate of decay then decreases with time and ceases after a while, leaving a high negative residual voltage on the sample which can only be erased by heating.

The initial discharge suggests that when the electrons are first injected into the polymer they are able to move relatively freely before becoming deeply trapped. If this is correct, then for a short time after bombardment the electrons will be drifting in their own space charge field and the decay should be space-charge limited, although modified by the presence of traps in the polymer. The dose (D_-) of electron bombardment of any sample is directly proportional to

the total charge or the integral of the electron beam current. It is also inversely proportional to the area which the electron beam is bombarding the surface of the sample. The electron beam current can be increased or decreased by modifying the electron gun accelerating voltage (Va).

When an electron beam, with beam current (Ib), acts on a surface of an electrically insulating body, the electrical charge transferred (Q) in a time t becomes

$$\dot{Q}_T = I_b \times t \qquad (3.4)$$

The electron beam transfers the electron to the insulating polystyrene surface with an area A. These electrons will be trapped in the polystyrene. To express the desired dose required for bombardment of the specimen, one may say

$$D_e = \frac{Ibx\ t\ x\ Ne}{A} \qquad (3.5)$$

where De is the desired dose of electron beam
A is the area of the surface cm sq.
Ne is the number of electrons per column
and t is the electron bombardment exposure time (S)

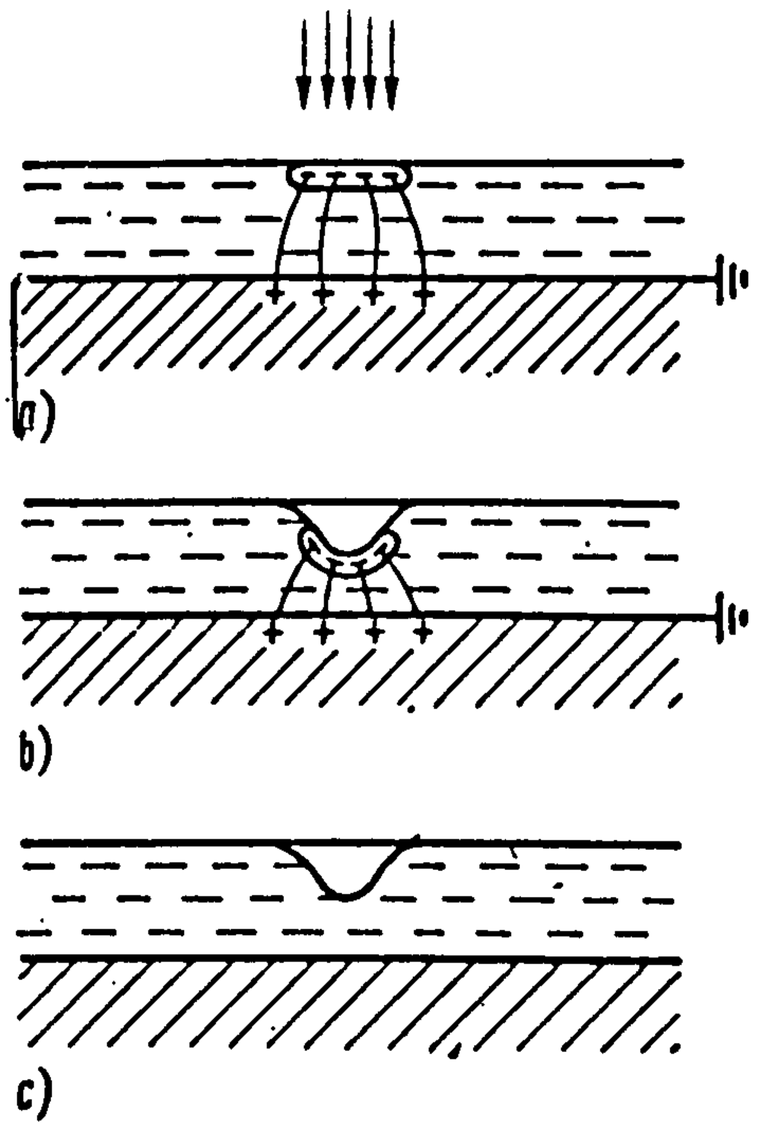

Fig. (3.2)
Surface deformation of an electrically insulating thermoplastic layer on an electrically conductive substrate caused by the action of electrostatic forces: (a) charge transfer by the electron beam, electrical influence of a charge of opposite polarity in the grounded substrate; (b) surface deformation due to the action of electrostatic forces, with the film heated to its softening temperature; (c) frozen surface deformation after the charge has been drained.

3.3 Isotope Separator

All heavy ion implants (to polystyrene petri dishes) performed in the course of this work were carried out using the Harwell Mk. 4 isotope separator at Salford University. This machine is best described in terms of its consisting of a number of distinct units. All the units are kept evacuated to a basic pressure $<10^{-6}$ torr using "diffstak"/rotary pumping systems.

3.3.1 Basic Data

3.3.1.1 Ion Source

The ion source, which "floats" at the required accelerating potential is known as a Freeman source it comprises:

(a) A carbon arc chamber in which lies a filament run at ~100-140 A. (4V). Between the filament and the arc chamber (electrically isolated) there is a 100V potential which will initiate a discharge if any gas (usually inert) is introduced to the arc chamber.

(b) Acceleration - up to 40 keV.is achieved within the source, and the arc and filament supplies from isolated transformers) and the input gas feed line are isolated from the earthed frame of the source by large insulators.

(c) Many solid compounds may be run in the source by loading them into a small carbon crucible which is moved into the source chamber temperature gradient by external movement of a steel rod (lear loader) connected to the crucible with an alumina rod as insulator. Corrosive vapours may also be run through the gas line and externally controlled by a low flow-rate leak valve.

3.3.1.2 H.T. Supply

(a) This is variable from 0-40kV and stabilised to 1 in 10^4.

(b) It is modulated by a sinusoidal voltage variable between 0-7 kV peak-peak in order to provide horizontal sweeping of the extracted ion beams.

Ions from the arc chamber are therefore velocity modulated until they reach the analysing magnet from where, according to momentum analysis, they emerge as convergent wedge-shaped beams, sweeping sinusoidally with time (50 c.p.s.) horizontally across the target area.

3.3.1.3 Analysing Magnet

The magnet is of a standard 'C' shape design with water cooled coils and provides a magnetic field variable between 0-11 kilogauss. It has a nominal radius (for central beams) of 40 cm and a deflection angle of 60 degrees. To facilitate the focussing of the incident divergent wedge-shaped beams (4 cm high), the pole tips are semi-circular shaped and rotatable (+ 25 deg.). Because of the vertical focussing action of the magnet (or defocussing due to fringe field), the incident beams are either vertically focussed or defocussed. Focussing occurs if the pole tips are turned inward from their neutral 60 deg. position and vice-versa for outward movement. Primarily, the pole tips are used to focus the vertical line beam; inward movement brings this focus point nearer to the exit pole face and vice-versa.

3.3.1.4 Target Chamber

The target chamber is a hollow steel cube in which there is a mounting for sample plates (2" x 2") which may be cooled or heated. In order to establish the desired beam parameters a dummy target may be swung in front of the real target mounting. The schematic of this system is shown in Fig.(3.3). For setting up the desired elemental ion beam is scanned across the slits in the dummy target plate and the transmitted pulses of ion current are collected on Plate A, connected to an oscilloscope Y amplifier. The X deflection is driven in-phase with the source modulation voltage - so the oscilloscope displays the horizontal intensity distribution of the scanning beams. Focus is

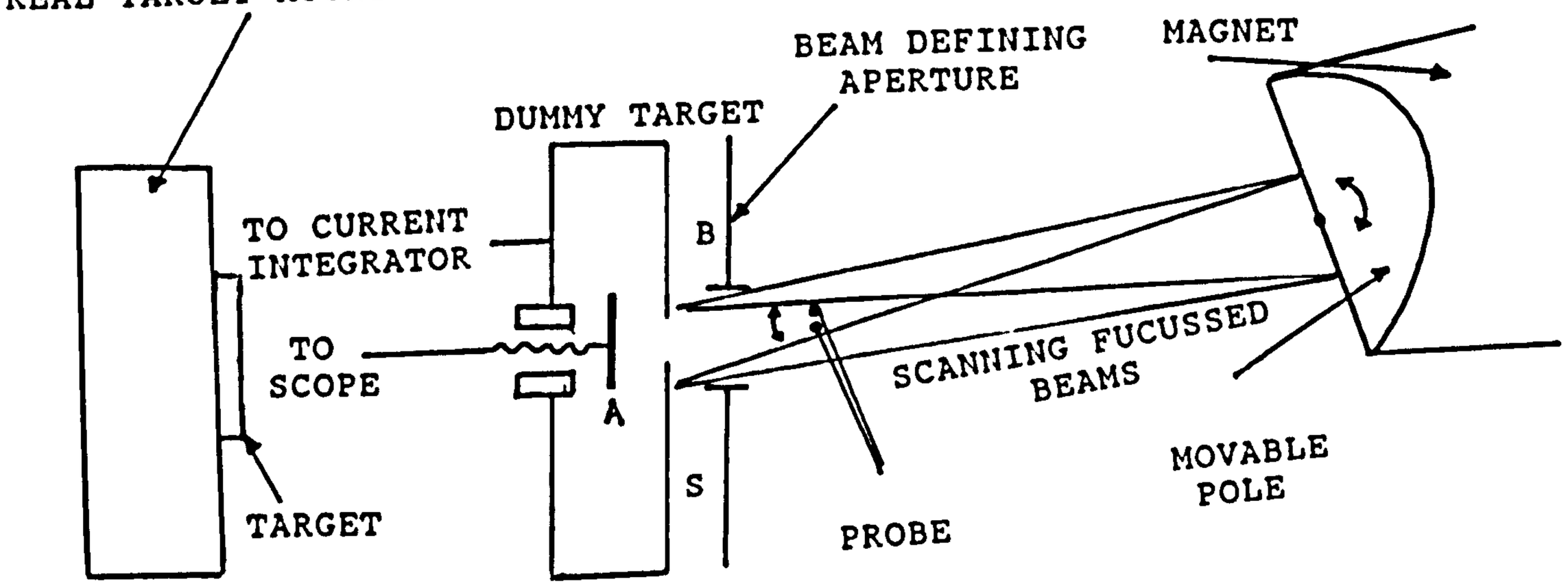

Fig. 3.3 Schematic diagram of a target chamber

obtained by movement of both pole tips to achieve the sharpest possible line focus as seen on the scope. Thus, beams are easily identified by comparison of scope trace with a chart of isotope natural abundance. The vast majority of the beam current is collected on Plate B however, and this is fed to the current integrator. Without going into precise

detail, the integrator incorporates two range switching devices - one a current range switch, the other a voltage range switch. When all the necessary parameters had been calculated, the defining apertures were manufactured to a range of different sizes and ascribed a number (1-4). The apertures are square with areas of 2.08-8.32 cm sq.; to achieve a desired dose D (ions/cm sq.) the counter on the integrator is set to a number of counts given by

$$\text{counts} = \frac{D \times (\text{Aperture number})}{10^{18} \times (\text{Voltage range}) \times (\text{Current range})} \qquad (3.6)$$

The integrator count rate may be switched to an order above or below the rate normally used (as in formula above). The normal count rate used is 3 counts per full scale second of the current meter.

3.3.2 General Data

To get horizontal uniformity of implant the beam must be swept over the largest area possible without bringing unwanted beams near the aperture. If high intensity unwanted beams (as shown on 'scope) are close to desired beams, then a small aperture must be used with a corresponding reduced beam sweep.

As arranged for most studies, the effective optical source of ions is at the line of the filament which ~76 cm from the magnet entry pole. The target plane is at ~70 cm from its exit pole.

As shown in the accompanying drawings (Fig. (3.4)), the focal plane is not normal to the line of beam exit from the magnet.

One-to-one scaling of the scope separation distances with the real

isotope separation at the plane of the target is obtained by inserting two probes into the lower extremity of the beams just before the aperture (Fig. (3.4). These are set 2 cm apart, therefore, by adjusting the 'scope display X gain until the signals from each probe are 2 cm apart, the display then shows the real physical separation of isotopes at the target place. In the normal mode of operation, the separation of masses M & M + ΔM is independent of beam energy and is approximately given by:

$$\text{separation} \simeq 40 \frac{\delta M}{M} \text{ CMS}$$

The machine must not be run if base pressures are $>10^{-6}$ torr. To get stable arcs, the pressure in the source chamber (<u>not</u> the arc chamber) must be $\sim 10^{-4}$ torr. Since the entire flight tube is $\simeq$14 cm wide and 6 cm high to allow transit of the beams, differential pumping to a high degree is not possible. However, target pressures should still not exceed $\simeq 5 \times 10^{-6}$ torr.

Targets are loaded onto the mounting through an air lock which is taken down to roughing pressure ($\sim 5 \times 10^{-2}$ torr) before opening the side loader gate valve.

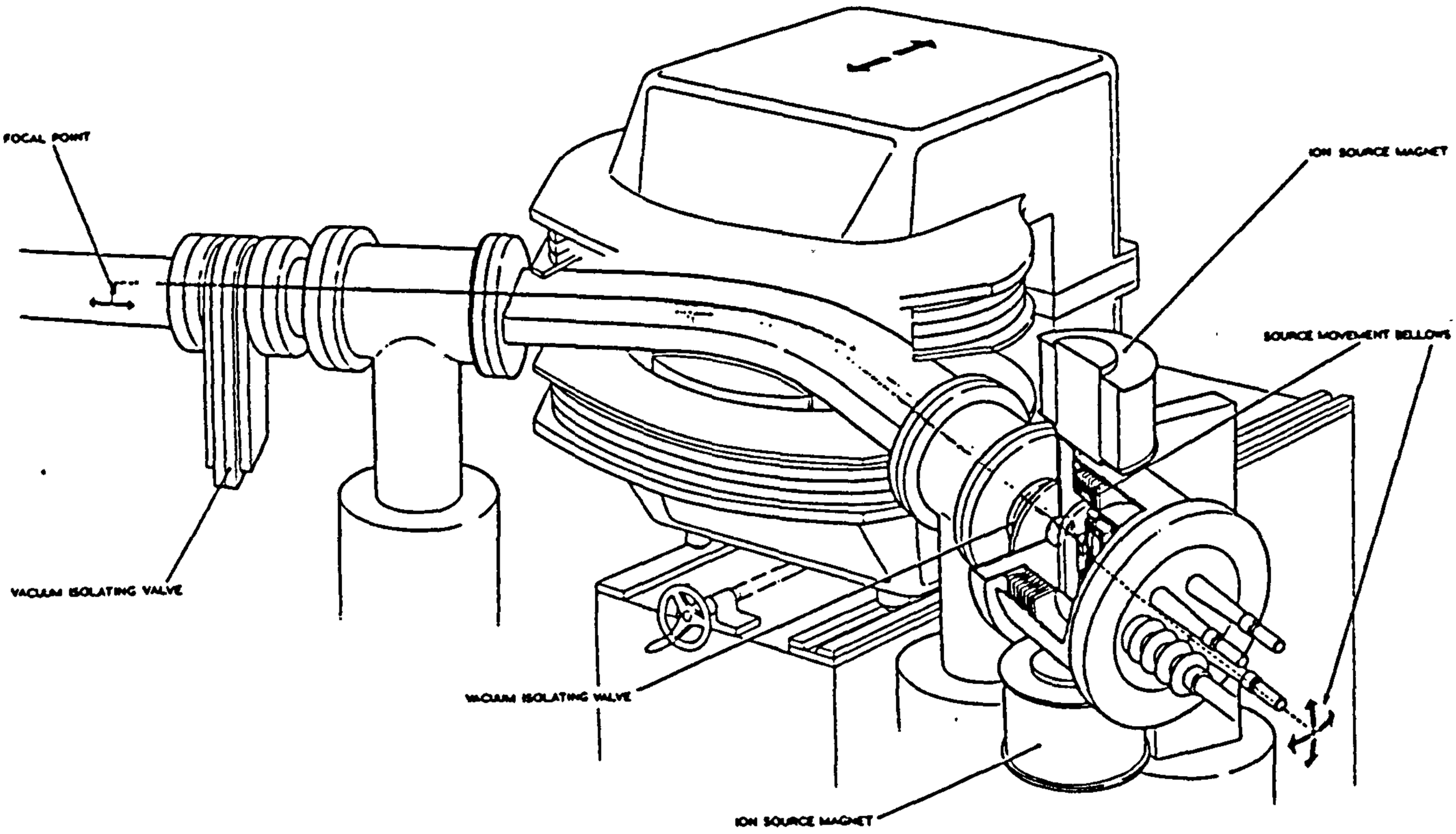

Fig. (3.4A) Central diagram of an isotope separator.

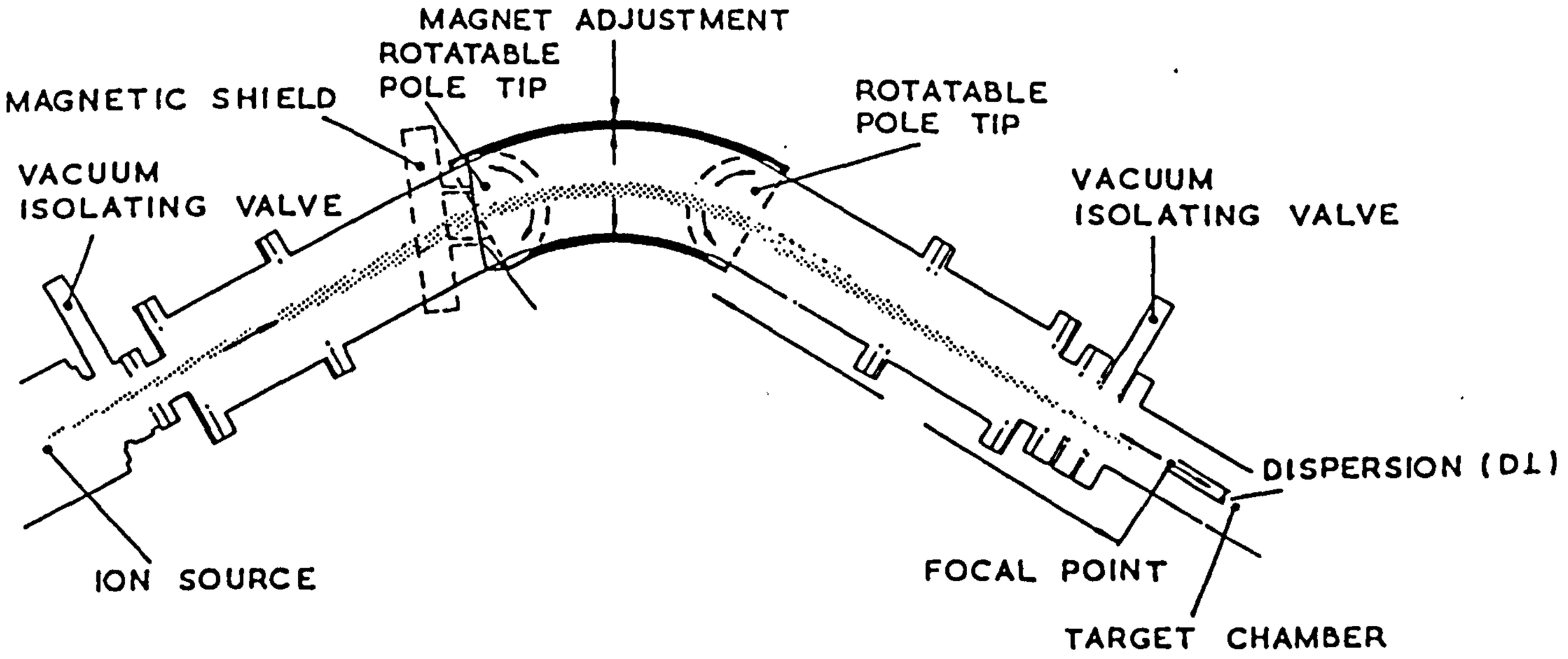

Fig. (3.4B) Schematic diagram of the I0n beam flight path

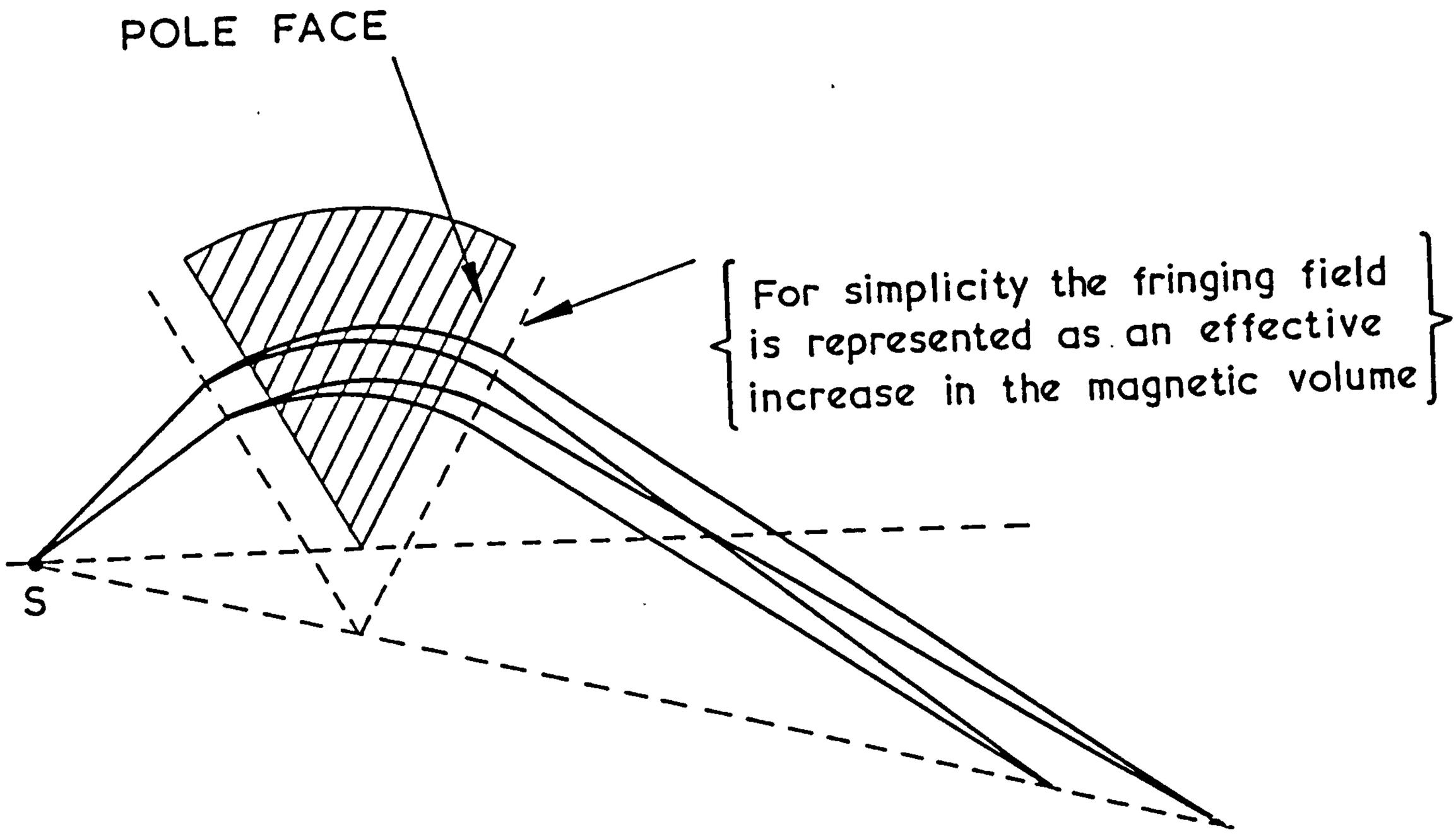

Fig. (3.5) Effective field boundary

3.3.2.1 Special notes

This type of ion source produces moderate quantities of multiply charged ion beams, so that doubly charged ion beams at up to 80 kev, (or triply charged to 120 keV) can normally be detected. Also, charge exchange taking place in the space between the ion source and the magnet has a reasonably high cross section.

Let m = isotope mass, V = accelerating potential
R = beam radius (normal) H = magnet field strength
V = particle velocity A.1 = charge on Accelerated ion
D.e = charge on Deflected ion

For acceleration $1/2\ mV^2 = AeV$ (3.7)

and for deflection $\frac{mV^2}{R} = H.D_{\blacksquare}\ v$ (3.8)

The effect of multiply charged extracted ions coupled with the

possibility of charge exchange ($A \neq D$) means that all beams appear at an apparent mass (based on A = D = 1) of $\frac{mA}{D^2}$

Examples for no charge exchange, A = D

therefore, singly charged ions appear at mass

doubly " " " " "

triply " " " " "

If a doubly charged extracted ion becomes singly charged,

Apparent mass = $\frac{m}{1}$ = 2m

NOTE! An ion energy is not altered by charge exchange and is equal to A x (accelerating voltage).

There is always the danger of confusion if predominently mono-isotopic molecular beams are interpreted as mono-atomic ones which have undergone a particular charge exchange.

EXAMPLE N_2 will appear at mass 28

but so will N++ reduced to N+ by charge exchange, therefore, within the one peak these will be:

(a) N^{2+} at V (KeV)

(b) N^+ (Reduced by $N^{++} \rightarrow N^+$) At 2V (KeV)

in calculating counts for a particular dose, the count number should be multiplied by the charge state at detection. Therefore, in the above

example, if the peak at mass 28 was assumed to be:

(a) N_2 singly charged at V and run to dose D

It could also be

(b) N^+ From ($N^{++} \rightarrow N^+$) At 2 V run to a dose D/2

However, generally, molecular species dissociate at the target into single atoms with shared energy. Therefore

(a) would enter the target A $\frac{V}{2}$ and run to a dose 2D

Thus if both N_2^+ & N^{++} are generated at the ion source and it was assumed that only N_2^+ entered the target, we would have at mass 28

Assumption - N_2^+ At energy V dose D

But Possibility - N At energy $\frac{V}{2}$ dose 2D

or Possibly - N^+ At energy 2V dose D/2

3.4 Van de Graaff

The high energetic electron bombardment experiments performed in the execution of this work were carried out using the High Voltage Ltd. AN2000 Van de Graaff accelerator at Salford University. This machine, like the isotope separator described in section 3.3, has an ion beam flight path evacuated to ~ 10^{-6} torr, but may be divided into four sections. Fig. (3.6) presents a simplified plan of the Van de Graaff and its ancillary equipment.

3.4.1 The high voltage terminal

The high voltage terminal is supported on a resistive column, built of equispaced metal planes. Adjacent planes are connected to each other by resistors of the order of 2000 MΩ, thus ensuring a relatively uniform electric field gradient along the ions acceleration path. The terminal itself can sustain a potential of up to 2 MV., but below 500 kV. the ion beams produced become progressively more difficult to control due to their increased sensitivity to parameters such as the beam focussing and small variations in the terminal potential. For this reason, acceleration energies in the range 2 to 3 MeV. have been selected for this present work.

The high voltage terminal contains the R.F. ion source, a selection of gases which may be accelerated, a high voltage probe used to eject ions from the source into the flight tube, and the ion beam focus power supply. Power for all these facilities is provided by an alternator housed within the upper pulley of the Van de Graaff charging belt. The support column and terminal are encased in a pressure vessel containing a mixture of nitrogen and carbon dioxide at ~370 p.s.i., which provides effective electrical insulation. A corona discharge is maintained through this gas to stabilize the terminal potential as described briefly in section 3.4.3.

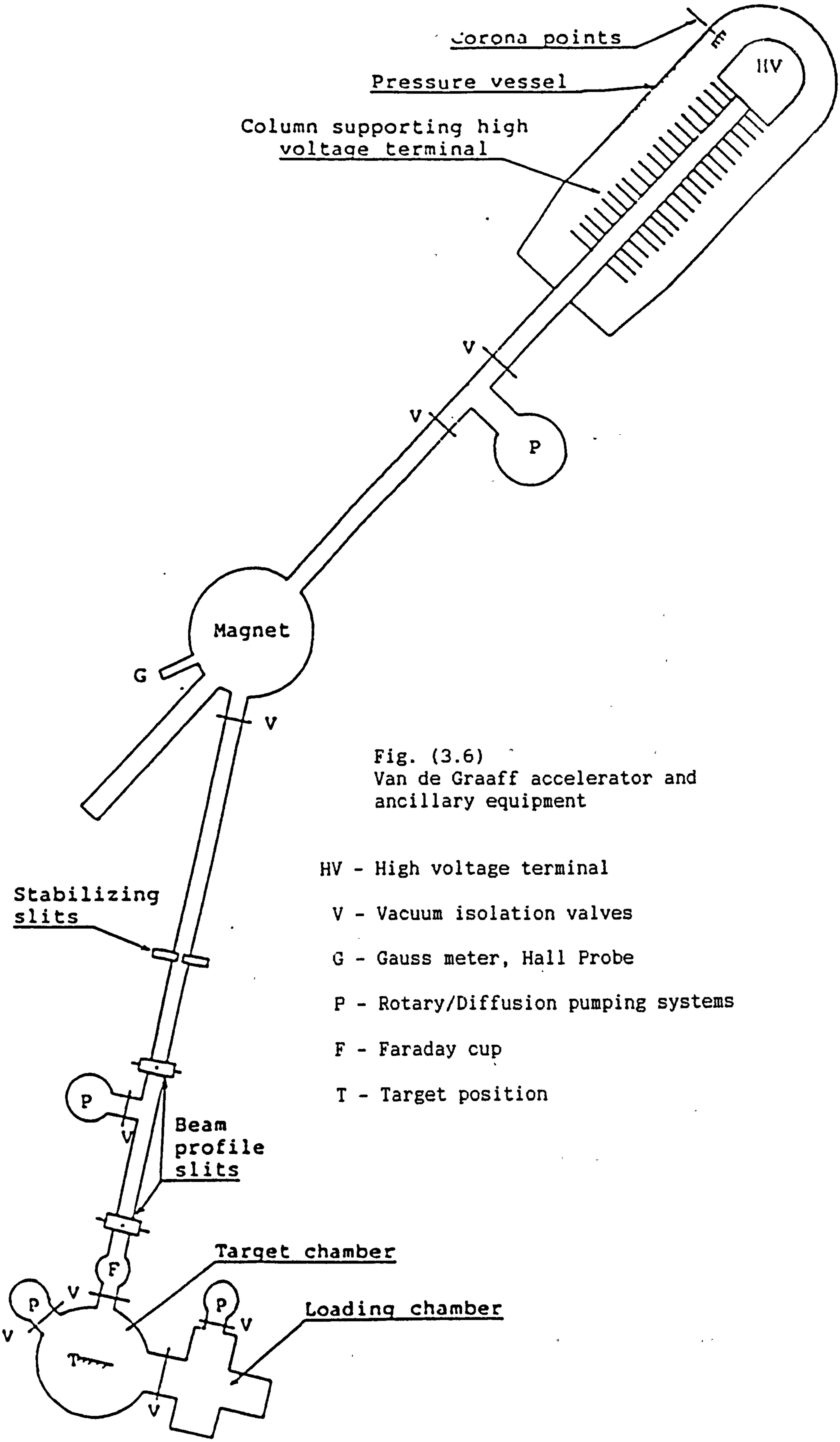

Fig. (3.6)
Van de Graaff accelerator and ancillary equipment

HV - High voltage terminal

V - Vacuum isolation valves

G - Gauss meter, Hall Probe

P - Rotary/Diffusion pumping systems

F - Faraday cup

T - Target position

3.4.2 Magnetic analyser

A high stability (0.01%) power supply is used for the analysing magnet associated with this equipment, and the magnetic field may be set to within 0.1 gauss in the range 0 to 12 k.gauss. These facilities enable ion beam energies to be reproduced accurately by using the appropriate magnetic field.

3.4.3. Ion beam flight path

The ion beam flight path between the magnet and target chamber is described here as it contains a number of important features. A pair of energy stabilization slits are located in the evacuated beam line. These slits extend into the ion beam at each side and intercept high and low energy ions respectively. Assuming the analysing magnetic flux to be stable, any motion of the ion beam to either side of its normal trajectory must be associated with a variation in the accelerating potential. The result of this change in trajectory is a variation in the magnitude of the currents measured on the stabilizing slits. To maintain stability, a feedback loop is incorporated. These currents are passed through a differential amplifier,output of which is used to alter the corona current in such a manner as to restore the terminal potential to its original level.

As the stabilizers are water cooled, they also serve a secondary purpose of greatly reducing the ion beam width. The helium beams employed throughout this work were normally used in a defocussed state, which resulted in a beam of ~3 cm. diameter. The stabilizers reduced the beam width to ~5 mm.

The helium beam profile at this point was still too large for

convenient use, hence two sets of beam defining slits, included in the beam line, were employed to reduce the beam to its final size of 2 mm. high and 0.5 mm. wide. These slits were well separated along the beam line, their spatial difference being ~2 m.

The final item before beam entry into the target chamber is a Faraday cup. This device was used to collect and measure the ion current as the initial beam was set up and stabilized to the appropriate value for use (5 nA to 30 nA). To permit the ion beam access to the target, the cup, supported through a sliding vacuum seal, was lifted out of the ion beam path. It is also inserted to monitor the ion beam current while targets are being changed.

3.4.4 Target Chamber

Access to the target chamber is gained through a side loading chamber which acts as an air lock, in a similar manner to the isotope separator target chamber system. However, in the case of the Van de Graaff, the air lock has its own complete pumping system to enable equalisation of pressures before opening to the target chamber. (Fig. (3.7))

Targets were mounted in stainless steel sample holders but were insulated from the holder and held in place by isolated spring clips which act as the current path for monitoring the ion beam. In the target chamber, the holder slides into a three axis goniometer, of which the rotation about each axis may be controlled to 0.01 deg. When positioned in the goniometer, a contact made to the spring clip was used for current measurement. Contact to the holder itself enabled the application of a 500 V. negative potential to the holder which served to suppress secondary electron emission from the target.

The system was designed such that the intersection point of the three goniometer axes was situated on the sample surface, and was coincident with the point of impact of the ion beam. As can be seen in fig. (3.7), the Z axis of the goniometer, about which the sample tilts backwards or forwards, is inclined at 30 deg. to the sample surface, rather than lying along the surface. This geometry enables back-scattered ions to enter detector No. 2 for the low angle emergence technique. It also allows the goniometer to be turned anti-clockwise about the vertical Y axis, to glancing incidence, where the ion beam enters the target at angles typically in the range of 5 deg. to 25 deg. to the target surface and the back-scattered helium ions enter detector No. 1, the normal detector.

A copper shield, cooled by liquid nitrogen, surrounds the goniometer. This type of cold trap in the proximity of the target improved the vacuum in the target chamber to ~10^{-7} torr and trapped most of the hydrocarbon contaminants that are usually present in small quantitites from the oils in the pumping system. Without such a cold trap, some of the hydrocarbons are deposited on the target surface and are cracked by reaction with the helium ions which would result in the build-up of a carbon deposit which would contaminate the polystyrene petri dish. Three openings are present in the wall of this shield, one to allow passage of the helium beam to the target and back-scattered helium ions to the detectors. A second aperture allows entry of the target and holder and the third opening is used to allow passage of the laser beam to the target for sample alignment.

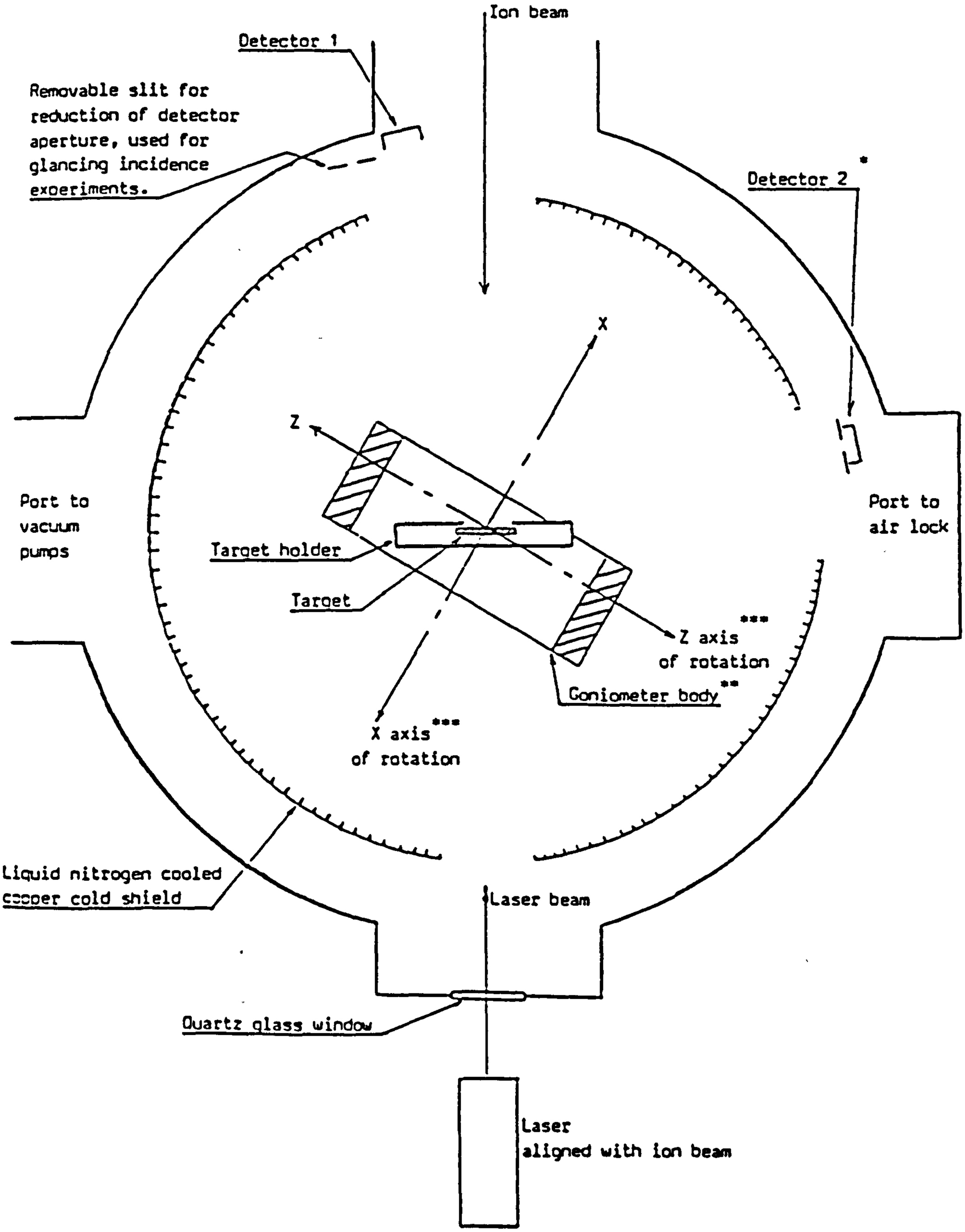

Fig. (3.7) Plan of the target chamber

3.5 D.C. Plasma ion bombardment

To ion-bombard any substrate in a low energy region, one may use ion-plating rig, except that the evaporation source is not required. Ion plating is a hybrid vacuum coating process that combines the benefits of vacuum evaporation and sputtering. The term, ion plating, is generally applied to high energy plasma deposition methods in which the surface to be coated is subjected to a small flux of high energy ions. A much larger number of continuous bombardment of the substrate by these energetic ions and atoms of both the coating material and the support gas, results in a wide variety of effects. In the ion bombardment experiments, there is no material to be vaporised. The working gas in the vacuum chamber will be ionized by a D.C. voltage between the two electrodes as shown in Figure (3.8). The ionized gas will form a plasma.

A plasma is defined as a region of high temperature gas containing large numbers of free electrons and ions. By a proper application of electrical potential, electrons can be extracted from the plasma to provide a useful energy beam.

Surfaces in contact with plasmas are bombarded by electrons, ions and photons. The electron and ion bombardment is particularly important. Less is known about the influences of the plasma radiation. The relative number of ions and electrons which are present on a surface depends on whether it is biased as a cathode or anode, or is electrically isolated. It is also related to the rate of gas flow and magnitude of applied voltage.

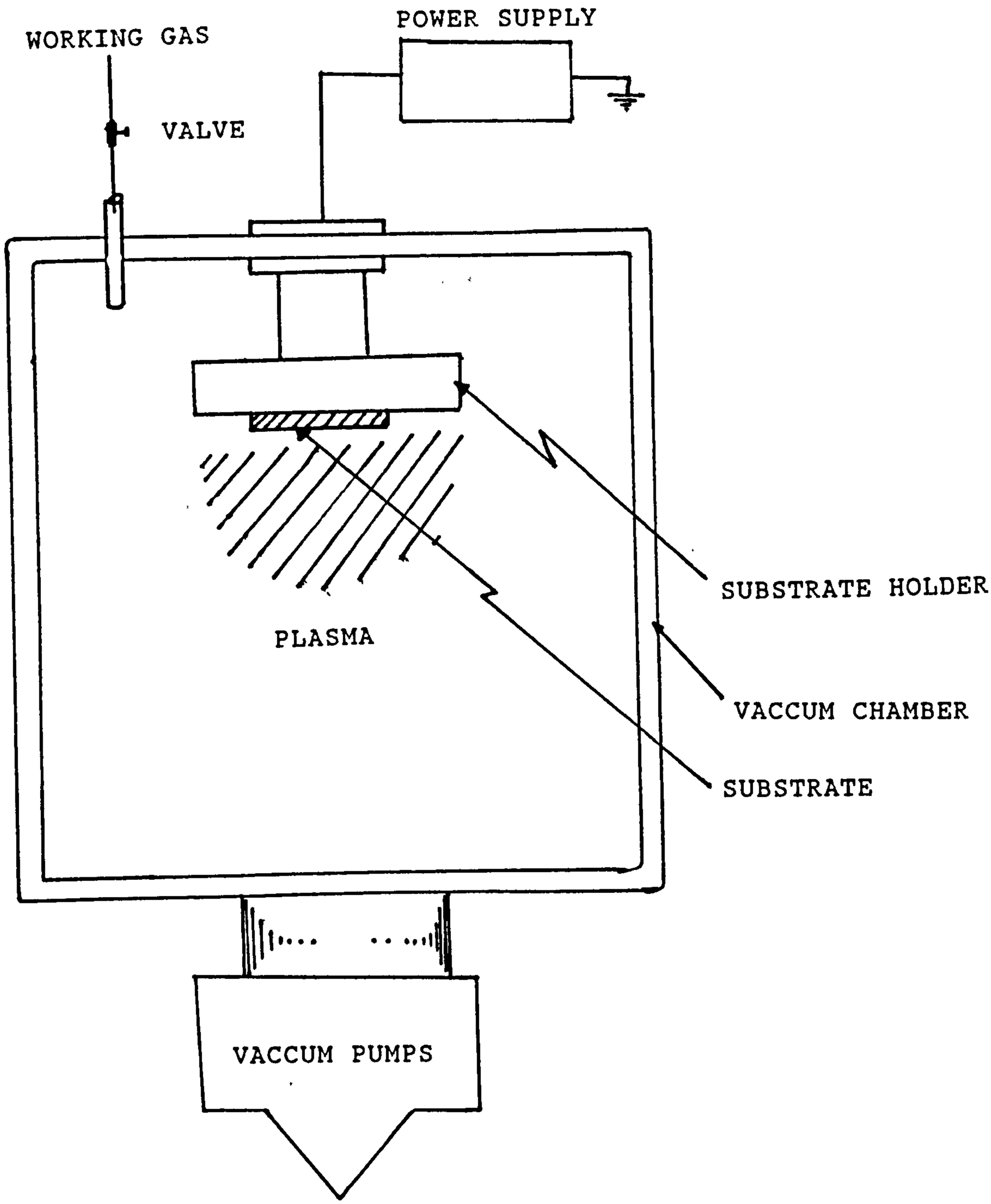

Figure (3.8). Ion bombardment process

For positive ion bombardment it is essential for the substrate holder (usually stainless steel) to be biased to a negative potential. This will then attract the positive ions and repel any negative ions in the plasma. A glow discharge is produced by biasing the substrate to a high negative potential. This glow discharge is due to the presence of the gas in the chamber and applied electrical potential, it is known as

a gas discharge, and is explained as follows.

3.5.1 Gas discharge

It has been known for a long time that if a D.C. voltage is applied between two electrodes in a vacuum chamber containing a gas at a pressure greater than about 0.1 Pa, then, a discharge can be initiated between the electrodes. The primary source of ionization of the discharge gas is the electron-atom collision, where collision between electrons and gas atoms results in the ionization of gas atoms and the emission of more electrons.

$$e^- + G^\circ \longrightarrow G^+ 2e^-$$

where G° is a ground state gas atom and G is a singly charged gas ion. At low voltage, only a few ionized particles will exist which can contribute to the current. As the voltage increases, the charged particles gain sufficient energy to produce additional charged particles by impact ionization. This can lead to a linear growth of discharge current. As the voltage increases further, an avalanche process takes place due to the ion bombardment of the cathode and the release of secondary electrons. The secondary electrons are then accelerated in the field of the cathode and due to collisions with the residual gas atoms and molecules, produce new ions. The ions are again accelerated back to the cathode and produce new secondary electrons. This process continues until a self-su.staining discharge is achieved. In this case, the gas starts to glow, the voltage falls and the current rises abruptly.

REFERENCES

1) EL-KAREH, A.B., EL-KAREH, J.C.J. "Electron Beams, Lenses and Optics", London: Academic, 1970.

2) SCHILLER, S., HEISIG, V., PANZER, S. Electron Beam Technology, New York: John Wiley & Sons, 1982.

3) WATSON, P.K. "The Transport of Electrons in Polystyrene", Electrical Insulation and Dielectric Phenomena, New York, 45th Meeting, 1976, p.10.

4) WATSON, P.K. "The Transport of Low Energy Electrons in Polystyrene", 52nd Conf. on Elect. Ins. and Dielectric Phenomena, 1983, p.421.

PART 2

EXPERIMENTAL WORKS AND OBSERVATIONS

CHAPTER 4

THIN FILM ELECTRODES

4.1 Introduction

The complete range of measurements reported in this thesis was obtained using several types of electrodes, the development which is also a part of the investigation (M Jaberansari, 1985 [1]). The details of these and the appropriate techniques for making the electrodes constructed for this work are discussed in detail under the following sub-sections 1 - Wire electrodes and problems associated with wire electrodes, 2 - Preparation of electrodes by evaporation technique, 3 - Preparation of electrodes by vacuum sputtering technique.

4.2 Wire electrodes and problems associated with wire electrodes

So far many experiments have been performed on biological systems by using wire electrodes. Different metal wires of different diameters (mm) have been tried. Experiments on pearl chain formation and cellular rotation have generally used either platinum or gold wire electrodes which could easily be made into spherical head shaped electrodes, thus generating a more controlled non-uniform electric field, but wires made of silver were equally successful, and cheaper than gold or platinum. Sometimes it was necessary to inject a very high electric field into the chamber by means of a sharp pointed electrode. Tungsten wires have a fibrous structure, therefore, to achieve a sharp point configuration, it was necessary to use an etching process which is discussed by Jaberansari [1].

In this experiment the wire types of electrodes described above were found not to be ideal for observing the cullular behaviour under a phase contrast microscope. In general, two drawbacks were encountered in experiments using wire electrodes:

1) Due to electrode thickness the chamber needed to be of a certain depth and that increases the magnification and focussing problem of the cells near the electrodes under the light microscope. This problem was greatly reduced by redesigning the electrode chamber so that the electrodes are located as near to the upper surface of the chamber as possible.

2) The individual cells could only be observed for a short period of time, because the cells settled in the chamber under gravity. To overcome this problem a density gradient layer was prepared to support the yeast cells whilst observing them under the microscope. The density gradient layer was obtained by mixing 0.1 M lactose (0.18 gram Lactose in 5 ml of distilled water) and 0.5 M xylose (0.375 gram xylose in 5 ml of distilled water).

All these problems were overcome by altering the electrode design and making the electrodes in a different way. To reduce the depth of the chamber the diameter of the electrodes was reduced. This problem was initially solved by painting the pattern of the electrodes in either silver or platinum liquid (Johnson Matthey Ltd.) over a microslide by means of a very fine brush. Once the picture of the electrode was drawn, i.e. that is either 3 electrode configuration electrode (each electrode 120° apart or 2 electrodes system (two parallel electrodes). The glass slide was carefully placed in an oven and then heated to 400°C. until the adherent metal film was formed. This method has an advantage over the other in producing a very thin strongly adherent metallic coating; the depth of the chamber can be very small and hence the magnification can be increased. However, due to errors in drawing the electrodes diagram by hand on a glass slide, it was decided to

prepare a mask and then evaporate the metal through the mask in a high vacuum system. This process was an ideal way for making the electrodes as far as this experiment was concerned, because both the thickness of the electrodes (near to 0.1 um) as well as the shape of the electrodes could be controlled to a high degree of precision and also the metal could be evaporated uniformly over the mask.

4.3 Preparation of electrodes by thin film vacuum

4.3.1 Preparation of mask

This is the most difficult part of the electrode preparation and requires patience and time to perfect the technique.

The procedure is given below:-

1) Cut a microscope glass slide size piece of a beryllium copper (BeCu) metal foil with a thickness of 1 mm. (Note: beryllium is highly toxic)

2) Clean BeCu in the detergent "decon 90" for approximately one minute in an ultrasonic cleaner and then rinse in water

3) Clean the BeCu in chromic acid for 1 to 3 seconds then rinse again in water

4) Electrolytically etch the BeCu in hydrochloric acid with a carbon rod as cathode and the BeCu as the anode and then rinse.

5) Spin coat the prepared BeCu mask with Kodak resist 747 at approximately 2000 r.p.m. for 60 seconds

6) Dry the mask by blowing hot air over it using a hand-held hot air dryer

7a) Expose the mask on Kodak resist under U.V. illumination for 8 second exposure

7b) After exposure, mount the mask in a vertical position and spray with "KTRF developer" for 1 minute at room temperature immediately follow this by a spray with "KTRF rinse" for 30 seconds. The mask is then allowed to dry in a vertical position in a stream of clean air for 10 minutes followed by heating in the oven at 80°C for 5 minutes. At this stage the image is checked with the aid of a low power microscope.

8) The mask frames and the rear surfaces of the BeCu were again coated with cellulose lacquer, except for one corner of each frame so that an electrical connection could be made in a plating bath. Since the masks had been well cleaned before being coated with photoresist, it was only necessary to give them a short cleaning before being plated.

9) For nickel plating, an Ni anode is used and the BeCu forms the cathode. The current density adjusted to 30 mA cm^{-2} , the plating bath consists of nickel chloride and is used at a temperature of 55°C., the time of electroplating is 20 minutes.

10) After plating, the masks were rinsed in water and then immersed in acetone to remove the cellulose lacquer from the rear surface. The photo-resist is then removed by soaking in "penstrip Y-1547 " for a

few minutes. The rear surface is again painted with cellulose lacquer and allowed to dry. The mask was then immersed in a vertical position in CR-20 etchant. When the etch is completed, the masks were thoroughly washed in running water. Finally the lacquer was again removed from the rear surface in acetone. Figure (2.7) shows the typical masks used for the electrodes described in this chapter.

Once the mask had been prepared, metal could be evaporated or sputtered through the mask in a vacuum chamber which was available for use in the Laboratory.

4.3.2 Pre-cleaning of the glass slide

Since the metal needed to be either evaporated or sputtered onto the microscope slide inside a vacuum chamber, the microscope slide needed to be cleaned in a special way. This ensured greater adhesion of the metal electrode to the glass microscope slide and in turn increases the electrode life.

First the glass slide was immersed in a detergent (decon 90) solution in an ultrasonic bath. The ultrasonic bath was switched on for 8 minutes, then, the glass slides were removed using a pair of clean forceps. The distilled water was sprayed over the glass slide which was then placed vertically in a clean room cabinet and left to dry.

4.3.3 Evaporation process

Any substrate such as a microscope glass slide may be covered by a thin film metal (in any desirable pattern by using a mask) by an evaporation process. In the evaporation process vapour is produced from the

material located in a source which is current heated through its resistance. The process is usually carried out in a vacuum (typically 10^{-3} to 10^{-6} torr) so that the evaporated atoms undergo an essentially collisionless line-of-sight transport prior to condensation on the substrate through the mask. The substrate is usually at ground potential (not biased). Figure (4.1) is a schematic of a vacuum evaporation system illustrating the filament supply.

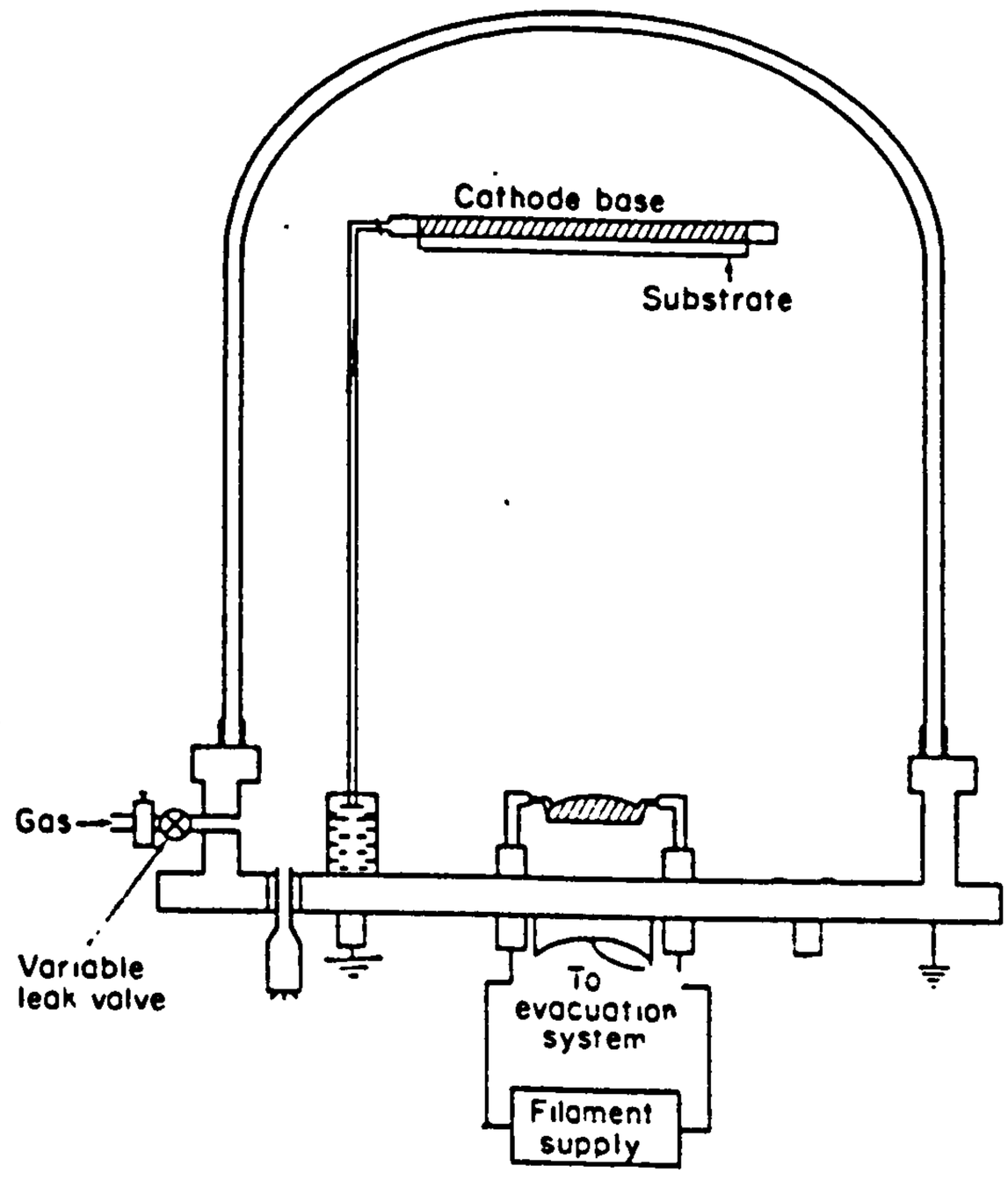

Fig. (4.1)
An evaporating system used in this project

4.3.3.1 <u>Evaporation method</u>

At this stage the mask was mounted carefully over the top of a clean glass slide which was already prepared. The assembly was then fixed on top of the evaporation chamber by using the special stand with the mask side facing downwards. The glass bell jar then covered the open space of the evaporation chamber. Silicone vacuum grease was used to prevent leakage. The rotary pump was a model QSB2 by Edward High Vacuum Ltd.

and it was then switched on (in conjunction with a diffusion pump, model ED75 by Speedivac Ltd.) already connected into the system), and it was left on for some hours and the vacuum was checked by a guage (model 2A, Pirani-Penning Ltd.) meter until a good vacuum of 10^{-5} torr (1torr-1mm of Hg) was achieved. The metal to be used (gold, platinum, silver or aluminium) for the evaporated electrodes was placed in the boat at the beginning of the procedure, and when the vacuum was satisfactory it was evaporated by increasing the current through the boat or coil from a 0-30 A power supply. After the evaporation of the metal over the microscope slide the pump is isolated with a flap valve and air is let into the chamber. The glass slide with the electrodes was then ready for the experimentation. The following photographs show some samples of the electrodes prepared by this technique.

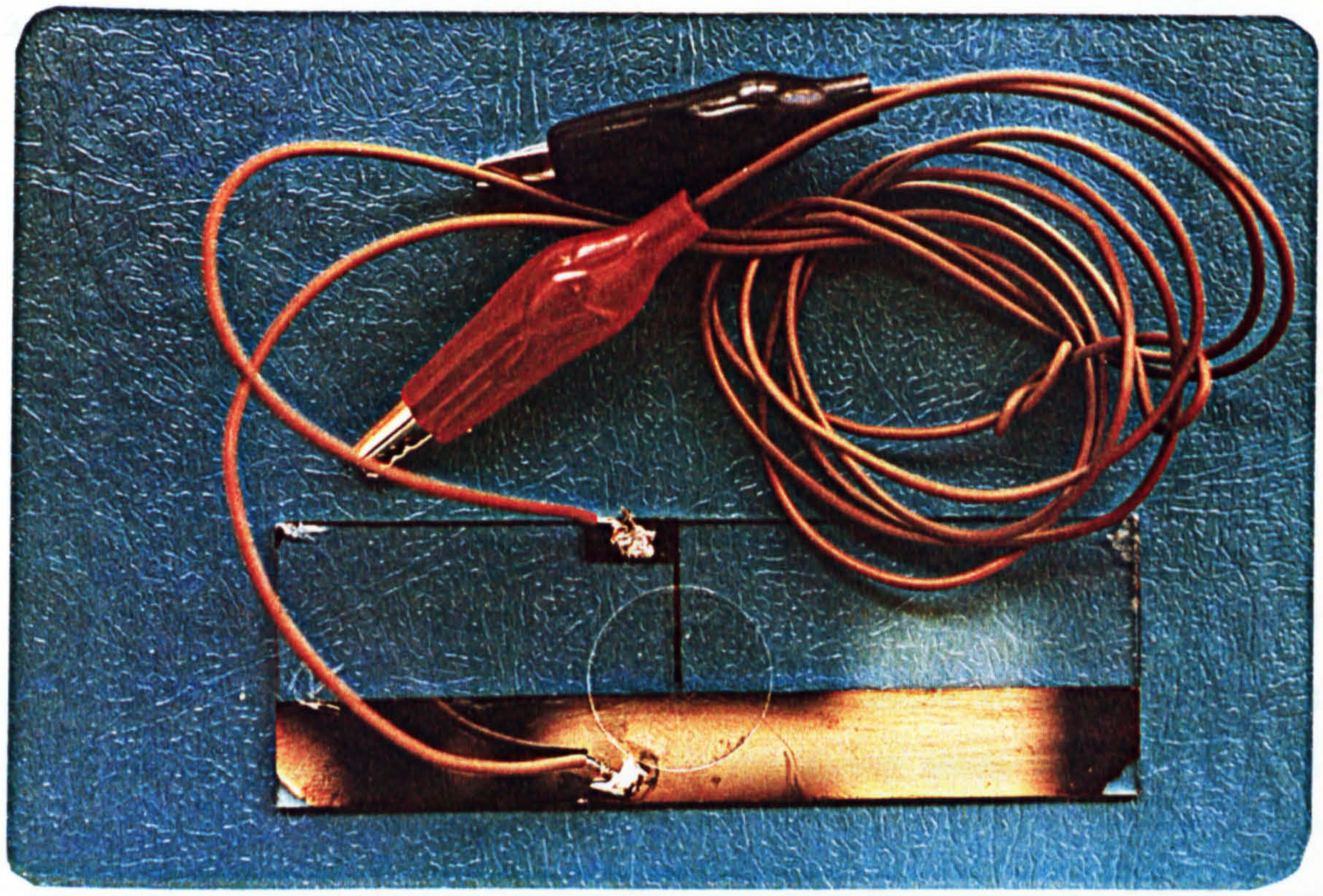

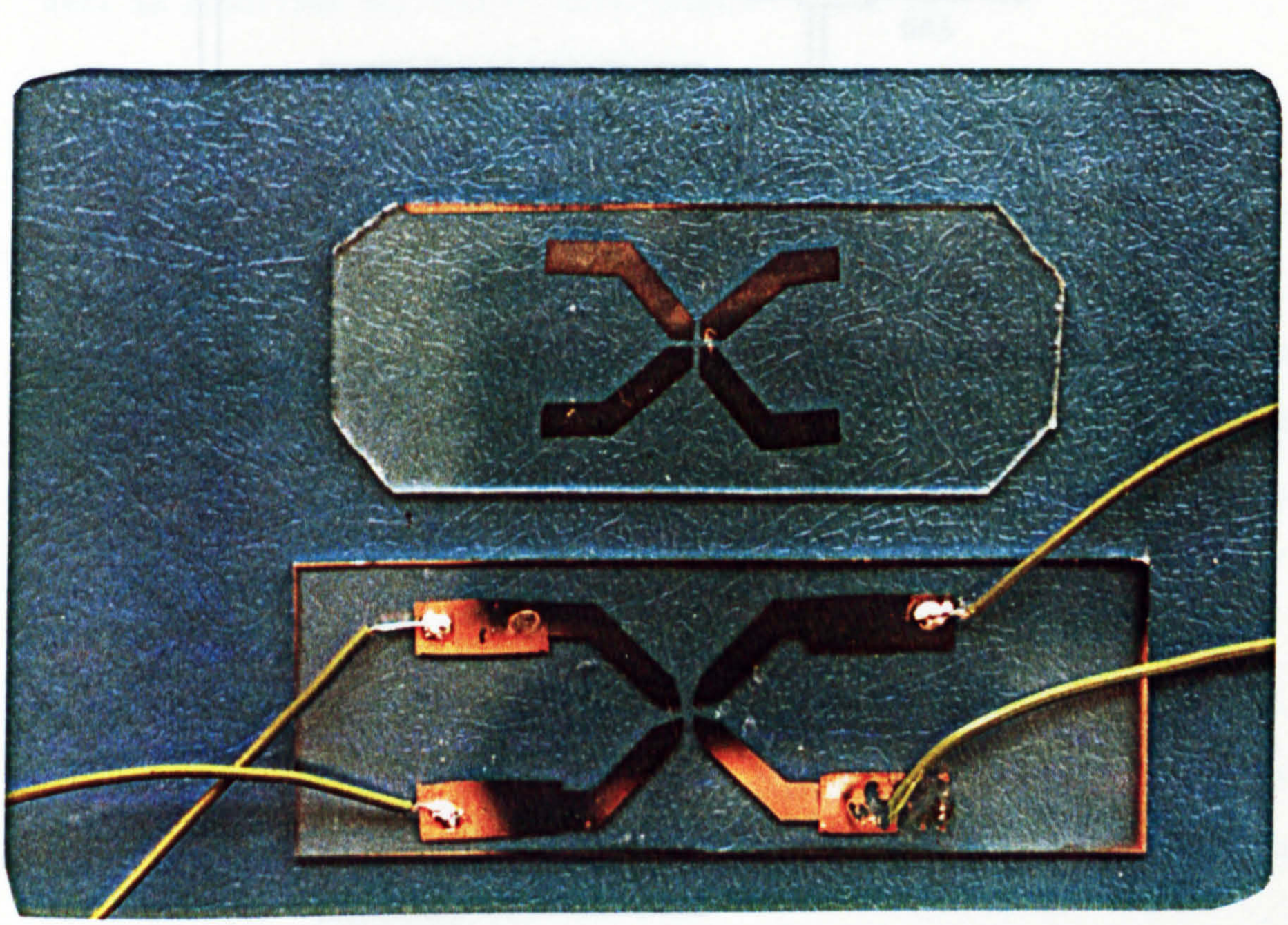

Fig. (4.2) Vacuum evaporated platinum electrodes prepared for studying the "pearl chain" formation (A) and cellular rotation (B).

4.3.4 Sputtering process

The frequent use of the thin film vacuum evaporated electrodes over glass slides caused the vacuum evaporated electrodes to wear and fresh ones often needed to be prepared. For a more reliable and permanent thin film electrode, it was decided to use the sputtering technique to replace the evaporation method. In this technique the life-span of electrodes was increased. This is also a physical vapour deposition process. In the sputtering process, illustrated schematically in Fig. (4.3), positive gas ions (usually argon ions), produced in a glow discharge, bombard the target material (also called cathode) dislodging groups of atoms which then pass into the vapour phase and deposit onto the substrate.

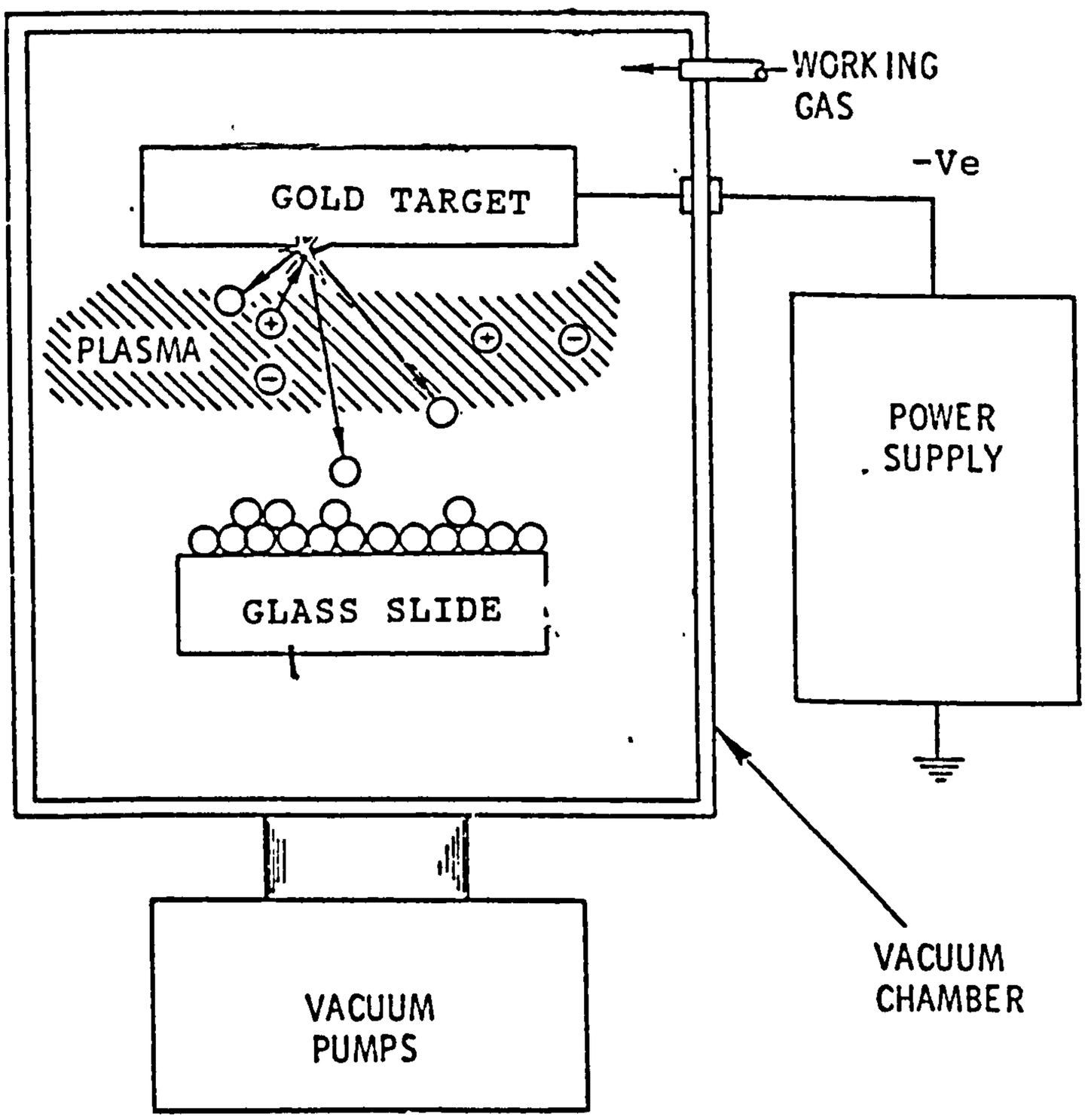

Fig. (4.3) Basic sputtering process used in this project (magnetic field is produced by magnetron between target and substrate)

4.3.4.1 Sputtering method

This method used the same rig as the evaporation rig with a few minor changes. One of the electrodes, which is the source of coating material and is called the 'target', was attached to a high negative potential power supply (from 10-5000 V.). The other electrode which has been referred to as the substrate holder, was situated opposite the target. After evacuating the vacuum chamber to a suitable pressure (1 x 10^{-5} torr) it was back-filled with an argon gas to a pressure of 0.1-10 Pa. A magnetic field was produced by magnetron between target and substrate (R.F.). The negative potential between the target and the substrate will ionize the gas. These energetic ions will bombard the target (in this experiment, a gold 'target'), knock out the gold ions and deposit them on the glass slide (substrate) through a pre-prepared mask as described earlier in this chapter.

4.3.4.2 Advantages

Since the gold ions (low energy) are more energetic they will bombard and adhere to the surface of the substrate (microscope glass slide), whereas, in the evaporation process all the deposited atoms were neutralised (only thermal energy). The sputtering process increased the life-span of the electrodes. It is important to note that in a sputtering process we create an energetic ion which "shallow bombards" the substrate.

It is possible to get atoms as well as ions but, the majority of particles are ions some of which may undergo further collisions with electrons and form atoms.

4.4 Electrode effect

Previous work done by other researchers on this subject always reported the use of either platinum or gold electrodes. But they never mentioned the reason for the use of such materials. In the present work electrodes of aluminium, gold, nickel, platinum, silver and tungsten were examined in conjunction with the cellular rotation experiments.

At very low conductivities, the bright platinum and then gold and silver electrodes gave best results, in that order; at medium and high conductivities of the suspension media, the platinum electrodes were superior. Often it was found that it was just not possible to reproduce results with this electrode. Aluminium electrodes were not satisfactory at all due to the anodisation of the aluminium which changed in colour from silver to grey.

Electrodes of nickel generated bubbles of gas in the field of view inside the test cell suspension and hence made it impossible to see any of the cells with the microscope. This could be due to electrode polarization which affected the electrode presented very much at low frequencies.

4.5 Electrode cleaning

Before beginning an experiment with a given electrode system, the electrodes should be as smooth as possible and they must certainly be very clean. After each experiment there is the problem of removing the collected cells from the electrodes. Merely turning off the applied field will not dislodge all of them from the electrodes. The best and simplest method is to rinse the slide with a high pressure jet of

deionized water from a hard plastic squeeze bottle. This usually removes all of the old cells. The electrodes can be dried in a current of air so as to avoid errors in the sample concentration. It should be remembered that any attempt to clean the electrodes with any form of paper tissue would remove or scratch the thin film vacuum evaporated electrodes and result in an open-circuit.

REFERENCES

1) JABERANSARI, M. "Dielectrophoretic, Electrodynamic and Magnetic Resonance Phenomena In Yeast Cells, M.Sc. Thesis. Salford University, 1985.

CHAPTER 5

ELECTRONIC CIRCUIT DESIGN AND APPLICATIONS

5.1 Introduction

This chapter introduces some of the circuits designed in the course of the research. Circuits were designed to produce the electric rotating fields, to supply a fixed regulated voltage, to measure the charge by a charge sensitive amplifier, to experiment on the effect of -ve ions formed by an air ionizer and to observe the pearl chain formation from lone cells by using a computer controlled oscillator.

5.2 Three-phase voltage generator circuit

A three-phase voltage generator circuit such as the one shown in figure (5.1) can be used to produce a rotating electric field. This generator uses one single-phase supply source and its three-phase output is to be connected to a chamber having the three electrode assembly. This circuit can be adjusted to operate at any frequency between 0.1 Hz to 80 KHz.

An external R.C. oscillator (type TG200, Levell Ltd.) was used as the reference phase output and as an input to the phase shifting network.

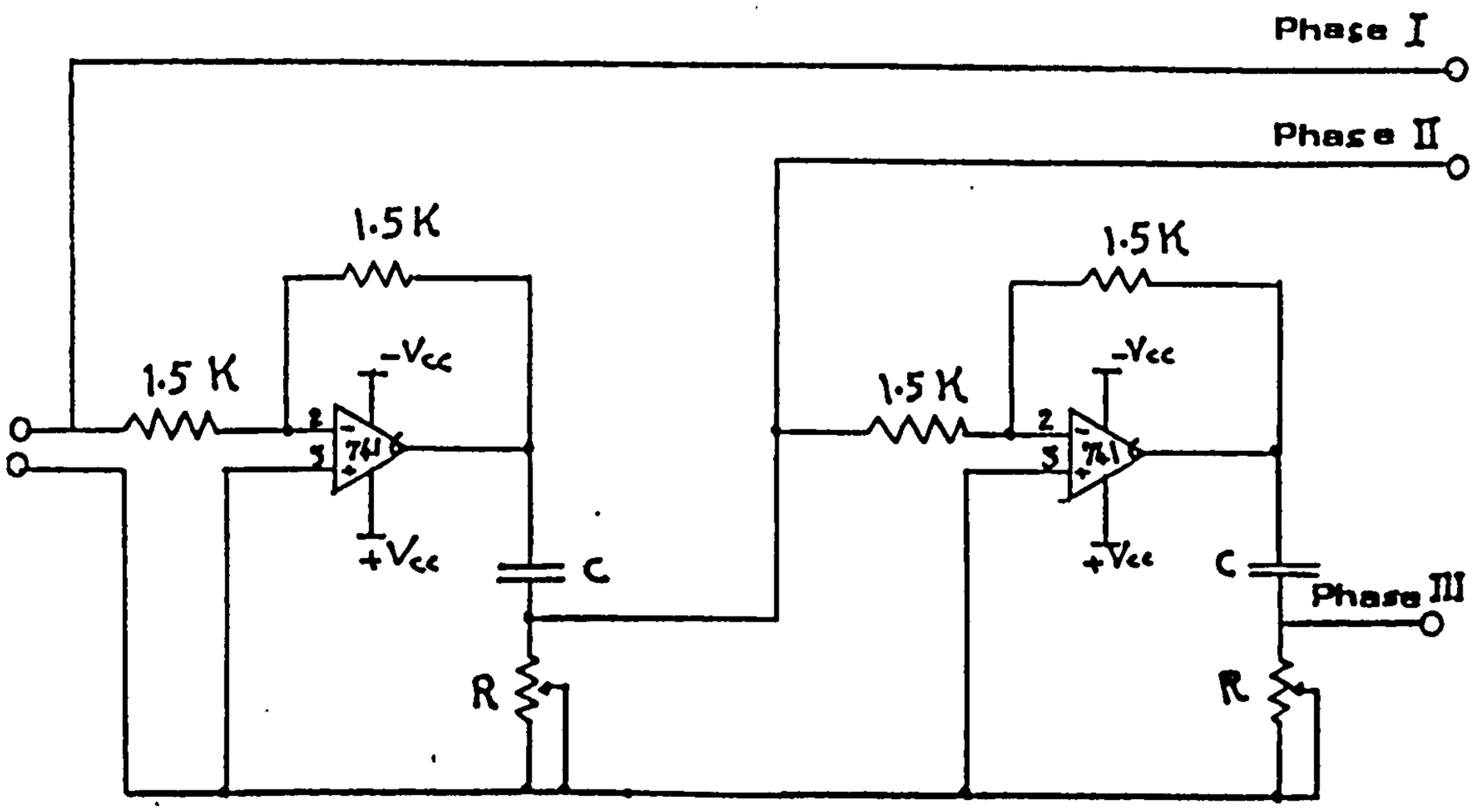

Figure (5.1) The circuit diagram of a three-phase oscillator

The phase shifting circuit comprises two operational amplifiers operating in the inverting mode, one for each phase output.

Each amplifier provides a phase change of 180 deg. between its input and output signals. The additional phase shift required is obtained from the series connected variable capacitor/variable resistor phase shifting network which is adjusted to set the phase angle of the output with respect to the reference input. The second amplifier operates on the same principle but its input is obtained from the phase 2 output, which is then referred to as its reference signal.

Both amplifiers have their gains set to ensure that all three-phase outputs are of identical amplitude and this is achieved by replacing the amplifier feedback resistor with variable resistors.

This circuit produces the three-phase outputs at equal amplitudes of 25 volts which could be amplified to provide higher voltages or power outputs as required.

An oscilloscope was used to set the phase difference to 120° between each adjacent phase of the three-phase system. However, for an easier and more accurate measurement of the phase differences a summing amplifier was designed which gave zero output when the amplitudes and phases were correctly adjusted, since each phase is 120° out of phase. Alternatively, if one of the phases is inverted and their sum obtained by the addition in summing amplifier, the magnitude of the output signal will be twice the magnitude of the input signal.

5.2.1 Three-phase rotating electric field

Now consider three electrodes arranged 120° apart in a chamber containing the biological cells. Each electrode is supplied from one phase of a three-phase supply generator. For three source voltages separated in time-phase by 120°, the phasor diagram of the source voltage is as shown in Fig. (5.2)

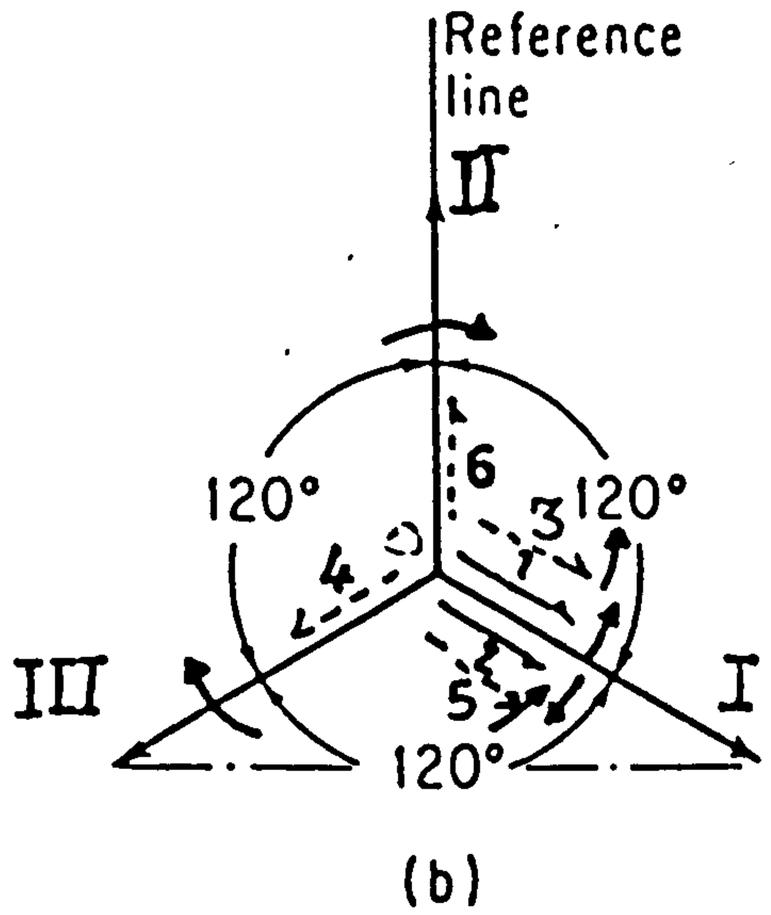

Fig. (5.2) The phasor diagram in terms of the maximum value of each phasor

Consider the instant at which the voltage in electrode I is at maximum. Then its two rotating field components I and II will at that instant be directed along the axis OA. The voltage at electrode II is 120° behind its maximum value and therefore, each of its component rotating fields, 3 and 4, has to travel 120° before pointing along the axis OB. Hence, one of them will at that instant point along OA, and the other along OC as shown, similarly the rotating fields 5 and 6, due to the voltage at electrode III, have each to travel 240° before pointing together along OC, hence field 5 is along OA, and 6 along OB. Collecting the clockwise fields we see that these are 120° apart and therefore neutralize one another at every instant, the counter-clockwise fields all point in the same direction and they therefore combine to produce a pure rotating field.

In this case, the direction of rotation is the same as the direction of the phase-sequence, first electrode I has its maximum voltage, then II, and then III. Thus, to reverse the direction of rotation of fields, the phase sequence must be reversed.

Let each of the phases in Fig. (5.2) produce an alternating field of maximum strength V along its axes, then, as with alternating voltage, one has the fundamental equation giving the instantaneous value with respect to time.

$v = V \sin w\tau$

where $w = 2\pi f$

Take as zero time the instant that the rotating vector giving the field v_1, is directed along OA, then:

$v_1 = V_1 \sin w\tau$

$v_2 = V_2 \sin (w\tau - 120^\circ)$

$v_3 = V_3 \sin (w\tau - 240^\circ)$

or

$v_1 = V_1 \sin w\tau$

$v_2 = -V_2 \{1/2 \sin w\tau + (3^{1/2}/2 \cos w\tau\}$

$v_3 = -V_3 \{1/2 \sin w\tau - (3^{1/2}/2 \cos w\tau)$

Now resolve these along OA and a perpendicular axis, and denote by $\underline{X}$ and $\underline{Y}$ the total component in these two directions. Then:

$\underline{X} = v_1 + v_2 \cos 120^\circ + v_3 \cos 240^\circ$

$\underline{Y} = 0 + v_2 \sin 120^\circ + v_3 \sin 240^\circ$

Now put $V_1=V_2=V_3$ then:

$\underline{X}=(3/2)\ V \sin w\tau$

$\underline{Y}=(3/2)\ V \cos w\tau$

Hence, the resultant field:

$V_R = (\underline{X}^2 + \underline{Y}^2)\ 1/2 = 3/2\ V$

Showing that the field is of constant strength, since its magnitude is independent of time. For its duration with respect to the OA axis

$\tan \theta = \underline{Y}/\underline{X}$

$= -\cos w\tau/\sin$

$= \tan (w\tau - 90^o)$

therefore $\theta = w\tau - 90^o$

In other words, the angle θ is proportional to the time, and therefore the resultant field V_R must rotate in the chamber with a uniform angular velocity of w. In the above work, the direction of rotation of this field is coutner-clockwise because the sequence with which the component alternating fields go through their changes in magnitude is, in order, I, II, III. Later, when it is required to look at the behaviour of cells in the chamber for the reverse direction of rotation of the field it is necessary to reverse this sequence, e.g. to change it to I, III, II. This is very easily accomplished by a switch.

5.3 Four-phase voltage generator

The four-phase generator circuit uses the same basic principle as the previous three-phase voltage generator, but each phase is 90 deg. out of phase by the next phase, and the phasor diagram is just like a cross. This uses four electrodes and the system is easier to manipulate given the usual microscope stage controls.

The block diagram circuit used for the four-phase voltage generator is shown in Figure (5.3).

Depicted in Fig. (5.3) is a diagram of the electronic setup to generate the rotating electric field. In the simplest way, the sine waves from a high-frequency generator are split up and inversed to obtain four outputs, each with a phase shift of 90°. To avoid transduction of a DC field, the generator is coupled to the vacuum deposited thin film electrodes by capacitors. A voltage of 10V is necessary for the experiments, depending on thin film to electrode distance. From the electronic point of view, it is also possible to apply simple square-topped pulses instead of sine waves.

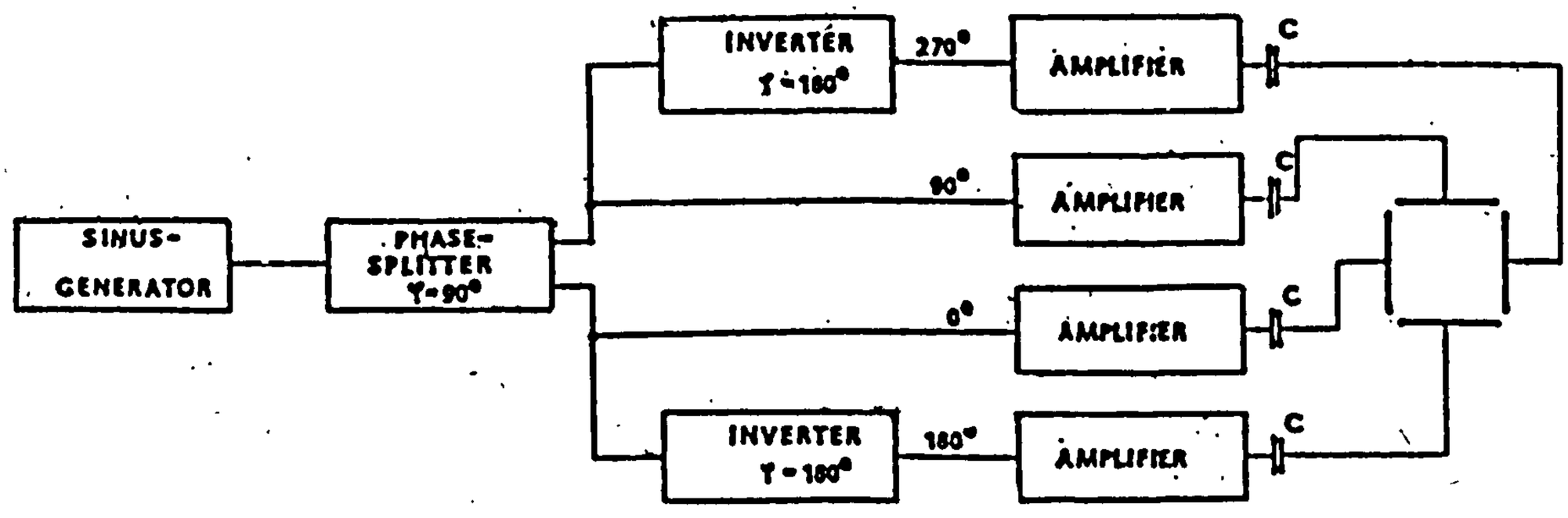

Fig. (5.3) Basic circuit diagram of the setup for a 4-phase generator

5.3.1 Four-phase rotating electric field

When two sinusoidally varying linear electric fields differing in phase by 90° are superimposed, the field E show in in Fig. (5.4) can be considered to be the result.

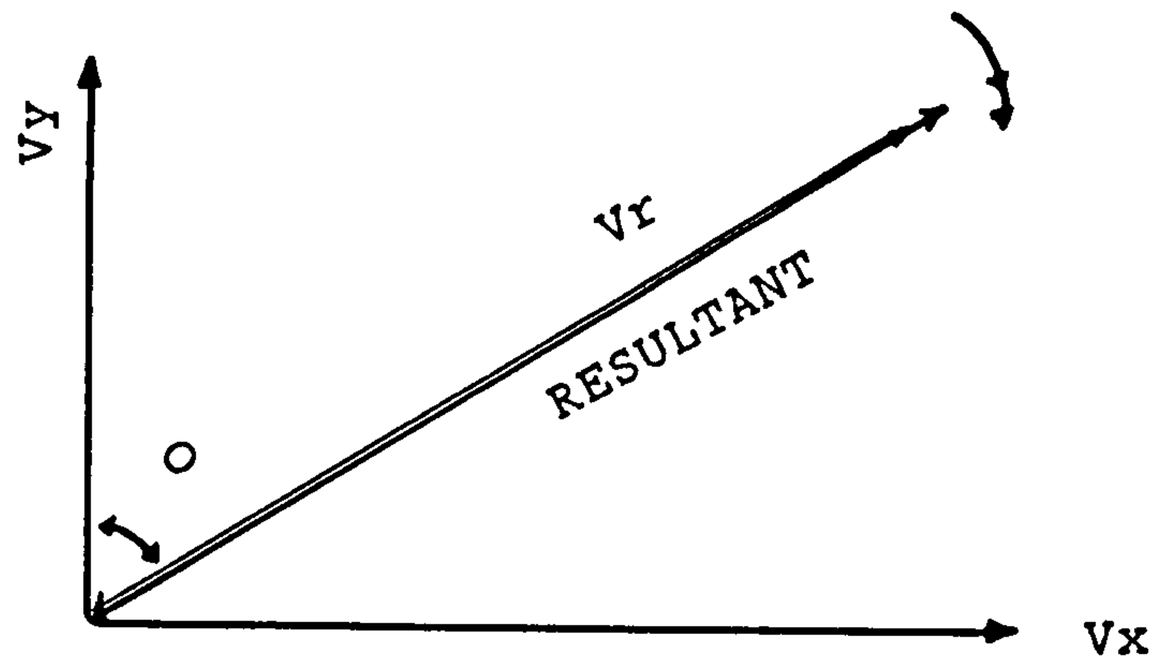

Fig. (5.4)
The superposition of two orthogonal linear field vectors and the resultant field, V_R, at a given instant in time

If both fields have peak amplitude V (V cm^{-1}) and frequency f(Hz), then

$$v_y = V \cos w\tau$$

and

$$v_x = V \cos (w\tau - 90^\circ) = V \sin w\tau$$

where

$$w = 2\pi f.$$

The amplitude of the resultant is given by:

$$v_R^2 = V^2(\cos^2 w\tau + \sin^2 w\tau)$$

Therefore

$$v_R = V \quad \text{(independent of } \tau\text{)}.$$

The angle θ in Fig. (5.4) is given by:

$$\tan\theta = \frac{V \sin w\tau}{V \cos w\tau} = \tan w\tau.$$

Therefore

$$\theta = w\tau$$

The resultant field rotates f times per second but has constant instantaneous amplitude V, which is the peak value of the component fields. The increase in average amplitude is due to the addition of two fields.

5.4 Fixed Voltage Regulator

For observation of cellular rotation of Leishmania major and (Saccharomyces cerevisiae) cells a rotating electric field needed to be created in a chamber containing the named suspended cells. To produce the rotating electric field the 4-phase voltage generator circuit was connected to the previously prepared electrodes. The 4-phase voltage generator circuit used 4 IC 741 operational amplifiers. These op-amps needed a + 15 volts supply which could be obtained from a standard DC power supply. Any experimental work on Leishmania parasites needed to be carried out in the Parasitology Laboratory and all electronic equipment needed to be carried to that Department. Fortunately the voltage regulator IC's offer the advantages of extremely good regulation, compact size and ease of use. Therefore an IC voltage regulator was constructed for a specific and fixed voltage output, such as 15V. For operational amplifiers. Figure (5.5) shows a circuit using RS IC no. 305-636 to give a fixed stable ± 15V. supply suitable for IC logic elements. The maximum output current is 100 mA and no heat sink is needed on the regulator.

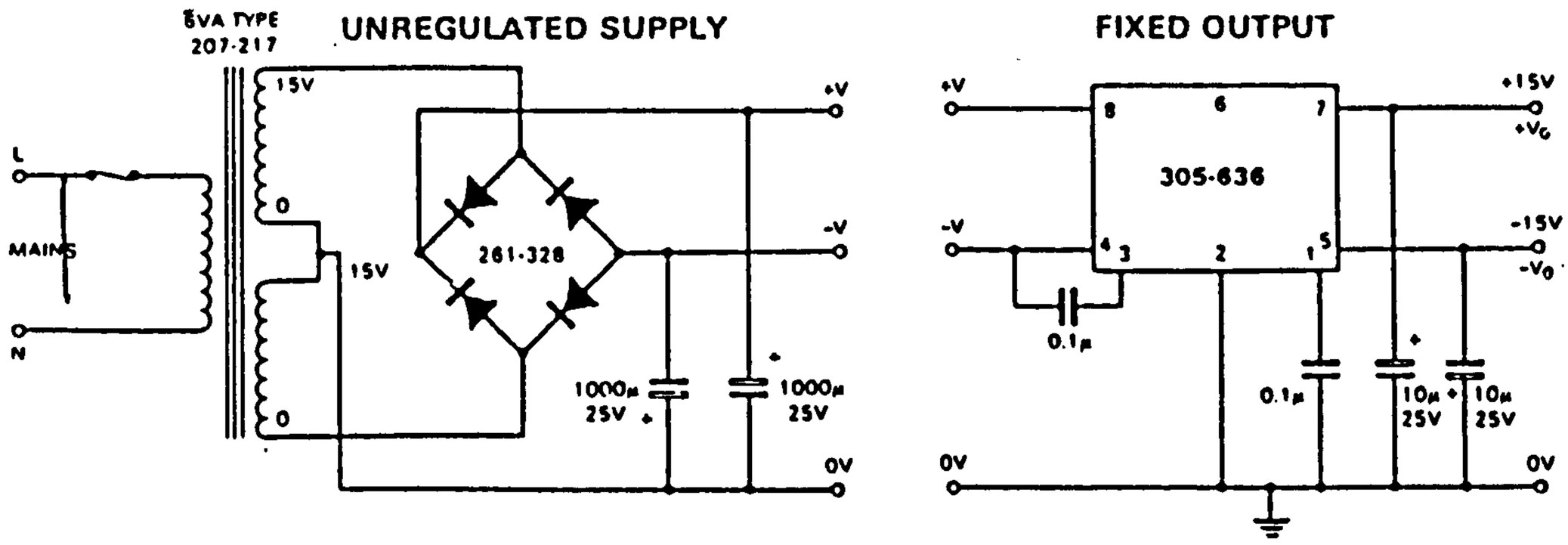

Fig. (5.5) Basic diagram for fixed output regulator

The transformer may be a standard 6VA type (RS No 207-217) and the full wave rectifier (RS No. 261-398) gave the unregulated DC voltage for the voltage regulator IC.

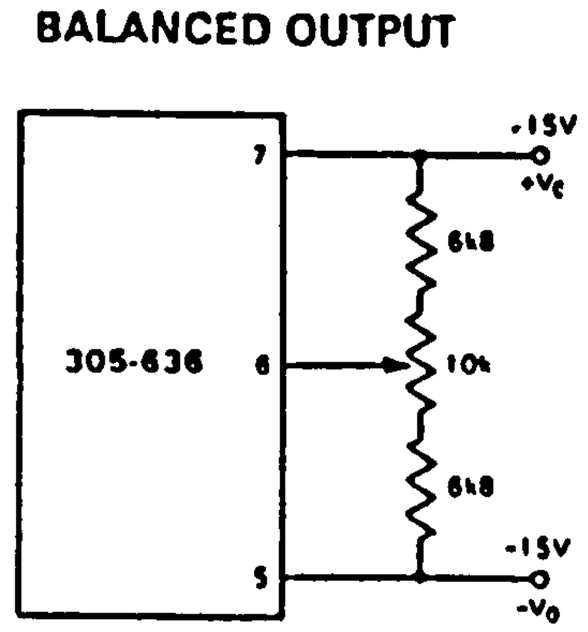

5.5 Charge-sensitive amplifier

The electron beam charge used in the experiments of chapter (7) could be measured in real time, while the electron beams are being injected into the target petri dish, by using a charge sensitive amplifier. This gave a direct reading of the surface potential of the sample and its variations with time.

A charge-sensitive amplifier (charge-to-voltage converter) will give an output voltage proportional to the quantity of charge transferred to the input. The operational integrator circuit is very useful in this application, the input resistor being removed and the input terminal connected straight to the inverting input (Fig. 5.8).

Because of the high input impedance of the op amp, negligible current flows into the inverting input, so that the input current i, resulting from charge q, flows only into capacitor C. Thus q is transferred to capacitor C.

Now, point E is a "virtual earth", so that the p.d. across C is v_{out}

Therefore, with charge q on C.

$$v_{out} = \frac{-q}{C}$$

The output voltage is thus proportional to the charge which has flowed into the input. A reset arrangement such as the FET in Fig. (5.6) will allow the summation of charge over a set period of time. Alternatively a resistor R can be connected across C to provide a discharge time constant. The arrival of a charge q on the input will then give an output pulse of peak magnitude q/C which will decay with time constant RC. Care should be taken in this case that RC is short compared with the intervals between pulses, otherwise C, will not have discharged sufficiently before the next pulse arrives and the pulses will pile up one on top of the other. This can lead to limiting in the amplifier and the loss of pulses at high pulse rates.

It is not so obvious why an operational amplifier circuit is necessary at all in a charge-to-voltage converter; after all, a simple capacitor to earth will work perfectly well, giving V = q/C. The advantage of the charge-sensitive amplifier Fig. (5.8) lies in the fact that the input feeds directly to a virtual earth. Inevitably the input circuit contains stray capacitance, which is subject to variation, due to changes in cable length and even changes in the internal capacitance of the particle detector.

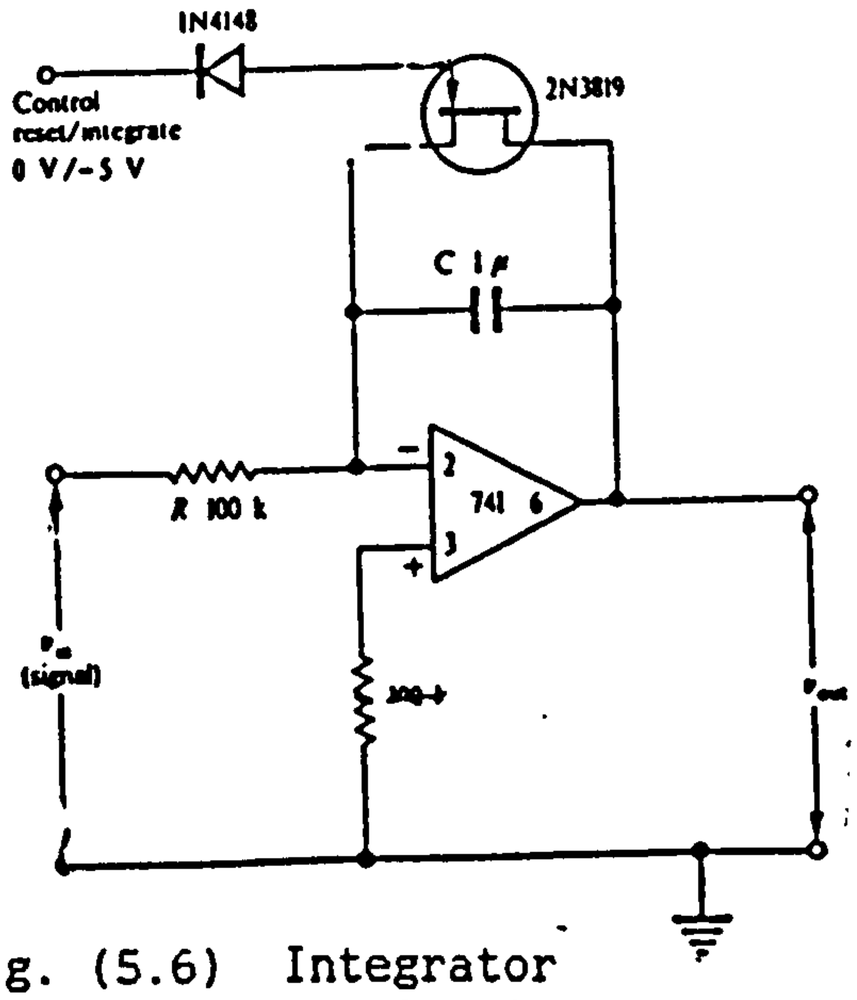

Fig. (5.6) Integrator with FET reset circuit

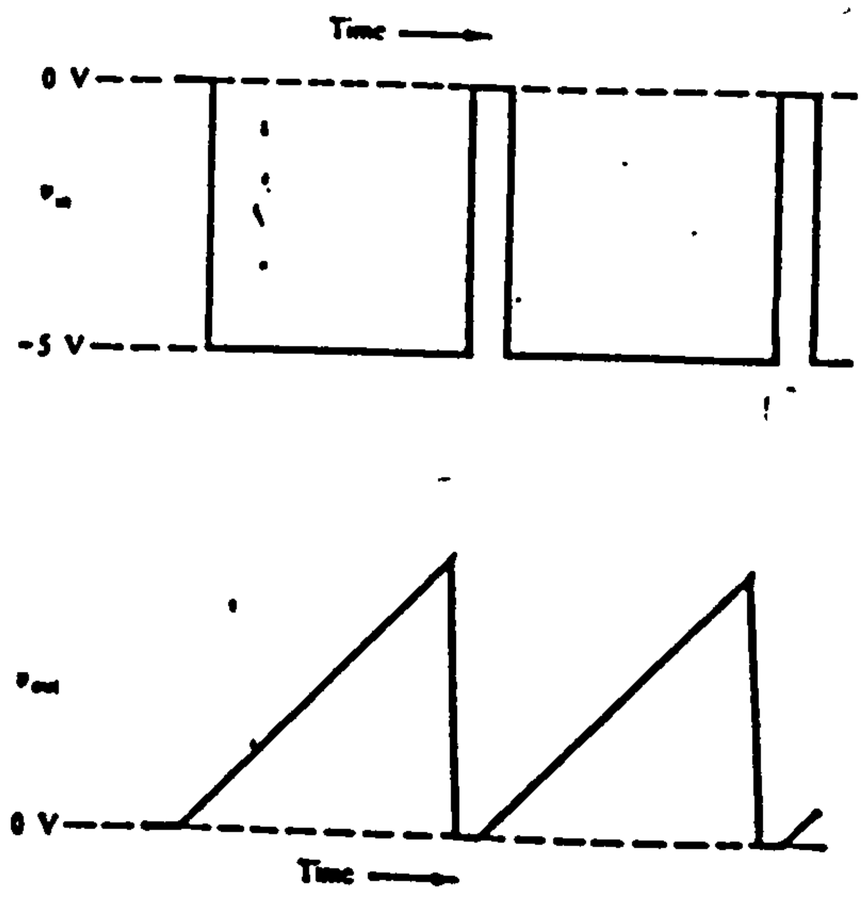

Fig. (5.7) Sawtooth output produced from rectangular wave input by integrator with automatic reset (control point coupled to input).

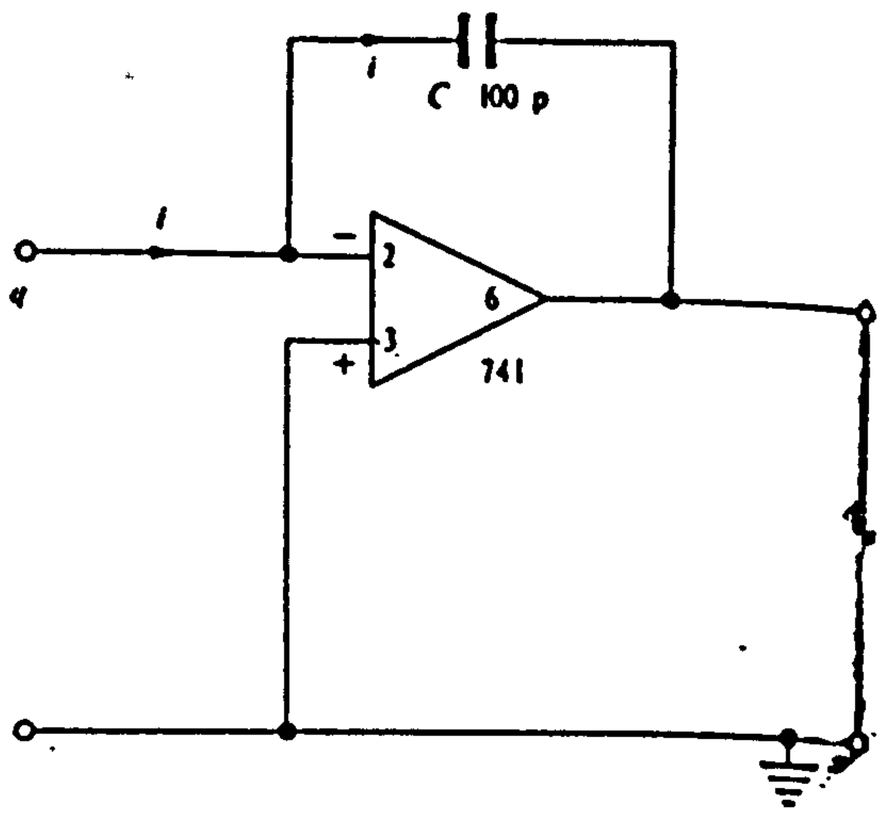

Fig. (5.8) Charge-sensitive amplifier.

This capacitance would be added to the 'known' capacitor converting charge to voltage and could cause errors. With the virtual-earth charge-to-voltage converter, however, the low impedance of the virtual earth swamps the stray capacitances. As with the other operational integrators, the effective capacitance seen when feeding directly into the virtual earth is equal to the value of C multiplied by the open-loop gain of the amplifier. A further advantage of the virtual-earth circuit is that the input device itself does not 'see' the output voltage pulse since the latter appears at the opposite side of the virtual earth. If a solid-state particle detector feeds a capacitor directly, it is possible that the capacitor p.d. might affect the bias voltage on the detector and upset linearity.

5.6 Ioniser

Air ions are electrically charged molecules which occur naturally in the air. They are formed when cosmic rays, ultra-violet light, radioisotopes or other forms of radiation interact with air molecules which either lose an electron (to form a position ion) or gain an electron (to form a negative ion). Ions are also formed by waterfalls, waves, lightning, hot dry winds and thunderstorms. The natural levels of ions and the balance between positive and negative ions vary considerably from place to place and change very quickly. For example, just before a thunderstorm the concentration of positive ion goes up, just after the storm the concentration of negative ion goes up. An air ioniser is an electrical appliance which produces negative ions (it also produces positive ions but this can be suppressed unless wanted too). A variety of ionisers are now available commercially, but all work on the same principle as the one designed and built for this project.

Ionisers are mainly used to clean the air. When lots of negative ions are in the air, smoke, pollen and dust particles in the air become negatively charged. It is thought that they are then attracted to surfaces which are positively charged or earthed. The reduction in the number of particles in the air likely to cause an allergic response could be the way ionisers make people who are sensitive to dust and pollen feel better. The method used is to apply a high negative voltage, several kV in fact, to a sharply pointed emitter. The negatively charged air is repelled from the emitter resulting in an ion breeze. There have been several published designs for air ionizers over the past few years, but no apology is made for offering yet another.

5.6.1 Circuit Design of an ioniser

Previous circuits have, almost without exception, been split into three stages. First of all, the mains voltage is reduced to 12V or so, then rectified and smoothed. Next there is an oscillator driving a transformer to step the voltage back up to a few hundred volts again. Finally, there will be a ladder of rectifiers and capacitors to step the voltage up to a few kV. In the present design as shown in Figure (5.10) the ladder runs directly from the mains. This cuts out the first two stages of the usual ioniser circuit. Larger capacitors will be needed and the final circuit can be run continuously (at 50Hz) for the experiments in this project without problems.

One advantage of the circuit at either 50 or 60 Hz (mains) instead of any other frequency like 50kHz is that 1N4007 rectifiers can be used. Ordinary rectifiers are not too keen to work at high frequencies, the main reason being their painfully slow reverse recovery time, which begins to degrade circuit performance at frequencies as low as 2kHz in the case of a 1N4007. The results of applying a sine wave of increasing frequency to the circuit is shown in Fig. (5.9).

At low frequencies, the output is a half-wave rectified sine wave, as you would expect.

At 2kHz, s small reverse conduction spike is already visible, and by 10kHz conduction does not stop until the input is at about -1.8V. From then on, the situation gets progressively worse. By 1MHz, whatever the 1N4007 is doing, it certainly is not rectifying

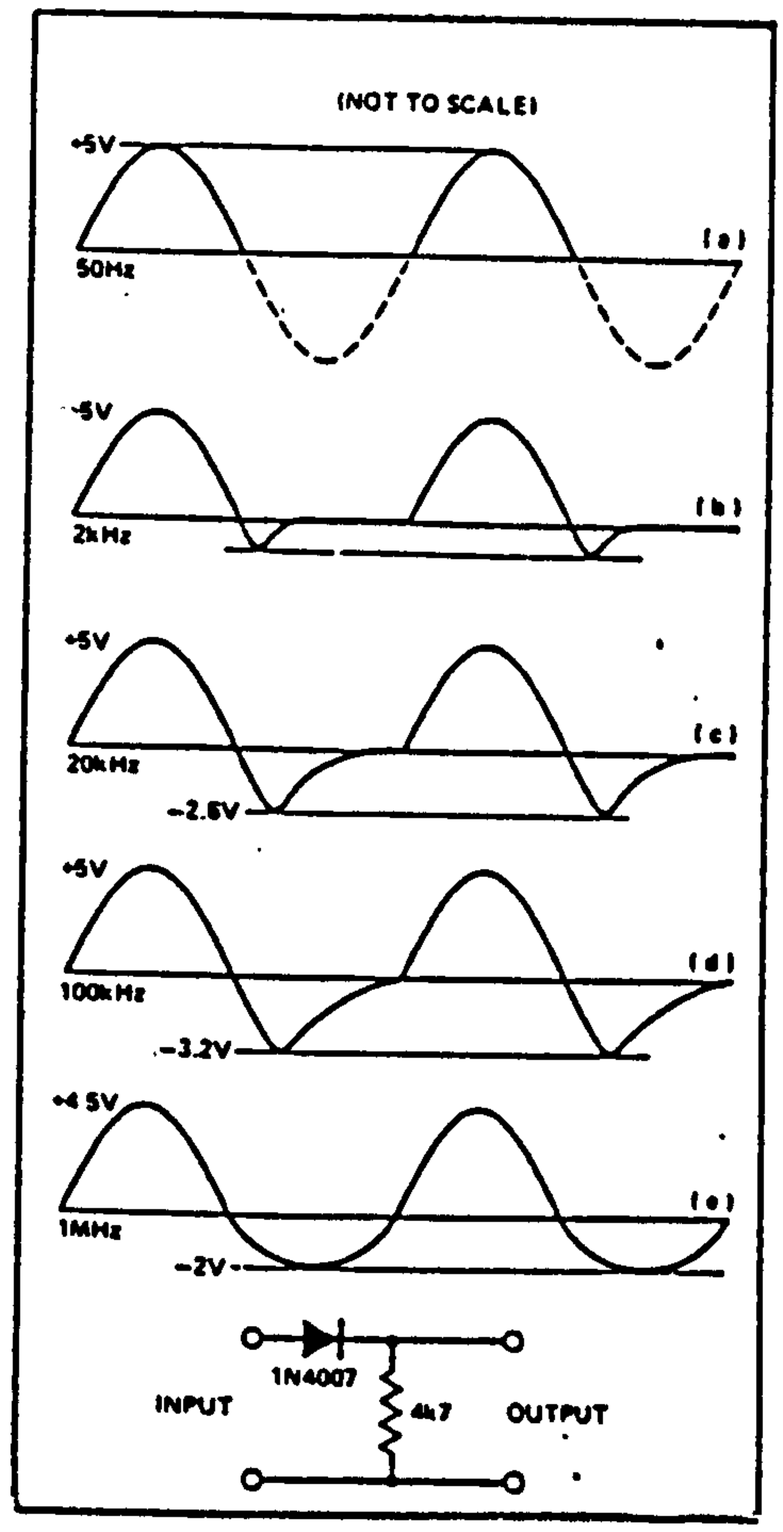

Fig. (5.9) The performance of the rectifier diminishes with frequency

The circuit is a standard Cockroft-Walton ladder network which steps up the mains voltage to -10KV or so (open circuit voltage). When the A.C. input is switched on, C_{16}, C_{17}, C_{18}, ...C_{30} gradually charge up until each has a P.d. of 2Vp (2 x main peak voltage), and since these are in

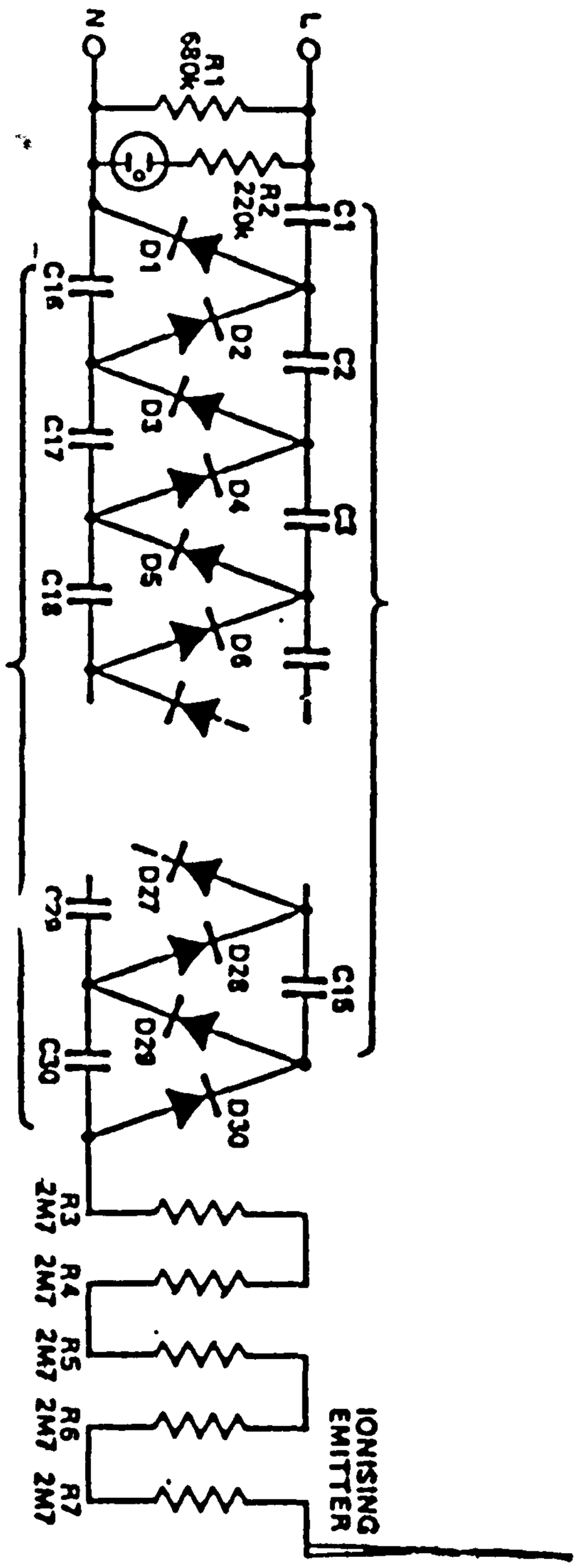

Fig. (5.10) Circuit diagram of an ionizer

series the output is 30 Vp. Capacitors c_1, c_2, c_3 .....c_{15} act as A.C. coupling capacitors, transmitting the A.C. wave to rectifiers D_1, D_3, D_5, so that C_{16}, C_{17}, C_{18}.....C_{30} receive their charge. Therefore the charge will be transferred backwards and forwards from one row of capacitors to the other on each main cycle, but always moving further up the chain because of the action of rectifiers. When all the capacitors are fully charged, there will be a voltage across each of them equal, in theory, to the peak-to-peak voltage of the mains.

In practice, the regulation of this type of circuit is very poor, and the full voltage will never be measured because of leakage, corona discharge, and so on. This nA ionizing current is quite enough to drop the output voltage to about 4kV, which by a strange coincidence is the ideal output voltage for an air ionizer. Voltages above this level tend to produce ozone rather than ions, whereas voltages much lower will not ionize the air efficiently. Touching the emitter directly is enough to reduce the voltage to almost nothing.

Having said that, a word of warning is in order. Although the circuit as a whole has a very high output resistance, individual capacitors do not. The capacitors will retain their charge for some time after the ionizer is unplugged and a painful shock can be received from the back of the PCB unless a leakage resistor is included to discharge them.

This ioniser can also be made to emit + ions than negative electrons if the polarity of the diodes are reversed.

5.6.2 Testing

A simple tester can be made from a 10 nF capacitor and a neon bulb (see Fig. (5.11)). The ioniser is plugged in and if all is well, its own neon lamp will glow; a few seconds later a soft hiss will be heard from the emitter, and the neon bulb on the tester will begin to flash when its free lead is about 1/2" from the emitter; the bulb flashes faster as it is brought closer. (The flashing will not be bright so it will not show up in direct sunlight). It is also very important for the emitter to be sharp pointed otherwise there will be no corona discharge and no hiss will be heard.

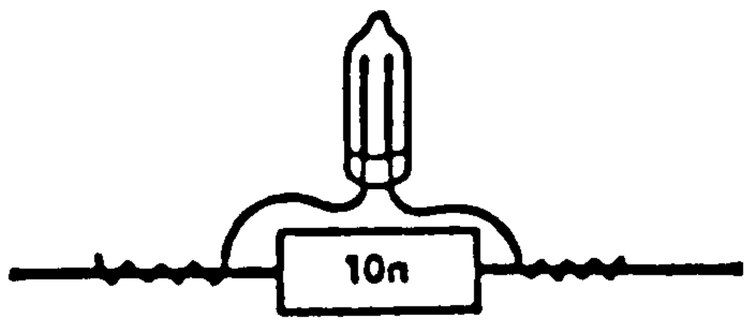

Figure (5.11) Abbreviated circuit of ionizer and a simple tester.

5.6.3 Measurements

Measurements have been made and interpreted from the following standpoint. If negative ions were infinitely long living and moved at a constant speed away from the ioniser in still air, the concentration would vary inversely as the square of the distance from the ioniser. However, some negative ions will combine with positive charges so that not all will reach the boundaries of the room, either as negative ions or attached to negatively charged dust particles. The mobility of negative ions in atmospheric air is approximately 1.7 cm/s per volt/cm of electric field strength, the field being increased by the ions themselves. Typically 10^{13} ions distributed symmetrically about the centre of a sphere of 1 m radius would create a field of 100V/cm at a distance of 1 m from the centre and therefore an ion velocity exceeding

1m/s might be expected 1 m from the ioniser. Since the mean free path of negative ions in atmospheric air is only a fraction of a mm a very large number of collisions of ions with neutral molecules will take place.

The approach was therefore adopted of measuring negative ion flux, i.e. ions/cm - using the apparatus shown in Fig.(5.12) that measures the charge arriving at the metal plate. The results are shown in Figs. (5.13) and (5.14)

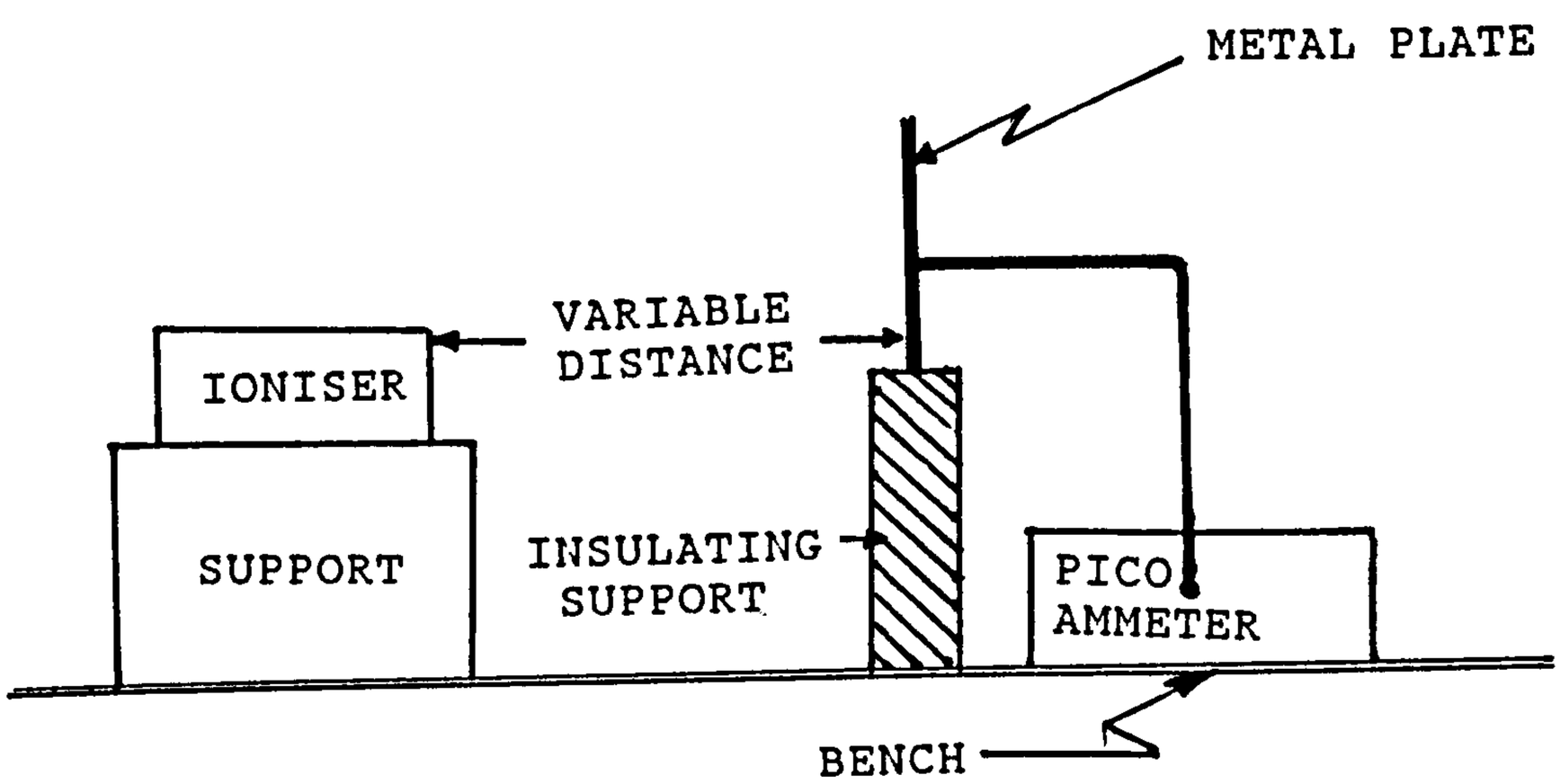

Fig. (5.12) Apparatus used to measure negative ion flux.

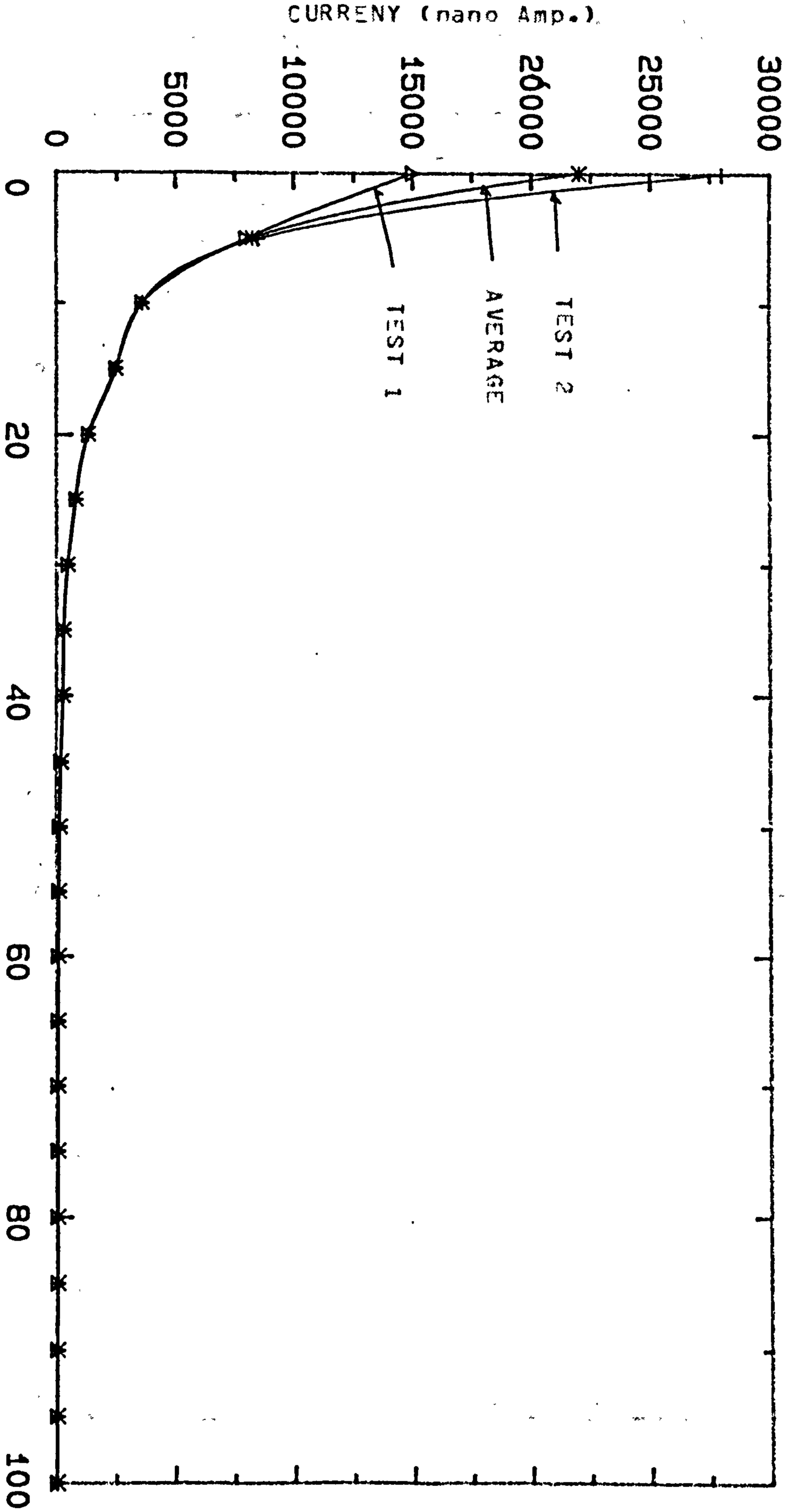

FIGURE (5.14), A GRAPH OF CURRENT AGAINST DISTANCE

FIGURE (5,13), A GRAPH OF ION FLUX AGAINST DISTANCE

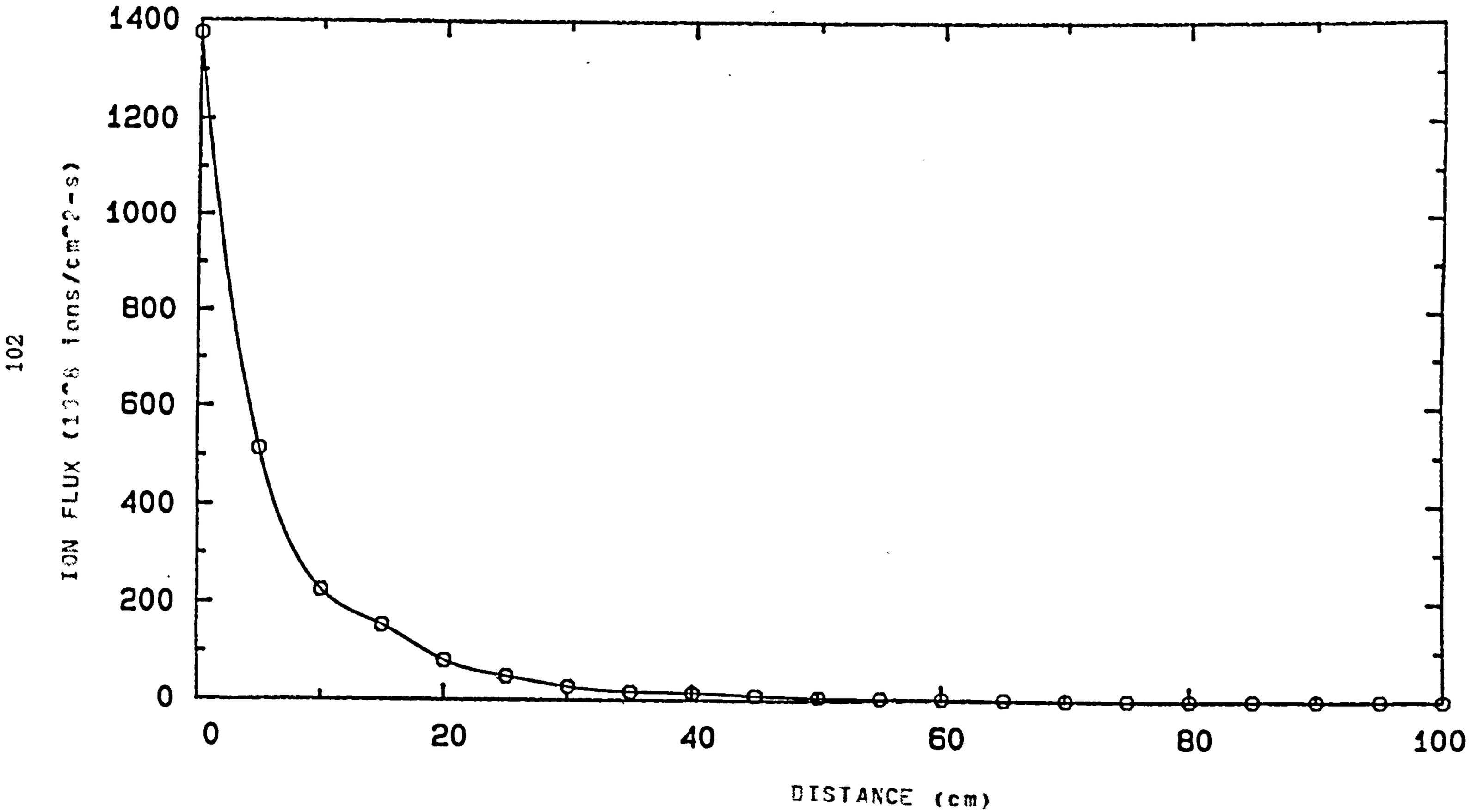

5.7 COMPUTER CONTROLLED OSCILLATOR

It has already been shown that alternating non-uniform electric fields acting on neutral particles can cause pearl chain formations. This is known as dielectrophoresis and has been described in Chapter (2).

Previous work on pearl chain formation for different oscillator frequencies using a single pair of electrodes showed a marked drop in yield over the region of between 2.55 kHz to 3 kHz. This drop is very strongly resonant, and any small change of oscillator frequency would change the number of lone cells in pearl chains. This drop of yield is consistent with resonance conditions in which the geomagnetic field strength satisfies the proton magnetic resonance condition. Unfortunately proton NMR observations are not easy to obtain because they are sharply resonant when working with a manually tuned oscillator. The aim of the work described in this Chapter of the project to design a computer controlled oscillator to ease and help the work of other researchers, working in this laboratory.

The oscillator needs to be computer controlled since the experimenter needs to study the number of pearl chain formations of lone cells.

There are a variety of ways to design a computer controlled oscillator: Two different methods were tried but the author believes the second method has a lot more potential to offer, the reasons being that it is simpler and easier to change, it is driven from the keyboard of a BBC microcomputer, the results may be stored in the memory of the computer by a slight change to the program, so the experimenter may go back to all the frequencies at which the experiments were done and finally, a hard copy printout may be obtained.

Each of these two methods are described, briefly, as follows.

Initially an oscillator was constructed by using a programmable crystal oscillator, an 8-bit synchronous up/down counter; an Eprom and an 8-bit D/A coverter. The programmable crystal oscillator (RS stock no. 301-858) is a standard 16 Pin package and could be used to generate 57 different outputs. Two different base frequency oscillators of 600 kHz and 1 MHz were available giving an output frequency from 0.005 Hz up to 1 MHz. The connections for this crystal oscillator are given in RS Data sheet 5027 (Nov. '84). The counter was an 8-bit synchronous 74193 up/down counter with pre-set inputs and was driven from the previously mentioned crystal oscillator. The outputs of the 8-bit 74193 up/down counter were input to an Eprom 2708. The Eprom was previously programmed to generate the sine output value of any input binary values. The data was programmed into the memory by using the Eprom programmer device in the microprocessor laboratory. There are many different types of Eprom. For example, the 2716 Eprom is an excellent device and requires only a 5V power supply however, its cost is quite high for this laboratory use therefore the smaller, but much less expensive, 2708 was chosen for this experiment.

The final digital sine wave output values were converted to an analog waveform by using a D/A IC (MC140828). Unfortunately this method had a few problems; each time the clock needed to be programmed, or to obtain any other waveform, the Eprom needed to be erased and re-stored with a new set of data to generate the desired waveform. This proved somewhat time consuming and the author decided to use a BBC computer to generate the desired waveform.

A nonlinear sine wave waveform was generated by programming a BBC microcomputer. Obviously, any desired non-linearity can be produced with a microcomputer and a D/A converter. Basically the desired values for each point on a waveform may be stored in a table in the memory and then sent out to the D/A converter (CMOS 4066) in proper order. Complex waveforms require lengthy tables which are somewhat tedious to produce. As an example of this powerful technique, a sine wave was chosen. Fig. (5.15) shows a program which plots and outputs the continuous sine wave digital values using the (?&FE60-61) function. The program is written in BBC Basic language. It has less than 50 statements and can be made to work on any frequency between 400-1600 Hz. It is important to note that the output digital values from the output port needed to be input to a D/A convertor. ss described in the next part of this Chapter.

```
10 HIMEN=&2000
20 DIM PROG 200
30 ?&FE62=255
40 FOR I=0 TO 2 STEP 2:P%=PROG
50 [OPTI
60 .WAVE
70 LDA £0:STA &70:LDA £&20:STA &71
80 .CYCLE
90 LDY £0
100 LDA (&70),Y
110 BEQ WAVE
120 STA &FE60
130 CLC:LDA &70:ADC £1:STA &70
140 LDA &71:ADC £0:STA &71
150 JMP CYCLE
160 ]
170 NEXT
180 MODE7:PROCtitles
190 I=0
200 REPEAT
210 A=A+F2
220 B=SIN(A)+1
230 C=B*127.5
240 C%=(C*Amp)/100
250 IF C%=0 C%=1
260 ?(&2000+I)=C%
270 I=I+1
280 UNTIL A>2*PI
290 PRINT TAB(10,20);"WE'RE OFF";SPC(20)
300 ?(&2000+I)=0
310 CALL WAVE
320 DEF PROCtitles
330 *KEY10 OLDIMRUNIM
340 PRINT TAB(8,1);CHR$(141);"SINE WAVE GENERATOR"
350 PRINT TAB(8,2);CHR$(141);"SINE WAVE GENERATOR"
360 PRINT TAB(2,5);"AMPLITUDE PERCENTAGE="
370 PRINT TAB(2,6);"FREQUENCY HZ(400-1600)="
380 PRINT TAB(10,20);"PRESS BREAK TO EXIT"
390 PRINT TAB(27,5)
400 INPUT Amp
410 IF Amp<1 OR Amp>100 GOTO 390
420 PRINT TAB(27,6);:INPUT Fre
430 IF Fre<1 GOTO 410
440 DIG=52945/Fre
450 F2=2*PI/DIG
460 PRINT TAB(10,20); "PLEASE WAIT A MOMENT"
470 ENDPROC
```

Fig. (5.15) Sine waveform generator programme

5.7.1 Using a D/A converter with a microcomputer

Digital to analog (D/A) conversion is basically simple: each bit is given its appropriate analogue value and the outputs summed up in an analog order. There are many D/A converter IC's, such as the MC1408 (see Appendix (2)). However, this part of the experiment used two 4066 CMOSS chips because of their ready availability. Figure (5.16) shows the 8-bit D/A converter designed for direct connection to the output port of the BBC micro.

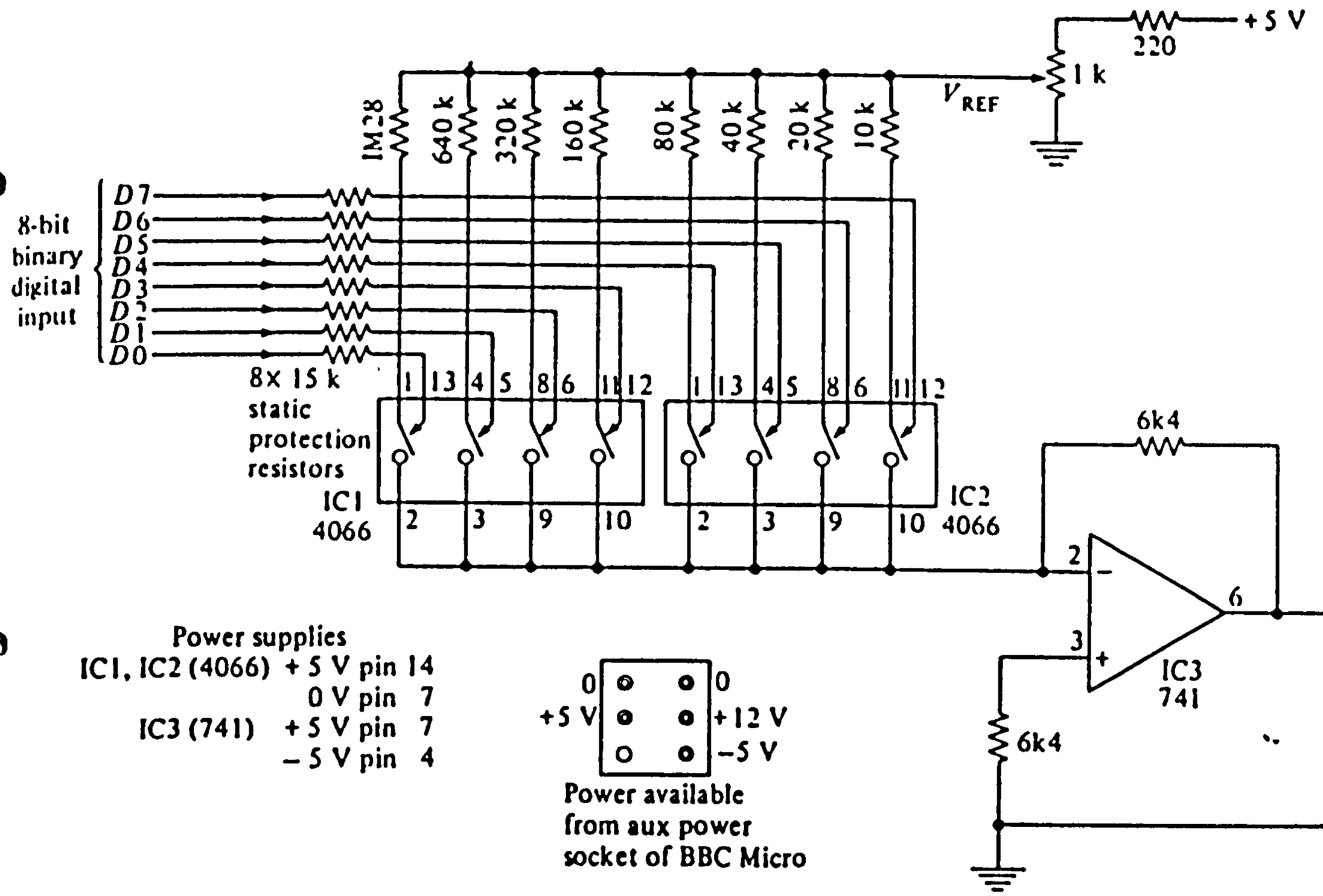

Fig. (5.16) Experimental 8-bit digital to analogue coverter

It was designed to be powered by + 5V supplies which are available from the BBC Micro auxiliary power socket. The two 4066 CMOS chips provided eight analogue switches which connected the appropriate input resistors to the virtual earth adder according to the logic state of the input bits. Calibration was determined by the reference voltage V_{REF} and adjusted by RV1. Each input resistor value was determined by the inverse of the 'weight' of the bit which switches it. Thus the 'LSB' resistor (IM28) was 128 times the value of the 'MSB' resistor (10k). The feedback resistor was chosen here so that the analogue output voltage Vo is given by

$$Vo = - \frac{V_{REF}}{100} \times D_{IN}$$

where D_{IN} is the decimal equivalent of the digital value (0 to 255)

With this circuit connected to an output port, a binary countup or countdown produces a linear ramp analogue output. Sine and cosine functions have already been displayed on an oscilloscope by using the computer to generate the function in the first place, as described earlier in this Chapter.

It is useful to note that the analogue output is proportional to the product of the digital input and the reference voltage. Most D/A converters have therefore an inherent ability to multiply an analogue voltage by a digital input. Some D/A converters are optimised for this application such as the multiplying D/A converter (MDAC), which is useful for the accurate digital control of analogue gain in a variety of applications.

5.8 Class AB emitter follower

For observations of possible effects of A-C magnetic fields on saline or water at high frequencies, an emitter follower was constructed. The details of such observations are explained in Chapter (10). The emitter follower was a complementary Darlington Class AB type as described below.

5.8.1 Class B and class AB push-pull operation

The reason for maintaining a quiescent current in the emitter follower is in order that the load current can swing both up and down to cope with the positive and negative half-cycles of the a.c. signal. With reference to the circuit of Fig. (5.17) where there are two complementary transistors: the NPN one handles the positive half-cycles and the PNP the negative half-cycles. This type of circuit is said to operate in Class B; each transistor handles only one signal polarity and the quiescent current can therefore be zero. It is sometimes known as push-pull output because T_2 'pushes' the negative half-cycles from below and then hands over to T_1 to 'pull' the positive half-cycles from above.

The Class B circuit is defined as one where the transitor operating point is chosen so that conduction only occurs for half the input cycle. This is contrasted with the class A mode, which applies to most voltage amplifier circuits, where the transistor is conducting at all points in the input cycle.

As might be anticipated from its simplicity, the circuit of Fig. (5.17) is inadequate for our application where low distortion is required. Each transitor requires about 0.6V across its base-emitter

junction before it begins to conduct significantly, so that small signals (‹1Vp-p) are not transmitted at all. The circuit will work with larger signals, but produces the crossover distortion shown in Fig. (5.18). Near the zero crossing of the wave, the gain drops to zero, resulting in the severe 'kink' shown.

Although the simple circuit of Fig. (5.17) is suitable for certain servocontrol applications, it needs improvement for our case, where high currents are needed. Some bias must be supplied to the transistors in order that the base-emitter junctions are ready to conduct on the smallest input signals. To obtain linear performance, it is usual to bias the transistors so that, even with no input signal, they are conducting a small quiescent collector current. For small signals, the stage is then operating in class A, with both transitors conducting, whilst, for larger signals, only one transistor will be operating on each half of the waveform. This mode of operation is termed class AB.

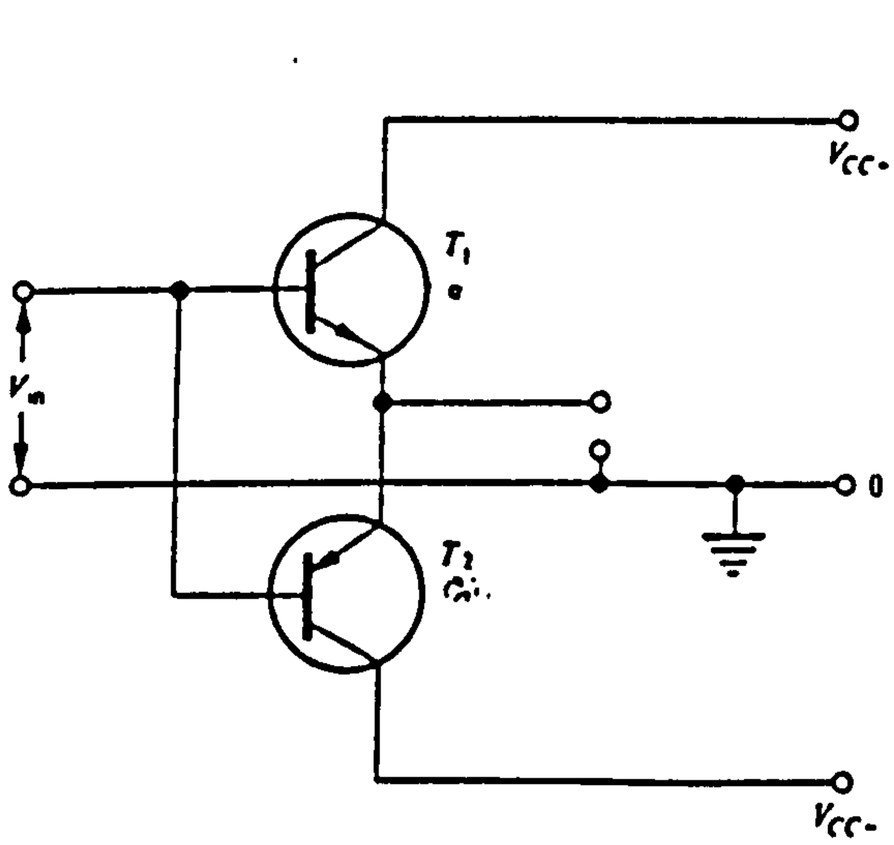

Fig. (5.17) Rudimentary class B complementary emitter follower.

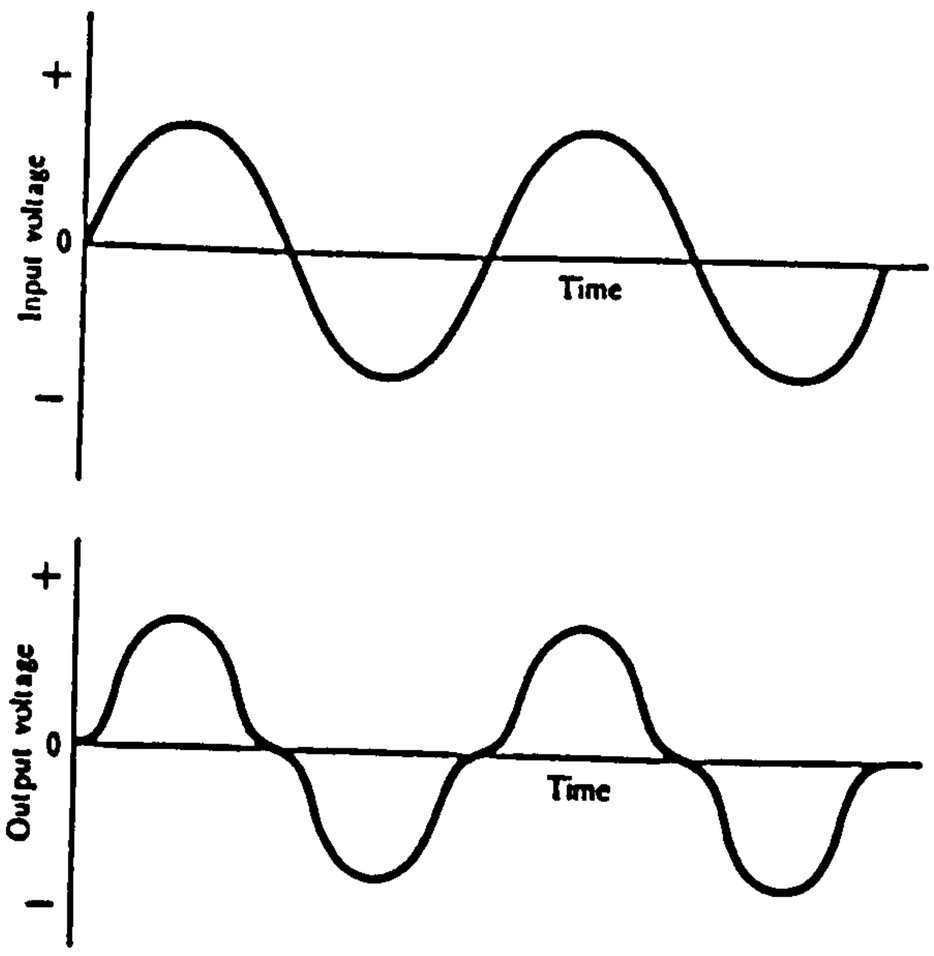

Fig. (5.18) Typical input and output waveforms from Fig. (5.18) showing severe distortion.

Fig. (5.19) shows the simple class B circuit modified for class AB operation. Instead of being connected together directly, the two bases are separated by a pair of forward-biased diodes, D_1 and D_2, which provide just sufficient bias to make the transistors conduct under quiescent conditions. Emitter resistors R_3 and R_4 provide a degree of current feedback to improve d.c. stability.

As with all class AB amplifiers, the quiescent conditions are closely dependent on the forward p.d. of the transitor base-emitter junction (V_{BE}). A small change in V_{BE} due to a change in temperature can produce a large change in quiescent collector current. The use of diodes to supply the bias provides temperature compensation; if the ambient temperature rises, producing a fall in V_{BE}, then the diode p.d. will also fall, keeping the base current, and hence the collector

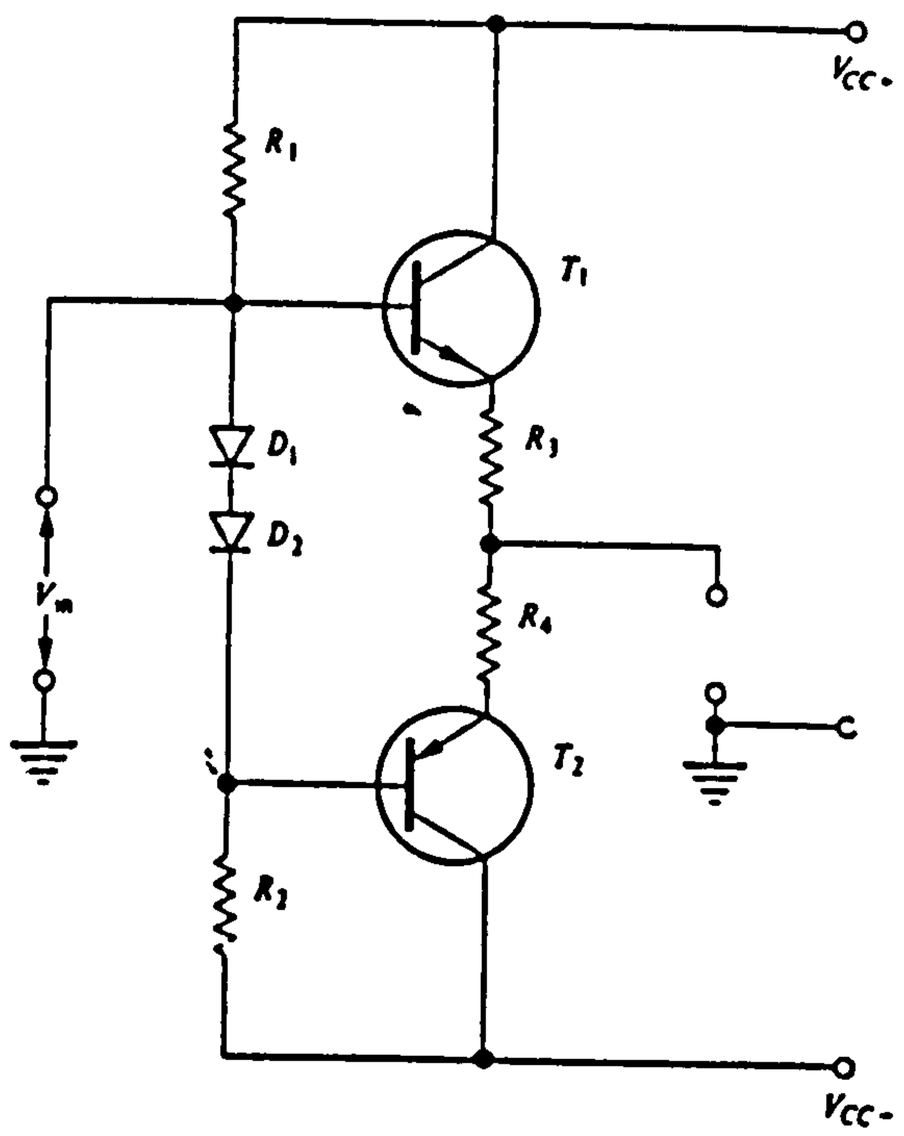

Fig. (5.19) Class AB complementary emitter follower.

current relatively constant. Ideally, the diodes are sited close to the transistors in order to be subject to the same temperature fluctuations.

In order to accommodate variations in transistor V_{BE} it is desirable to be able to adjust quiescent current manually to the required value. The modification of Fig. (5.20(a)) provides this facility. The bias voltage is derived from a transistor (T_3) in a 'V_{BE} multiplier' circuit shown in isolation in Fig. (5.20(b)). This latter part of the circuit is really a small voltage amplifier, with its own V_{BE} as input and having negative feedback applied via the potential divider R_x and R_y. Here feedback fraction $\beta = R_y/(R_x + R_y)$. The output V_{BIAS}, is therefore given by

$$V_{BIAS} \sim \frac{V_{BE}}{\beta} = \frac{V_{BE}(R_x + R_y)}{R_y}$$

In the circuit of Fig. (5.20(a)), potentiometer R_3 is adjusted for a quiescent current. Temperature compensation is again present because the V_{BE} of T_3 will change by the same factor as the V_{BE} of T_1 and T_2

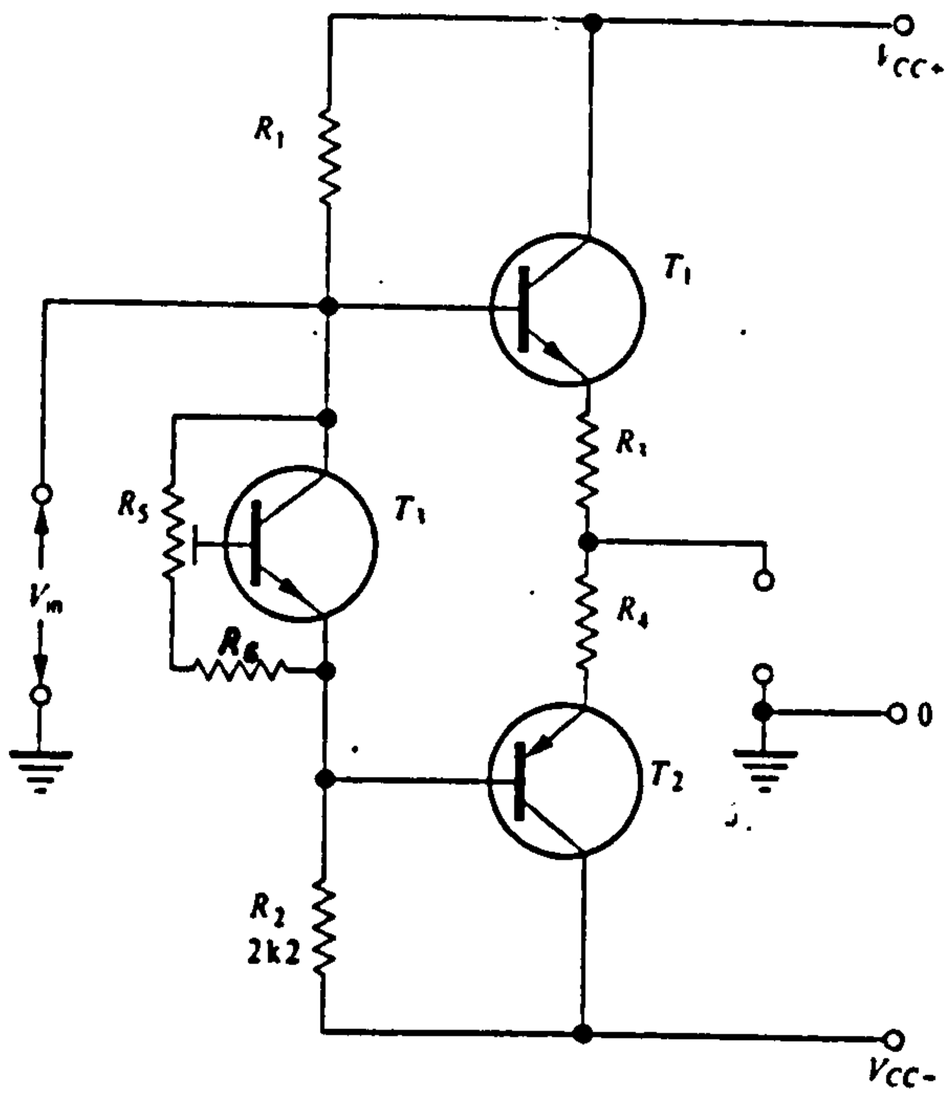

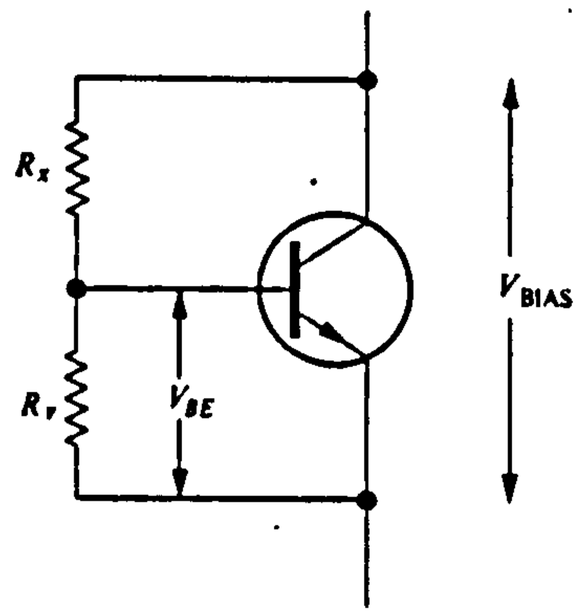

Fig. (5.20(a) Class AB complementary emitter follower with bias provided by a V_{BE} multiplier. The latter is shown separately in (b)

Where higher powers are required power transistors are used, usually in the complementary Darlington arrangement of Fig. (5.21). This circuit will safely give at least 3 A to the load. Quiescent current should be set to about 40 mA. The advantage of the complementary circuit is that the bias p.d. needs only to be $2V_{BE}$ instead of the $4V_{BE}$ that would

otherwise be required; this leads to improved thermal stability.

Resistors R_7 and R_8 across the base-emitter junctions of the power transistors improve high-frequency response by providing a path for the current carriers that would otherwise linger in the base region on turn-off. This circuit was constructed to study the effect of high frequency A.C signals on ice crystals as described in Chapter (10).

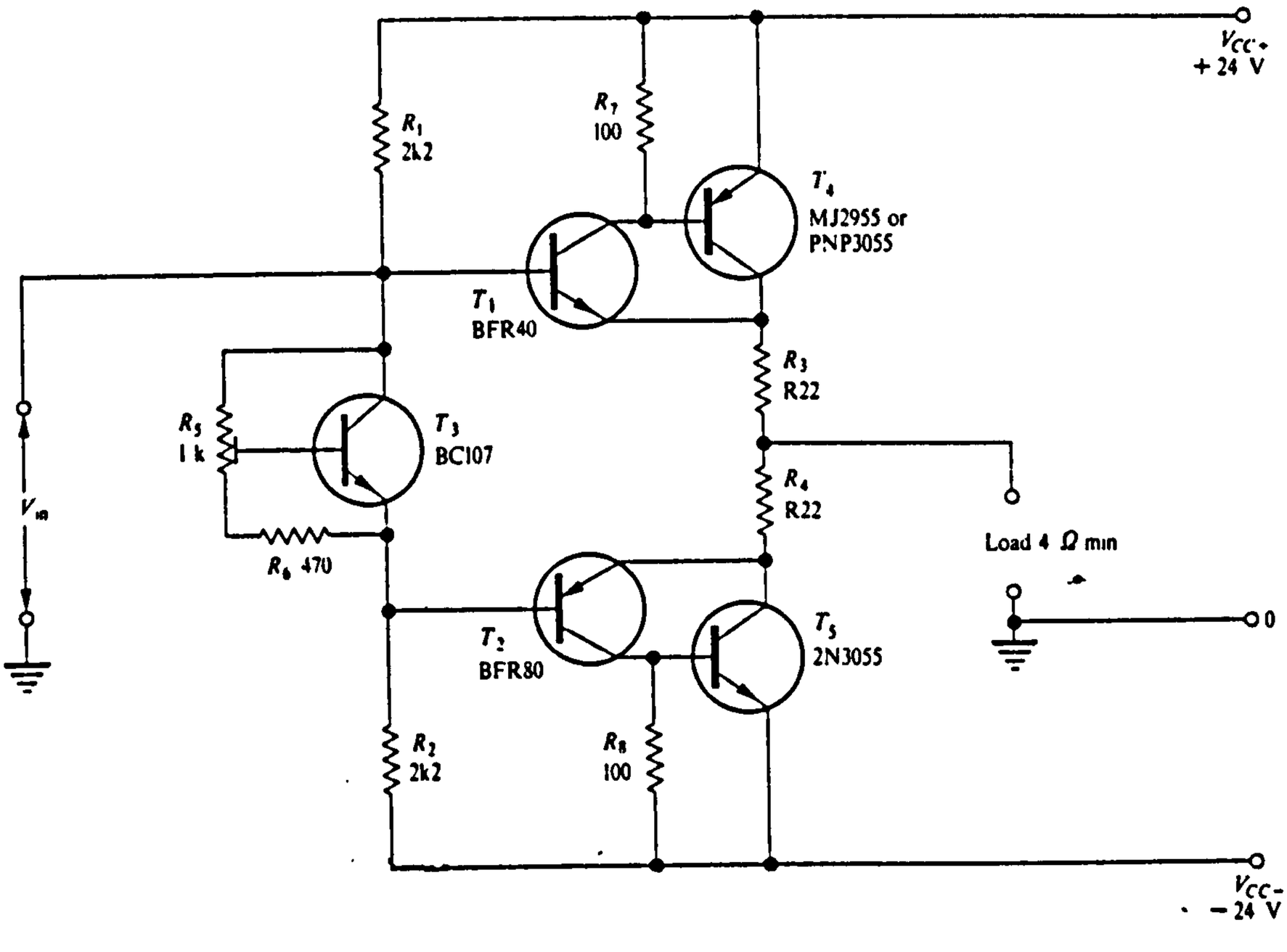

Fig. (5.21). The Complementary Darlington class AB emitter, giving 3 A output capability, used for this project (details of the experiment are given in Chapter (10)

CHAPTER 6

CONSTRUCTION OF THE ELECTRON BEAM GUN

6.1 Introduction

This part of the programme aims to study the effects on cellular adhesion of Leishmania parasites (L.major) cells of e-bombardment of polystyrene petri dishes. The first step was the construction and operation of an electron gun.

It was also intended to focus the electron beam produced by such a gun into a fine beam for localised bombardment of the polystyrene petri dishes. The electron gun as constructed had to be a low energy electron gun in view of the fact that at high voltage X-rays are generated in the apparatus which are hazardous to persons nearby and difficult to screen in a confined space. However, measurements were taken using a gun which did cover high energy levels as well as low. This high power electron gun differs in design from that constructed for low energy, and, whilst existing in the Department, was not always easily made available for this project.

6.2 Requirements for constructing the electron gun

An electron gun is a device which accelerates, controls and focusses a beam of electrons. The requirements of any electron gun are:

a) An electron source which usually consists of a heated filament of tungsten on tantalum acting as a cathode and a source of free electrons.

b) A potential difference to accelerate the free electrons from the source towards the anode, this potential difference is maintained between the source and the anode.

c) An electron optical system which accepts a broad beam of electrons and focuses them onto a target.

The electron gun is operated in a high vacuum below 10^{-4} torr where the control of the beam is easier and the density higher.

There are many varieties of electron gun which could be used for beam generation at different energies. Simpson and Kuyarr [1] have designed an electron gun which supplies 10A of current at 30 eV. They used a multi-stage technique in which electrons are extracted from a source and are subsequently decelerated to the required final energy.

The present gun design is similar to one designed by Pierce [2], which supplies (100-150) mA current at (2-10) KeV. This gun has high efficiency ~ 99.5-99.99% and operates with a space-charge limited cathode which produces a uniform current density over the beam.

The electron gun used in this project is based on a two piece gun of the above design and is shown in Fig. (6.1).

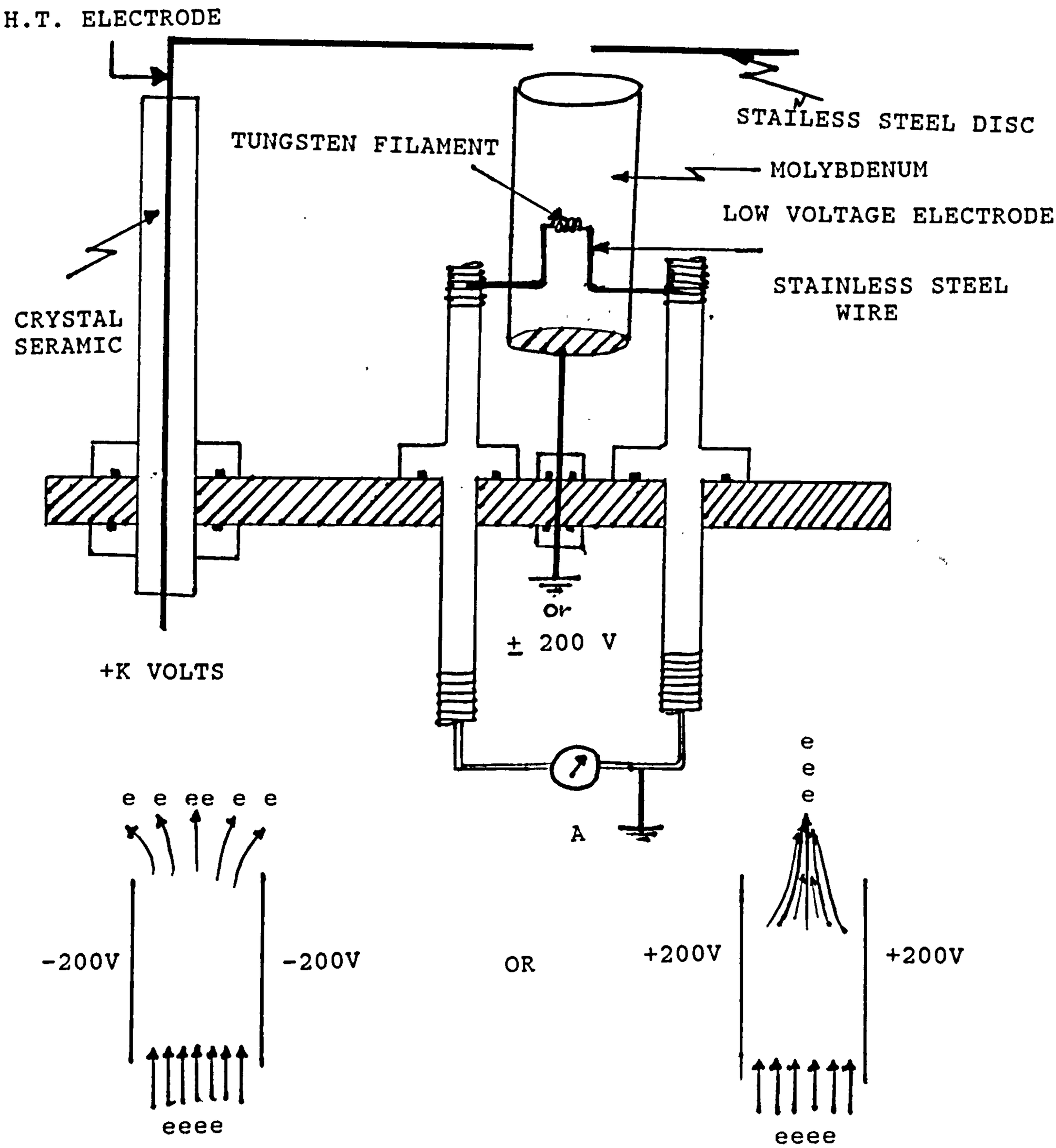

Fig. (6.1) Schematic diagram of an electron gun constructed in this project

There are two electrodes, one based to several thousand volts positive

(HT), while the other is held at ground or + 200 volts.

The high voltage electrode is manufactured from non-magnetic stainless steel while the lower voltage electrode is cylinder shaped around the cathode and is manufactured from molybdenum.

A tungsten wire (ϕ = 0.1) mm, 0.8 cm length is used for the filament because of its high melting point and low volatility; it requires a current of 6A at 7 volts a.c.

Each end of the filament wire is spot-welded to stainless steel wire (ϕ = 0.8 mm) and the whole of it is mounted on a ceramic disc with central holes as shown in Fig. (6.2).

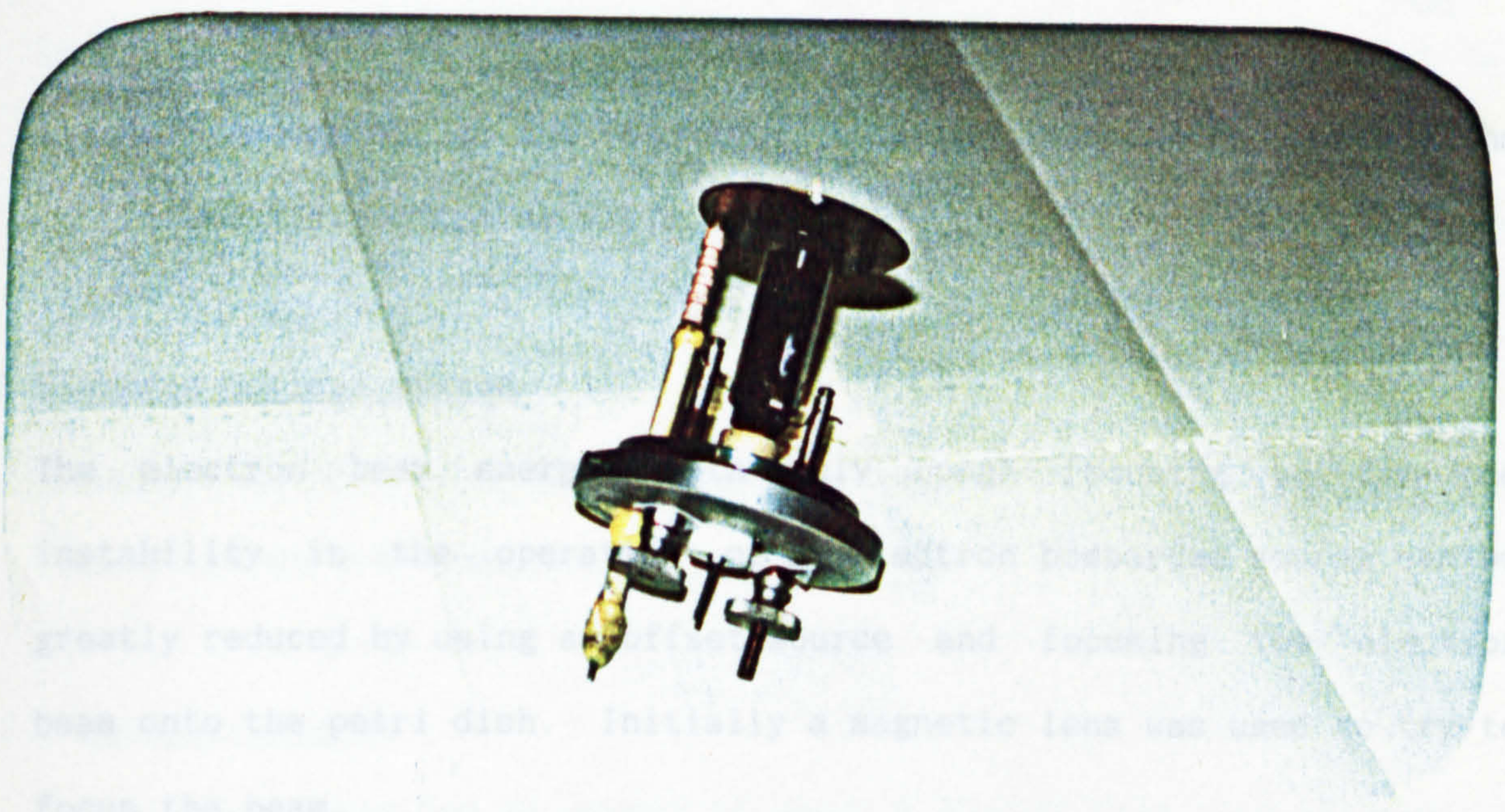

Fig. (6.2) Filament picture

The electrodes and filaments are mounted onto the back flange by ceramic which isolates the electrodes from each other.

There were difficulties with the design of the electron gun which needed to be corrected; these are summarised below:

1) Breakdown between the high voltage electrodes and the flange of the vacuum chamber

2) Insulation problems which arose because the insulators cracked after only a small amount of use of the gun. It is important to heat the fabricated ceramic to a high temperature in air which hardens it and evaporates any water vapour from within the ceramic structure.

3) Short running life of the filament (~ 6 hours). This caused problems because, to change the filament, the electron gun had to be dismantled. This problem was solved by modifying the design of the filament (as shown in Fig. (6.2)).

4) Heat produced by the filament. This was improved by changing the filament structure as explained in (3)

6.3 Electron optical system

The electron beam emerges with only rough focusing because the instability in the operation of an electron bombarded source can be greatly reduced by using an offset source and focusing the electron beam onto the petri dish. Initially a magnetic lens was used to try to focus the beam.

6.3.1 Magnetic lens

A thin magnetic lens was used to focus the electron beams. It was placed symmetrically between the object and the image. A static magnetic field does not change the kinetic energy of the electron but changes only the curvature of the path. This depends on the direction of the movement of the electron and the direction of flux of the

magnetic field (See section (3.3.2.1)).

800 ampere-turns was employed. A single copper wire was used with diameter 0.8 mm. It was wound on a cylinder yoke, having an inner diameter 8.4 cm, outer diameter 10.2 cm and length 4 cm. The number of turns was nominally 400 (8 layers each 50 turns). The total magnetomotive force H_M generated by the coil was

$$V_M = nI. \qquad \text{Equation (6.1)}$$

If all the flux along the axis is concentrated between the object and image, it gives high efficiency, hence the dimensionless factor $\frac{Br}{\mu NI}$ has been termed the focusing efficiency under given geometrical conditions, where B is the flux density of the magnetic field, r is the radius of curvature of the path of electrons, n is the number of turns, I is the current and μ is the permeability.

This expression indicates the number of ampere-turns required to focus rays of given momentum (Br)e.

6.3.2 Phosphor screen

The electron beam had an energy of about 5 kV and this is sufficient to make a bright spot on a phosphor plate bombarded target. During the experimental work outlined in this chapter a phosphor coated plate was used to check the focus of the electron beam. The preparation of the phosphor screen is as follows:

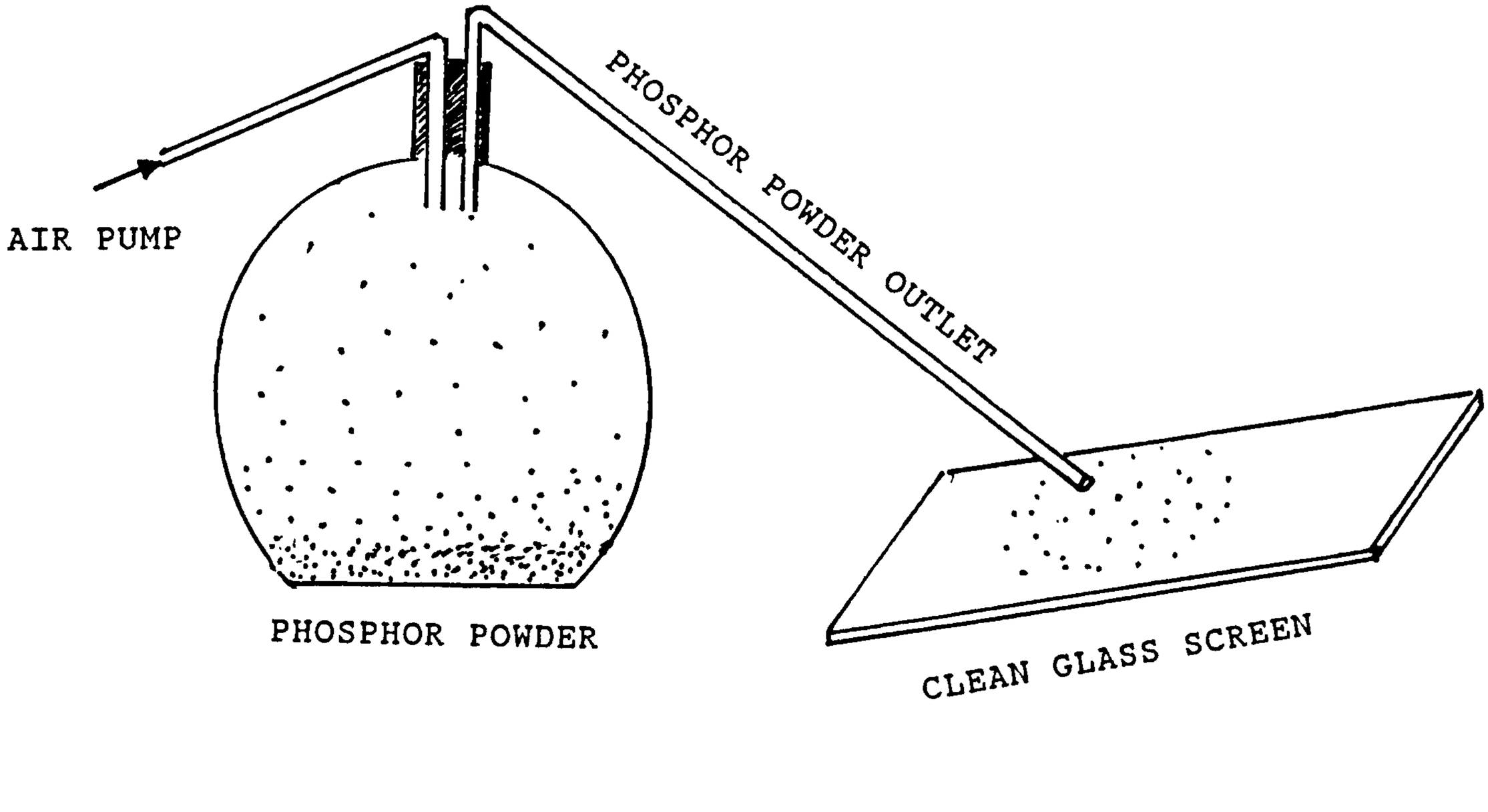

Fig. (6.3) A basic diagram to prepare the phosphor screen

6.3.2.1 Preparation of the Phosphor Screen

A uniform layer of phosphor powder was deposited on a glass slide by the following method.

A few drops of a solution of 1 : 9 phosphoric acid in methanol were thinly spread on the surface of the substrate (the glass slide) to act as an adhesive.

The phosphor powder was then scattered over the glass slide using an air jet as shown in Fig. (6.3).

To make sure the sample was clean and dust particle free, the whole process was performed in a fume cupboard in a clean room.

6.4 Experiments

The system used in the present work consisted of a vacuum chamber which was evacuated by a diffusion pump backed by a rotary pump. A Penning gauge was attached to the chamber to measure the pressure. The operating pressure was varied from 1 x 10^{-5} to 0.4 x 10^{-4} torr. A diagram is shown in Figure (6.4).

The electron gun was mounted on top of the 15 mm thick glass chamber and all the electrodes were held together by a stainless steel base. The high tension electrode and molybdenum anode cylinder were insulated from each other by ceramic washers and were fixed to the base of the electron gun (stainless steel) by means of rubber 'O' rings. The ceramics were all prepared and machined by the Department's workshop and were then heated to a high temperature (above 150°) to be hardened. Either a pin point or multi-strand (1 cm length) helical filament was constructed from tungsten 2 mm diameter. The filament was mounted between two 0.8 mm diameter stainless steel wires. These were then connected to two insulated current feed-throughs.

The uniformity of the beam was measured by a probe composed of two plates 1 cm apart and insulated by ceramic spacers. The front plates consisted of two stainless steel plates ϕ = 2.5 cm and 0.5 m apart as shown in the diagram (Fig. (6.5)). The probe was connected to the stainless steel bar which is mounted via the glass chamber placed near the bottom of the chamber.

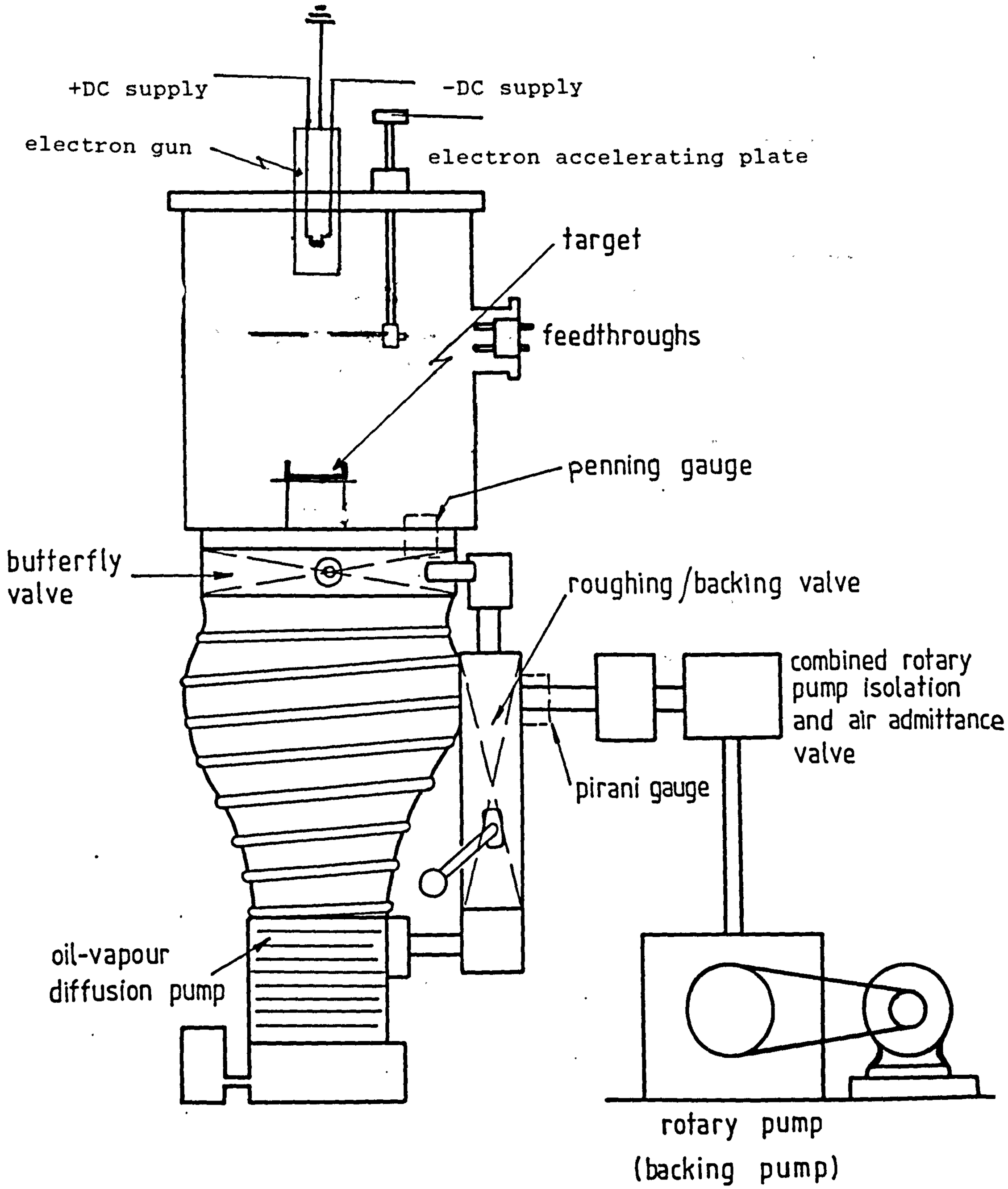

Fig. (6.4) Whole electron gun system

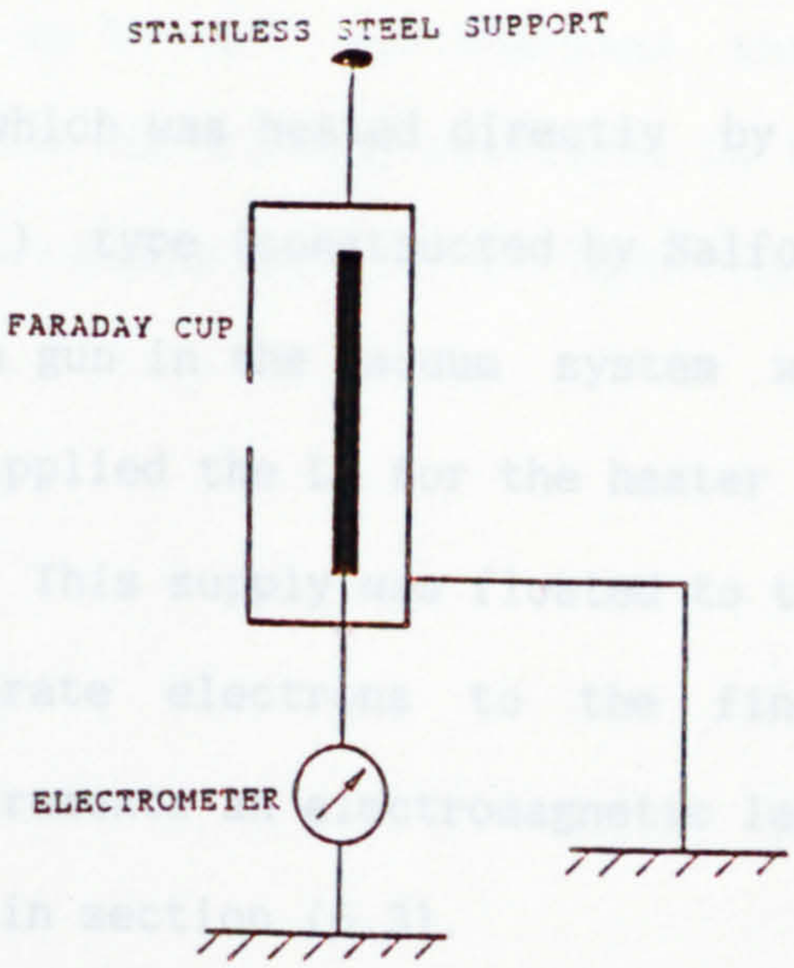

Fig. (6.5) The Probe

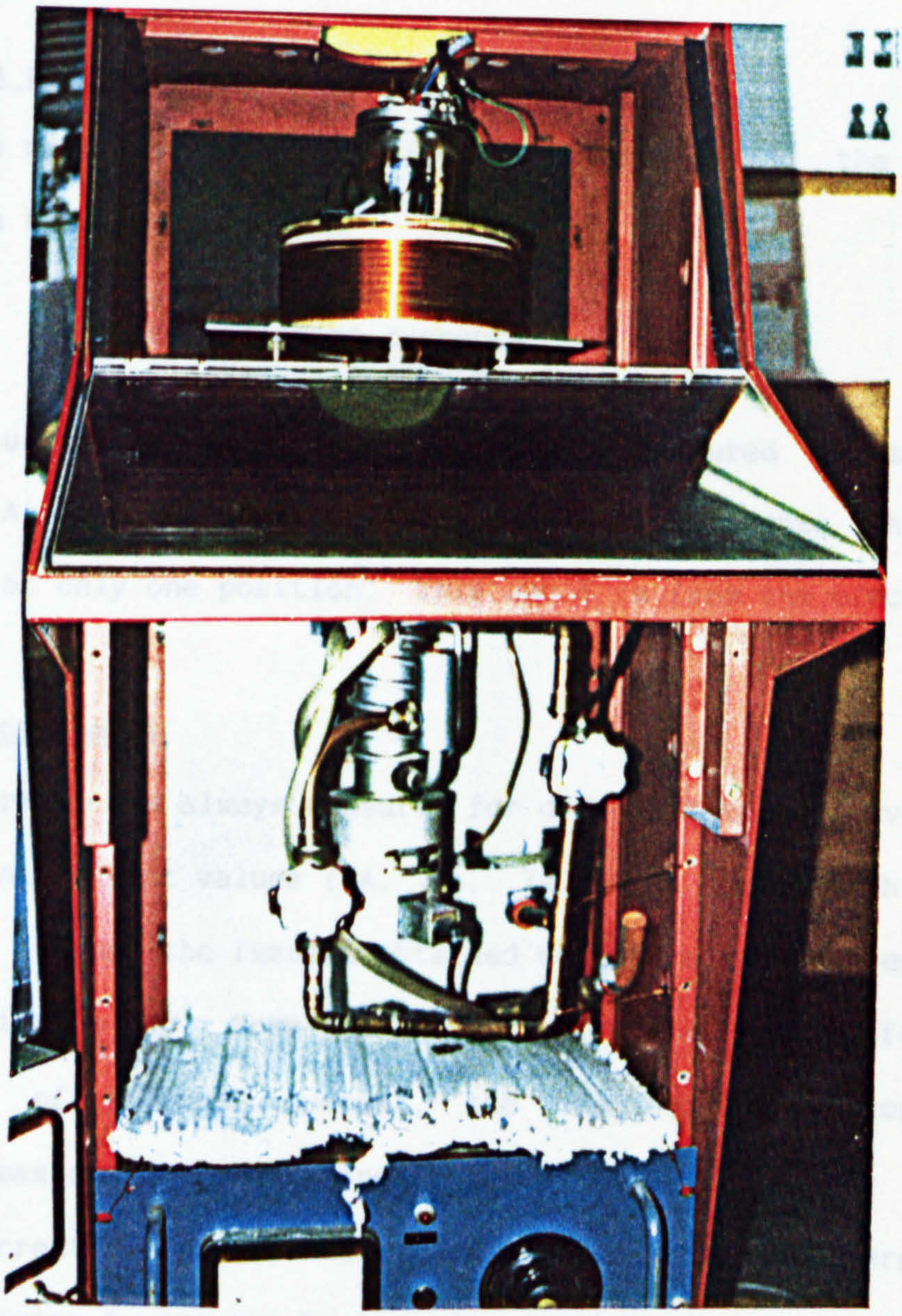

Fig. (6.6) Picture of electron gun with magnetic lens

6.5 Operation of the Electron Gun

Electrons were drawn from the filament which was heated directly by a constant current source (A.C + D.C.) type (constructed by Salford University). Connection to the electron gun in the vacuum system was made by two insulated HT leads which supplied the LT. for the heater to maintain the constant current emission. This supply was floated to the negative high voltage required to accelerate electrons to the final energy. During the electron beam measurements an electromagnetic lens was used to focus the beam as described in section (6.3).

6.6 Measurements on the Electron Gun

Measurements were carried out to find the uniformity and the size of the electron beam for different

a) Energies
b) Filament currents
c) Vacuum pressure

The beam current distribution was always measured in a vertical direction. A probe was used to make these measurements which were carried out at only one position. This was 5 cm from the electron gun.

6.6.1 Beam current/Energy

The beam current was always measured for different energy levels for a fixed filament current values (4A, 6A, 7A and 8A - see graph (6.1)). Graph (6.1) shows the results obtained while the vacuum pressure was held at 1 x 10^{-5} m bar. From the graph it is clear that for every fixed value of filament current, the beam current is proportional related to beam energy. Any increase in energy will directly increase the beam current. However, it is necessary to keep the energy at low voltage otherwise X-rays may be introduced which are hazardous to the operator and need protective shielding.. Because of this problem this

electron gun was used only for energies up to 5kV. For energies above 5kV different electron gun was used, this was already available in the Department and it had a stainless vacuum chamber with a 1 inch thick lead glass window for X-ray shielding.

GRAPH (6.1), A graph of beam current against energy

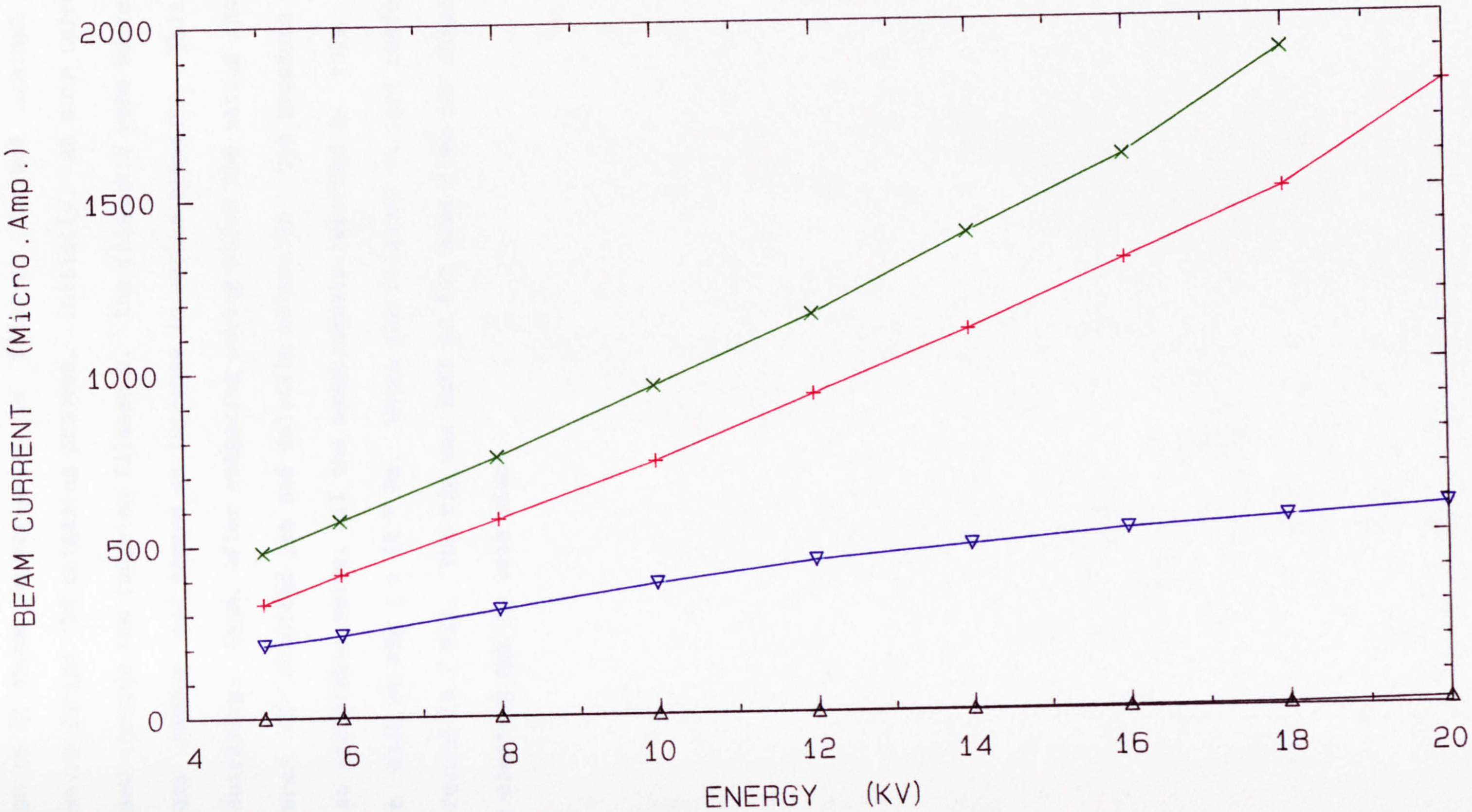

Graph (6.2) shows the variation of filament current against vacuum pressure during the outgasing process. Initially, as more current was passed through the tungsten filaments, the filaments were heated more, became redder and caused an increase in vacuum pressure. This is due to outgasing; then, after outgasing during which the vacuum chamber is cleared of absorbed gas and volatile molecules, the pressure dropped to an acceptable value. All the measurements reported in this chapter were made at the 1×10^{-5} Pa. Where the filament current needed to be increased to 7 Amp, the rig was left on for some time for outgasing of the electron gun to take place.

GRAPH (6.2) A graph of filament current against vaccum pressure during outgasing process.

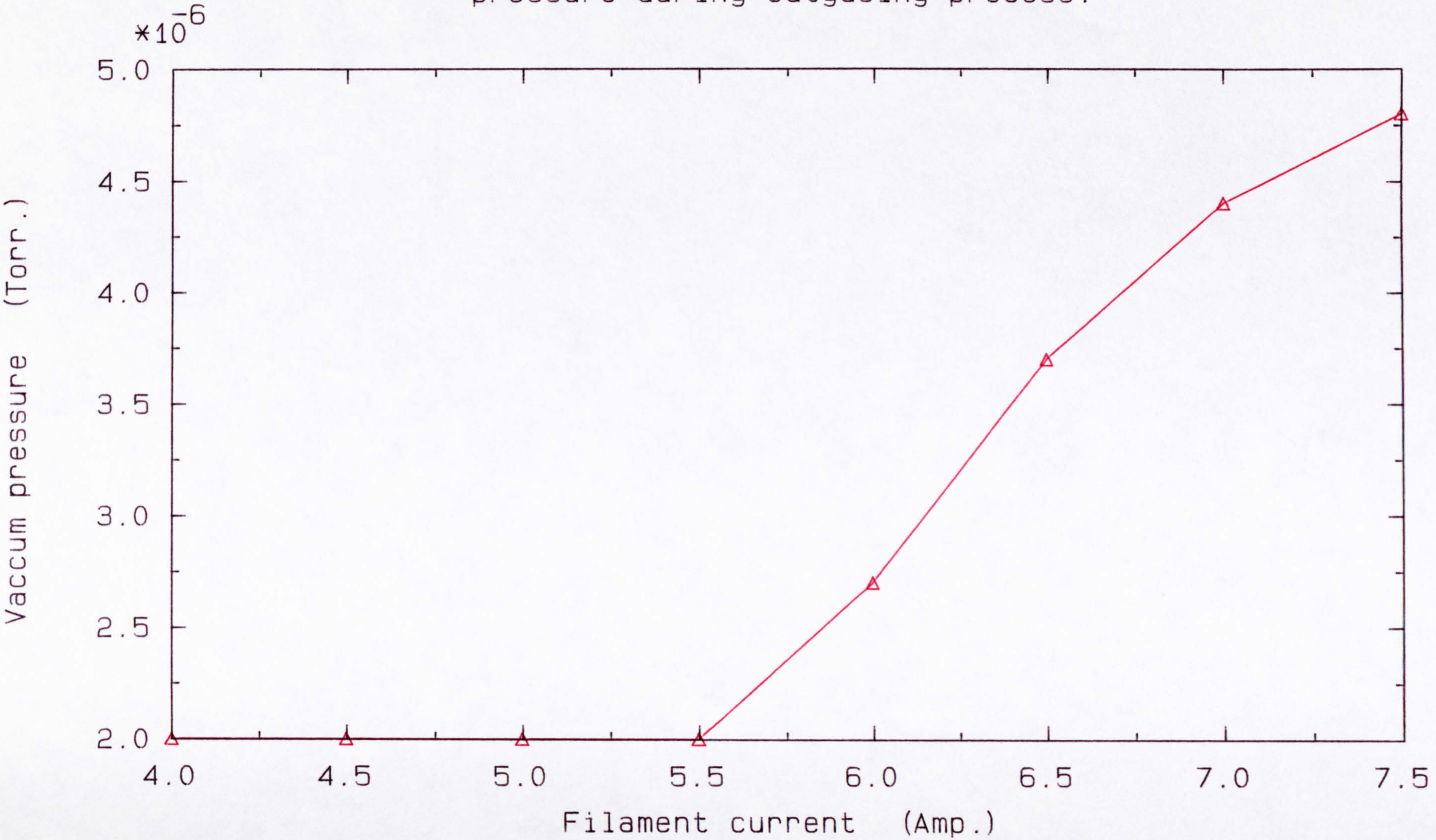

6.6.2 Beam current vs Filament current

In this part of measurement the energy levels were always held fixed at 5, 10, 15 and 20 kV as seen in Graph (6.3) . Again the vacuum pressure was kept at 1 x 10^{-5} Pa and the beam current was measured as the filament current was increased from 4 A to 7.5 A in steps of 0.5 Amp. as shown in Graph (6.3). For a filament current of less than 4 Amp, there was zero beam current. Further increase in filament current produced a measurable beam current which was greatly increased as the filament current was increased above 5.5 A. However, electrical breakdown between the vacuum flange and the high voltage electrodes. resulted when the filament current increased to more than 7 A at an anode voltage of 20 kV.

GRAPH (6.3) Energy 5, 10, 15, 20 KV, pressure 1×10^{-5} Torr.

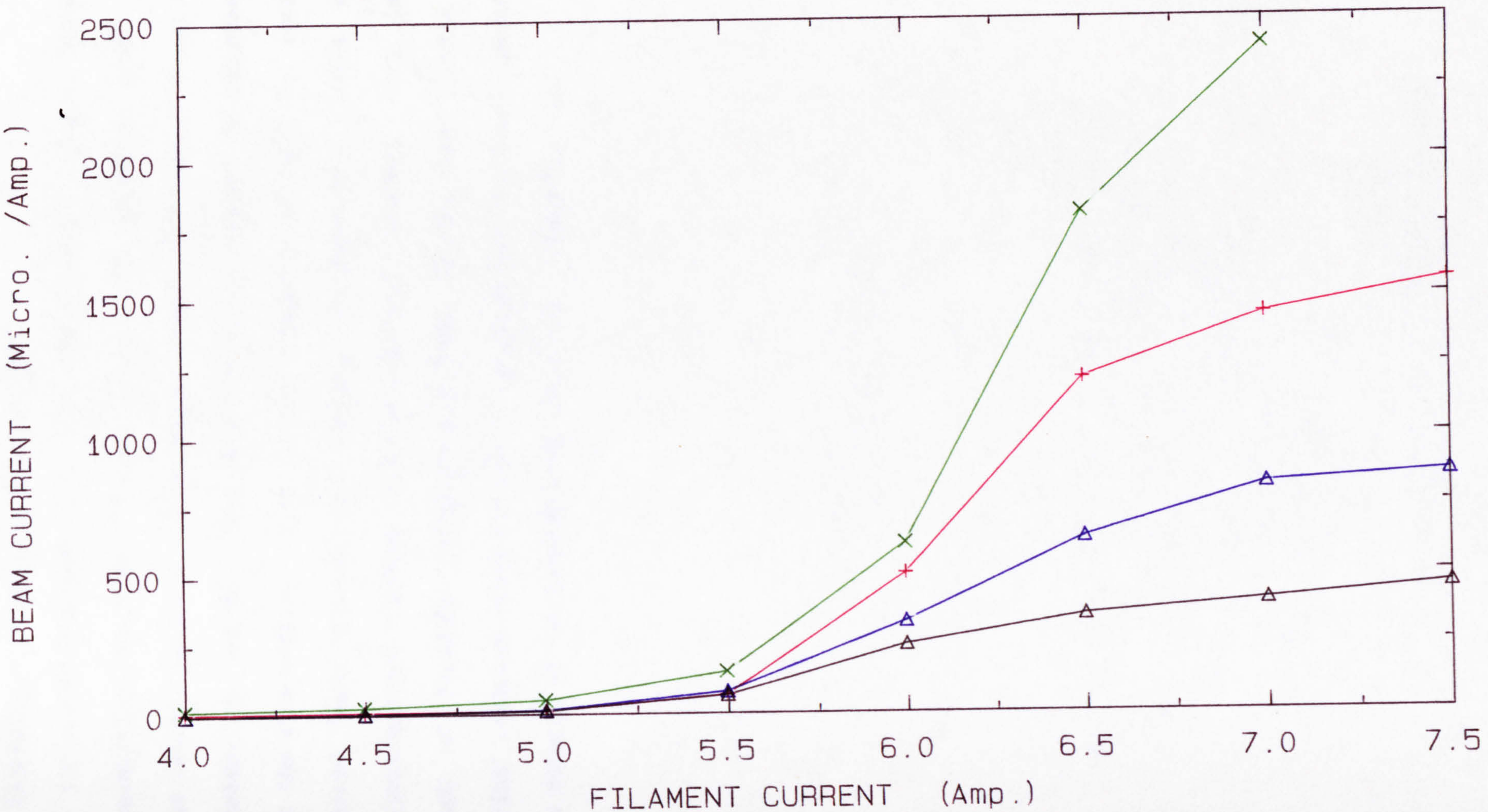

6.6.3 Filament current/Energy/Beam current

As the previous graphs show, the beam current is largely dependent on accelerating energy and filament current. An isometric graph of the beam current is given for different values of filament currents and of accelerating energy. This isometric graph enables the experimenter to set the accelerating energy and the filament current to obtain the desired beam current. This graph was especially useful when the polystyrene petri dishes were electron beam bombarded. This isometric graph of filament current/energy/beam current was plotted on the "Prime" computer using Fortran 77 language and is shown in Graph (6.4). The details of the program used are given in Appendix (3).

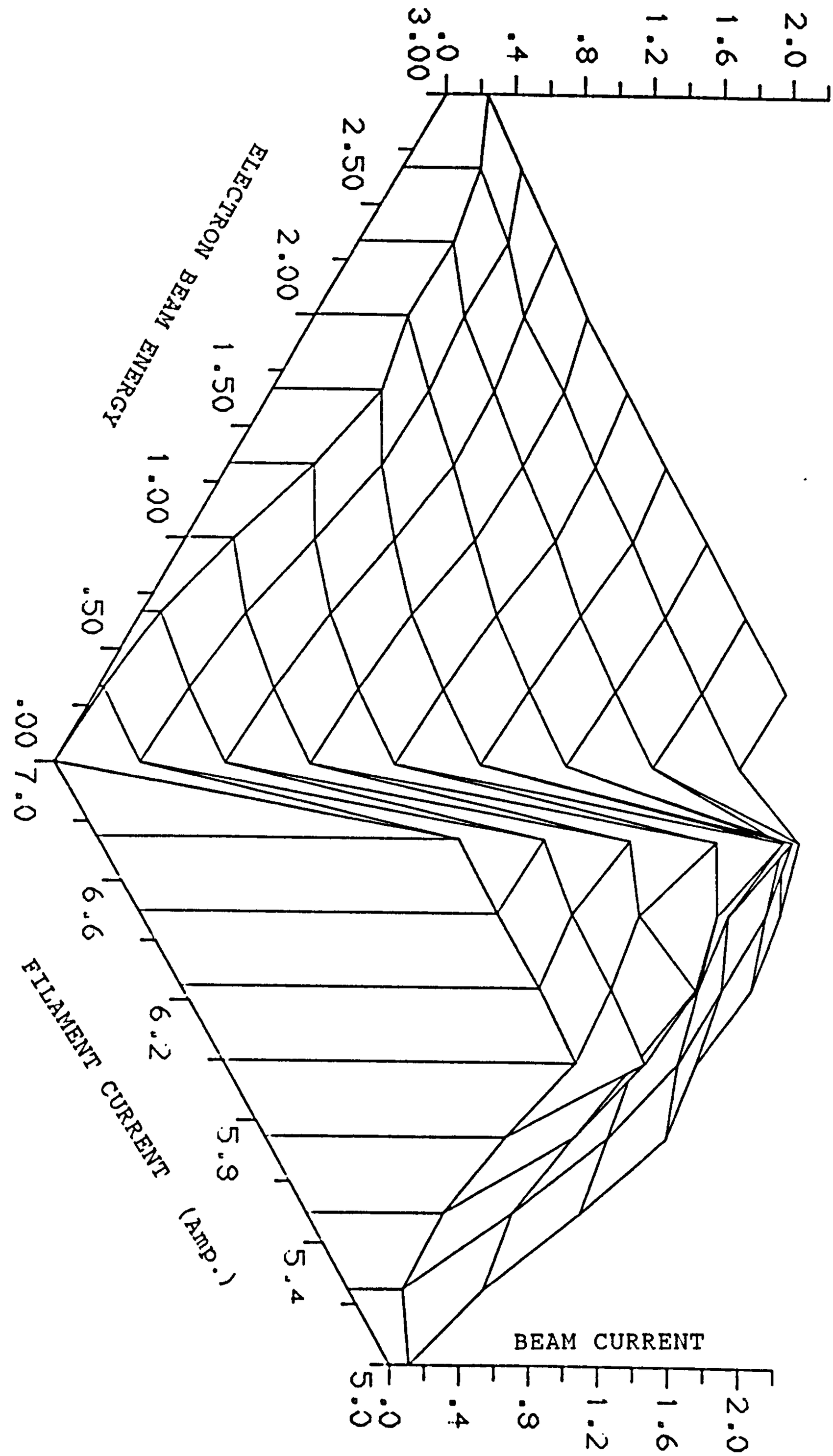

GRAPH (6.4), Three dimensional spectrum of filament current, Beam current and electron beam energy.

REFERENCES

1) SIMPSON, J.A. and KUYATT, C.E. Rev. Sci. Instrum., 1963, 34, p.265.

2) BAKISH, R. "Introduction to Electron Beam Technology", John Wiley & Sons, 1962.

CHAPTER 7

CHARGE IMPLANTATION EXPERIMENTAL: EQUIPMENT AND PROCEDURE

7.1 Introduction

It has already been shown that the physiology of the cells may be varied after being placed in a charged environment. However, this is strongly dependent upon the nature of the charge and whether it is negatively or positively charged. This Chapter reviews briefly experimental details of electron beam injection techniques and procedure, and the charge decay process in polystyrene insulators. Following this, it outlines some main experimental results obtained using positive ion bombarded polystyrene petri dishes. This is firstly for high energy He+ ion beams produced in the Van de Graaff and secondly for medium energy N+ ion beams using the isotope separator, and finally for low energy N+ ions generated by a D.C. plasma ion system in the experimenters own laboratory.

7.2 Electron Bombardment and Injection

For the experiments described in this section, two kinds of electron gun were used, high and low energy electron guns.

The high energy electron gun was a commercial electron gun designed and manufactured by Oxford Applied Research Ltd. The low energy electron gun was constructed by the writer during this research programme. Details of its design and construction were given in Chapter (6). These electron guns both have electrostatic acceleration and focussing. The electron beam could be deflected with either magnetic or electric fields to enable the beam to be guided into the work chamber through the aperture of the electron gun. The targets to be bombarded were polystyrene petri dishes produced by Sterilin Co. (Teddington, Middlesex, TW11 8OZ, England, UK. Part no. 1.206.475). Polystyrene has a density of 1.05 g/cm^3. and these petri dishes are commercially

available in different sizes and are vacuum compatible. The dishes were covered with a mask which was made of aluminium. The mask was similar to a matchbox cover, as shown in Fig. (7.1). A 1 cm diameter window was located centrally to allow the electron beam to irradiate a circular path in the centre of the petri dish (as illustrated in Fig. (7.2)).

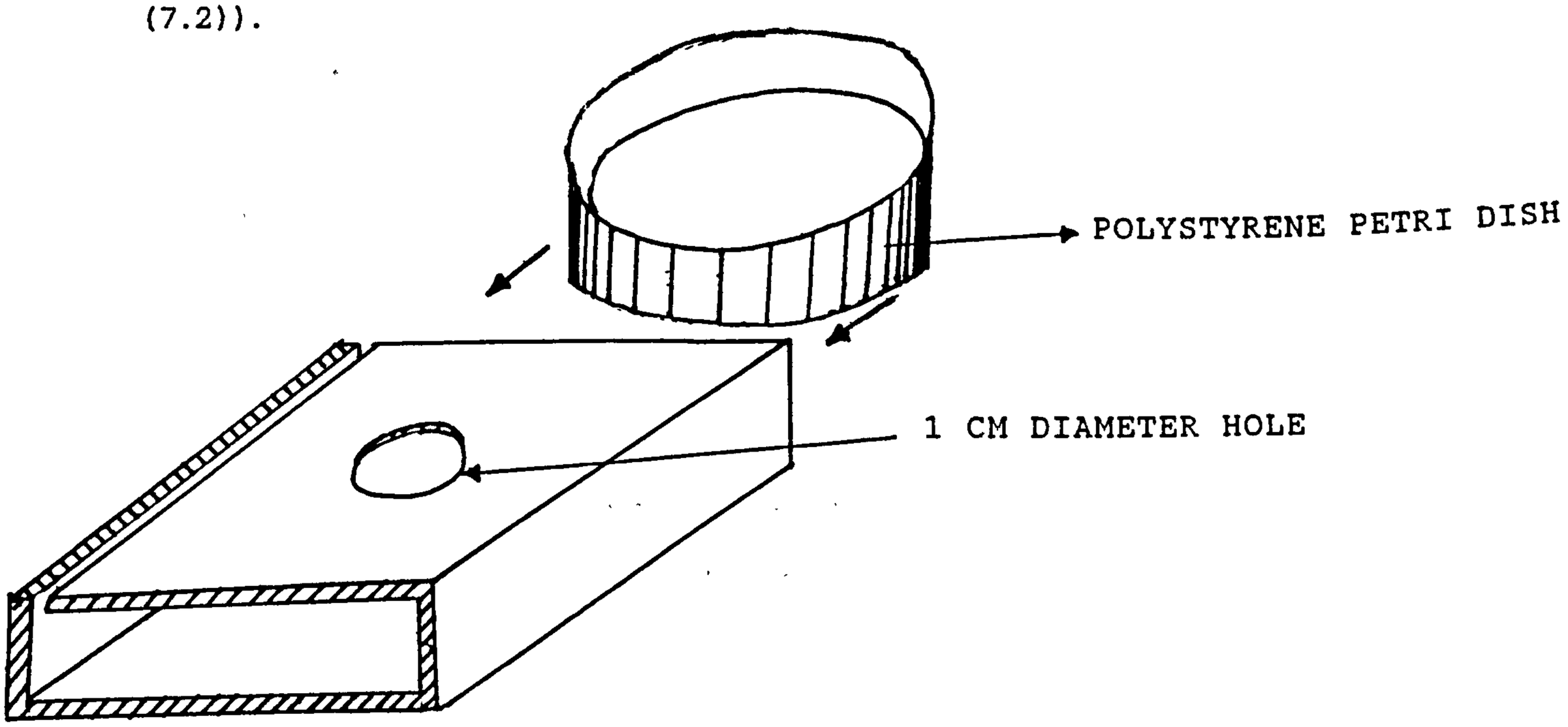

Fig. (7.1) An aluminium mask where the polystyrene petri dish could slide in with the open side of the dish facing towards the 1 cm diameter window of the mask. This would allow the electron beam to pass through the window into the surface of the petri dish.

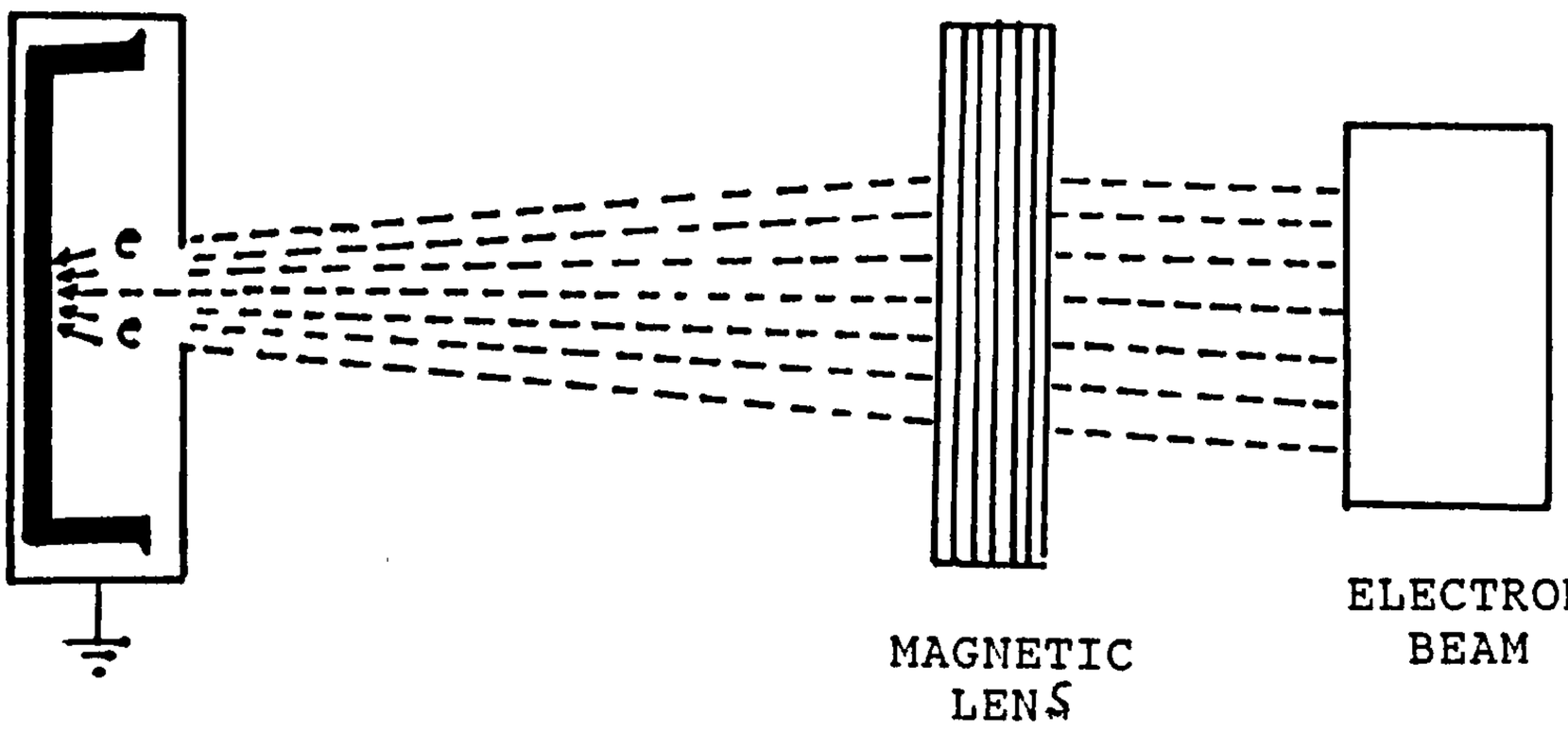

Fig.(7.2). The electron beam is directly hitting a circular path along the surface of a polystyrene petri dish, through 1 cm centrally located mask. The electron beam sits inside the polystyrene and charges the surface of the dish negatively.

It is important to note that in all the electron bombardment processes used here, the electron beam was always incident on the target material normal to its surface. This results in a higher penetration depth, since all the EB's will be resolved perpendicular to the surface of the material and it also minimises electron back-scattering which increases with the angle between the direction of the incident beam, and the normal to the surface (Chapter (3).

To achieve a perpendicular electron bombardment the target material and the Faraday cup were fixed opposed to each other back to back at 180 deg. The cup was initally incident to the Faraday cup. The cup was adjusted to reach the highest magnitude of the electron beam current. The position of the external handle which held the Faraday cup and the sample were marked. This was then turned by 180 deg. so that the sample face was normal to the beam and the Faraday cup was at its back where the sample was previously held.

The whole assembly was installed inside the work chamber of the vacuum system. Since the production and unrestricted propagation of an electron beam is only possible in high vacuum, the system was pumped down to 5 x 10^{-6} mbar. The acceleration voltage for the electron beam was set to 20 kV, and the beam current set to 6 A by adjusting the filament current.. The specimen was then irradiated for the time required to give the polystyrene the desired surface charge density.

The distance beneath a perpendicular target surface within which the electrons give off practically all their energy is called the Electron Range S. It is determined solely by eletron energy and the density of polystyrene and is defined by Equation (3.3). The penetration depth of

20 kV electron in polystyrene is 8 μm. With 5 minutes of electron beam exposure time. An electron dose of $\frac{6 \times 10^{16}}{0.445}$ $e^{-}cm^{-2}$ can be obtained.

7.2.1 Electron charge measurement

Once the electron beam enters the free surface of the polystyrene petri dish, the electrons will start to dissipate their energy in the target material. The surface of the polystyrene carries a -ve charge and this is localised in the centre of the petri dish where it was localised by the masking. The surface negative electron charge density and potential of the polymer was measured as a function of the exposure time.

7.2.1.1 Decay time

The technique used in these experiments is to measure the decay of surface potential by an Electrometer (Keithley Instruments (602)) following the injection of a beam of electrons. The procedures are as follows:

i) Electron bombard a polystyrene petri dish for a time. Accelerating energy and current required to give the specimen the desired surface charge density.

2) Once the target is bombarded, lightly touch an electrode to the surface of the target plate where it has been electron beam scored.

3) Earth the electrode while it is touching the surface of the target plate. The electrode can be easily earthed by lightly touching it with a finger

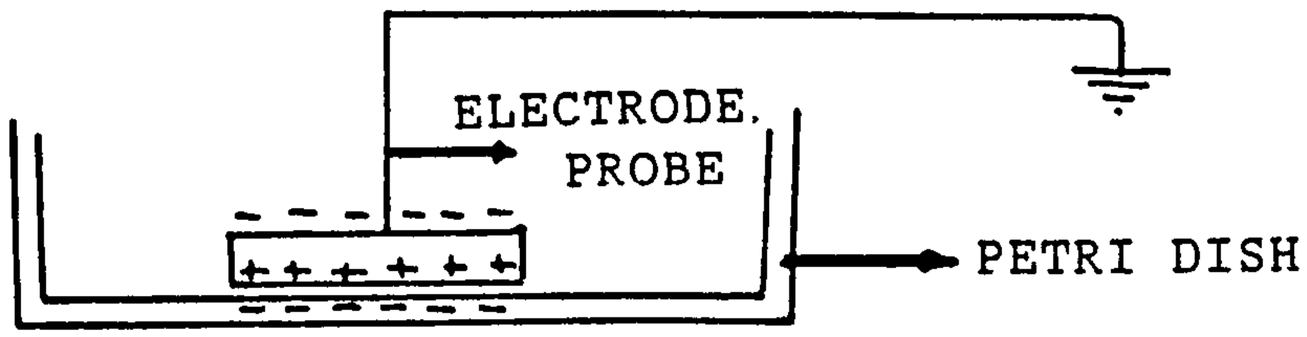

4) Connect the electrode terminal to an electrometer and then very quickly remove the finger from the surface of the electrode; lift up the electrode by pulling the insulated wire connected to the electrode. (The handle of the electrode was insulated by placing a cover off a pen around the metal handle of the electrode. The insulator was glued by Rapid Araldite adhesive).

5) Read the highest meter deflection of the electrometer. This is the charge on the specimen at that time.

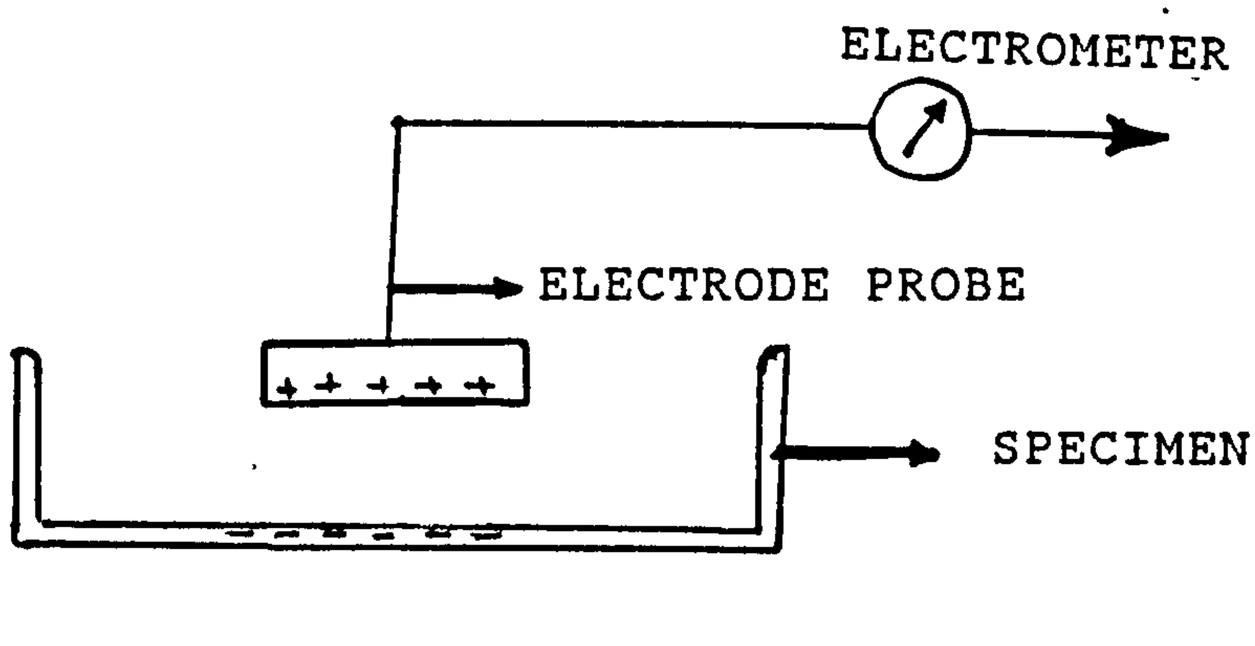

6) Repeat the same procedure (2-5) for different time periods following the first reading.

7.2.1.2 Errors

It was advisable to repeat this experiment a number of times. Also, step 4 needed to be carried out more carefully and neatly, hence the electrode probe was connected to a spring. The spring saved the trouble of pulling the electrode up since the elasticity of the spring did this at the same rate (throughout the experiment) each time the fingers were removed from the surface of the electrode.

7.2.1.3 Results

Graph (7.1) shows the change decay of a specimen which was bombarded for 5 minutes on accelerating energy of 20 kV and the beam

ELECTRON CHARGE TRAPPED INTO
POLYSTYRENNE PETRI DISH

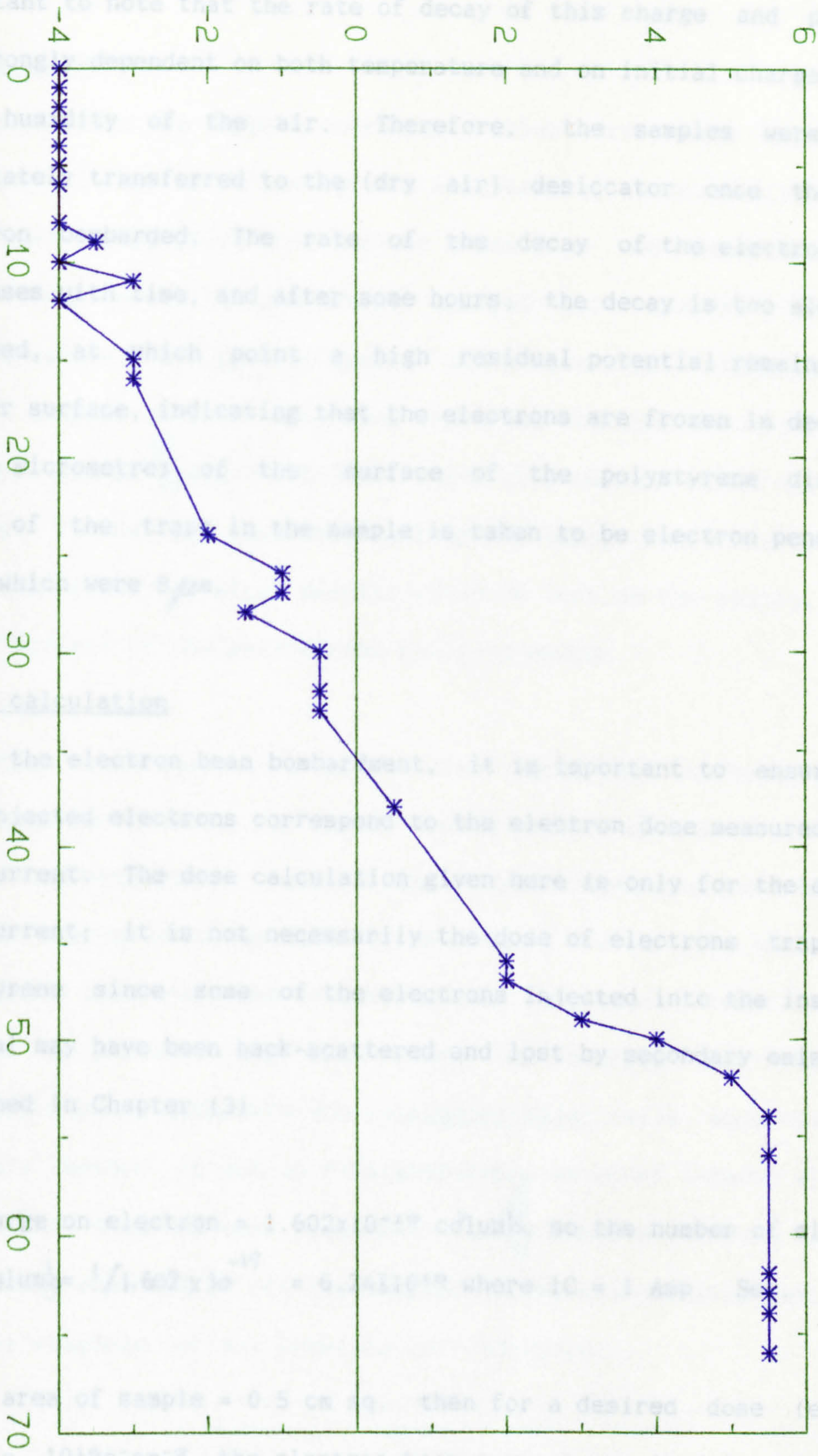

current of 6 A. (Charge is 13.5 x 10^{16}). As the graphs show, the charge in the injection is falling experimentally and it is also important to note that the rate of decay of this charge and potential is strongly dependent on both temperature and on initial charge density and humidity of the air. Therefore, the samples were always immediately transferred to the (dry air) desiccator once they were electron bombarded. The rate of the decay of the electron charge decreases with time, and after some hours, the decay is too slow to be measured, at which point a high residual potential remains on the polymer surface, indicating that the electrons are frozen in deep traps within micrometres of the surface of the polystyrene dish. The depth of the traps in the sample is taken to be electron penetration depth which were 8μm.

7.2.2 Dose calculation

During the electron beam bombardment, it is important to ensure that the injected electrons correspond to the electron dose measured by the beam current. The dose calculation given here is only for the electron beam current; it is not necessarily the dose of electrons trapped in polystyrene since some of the electrons injected into the insulating material may have been back-scattered and lost by secondary emission as explained in Chapter (3).

The charge on electron = 1.602×10^{-19} coulomb, so the number of electrons per coulomb = $1/1.602 \times 10^{-19} = 6.24 \times 10^{18}$ where 1C = 1 Amp. Sec.

Assume area of sample = 0.5 cm sq. then for a desired dose (electron beam) = $10^{16} e^{-} cm^{-2}$ the electron beam current required for 30 minutes exposure time = $\frac{10^{16} \times 0.5}{(1/1.602 \times 10^{-19}) \times 30 \times 60} = 0.44\mu A$. Therefore, the target

material can be bombarded by a fixed electron beam dose by adjusting the electron beam current and fixing the exposure time.

7.3 VAN DE GRAAFF

Van de Graaff's are large electrostatic generators which can develop energies of up to a few MeV for accelerating atomic particles. The electrical energy which they deliver comes from the work done by a motor which draws a positively charged belt towards a positively charged sphere, electrocute against the electrostatic repulsion. More than 14 samples of petri dish were bombarded with positive particles in the low energy range of 2-3 MeV (He+) at a current of 30 nA. for 25 minutes. It was very important to keep the energy as low as possible, otherwise first a black deposit would be left on the sample, and at higher surface of the polystyrene could be melted.

With this technique, the petri dish could not be bombarded by a particle directly since the sample needed to have an area smaller than 1 cm^2. Unfortunately, such a small petri dish could not be found. However, some polystyrene discs of an area of 0.8 cm^2 were available in the Physics Laboratory and it was decided to score these discs by positive α particle and then place the charged disc inside the polystyrene petri dish with the Leishmania major cells suspended over it. This method is not as straightforward as other methods where the actual petri dish has been bombarded. So it needs a lot more care and attention; some 40% of all the samples became contaminated before they could be examined for any possible cell adhesion.

7.4 Isotope Separator

The Isotope Separator available in this University is the Harwell Mk. 4 type. Basically it consists of a high current tungsten filament. Nitrogen gas entering the chamber is ionized and leaves the source through a rectangular slit, primarily attracted by an extractor plate at 2 to 5 kV w.r.t. earth. This produced a high intensity N+ ion beam for extended periods of time. When in operation, the pressure measured in the region of the ion source was allowed to rise to the range 5 x 10^{-5} to 2 x 10^{-4} Pa which enabled a plasma to be maintained.

Although designed to operate at up to 40 kV, and single charged nitrogen ions, 10, 20, 30 kV energy were used throughout this research, it is possible for this type of ion source to produce lower intensity beams of double or triply charged ions at up to 80 Kev or 120 keV respectively.

A magnetic separation unit deflects the (N+) ion beam, at the same time separating the beam into its separate ionic components according to the projectile mass and energy. This field was adjusted until the required ion species entered the polystyrene petri dishes inside the target chamber. The target chamber used to perform the N+ ion implants had a side loading chamber capable of being evacuated by rotary pump. This allowed a small number of polystyrene petri dishes to be ion implanted every day, thus avoiding the necessity of allowing the target chamber's atmospheric pressure to increase during the target insertion. Permanent magnets mounted above and below the target chamber provided a magnetic field which prevented the emission of secondary electrons from the target during the experiment.

To produce a uniform implant in polystyrene petri dishes, the N+ ion beam was swept across the target by superimposition of a sinusoidal wave form on top of the 30 kV. acceleration voltage. At this energy, the ion beam will scan approximately 6 cm. Hence, providing the target is relatively small compared to this scan, and is situated centrally in the scan, thenthe (N+) ion beam dwell time on each part of the target is fairly constant.

However, care had to be taken using this type of N+ ion beam scanning because, although the original (N+) ion beam is analysed into its separate components by the magnet, all the components will be scanned. This may lead to contaminated ions of a suitable mass and charge reaching the target at the end of each sweep of the beam, and although the concentration of such ions in the beam may be very low, the extended dwell time on target of this component can cause measurable quantities to be implanted.

Using a circular aperture in front of the target, the total area swept by the ion beam (the implant area) was defined to be a circle with a diameter of 1 cm (precisely $\pi/4$ cm^2. Hence, by alteration of the measured beam current to the required level, the dose rate, in units of ions/cm^2/sec had been set to a desired value of 10^{16} .

In the case of this present work, more than 47 samples were N+ ion implanted with total currents of 10, 20, 30μA at energies of 10, 20, 30 kev to give a total dose of ~ 10^{16}. as this rate of implantation was concomitant with the prevention of excessive target heating for exposure times up to 10 minutes. The total flux of ions implanted, in units of ions/cm^2, was controlled by the inclusion of a current

integrator in the beam current measurement circuit. This device gave a pulsed output after the passage of a pre-set amount of electrical charge. As this charge is proportional to the number of ions that have been implanted, the number of pulses required for the implantation of a given flux may be calculated. A pulse counter was used to interpose a shutter into the ion beam path after implantation of the requisite number of ions.

Following the ion implantation of N+ on polystyrene petri dishes they were carefully inserted into de sicator (dry air) and were then taken to the Parasitology Laboratory in the Department of Biology where they were ready for use in the experiment. The results of possible attachment of Leishmania major cells to these N+ ion bombarded petri dishes is discussed in Chapter (9)

7.5 D.C. Plasma Ion-Bombardment System

As we have said in Chapter (3) the ion-bombardment system can use the ion-plating system with no evaporation sources. There was already an ion-implanting system available in the laboratory and it was easily converted for use in the ion-bombardment process. The basic features of a simple ion plating unit used in this project are shown in Fig (7.3). There are three main units as follows:

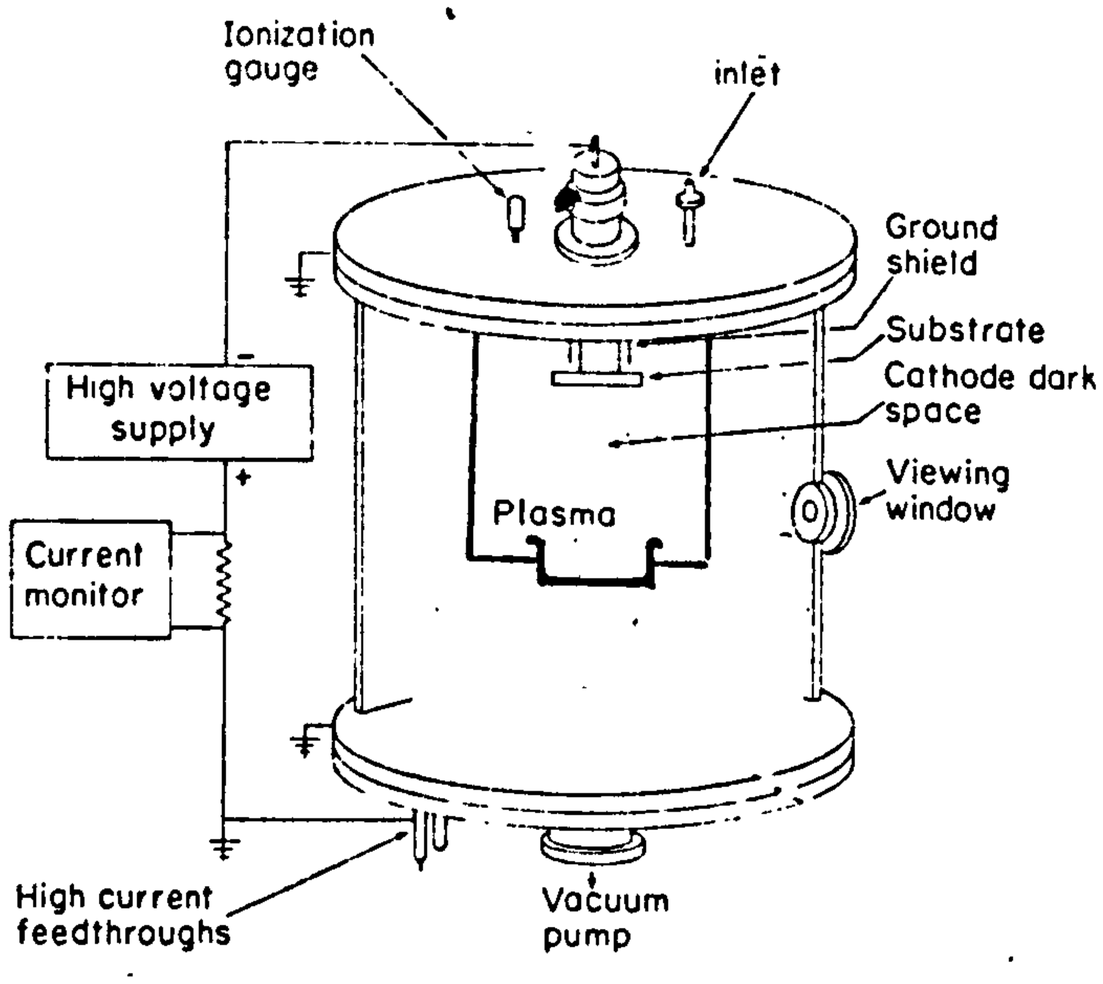

Fig. (7.3) Schematic diagram of a D.C. plasma bombardment set-up

A - <u>The vacuum and gas control unit</u>

The reproducibility of ion bombardment required a high vacuum system and a working gas (plasma). In the ion bombardment processes, suitable pressures were achieved by using a mechanical rotary pump to rough out the vacuum chamber from atmospheric pressures down to about 10^{-1} pa and then a silicon oil diffusion pump with a liquid nitrogen trap to reduce the pressure in a short time to 10^{-4} Pa. Gas used in the ion bombardment process was nitrogen. The gas flow rate could be monitored using a suitable flow meter and the flow rate could be controlled using a fine needle valve or a mass flow controller combined with a magnetic isolation valve.

B - The gas discharge chamber

The conventional ion bombardment process was carried out in a gaseous discharge and it is essential that the whole substrate (polystyrene petri dish) sees the same discharge conditions. It is therefore of prime importance to have a uniform environment to achieve uniform electric field distribution and uniform plasma. The system was already designed symmetrically and if the system is not symmetric, the electric field will be distorted and there will be a plasma density variation due to wall losses.

C - The high voltage electrode

As the ion bombarded substrate is usually held at high voltages, it is necessary to use a reliable electrode that can operate successfully at different ranges of voltages and temperatures. The system was previously designed with a substrate holder with a high breakdown voltage by having a PTFE insulator. Since most of the input power appears as substrate heating, it was necessary to use the existing cool-down system for the substrate and the holder which circulated cooling water through.

The H.V.- d.c. power supplies used in conventional ion bombardment were capable of supplying a negative voltage of 0-5kV to the cathode. This was not a highly smoothed or regulated power supply but was suitable for this work. It is important to make sure that the output cable is strong enough to withstand the maximum d.c. output voltage.

Samples were bombarded by N+ ions in an energy range of 700 to 1kV. The beam current was started at 150 mA (when the voltage was 1kV) and was gradually reduced to 25 mA as the voltage was dropped to 700 volts.

The positive ion was nitrogen and the plates were exposed from as much as 15 minutes to 90 seconds (700 volts). It is important to point out that at an energy level of 1keV. with a beam current of 150 mA for an exposure time of 15 minutes, the surface of the polystyrene was turned to pale yellow in colour, only at the place where the beam was bombarded. (The target plate was always covered by a mask with a window of 1 cm. in diameter in the centre of the polystyrene petri dish). However, this did not happen as the energy of the beam was dropped to below 800 volts regardless of the beam current. Therefore, it was decided to get some infra-red measurements on comparison of bombardment and non-bombardment of polystyrene petri dishes which have been exposed to D.C. plasma +ion beams.

7.5.1 Ion bombardment method by D.C. plasma ion

The ion bombardment process was carried out in a nitrogen gas discharge (similar gas to ion separator). The substrate was continuously bombarded by the energetic singly charged nitrogen positive ions and neutrals of the gas subjected to the action of the ultraviolet radiation emitted from the positive column of the abnormal glow discharge. When the atoms of the polystyrene petri dish material are subjected to ion-bombardment of N+ ions, the surface of the polystyrene would be fractionally ionized.

7.5.2 Infra-red Measurement

Infra-red spectrum of the samples were taken by the 1710 Fourier Transform spectrometer. It comprises an optical unit, a visual display unit (VDU) and control keyboard, a microprocessor control and data processing system, together with a printer (model PPI). Spectra are computed from a program by Fourier transformation. The instrument has

a single beam and the spectra of a non-bombarded polystyrene petri dish (control) is obtained from the ratio of spectra with the control in the beam against a background spectra obtained without a sample. The control spectra is stored in the instrument and is shown in graph (7.3).

The control spectra is inverted and which is controlled from the keyboard. There are three spectra data memories, A, B or C, in which the inverted control spectra can be stored. A new spectra of +ion irradiated polystyrene petri dish is obtained. The new spectrum is added to the inverted control spectrum which is stored in one of the memories and the difference between the two spectra is obtained as shown in Figure (7.4). Facilities are provided for absorbance expansion, digital smoothing and quantitative analysis.

Unfortunately the graph (7.4) does not give any definite answer to the ion charge effect and more likely the change of colour in the polystyrene petri dish is either due to UV from ions in plasma or thermal decomposition during the collision of high energy N+ ions with polystyrene atoms.

GRAPH (7.3), Infra red spectrum of a polystyrene petri dish (control specimen).

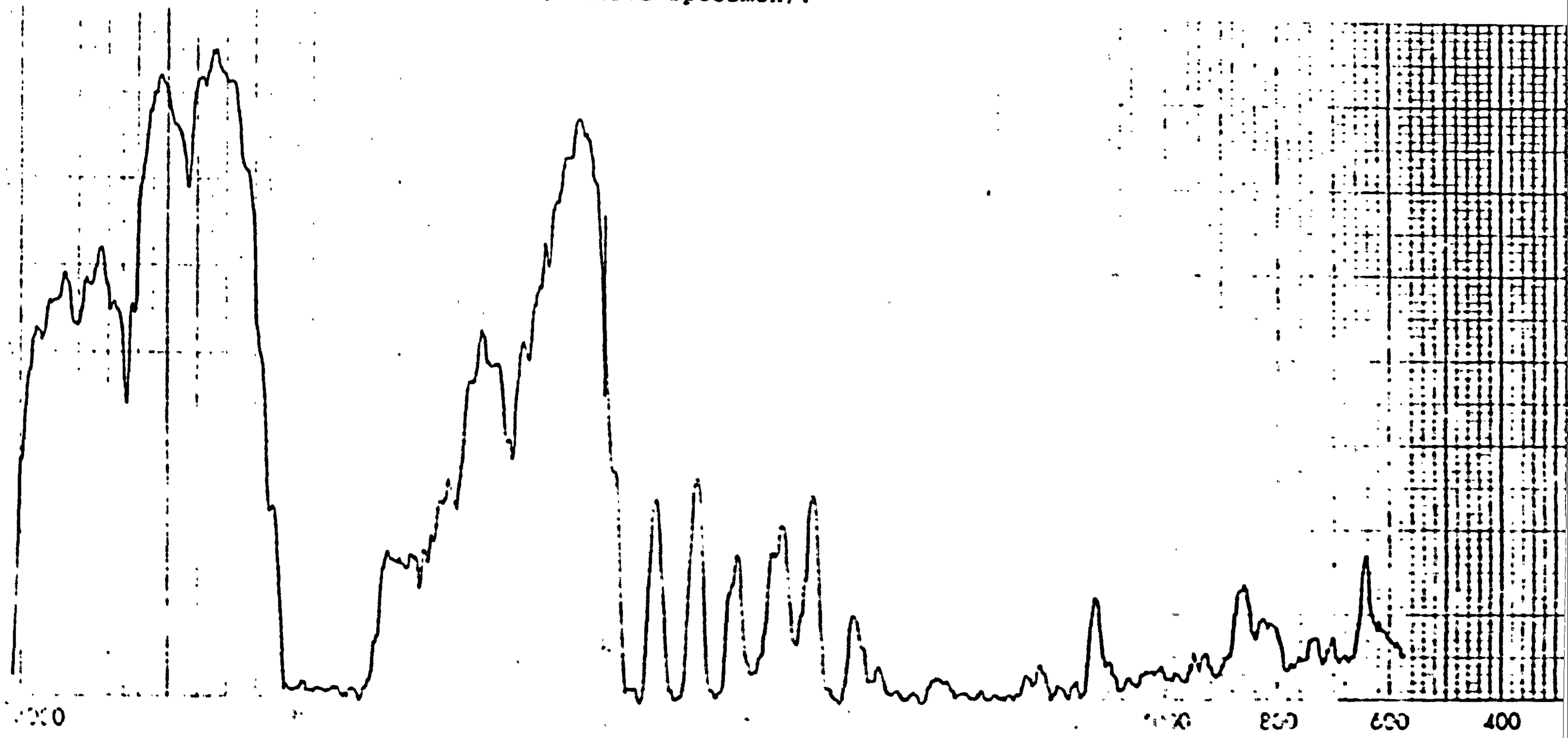

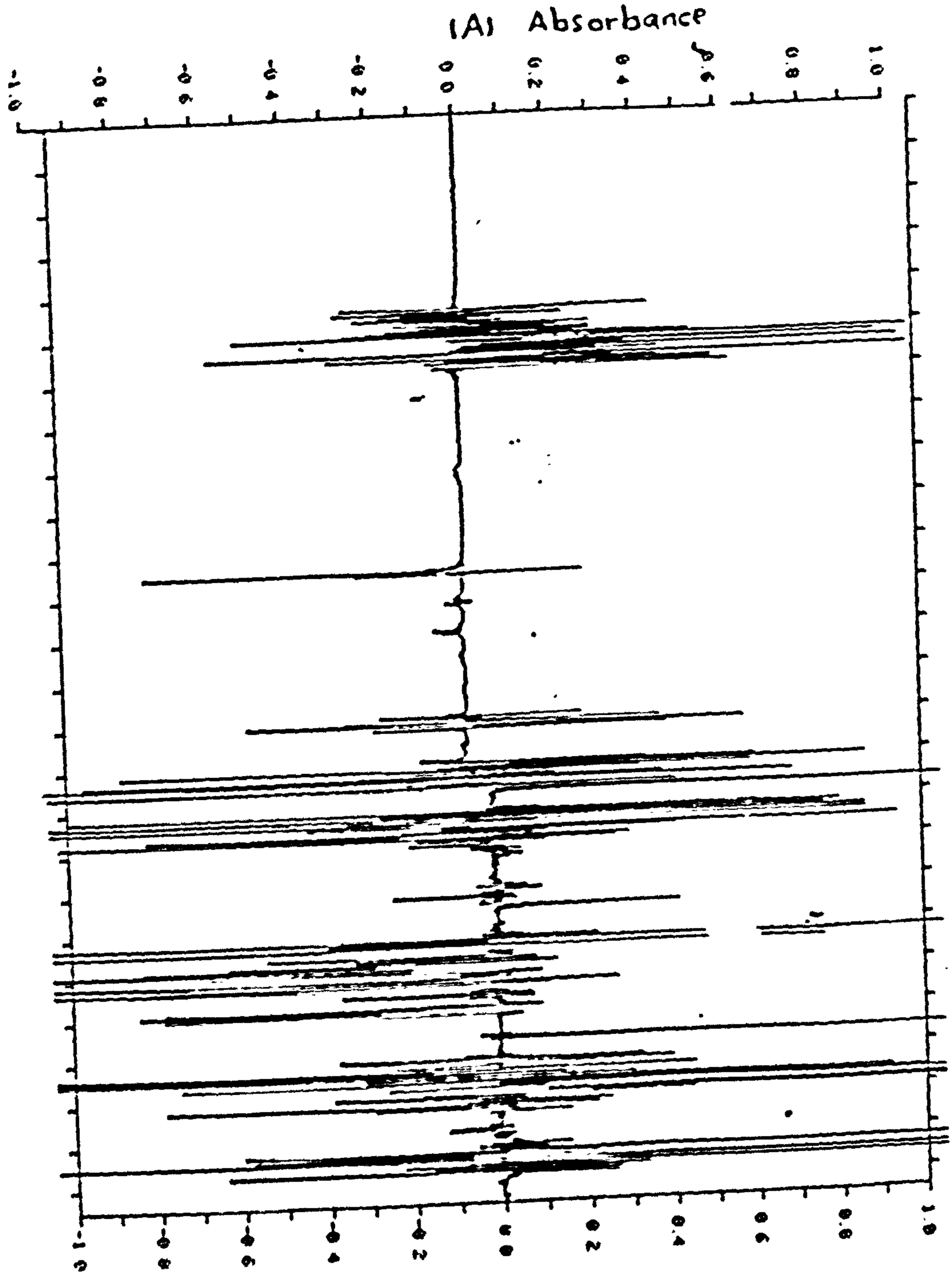

GRAPH (7.4), Difference Infra red spectrum of an ion bombarded polystyrene petri dish (sample) and an unbombarded polystyrene petri dish (control).

REFERENCES

1) TUANRU, C., SHANGWU, M.O. and SHUHUA, Q. "Effect of N+ Ion Implantation on Wheat Growth", Institute of Nuclea Sci. & Tech., Chengdu, China, 1985.

CHAPTER 8

EXPERIMENTS WITH CELL OSCILLATION AND ROTATION

8.1 Introduction

Fröhlich [1] has considered that enzymes and other biological systems might possess a metastable state with high electric dipole moment, which would become established when the system is forced into large vibrations through the supply of random energy in excess of some critical value, and result in the coherent excitation of a single mode of oscillation, the excitation of a metastable highly polar state and the possibility of limit cycles.

There are now many published reports that living cells produce natural A.C. fields [2]. Pohl and Braden [3] concluded that the presence of natural r.f. electrical oscillation in living cells is well established. They are present in a wide variety of organisms, and vary with the physiological state of the organism. This A.C. field pattern produced by living cells is made evident by a gentle dielectrophoretic force on tiny dielectric particles [4]. Previous works on pearl chain formation of yeast cells (Saccharomyces cerevisiae) has proved that there will be a repulsion force between some of the cells along the pearl chain as the proton magnetic resonance conditions are satisfied exactly with a frequency and a combination of steady and swept magnetic fields [5].

In this project, the natural A.C. field is shown by subjecting either Leishmania major parasites or yeast (S.C.) cells to rotating electric fields.

Pohl and Zimmerman (6-7) were two of the early scientists who observed the rotation of lone cells while they were studying the pearl chain formation. [Pearl chain formation is the collection of lone cells].

This is an effect of alternating non-uniform electric field (dielectrophoresis) on neutral particles.

In the spinning studies of the given living cells to the rotating electric field, it was observed that the rotation of these cells responded rather sharply and in a resonant manner at several frequencies, hence the term "cellular spin resonance" (CSR). This thesis reports on a resonance frequency at which nearly all cells simultaneously spin perpendicular to their axis in the field. the frequencies of the applied field can be in the order of magnitude higher than the actual spin rate. The CSR varies with the conductivity of the medium, with the square of the applied field, with the cell type and phase of the cell life cycle, and age of the colony. Living cells respond readily and individually and are sharply resonant. Dead cells show no response.

There is no CSR in D.C. signals, from the behaviour of the CSR in sinusoidal A.C. signals, it appears likely that one cause of CSR at least that in high frequency electric fields is the presence of natural r.f. oscillations arising from the cells. The cell resonance frequencies observed vary from species to species for yeast cells (Saccharomyces cerevisiae) it is 12 kHz, (Leishmania major) parasites it is 10 kHz.

The present work reports on the sharply resonant character of the spinning response of (Saccharomyces cerevisiae) and Leishmania major cells to applied frequencies.

All the measurements reported in this chapter made use of either

platinum or gold vacuum deposited thin film metal electrodes. The electrodes were 50 μmm thick which will generate a very strong field at the edges. The use of such electrodes allows the observations to be carried out at high optical magnification so that a single cell can be observed directly in the centre of the chamber and far from the electrodes and other cells. It can be seen rotating or spinning in the rotating electric field, with a rotating frequency of about 10 Hz (strobe illum.) - something that no other researcher cited in this area has managed to observe. This method also provides a simple and straightforward method for obtaining the dielectric properties of individual cells [8]. However, before we describe the CSR of both Leishmania parasites and yeast cells, attention needs to be directed to some interesting effects of non-uniform electric fields on these biological organisms in Hz. and sub-Hz. ranges.

8.2 Action of Non-uniform Electric Fields on Leishmania and Yeast Cells in Hz. and sub-Hz. Ranges

Dielectrophoresis - the action of alternating non-uniform electric fields on neutral particles has recently been receiving increased attention. The most obvious effect is the "pearl chain" formation of cells (or yield) along the field lines in the space between and at the surface of the electrodes.

In the experimental study of pearl chain formation of cells, numerous experimental techniques are now available. It is our purpose here to add a new and simple physical technique to the array of methods available for the study of pearl chain formation in sub-audio range. Recently Pethig et al [14] has employed an optical technique for studying the dielectrophoretic behaviour of colloidal particles at low

frequences. He has shown that the large, low frequency, dielectrophoretic response for their particle is associated with surface charge and surface conductivity effects. The "pearl chain" formation technique used in this work consists of placing a suspension of cells between two parallel plate vacuum sputtered metal electrodes prepared as explained in Chapter [4].

Cells of Saccharomyces cerevisiae and Leishmania major cells in media of low conductivity were prepared by centrifuging freshly harvested cells from the growth medium, rejecting the supernatant liquid, rediluting the cells with 0.25 M sucrose in deionised water, centrifuging again, until the overall resistivity of the suspension was at least 200 kΩcm. This conductivity was checked by a conductivity measuring bridge (Type MC3, Switchgear Ltd.). The preparation was then examined for observation and concentration measurements.

It is important for all the cells to be synchronised in respect of cell division cycles so the cells are in some period of growth while the experiment is taking place. The procedure for cell synchronisation is described in Chapter (1).

8.2.1 Observation of Pearl Chains at Sub-audio Frequences

Observations of pearl chain at Hz. and sub-Hz. range frequencies for given cells revealed the oscillatory motion of "pearl chains". For this experiment a low frequency function generator (model 202A Hewlett Packard Ltd.) was connected to a pair of thin film vacuum metal electrodes and the "pearl chains" were observed under the microsope. The majority of the "pearl chains" were oscillating "back and forth" towards each electrode except for a minority which were oscillating in

the opposite direction compared to the majority chains as illustrated in Figs. (8.1 and 8.2).

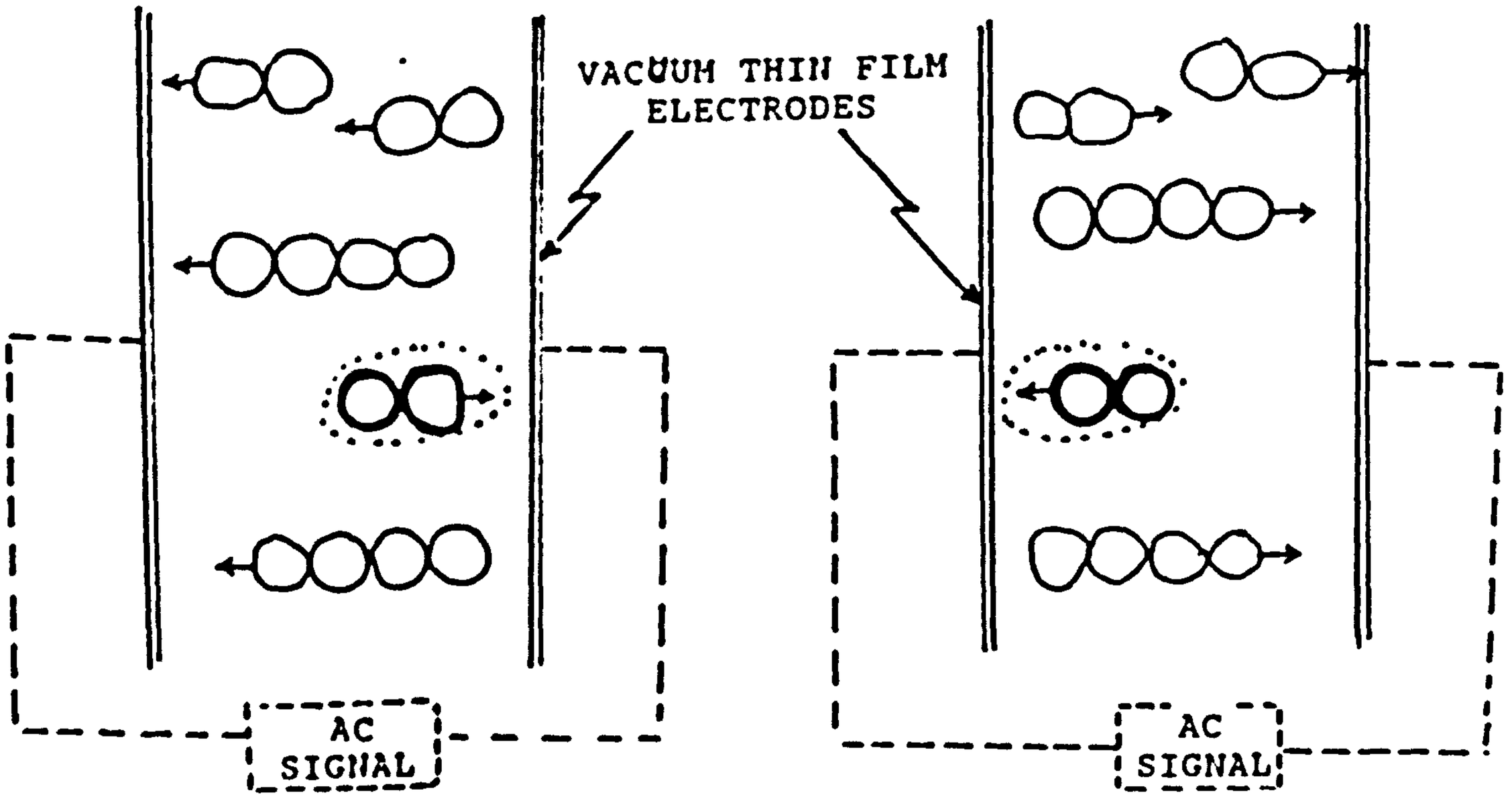

Fig. (8.1) The oscillatory movement of Saccharomyces cerevisiae cells at low applied frequency

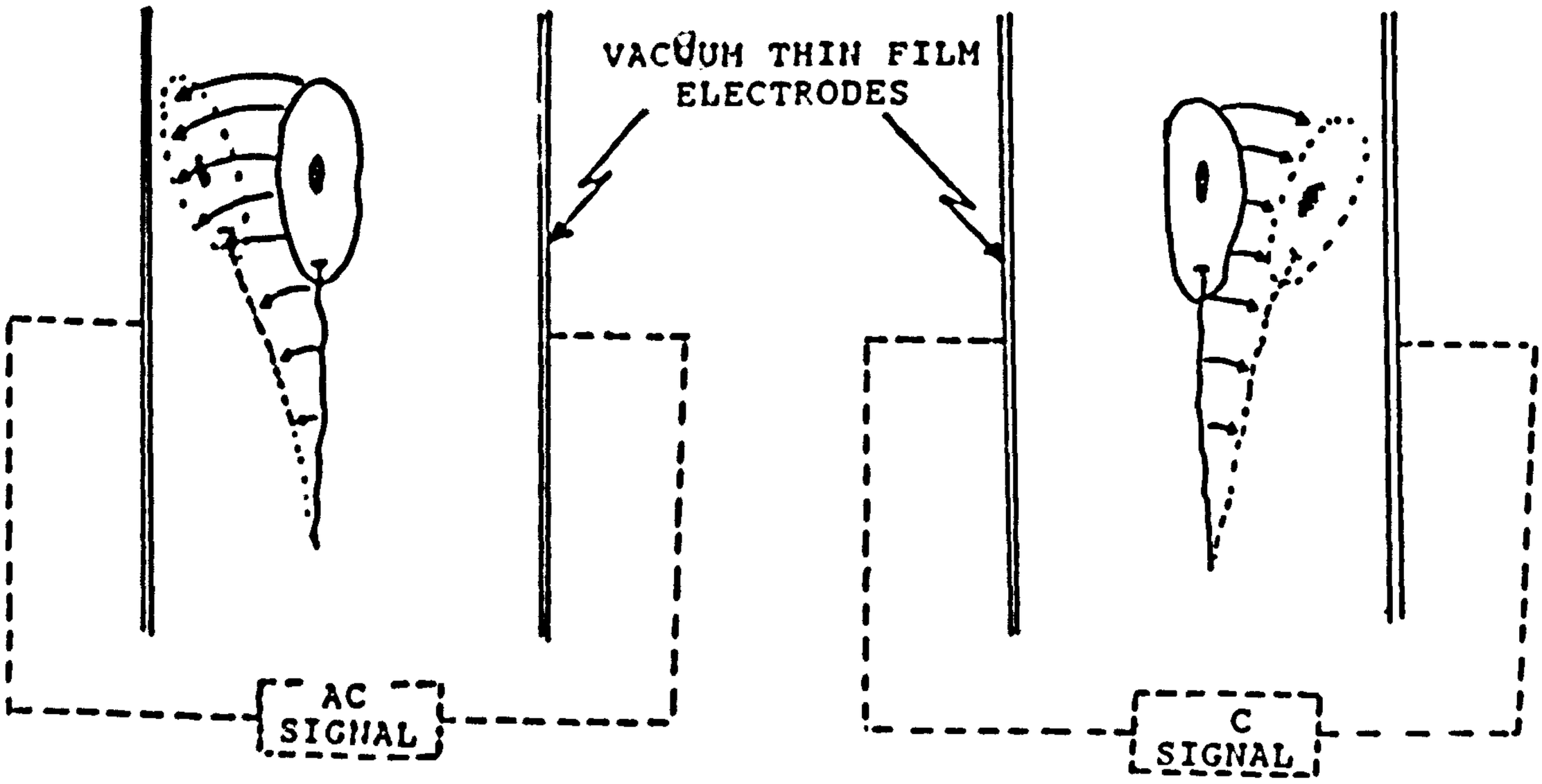

Fig. (8.2) The harmonic motion of Leishmania major cells at low applied frequency

This alternating movement of chains of cells implies that there are the charge phenomena of electrophoresis associated with the cells. Different groups of cells in the same suspension appear to have different surface charges. The behaviour of a chain of cells at low frequency is known to be an electrophoresis effect. As described in Chapter (2) the electrophoresis force is directly proportional to the field and to the charge, and its polarity reverses the effect while the dielectrophoresis force (equation (2.7)) is directly proportional to the square of the field, across the electrodes, and is independent of any sign of change of the charge across the electrodes.

One interesting point about the oscillatory motion of parasites is the way in which Leishmania major cells move back and forth in a sub-audio frequency range. Leishmania major cells do not have the sphere shaped body of yeast (S.C.) cells. They have an elongated unflagellate measuring 4 to 40μm in total length; they are free-swimming and are attached to the anterior sites (cell body) of the organism. Their oscillation can best be described as a simple harmonic motion where the anterior sites of the organism (cell body) would look as a small mass attached to the end of a 40μm length of wire (flagellum), where the other end of the wire (flagellum) is fixed (pivoted) with no oscillation, and the cell body oscillator swings to-and-fro along the arc of a circle off centre of the free end of the flagellum.

Any increase in voltage amplitude of the waveform generator for a fixed frequency of the sub-audio waveform generator would increase the angle of the oscillation of the cell body. Obviously the angle of the oscillation decreases if the voltage of the generator is reduced. Very similarly to yeast cells, as the frequency increases, the frequency of

oscillation increases and they are very nearly related. As a typical example, when the frequency of the oscillation was kept at 0.5 Hz., the Leishmania cells were oscillating at 0.6 Hz. However, when the frequency of the oscillation was increased to 3 Hz. it similarly increased the oscillation of the cell to 2.89 Hz. At a waveform frequency of 11 Hz. the cells were still oscillating very rapidly although they appeared to be stationary because the amplitude of oscillation is small while its frequency has increased..

Graph (8.1) shows more such results for Leishmania major parasite cells.

During the work reported in this chapter, a rotational phenomena of the cells about an axis through their centres was noticed. Here the cells spin on an axis normal both to the magnetic field lines and to the surface of the slide, at a rate of a few revolutions per second. This can be seen to occur with certain cells at almost any applied frequency and anywhere in the field, irrespective of whether the cell is attached to an electrode, attached to another cell, or floating freely in the medium. It is not unusual to see several cells of a long attached chain rotating individually in their places. This implies that the contact is non-adhesive.

From the preliminary observations of the cell rotation, it was clear that it definitely needed further investigation, and the results of these investigations are presented in the next part of this chapter.

8.3 Experiments involving cell rotation

Previous investigations [2] have shown that the live microscopic

GRAPH (8.1), Oscillatory motion of cells

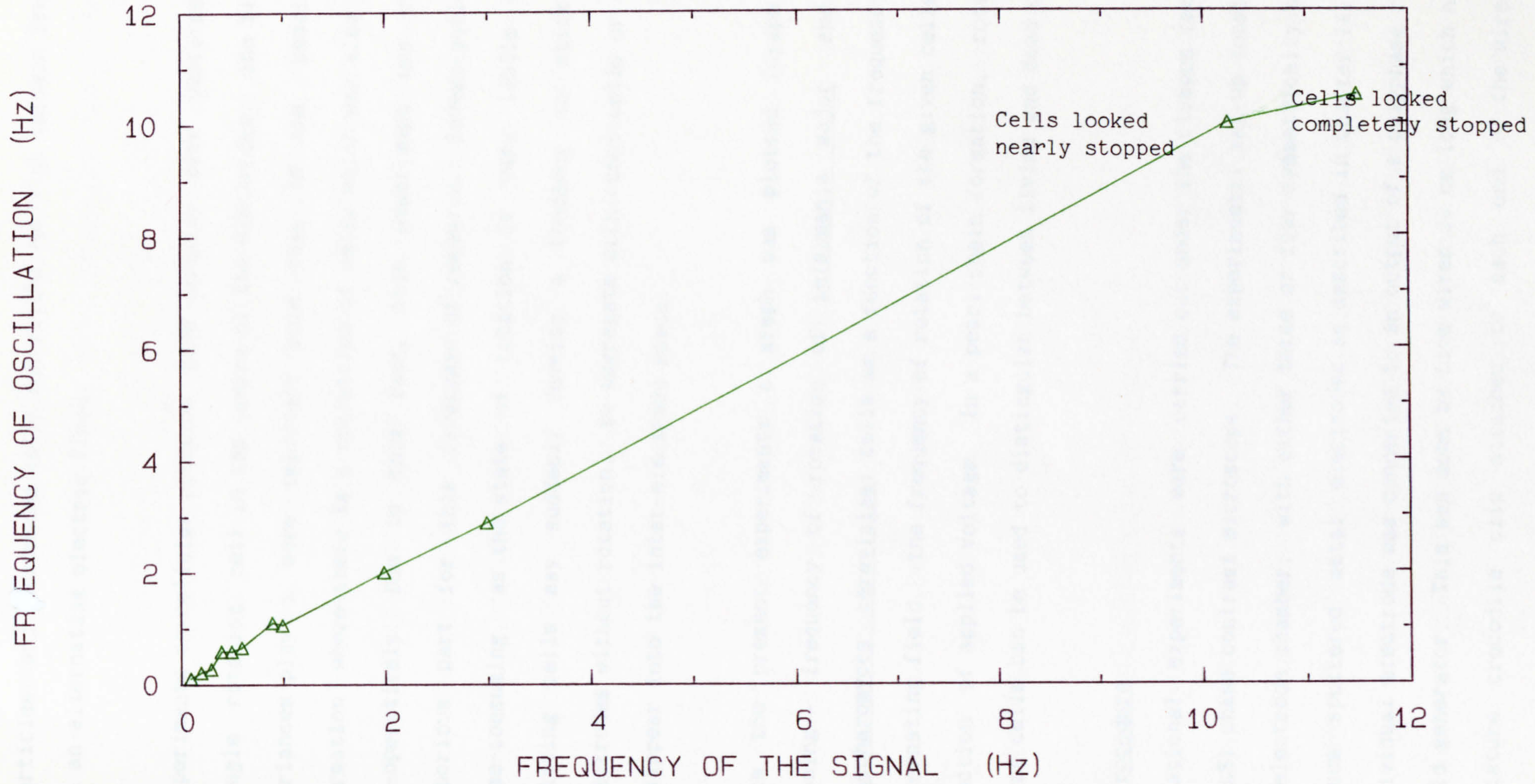

particles and suspended cells can rotate (6-7) at certain frequencies in an alternating electric field.

Experiments on cellular rotation have usually been performed on a single rotating cell in the centre of the electrodes. The biological variances play a more important role than in the "pearl chain" formation where there is a collection of cells which may also interact co-operatively. Due to this fact, this experiment was the most laborious part for this programme of research. Investigations were time-consuming, as the state of rotation is very labile and the rotating cells may suddenly develop a tendency to stick to the electrodes without rotation, to aggregate with other cells or just to disappear into the inter-electrode space.

From the present experiments a graph was plotted [Graph (8.2)] showing:- frequency of rotation of Leishmania major and yeast (Saccharomyces cerevisiae) cells as a function of the frequency of the alternating field, the frequency of rotation of the given cells as a function of applied voltage. In a pearl chain formation, rotation of given cells can be used to distinguish between living and dead cells.

8.3.1 Procedure

Rotational experiments were carried out under the Olympus (model BHB 413LS) phase contrast microscope. The experimental set-up consisted of an electrode chamber, with either three or four symmetrically arranged vacuum sputtered metal electrodes as described in Chapter (4). Each individual electrode was connected to an output of a polyphase rotating field generator. This was done by fine wires 30 cm long which had one miniature crocodile clip attached to each end of the wires. The

circuits that produce the rotating electric fields are discussed in Chapter (5). All the experiments were performed at room temperature.

Yeast cells (Saccharomyces cerevisiae) were grown on sterile liquid medium (Appendix (1)) for various periods until the reached the expontental phase. The cellular suspension was then centrifuged at 200g for 2 minutes, and the supernate rejected. The cells were re-suspended in deionized water and again sedimented by centrifugation at 200g for 2 minutes, and the supernate again rejected. This purification, or washing was repeated 4 times, the final suspension typically having a specific resistivity in excess of 200 KΩcm. This suspension was then diluted with deionized 0.25M sucrose in water and used in the CSR studies.

For cell rotation experiments Leishmania major promostigotes, cultured in Schneiders Drosophila medium, were rinsed twice in phosphate buffered saline (PBS) PH 7.2 by centrifution (1000g - 10 mins) and re-suspended in 10% (w/v) glucose in distilled water to reduce the conductivity of the medium without subjecting the cells to hypo-osomotic shock.

8.3.2 Problems associated with CSR studies

In this experiment it was observed that once the magnitude of the voltage applied to electrodes was increased at high frequency (>60 kHz), the rotation speed of cells were also increased in the same direction. Therefore it was not possible to measure the frequency of cellular rotation by a naked eye through the eyepiece, and it was decided to do stroboscopic measurements as described below.

The principle of stroboscopic measurements rests on a comparison of the known flashing speed of a lamp with the unknown speed of rotating yeast cells. If a rotating yeast cell with a nearly constant speed is viewed through an optical microscope when illuminated by a flashing light of controllable frequency. The continuous train of flashes coming from the stroboscope was shone into the mirror of an optical microscope (Olympus model HSC) and was thereby directed to the electrode chambers. The eye then perceives conditions of motion of this cell which depend upon its speed relative to the frequency of the light source, i.e. upon the particular positions, during its rotation, at which the yeast cell is seen.

When the rate of viewing is identical with the rate of rotation of yeast cells, movement of the cell appears to be arrested, since any given point on it is in the same position each time it is illuminated.

If the rate of viewing through the eyepiece is slightly lower than the rate of rotation, the body appears to rotate at a slow speed in its actual direction of rotation. This is because any given point on the cell advances slightly each time it is seen, owing to the longer time between observations.

Should the rate of viewing be slightly faster than the rate of rotation, the cell appears to rotate at a slower speed in reverse because the interval between observations is shortened and thus each successive view is of points on the cell which follow each other into the field of vision in the direction opposite to the actual rotation. In practice, the cells never seemed to be stationary and they always had a very slow rotation even at the minimum rotation which was always

looked for. This is probably because the cells do not all have the same and uniform rotation speed.

8.3.3 Sources of error

One of the most likely sources of the error is the accidental change in the conductivity of the suspension, especially when working with low conductivities. This can occur when the suspension comes in contact with any surface where ions are present. Ions can be easily transferred from fingers to the suspension. It is good practice for the experimenter to wear sterilized plastic gloves during the experimental procedure.

Another source of the error, is enhanced evaporation due to draughts in the laboratory. It was found advisable whenever the experiment was in progress, to have all the windows and doors closed. Any change in conditions was especially troublesome. Any draught occurring in the middle of the experiment might increase evaporation and by surface tension effects move the position of the cell in the chamber. The CSR experiments in particular, were performed using a single cell throughout.

Draughts either resulted in evaporation from the edges of the cover slips and hence gave rise to concentration gradients in the suspension of the cells, or resulted in thermal gradients due to heating or cooling of the slide.

8.3.4 Results

During the course of this experiment, several phenomena were noticed concerning the rotation of yeast cells. These were associated with (a)

AC and DC responses (b) concentration, (c) conductivity, (d) age of the colony, (e) resonance behaviour, and (f) voltage dependent.

(a) AC and DC responses

The cellular rotation of both yeast (Saccharomyces cerevisiae) cells and Leishmania major cells for both AC and the pulsed DC spectra were quite similar in that the cells continued to spin in either field of the same basal frequency and applied field strength (30 kHz - 20 V p-p). This finding assures one that the cells are possessed of natural, intrinsic, oscillating electric fields.

(b) - Concentration

Unlike the pearl chain formation technique the rotation of the cells is not dependent on the concentration of cells and it was even possible to observe the rotation of a single cell in the centre of the chamber. When a high concentration of yeast cells were used, it was possible to see most rotations were in places where the electric field existed between the electrodes.

(c) Conductivity

The higher the conductivity of the solution, the higher frequency at which the cells started to spin. The conductivity of 0.5 x 10^{-3} S/m was the maximum conductivity at which the cellular rotations were observed, beyond this the cells just drifted out of the viewing field. The cells were usually suspended at a conductivity of 0.5 x 10^{-6} S/m.

(d) Age of the colony

The rotations of cells were proven to be dependent upon the age of the colony being examined. When yeast cells were grown to the stationary phase (incubation time = 24 hours) and then examined for rotation, the maximum cellular rotation was 0.1 rev/sec at a voltage = 40 V peak-peak and frequency of 30 Hz. Whilst the yeast cells were in the exponential phase (incubation time = 14 hours) and then examined in a similar experiment, the rotation speeds were increased by a factor of four to 0.4 rev/sec. Cells killed by heating did not spin at all when subjected to high frequency rotating electric fields, AC or pulsed DC.

(e) Resonance behaviour

A study of cell rotation as a function of frequency was made for both parasites and yeast cells which were grown to exponential phase (incubation time 14 hours). This experiment was repeated for three similar samples each with a one day interval. The results of the experiment are shown in Graphs (8.2) and (8.3). The spectra of the rotation of the given cells for different values of supply frequency of the oscillator, show the sharply resonant character of the spinning resonance of the cells in respect to the applied frequency, which led to the adoption of a descriptive term, "cellular spin resonance (CSR)", [2, 3]. CSR frequency is the applied frequency at which all the cells in the suspension would spin at their greatest speed under the applied field and the CSR frequency varies from one cell type to another.

When the direction of the rotation of the electric fields inside the chamber were reversed, the direction of rotation of the cells were also reversed, and when the distance between the electrodes was increased, the rotation speed decreased.

(f) Voltage dependent

The speed of cell rotation was also found to be voltage dependent in that an increase in applied voltage increases the rate of revolution.

A wide study of cell rotation as a function of the applied voltage for different values of supply frequency were made and the results are shown in Graphs (8.4-8.11 & 8.12-8.16). As one may observe the relationship between the rotation frequency and the voltage (peak-peak) in linear at low supply frequencies as shown in Graph (13.3), and, as the supply frequency increases, the relationships change to square law dependence as seen in Graphs (8.6-8.11) & (8.14-8.16).

GRAPH (8.2), Cellular spin resonance for Sacromyces cerevisiae cells

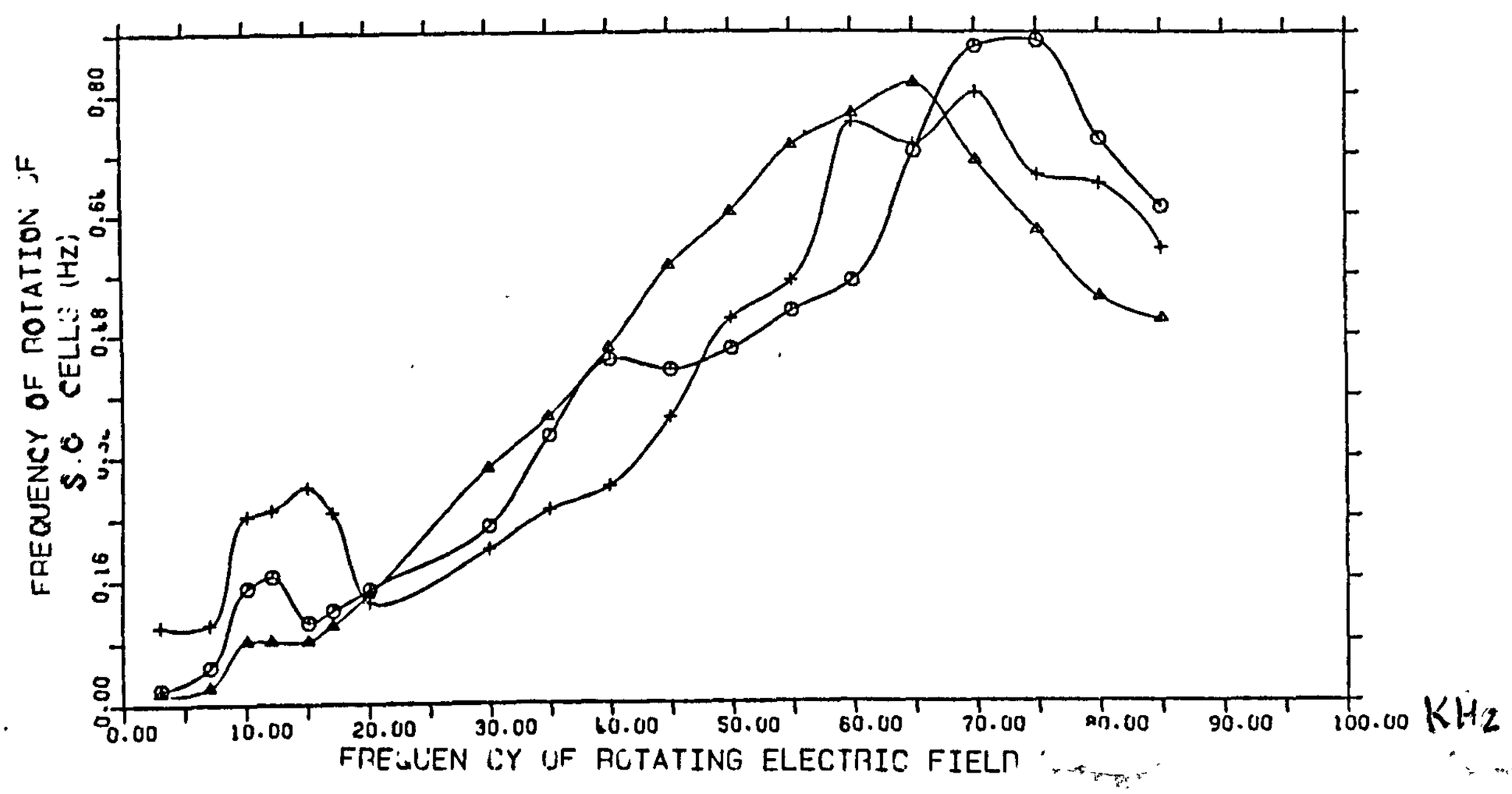

Graph (8.2) Cellular spin resonance for Saccharomyces cerevisiae cells

GRAPH (8.3). Cellular spin r sonance for Leishmania major cells

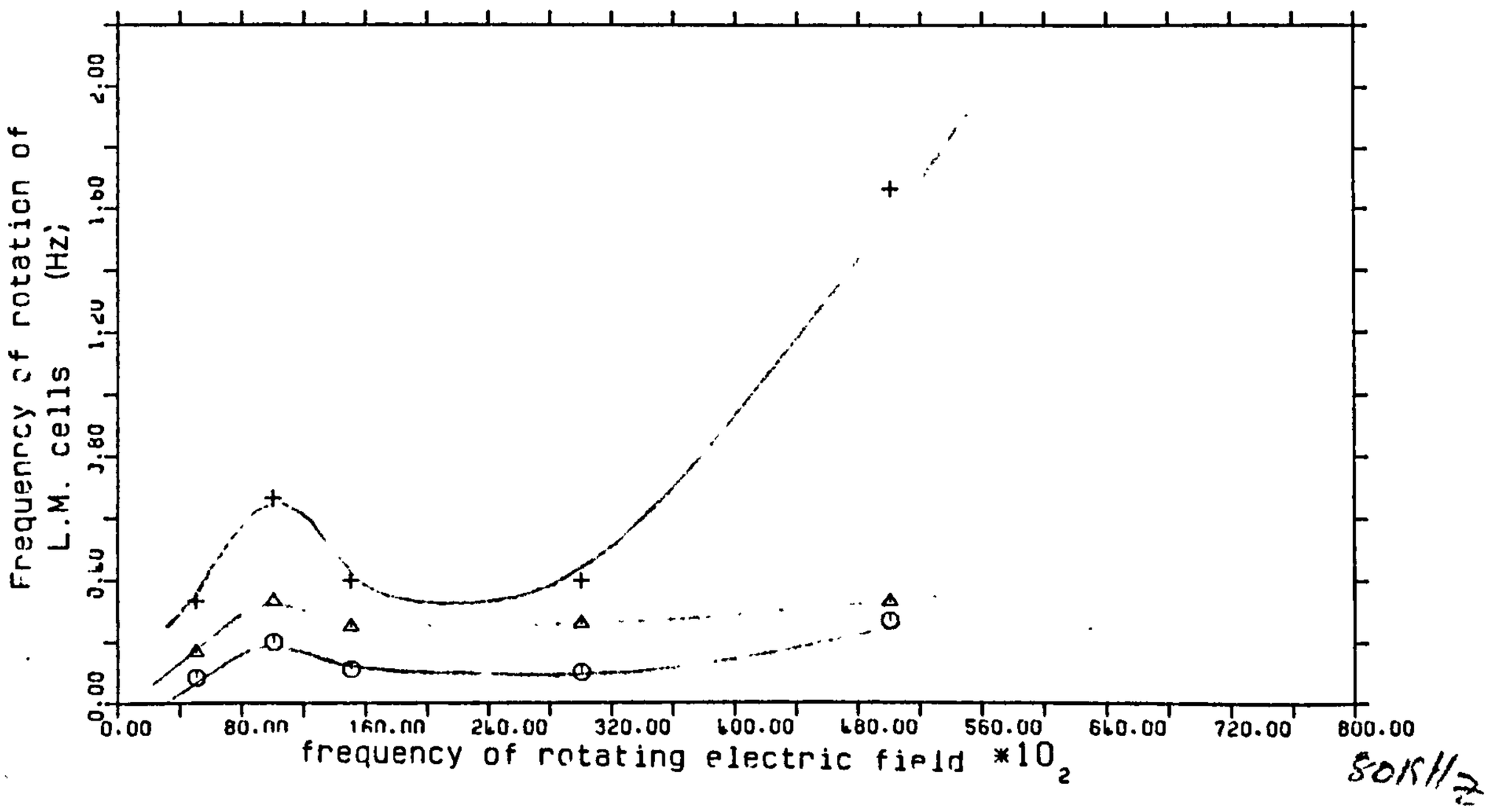

Graph (8.3) Cellular spin resonance for Leishmania major cells

Furthermore, as the graphs show, the gradient of these lines is not of the same magnitude. However, the experimental condition for each type of cell tried was made to be the same. Since there is a significant variation between them, it is a good idea to plot one single line for kinds of cell in a graph to represent the variation of gradient with respect to any change in voltage between the electrodes. The gradient of the lines in graphs (8.4-8.16) was determined by using the least square method. Appendix (4) covers all the necessary formulae to determine the constant gradient and intercepts, as well as the percentage error in the gradient and intercepts, for a straight line graph. To prepare the calculation using these formulae using a prime computer, a program was written in BASIC language. The program is listed in Appendix (4) and has a lot of other features incorporated.

GRAPH (8.8). Signal frequency 40 KHz.

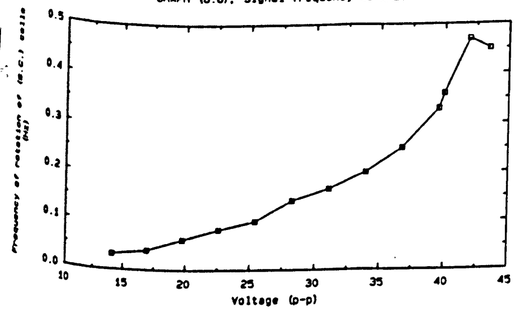

GRAPH (8.9). Signal frequency 50 KHz.

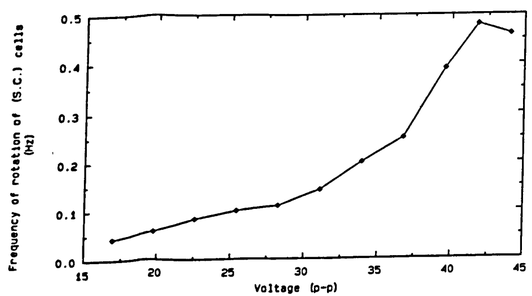

GRAPH (8.10). Signal frequency 60 KHz.

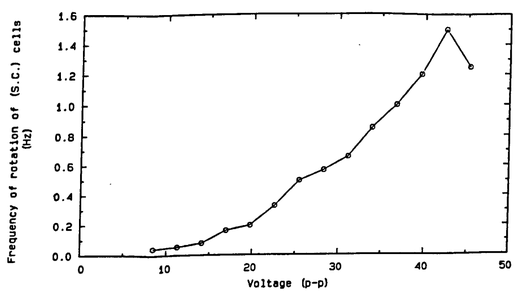

GRAPH (8.11). Signal frequency 76.5 KHz.

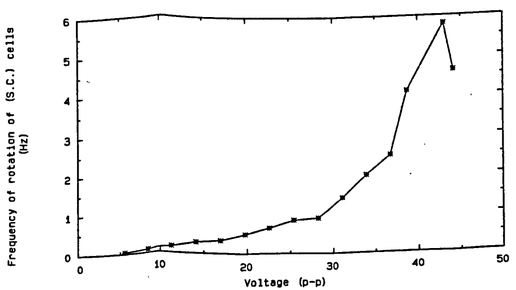

GRAPH (8.4). Signal frequency 3 KHz.

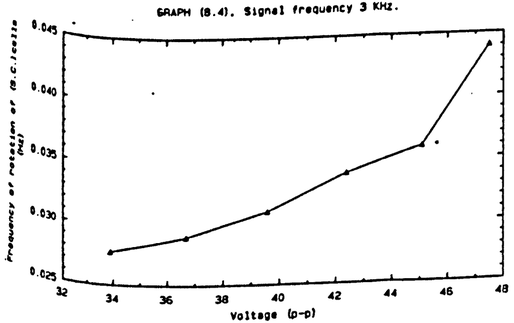

GRAPH (8.5). Signal frequency 10 KHz.

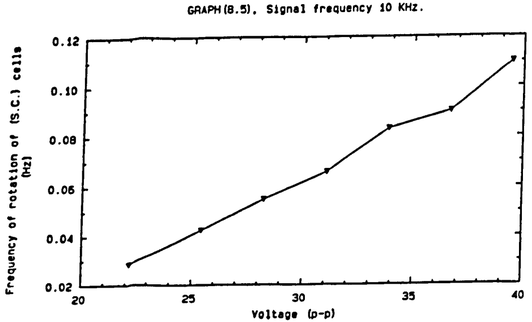

GRAPH (8.6). Signal frequency 20 KHz.

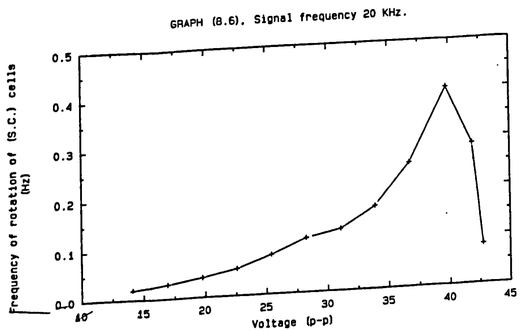

GRAPH (8.7). Signal frequency 30 KHz.

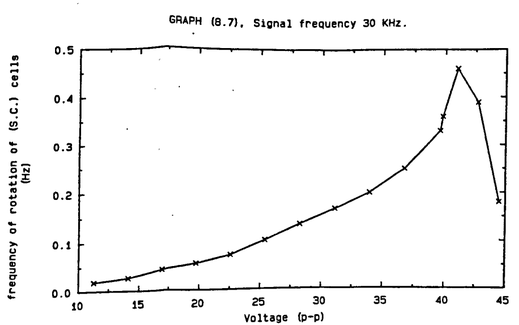

GRAPH (8.12). Signal Frequency 5 KHz.

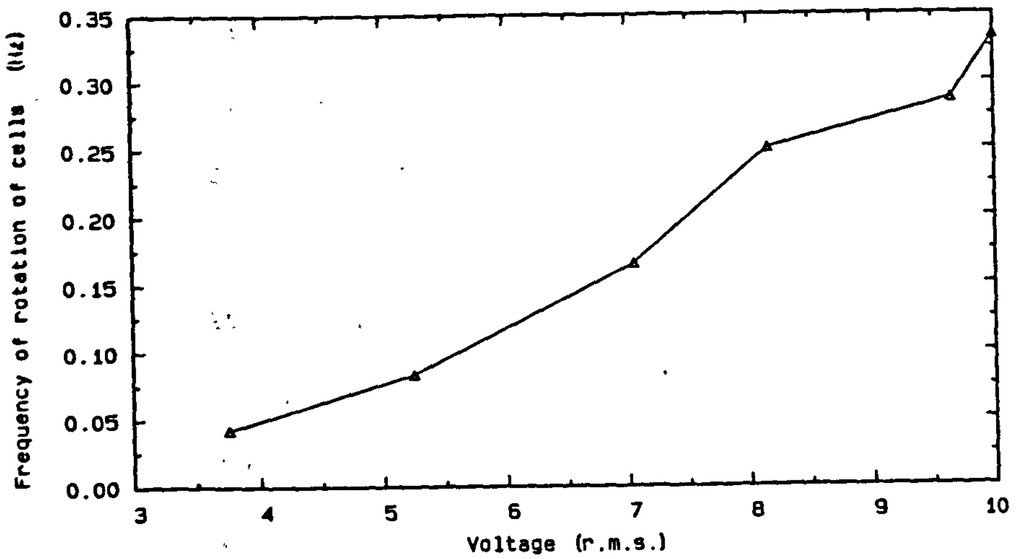

GRAPH (8.13) Signal frequency 10 KHz.

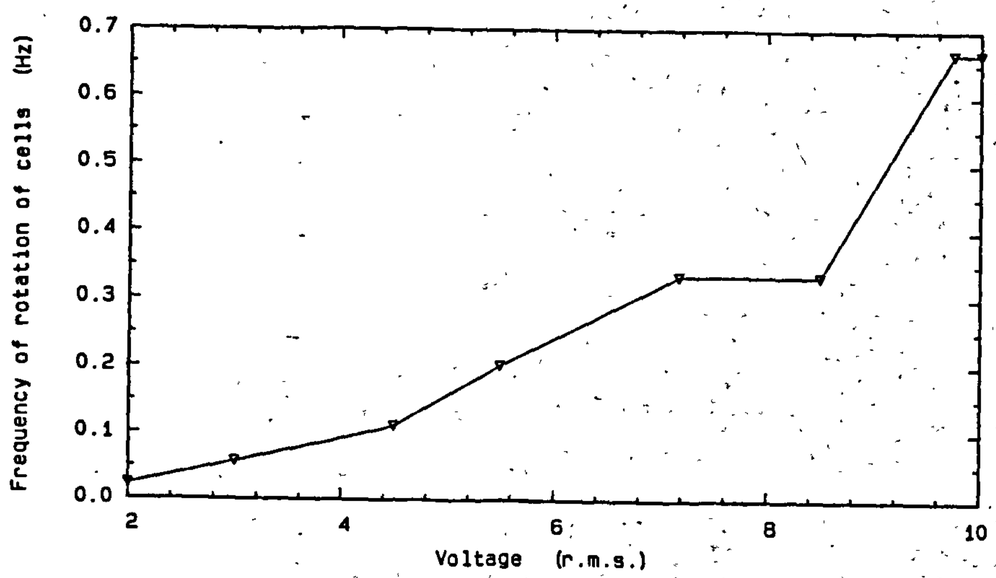

GRAPH (8.14). Signal frequency 15 KHz.

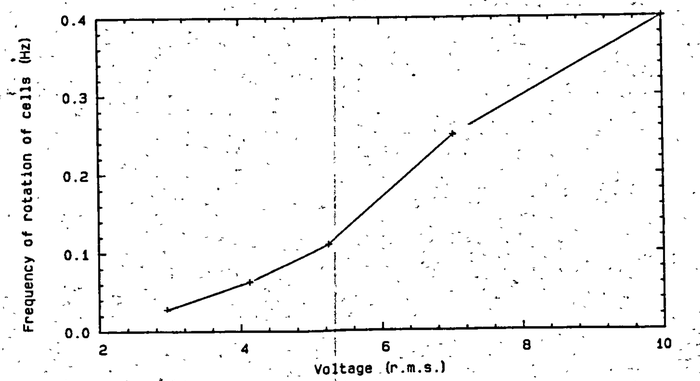

GRAPH (8.15). Signal frequency 30 KHz.

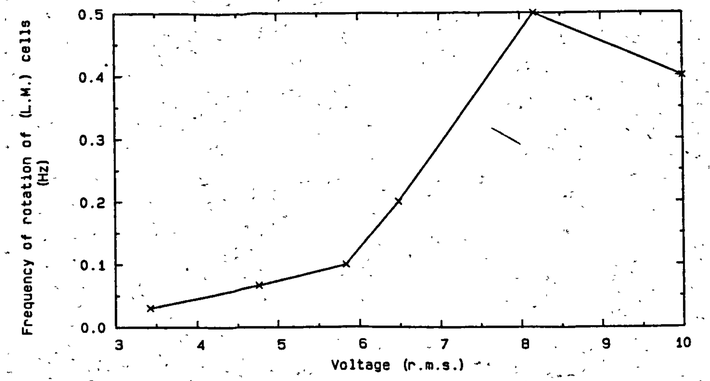

GRAPH (8.16). Signal frequency 50 KHz.

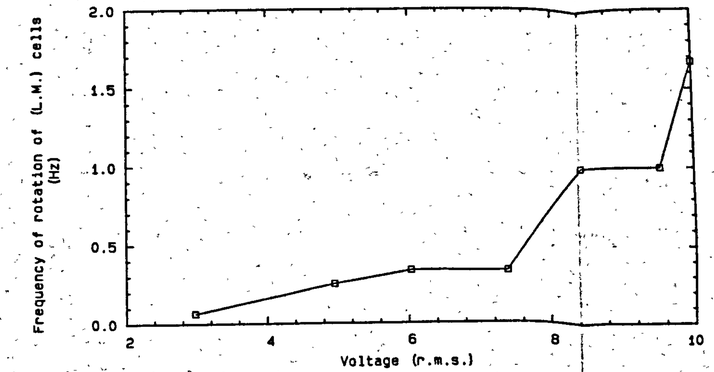

Once the program has been loaded, it will ask the user to input a set of data points. These data points can either be 'input' at a terminal on real time, or they can be transferred from a file already 'exited' in the user's file. Graph (8.17) shows the variation of gradient for both yeast (S.C.) cells and Leishmania major cells for any change in voltage between the electrodes.

8.4 Discussion

The use of sputtered thin film metal electrodes allows the obervations to be carried out at high optical magnifications so that a single cell, right in the centre of the chamber far from the electrodes and other cells, can be seen rotating or spinning in the rotating electric field. This provides a simple and straightforward method for obtaining the dielectric properties of individual cells.

At Hz. and sub-Hz. frequencies, the alternating movement of pearl chains towards each of a parallel plate electrode confirms the idea that there are charged phenomena associated with the cells, and different groups of cells in the same suspensions which appear to have different surface charges at different times.

The use of a rotating electric field can simplify and improve the accuracy of cellular spin experiments.

When increasing the distance between the electrodes the rotation frequency decreases. This is on the contrary to effect of voltage between the electrodes. Furthermore, if two cells of different radius are examined under the same conditions, the cell with the smaller radius will rotate with a higher speed than the larger one. Further

GRAPH (8.17), GREEN LINNE >>> L.M. CELLS, BLUE LINE >>> S.C. CELLS

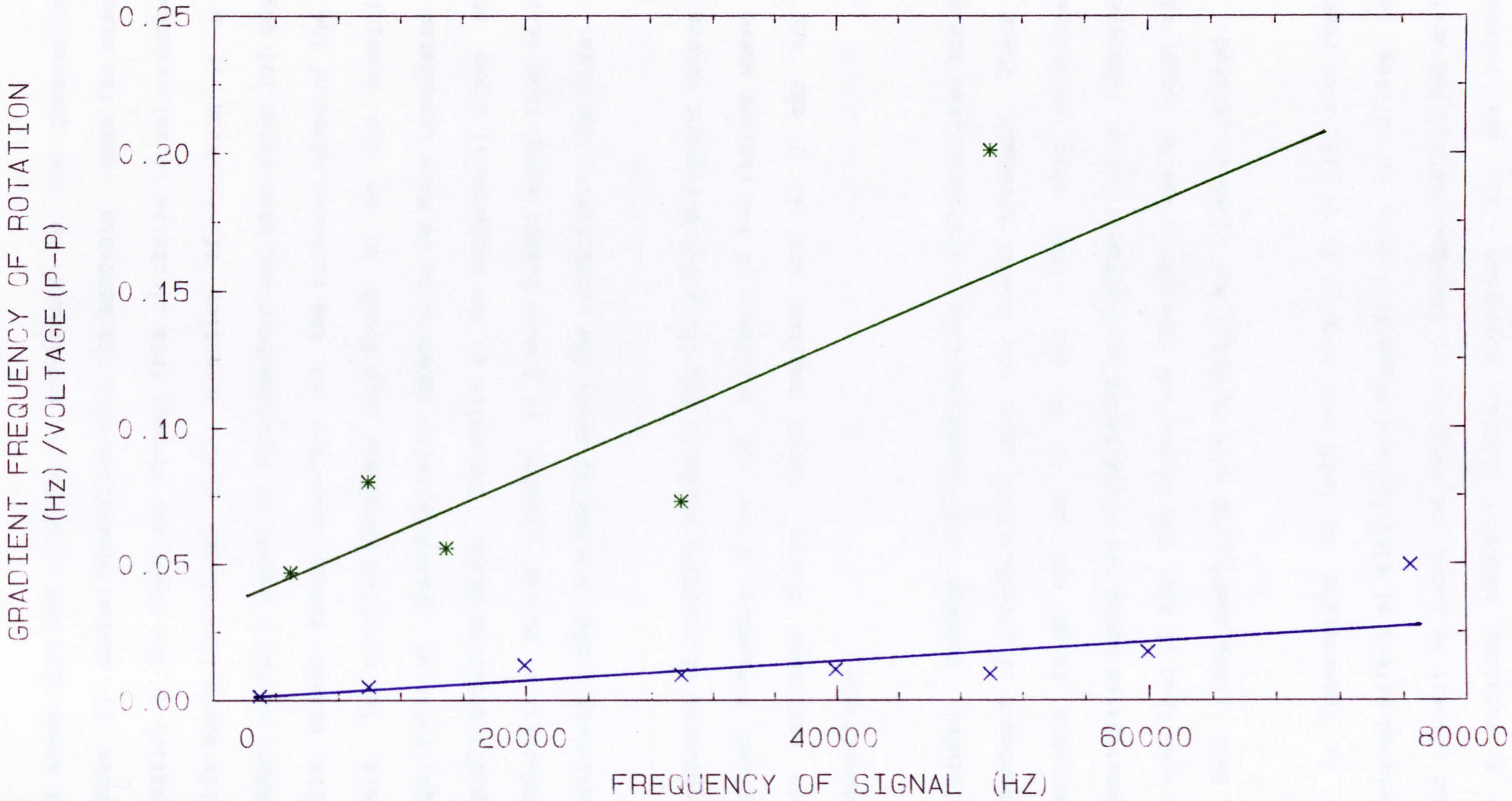

work shows that the rotation is attributed to the generation of a dipole by charge separation with the membrane, when the direction of rotation of the field was changed from clockwise to anti-clockwise, the cells would also change their direction of rotation in a similar manner, unlike a number of experimenters who have shown [9] that living cells always rotate contrary to the rotation sense of the electric field. The rotation speed was also found to be age sensitive. The high rotation frequency value appeared to be more associated with the rapidly dividing state. The cells at the exponential phase in a low conductivity medium rotated at a much higher speed than cells at the stationery phase in a medium where the conductivity was high.

A spectrum of rotation speed of the cells for different values of the applied frequency shows the existence of two regions where cellular spin resonance occurs. These regions are at 3 kHz and 70 kHz respectively.

Halzapfel, Vienken and Zimmerman [10], also predicted the square law dependence of rotation rate upon the field strength. Their optimum frequency range was 20 to 30 kHz. When this relationship was investigated using the 4 electrode arrangements for a frequency range of less than 20 kHz, the square-law dependence was no longer valid, and in fact, these quantities were directly and linearly related.

It is interesting to note that Ribeiro et al [11] also reported the combined effect of electric and magnetic fields on living cells. In this context he noted the rotation of deoxygenated sickled erythrocytes in a rotating magnetic field. Zimmerman [12] also points out the

occurrence of rotating fields and the generation of cell rotation by rotating fields were linked with the occurrence of magnetic fields.

The evidence that living cells naturally produce oscillating electrical fields in the rf region is by now quite strong, and proceeds from a variety of pieces of experimental evidence.

i) CSR is observable with sharp resonance in living cells but not dead cells (see, however, Zimmerman, et al. [13].

ii) Living cells continue to exhibit CSR in either AC or pulsed DC fields. If the cells possessed induced-polarization dipoles only, they would be expected to librate but not spin in high frequency pulsed DC fields.

The presence of natural electrical oscillations in living cells is well-established. They are present in a wide variety of organisms, and vary with the physiological state of the organism. The above evidence pin-points the rf range as also being of importance.

REFERENCES

1) FRÖHLICH, H. and KREMER, F. "Coherent Excitations in Biological Systems", York: Springer-Verlag, 1983.

2) RIVERA, H., POLLOCK, J.K. and POHL, H.A. "The A.C. Field Patterns About Living Cells", Cell Biophysics, 1985, 7, p.43.

3) POHL, A. and BRADEN, T. "Cellular Spin Resonance of Aging Yeast and Mouse Sarcoma Cells", J. Biol. Phys., 1982, 10, p.17.

4) JAFARY-ASL, A.H., SOLANKI, S.N. AARHOLT, E. and SMITH, C.W. "Dielectric Measurements on Live Biological Materials Under Magnetic Resonance Conditions", J. of Biological Physics, 1982, 11, p.15.

5) JABERANSARI, M. "Dielectrophoretics, Electrodynamic and Magnetic Resonance Phenomena In Yeast Cells", M.Sc. Thesis, University of Salford, 1985.

6) POHL, H.A. "Electrical Oscillation and Contact Inhibition of Reproduction In Cells", J. Biol. Phys., 1981, 9, p.191.

7) ZIMMERMAN, U., VIENKEN, J., PILWAT, G. "Rotation of Cells In An Alternating Electric Field", Z. Naturforsch, 1981, 36C, p.172.

8) FUHR, G., GIMSA, J., GLASER, R. "Interpretation of Electrorotation of Protoplasts", Studia Biophysica, 1985, 103(3), p.149.

9) HAGEDORN, R. "Calculation of Rotation of Biological Objects in the Electric Rotation Field", Studia. Biophysica, 1984, 102(3), p.229.

10) HOLZAPFEL, C., VIENKEN, J. and ZIMMERMAN, U. J. Membrane Biol., 1982, 67, p.13.

11) RIBEIRO, P.C., DAVIDORICH, M.A., WAJNBERG, E., BEMSKI, G. and KISCHINEVSKY, M. Biophys. J., 1981, 36, p.443.

12) ZIMMERMANN, J. "A report About Bioelectromagnetics", Bio-Electro-Magnetics Institute, Boulder, Colarado, 1988.

13) ZIMMERMANN, U., SCHEURICH, P., GUNTER, P. and BENZ, R. "Cells with Manipulated Functions: New Perspectives for Cell Biology, Medicine and Technology", Agnew Chem. Inst., 1981, 20, p.325.

14) BURT, P.H. and PETHIG, R. "Applications fo dielectrophoresis to the study of colloidal suspensions". IOP Short Meetings Series, 1989, No. 21, London.

CHAPTER 9

CELLULAR ATTACHMENT

9.1 INTRODUCTION

It is well acknowledged that while many cell lines can grow in suspension, other cell lines and most primary cells require a substratum, on which they can adhere and spread for growth. In 1968 Stoker et al, [1] demonstrated such anchorage dependence of growth by adding glass fibrils 500 μm in length to cells held in soft agar or methyl cellulose suspension. In the absence of fibrils, or in the presence of silica fragments smaller than the cells themselves, the cells did not grow. When the fibrils were added the cells attached to them, spread, and grew into colonies. This indicates that the cells must attach and spread in order to grow.

Cell adhesiveness plays a role in developmental process such as cell migration during embryogensis and morphogeneses in response to particular extracellular matrices. It plays a role in homeostatic processes such as tissue and organ stability, thrombosis, inflammation, and wound healing, and it plays a role in the pathology of various disease states. [2]

Polystyrene dishes have been used for cell cultures for at least the past twenty years. Many cell types adhere to, and move on, the surfaces of such materials and present a morphology that is very similar to that seen when the cells are grown on glass. However, it is known that when the polystyrene is subjected to a chemical surface treatment it becomes suitable for cell attachment.

Polystyrene surfaces, as pressed by the manufacturer, are unsuitable for cell attachment. This has been attributed to the surface chemistry of the polystyrene, and many different suggestions have been made as to

the precise chemistry involved in the non-adhesive nature of polystyrene. [2, 3]

Several processes appear to be in use commercially for making the dishes suitable for cellular adhesion [4] though, regrettably, little information has been published by manufacturers about their own techniques. Martin and Rubin [5] reported that treatment of polystyrene with concentrated sulfuric acid followed by exposure to ultraviolet light (used by them for sterilization), converted the surfaces of the dishes into a state suitable for the adhesion of fibroblasts. Maroudas [6] suggested that this treatment leads to the sulfonation of the polystyrene with a consequent increase in the number of charged groups per unit area. However, it seems likely that the treatment used by commercial manufacturers is a corona discharge, which might induce mild oxidation of the surface of the plastic or destruction of any mould release agent used in manufacture. Klemperer and Knox [3] found that treatment with chromic acid, which might produce hydroxyl, aldehyde, or carboxyl groups on the surface, led to increased cell adhesion. They suggested that cell adhesion required the presence of charged groups, which might be either carboxyl or sulfonate. However, in 1973 and 1980, Curtis et al [7] and Gingel et al [8] respectively, reported that the attachment to surface decreases rather than increases as the surface charge density is raised. This evidence appears to be a direct contradiction to the idea that charged groups on the surface are responsible for cell adhesion. Moreover, the two studies on modification of polystyrene both used the crystal violet dye method for measuring the surface density of charged groups. This method is suspect because it requires the binding of several hundred dye molecules per A° of the surface in order to detect one charged

group. Furthermore, measurements of the surface charges produced by sulfonation, by Gingell et al [8], using electroendosomosis, gave a low value of only 1.3^{3} esu cm^{-2}. Thus there are two reasons for doubting whether the presence of charged groups on polystyrene is required for cell adhesion. In addition the results of work by Martin and Rubin (5) suggested that there is a correlation between cell attachment and the number of negative charges on the surface, therefore it can be assumed that the charged groups are all anions: and surfaces bearing cations which are very adhesive for cells.

This chapter investigates the cases of the attachment of Leishmania major cells to scratched polystyrenes or charged substrate, and includes measurements of attachment on electron and positive ion charged surfaces using Leishmania major cells. Perhaps somewhat arbitrarily this research is felt to be very relevant to reaching an understanding of the mechanism of cell adhesiveness.

9.2 Scratched plastic as a substrate for attachment

During cultivation of some flagellates [12], in Schneider's Drosophila medium and Grace's insect tissue culture medium, some flasks were initially inadvertently scratched with the tip of a metal needle or a pasteur pipette, or a diamond, and Leishmania major cells were cultured in them. All Leishmania major cells were attached to the scratched area (after 48 hours) and formed colonies. Attachment led to an increase in the division rate of the major cells. After 13 days the number of Leishmania cells cultured in scratched flasks was approximately increased to about five times compared with unscratched controls. An example of attachment of Leishmania major cells to a scratched polystyrene is shown in Fig (9.1). Fig. (9.3) magnifies the

same attachment of parasites to the scratched polystyrene by an electron micrograph about 3.000 times. Notice how the parasites are attached to the side of the scratch in tissue culture plastic and not to the original surface of the plastic.

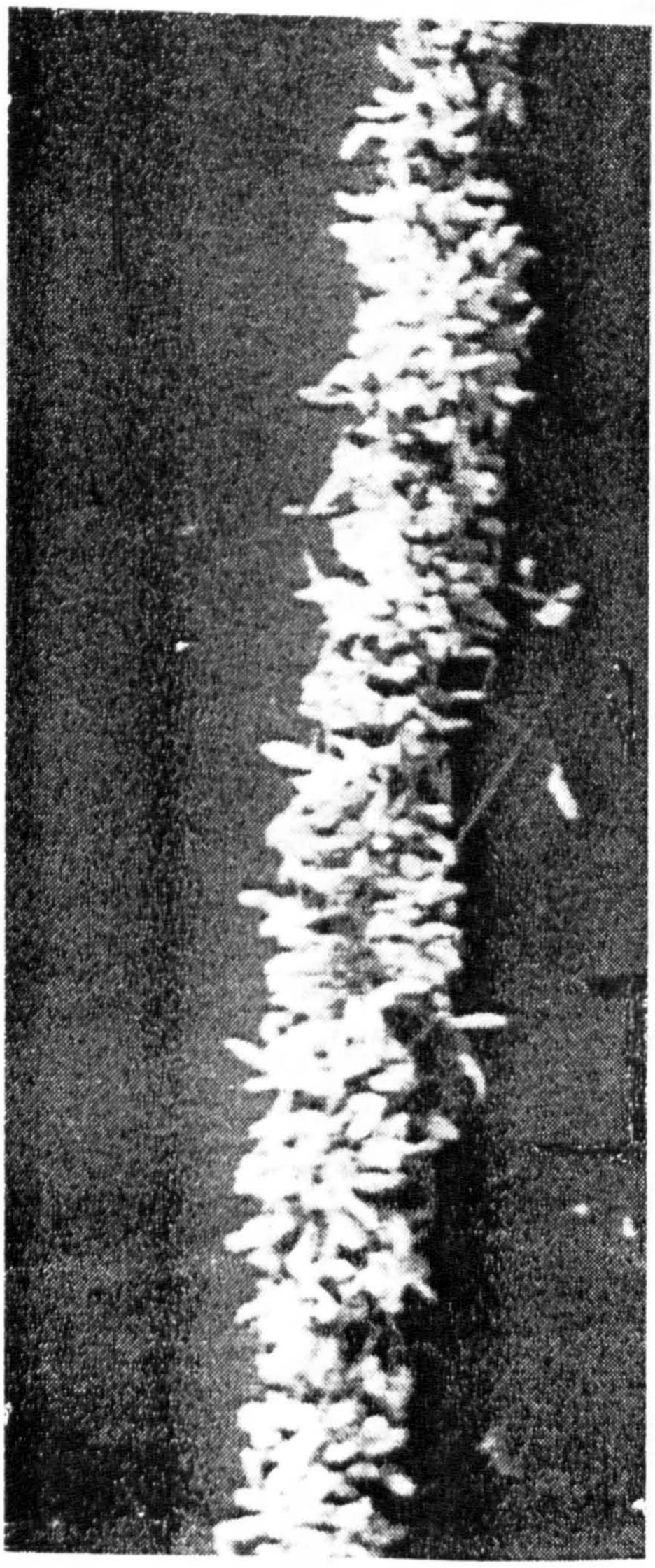

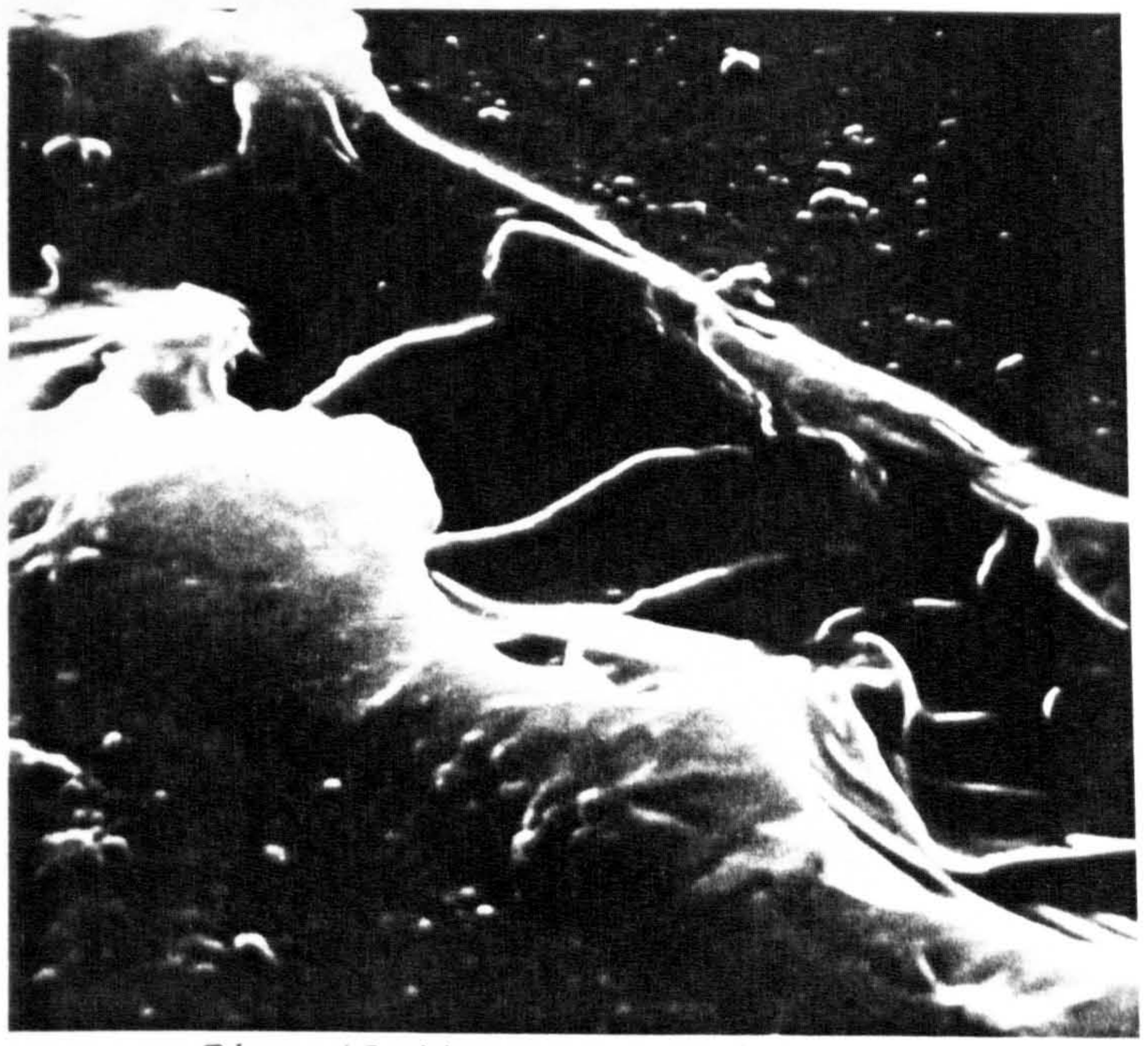

Fig. (9.1) A type of scratch made by the tip of a metal needle or a pasteur pipette over polystyrene petri dishes (x 1000)

Fig. (9.2) Shows how L.major parasites may attach to the scratched area as shown in Fig. (9.1) (scanning electron micrograph)

Fig. (9.3)

Leishmania major promastigotes attached to the side of a scratch in tissue culture plastic (S) and not to the original surface (OS). Electron micrograph x 3.000

9.3 Surface of substratum

Many of the recent studies indicate that there may be specialised regions of negative charges on the cell surface [9]. The posterior sites of a Leishmania major cells may have higher negative charge density than its anion sites. Also, as said before, Martin and Rubin [5] suggested that the substratum may have a surface bearing cation. For a polystyrene dish this will only be true when it is subjected to a surface treatment, something similar to a scratch made by a needle, which would be suitable for cellular adhesion. This causes electrification of polystyrene by friction between needle and the polystyrene surface.

The surface of these scratches appears to carry a higher negative charge than the surrounding plastic resulting in an electron dense subsurface layer visible in electron micrographs (Fig. (9.3)).

However, the possible role of the distribution of cations on polystyrene surfaces require further study.

When adhesion of Leishmania major cells was examined under a microscope, it was noticed that all Leishmania major cells were adhesed to the surface of the scratch by their anterior sites. A typical example of them is shown in picture (9.3). This tells us of the possibility that the posterior sites of a L.major cells has a higher density of negative charge compared to its anterior sites, and hence, this causes the anterior sites to be attached by the surface of the scratch (unlike charges attract) and the posterior sites to be repelled comparatively (like charges repel).

Whether or not this attachment is a result of a substrate surface charge, which is probably negative, remains to be seen. [10] Eukaryotic cells usually carry an overall negative charge and thus might not be expected to attach to like charge substrates. In bacteria, which adhere to epithelial surfaces in vertebrates, the attaction between hydrophobic molecules on the bacterial surface and the hydrophilic phospholipid molecules in the lipid bilayer membrane of the epithelial cells, probably overcomes a similar charge repulsion.

9.4 The physical implications of the attachment of L.major cells to electron bombarded surfaces

The treatment of polystyrene petri dishes to give electrostatically charged surfaces showed that attachment may be mediated through an electrostatic charge phenomenon at least as a contributary mechanism. Clearly, the L.major cells have decided that the electron charged surface is a good place to stick. Such an observation suggests that 'in vivo' in the insect host, a combination of mechanisms must be involved. Some host surfaces certainly carry negative charge within which can be visualised using cationic ferritin. [10] To investigate the polystyrene surface effect, a small piece of polystyrene was dissolved in toluene. Once the solution was liquified and prepared, a very small amount of it was poured by pipette over the base of a prepared flat glass beaker. The beaker was then spun rapidly in a photomist spinner at 1000 revolution/sec. This formed a nice uniform thin film polystyrene over the glass. The thin film polystyrene was left overnight in a clear air room cabinet. Once the thin film was dried, U.V. light was shone over it for the following 24 hours. The sample was finally scratched by a sterilized diamond and the plate was then carefully taken to the Biology Department for cell attachment

experiments.

Experiments carried out on these thin film polystyrenes gave the same sort of attachment as petri dishes. However, since the polystyrene was a thin film, it floated on the surface of the culture medium in the beaker with the cells attached to the under surface of polystyrene. Furthermore, to eliminate the possibility of attachment by surface effects with polystyrene, it was decided to repeat the attaching of parasite cells with the glass petri dishes. A glass petri dish (Labap Laboratory Equipment (50ml capacity)) was created by electron beam bombardment with a dose of 5×10^{19} e/m^2 . The L.major cells were cultured and left in an incubator for 48 hours. Observation of this glass beaker revealed the same sort of cell attachment as was obtained by polystyrene petri dishes. There was no attachment of any kind to a control glass petri dish which had not been bombarded by an electron beam. This strongly supports the idea that cell attachment is mediated by a negative charge phenomena. It was then decided to repeat this using polystyrene petri dishes.

This part of the chapter summarizes some results obtained when the petri disches were

a) negative electron bombarded

b) position ion implantation

9.4.1 Electron bombardment

This experiment was tried many times for different ranges of doses of -ve electron charge and the following effects were observed.

attachment	strong attachment	50% attachment				
16	17	18	19	20	21	electrons/m^2
10	10	10	10	0.5x10	10	

Figure (3) dose chart

In the dose range of 10^{16}-10^{17} electrons/m^2 some attachment of cells to the surface of polystyrene may start and can be observed.

The attachment is more or less a twin type attachment (as shown in Figure (9.4)) and the parasites can be detached easily by a jet of water from a plastic bottle.

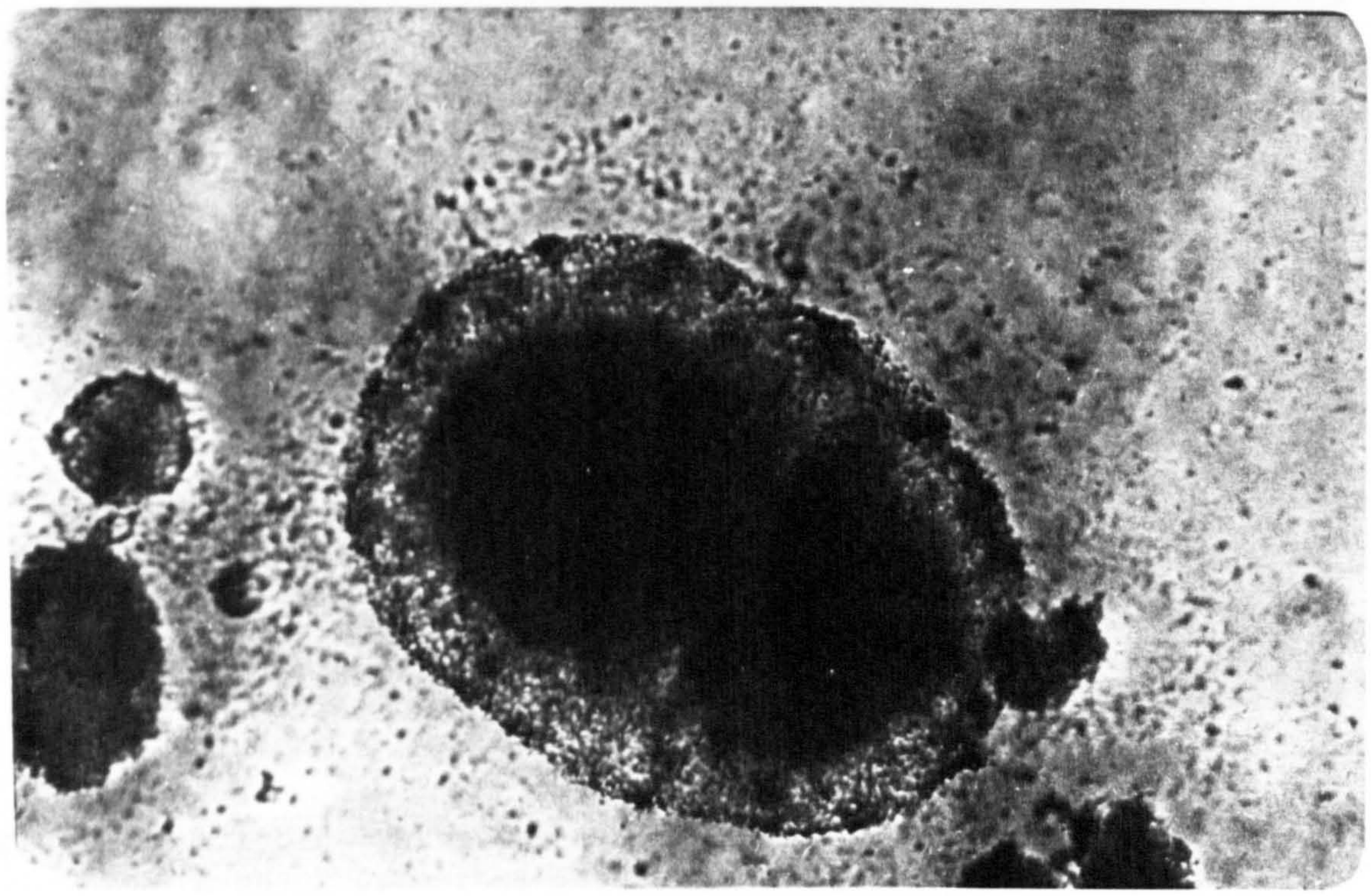

Fig. (9.4) The attachment of L.major cells to low dose elctron bombarded polystyrene petri disches (x 100)

The negative electron beam bombardment dose range of 10^{17}-10^{20} electrons/m^2 presented a stronger cell adhesion than the previous 10^{16}-10^{17} electron m^2 dose range. This dose gave the strongest attachment which could be produced. In this range the parasite flagellum also becomes an attachment organ as in its sandfly host, often expanding its

membrane to increase the area of cell-substrate contact presumably to facilitate adhesion (Figure (9.6)). These cells could not be detached easily with something like a jet of water from a plastic bottle. Usually removing these parasites, a paper tissue had to be smoothly rubbed over them. Rubber gloves were always worn whilst carrying out these experiments under supervision.

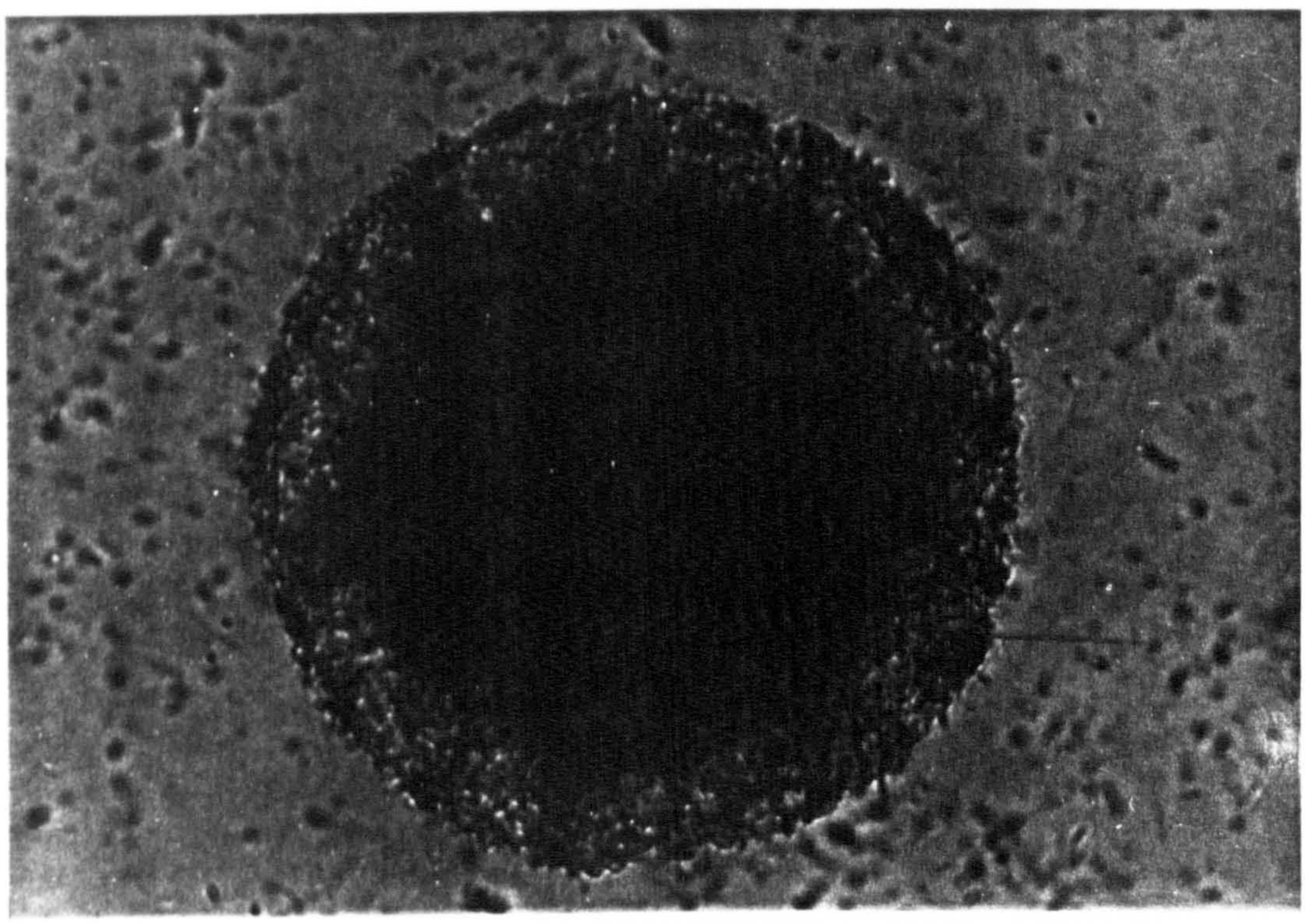

Fig. (9.5) A typical attachment obtained in mid-region dose (10^{19}). L.major parasites attached strongly to a plastic electron bombarded petri dish forming circular colony phase-contrast light micrograph (x 600)

Fig. (9.6) L.major parasites scraped from the petri dish surface (Fig. (9.5). The two cells on the right show short, greatly expanded flagella. Bright field light monograph, Giemsa stained. (x 2000)

Any electron beam dose higher than 1/2 10^{20} electrons/m^2 gives only a 50% effect. More than 19 plates were exposed to an electron beam in doses of more than 1/2 10^{20} electrons/m^2 and only in 9 of them was an attachment observed. The exact cause of this is still not very clear but when a L.major cell attachment was obtained, it was a very strong attachment. The author believes there is a need to extend such studies especially in this high dose range. Unfortunately, this did not prove to be possible since there was only a single high energy electron machine in the Department and that had to be shared with many other researchers in the University. Finally, when this machine broke down, the Department did not manage to find the resources to get it repaired during the time available for doing this research.

9.4.2 Ion Implantation

If electrons can charge the polystyrene surface of a petri dish to a negative potential, then positive ions should charge the surface of a polystyrene petri dish to a positive potential. Previous work on electron beam bombardment of attachment surfaces has shown that the (L.major) parasites have found a negatively charged surface a good place to stick. This was evidenced by an increase in their growth rate and the total number of viable cells; about 5 times compared to those cells grown in the presence of a non-bombarded but otherwise similar surface (the control). The present section of this Chapter reports the results of a set of investigations of attachment of parasites to positive ion implanted surfaces. The researcher was looking for any sort of attachment or any other sort of effect on the L.major cells that may arise once the polystyrene petri dishes have been subjected to either positive or negative ion implantation. There was a wide variety of equipment available to be used and the theories and procedures have been given in Chapter (7). A total of 86 plates were ion bombarded covering a wide range of energies. The total energy spectrum is shown in Figure (9.7).

VAN DE GRAAFF (High energy)		ISOTOPE SEPARATOR (Medium energy)		DC PLAZMA ION (Low energy)	
3 Mev	› 2 Mev	30 kev	›10 kev	1 kev	› 700v
I=5 nA	I = 30nA	I = 30MA	I = 10MA	I = 150MA	I = 25 MA
Exposure time = 25 min.		Exposure time = 7.4-›5 min sec		Exposure time = 15-›1 min	

Fig. (9.7) The energy spectrum of ion implantation.

The plates were either ion bombarded by high energy (MeV) particle ions in Van de Graaff or in a medium range of energy (keV) by N + ion in an

ion separator or lower energy state (volts) by DC Plasma N+ ions.

Unfortunately, none of the samples which had been ion bombarded caused any attachment of L.major parasites, regardless of the energy with which the ion had been implanted.

The most laborious part of this research was the work on medium energy and particle implantation. Many of the samples were often contaminated, due to the limitations on sterilizing and cleanliness possible and the conditions in which the samples could be cared for.

During the course work of DC Plasma Ion in low energies, the surface of the polystyrene petri dish had a change in colour in the place where it was subjected to ion implantation probably due to carbonisation beginning. This had no effect on the cultured cells. Therefore, an ion implantation will not have any effect on attachment of parasites to the implanted substrate, regardless of ion energy state.

This result however, confirms the idea that (L.major) parasites carry a positive charge and they will be repelled by a similar charge (in this case, the + ion implanted surfaces) but they will be attracted by a dissimilar charge (-ve electron bombarded surface) to which they will attach and grow.

9.5 Effect of ionisers on Leishmania cells

It has been ascertained that ionisers will help people to feel in 'top form'; or that ionisers help to relieve specific complaints such as hayfever, bronchitis, asthma, migraine, headaches and sinus infections. And they are also supposed to clean the air. The idea has been put

about that air with lots of negative ions makes a person feel better than air with low levels of ions. Areas such as mountains, the seaside and near waterfalls, have a particularly high concentration of natural occurring ions with the balance tipped in favour of negative ions. These tend to be popularly associated with a feeling of well-being. Equally, many hot, dry winds, like the Sahara in the Middle East and the Fohn in the Alps, are also associated with particularly high concentrations of ions, but in these cases the balance is tipped in favour of positive ions, and these winds have a popular reputation for causing sickness, irritability and erratic behaviour in some people.

Although ions are a very small component in the air, it has been proved that they can have an effect on living things. Evidence for this comes from experiments on bacteria and laboratory animals. This section reports preliminary work looking into any possible effect of air ions on (L.major) parasites. It had already been proven that negatively charged plates resulted in the attachment of Leishmania cells to the charged surface of the plate and gave rise to faster growth of the cells. Exactly what effect, if any, air ions can have on Leishmania cells forms the subject of this section of the chapter.

Proposals

If some negative ions are good for humans perhaps they are also good, or have an effect, on L.major parasites.

The ioniser used in this research was the one designed and built as described in Chapter (5). The basic principle of this ioniser is the same as the other ionisers, a high voltage is applied to a needle sharp point of fine wire; this wire is placed inside a polystyrene petri

dish, pointing downwards, just above the surface of liquid medium with Leishmania cells suspended in it. The wire needed to be sterilized by heating, however, it still often caused contamination of the medium possibly because it attracted contaminants from the air. This wire generated a high concentration of positive and negative ions in a small area above the surface of the medium around the point, the negative. The Polarity ioniser needle is such that it attracts the positive ions and repels the negative ions in the small volume around the point and into the cell suspension (because the needle has negative applied potential). Although the voltage is high, there is no risk of an electric shock if the needle is touched, but ... there might be a static discharge similar to that obtained by shuffling across a synthetic carpet and then touching a metal object.

Some twenty plates have been tested for 48 hour exposures on the theory that lots of negative cells could have an effect on Leishmania cells. The test was negative in all cases and there was not a single piece of evidence that the ions gave rise to any abnormalities in the cells or an increase in the number of cells, except for a few contaminations which were due to the wire not being properly sterilized. Overall, ionisers can help to clean the air, but they had no beneficial effect on Leishmania cells. A lot more research is necessary before we shall know for certain whether ions have an effect on biological cells as distinct from organisms and, if so, how they work. But this research reports that the Leishmania cell cultures do not benefit from ionisers and there are no attachments of L.major cells to the surface of polystyrene petri dishes in the presence of an air ioniser.

9.6 Charge Distribution

In April 1987 Watson [11] reported that the electrons may be thermalized and trapped in polystyrene. This project used an electron beam to inject electrons into the free surface of a polymer. Once these electrons dissipate all their energy in their target material, the surface (polystyrene) carries a-ve charge. The charge was localised in the centre of the petri dish where it was bombarded through a mask but once the suspension of cells was poured into the petri dishes the charge may tend to spread over the whole surface of the suspension. Fig.(9.8) shows the sort of cell adhesion which may occur once the charge is spread all over the surface of the polystyrene.

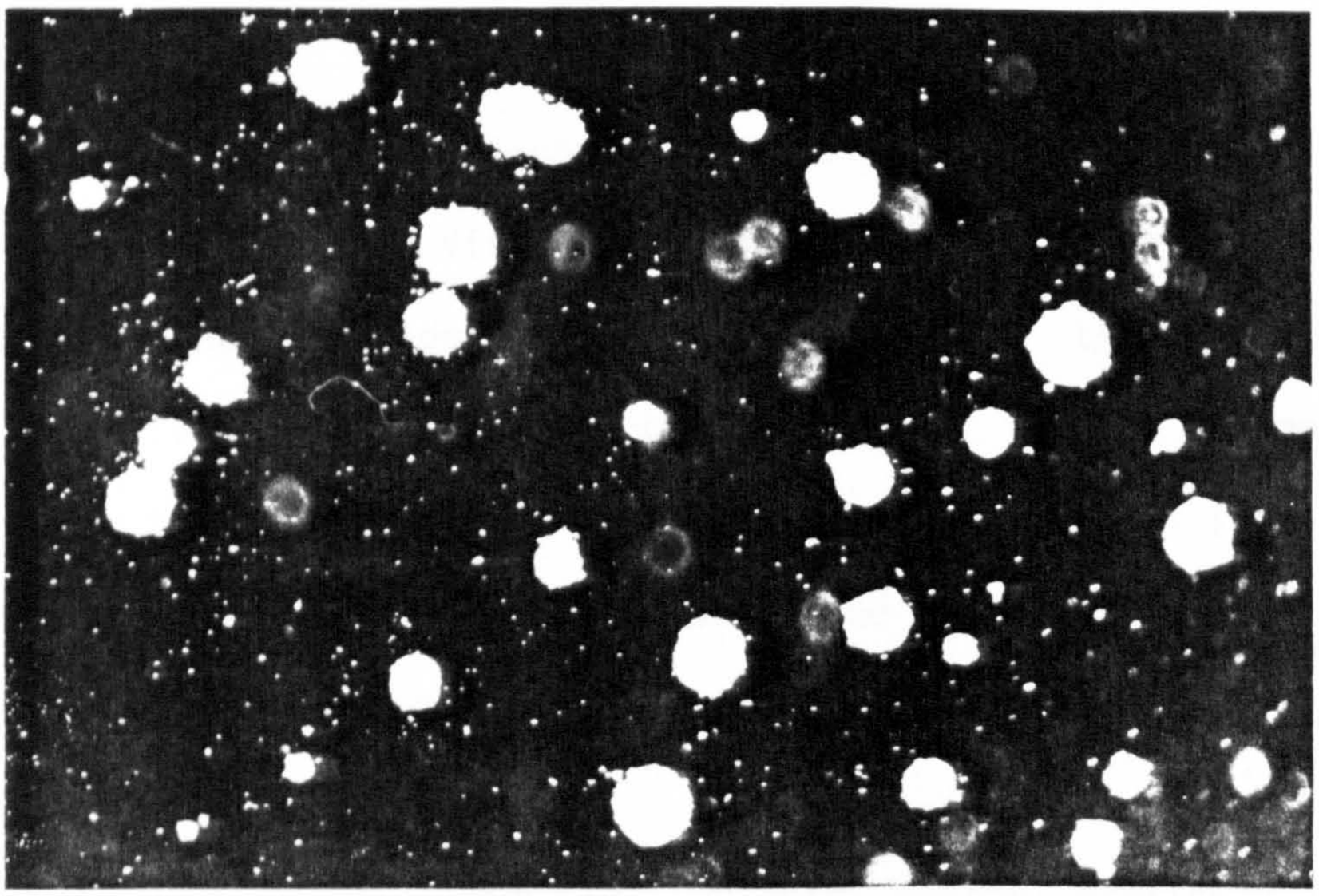

Fig. (9.8) Some circular colonies of L.major parasites have been found and detached to the polystyrene electron bombarded petri dish as a result of negative charge distribution over the surface of the target.

9.7 U.V. Sterlization Effect

When these petri dishes were bombarded by electrons and subsequently sterilized by shining T.U.V. light directly over the polystyrene surface. Unfortunately, this T.U.V. light always dissipated the negative charge and there was no parasite attachment at all in any electron dose range. Therefore, the plates could not be placed under the T.U.V. light for sterilization and each step of the experiment had to be done very carefully, and always wearing plastic gloves. This reduced the contamination risk to an acceptable level and the effect of electron bombardment could be easily seen. This drastic effect of the T.U.V. is probably due to the release of the trapped electrons and the increased conduction of the polystyrene.

It is also found to be advisable to place and keep the electron bombarded petri dish in dry air , apparatus is a glass desiccator over silica gel and to carry the samples about while still in a desiccator.

9.8 Advantages of 'In Vitro' Attachment

One advantage of an 'In Vitro' attachment system for culturing L.major parasites is that it allows a detailed study of the mechanism of attachment. The ultrastructure of attachment "foot" is remarkably similar for both "in vitro" and "in vivo" culturing [12]. Large numbers of parasites can be obtained and cultured and more readily studied in vitro, than when cultured in live insect hosts.

There are already some commercial culture plates available with a microporous membrane surface for cell attachment. (Appendix (5)). However, the attachment of Leishmania cells may easily be oberved when the plates are scored with an electron beam in the right dose range.

The writer points out to those working on the culture of Leishmania parasites that large numbers of flasks, dishes, culture dishes and roller bottles may be "scored" or bombarded with electron beams to improve cell growth at little expense given the basic apparatus.

9.9 Discussion

During investigation of cases of the attachment of Leishmania promastigotes to scratches made in polystyrene petri dishes, it was found that scratches made both with a metal stylus and with a diamond were equally effective, thus eliminating the possibility of surface contamination with metal and consequent chemical or ionic effects.

Polystyrene is a very good electrical insulator having a nominal resistivity of 10^14 ohms.m,the possibility that the attachment effects were due to surface charging by friction when the polystyrene was scratched, was considered. Surface charging of the polystyrene, without gross mechanical damage as described and the resulting enhanced attachment of the L.major is the subject of this section.

By way of a preliminary estimate, the surface density of electron charge which was deposited into the top 8μm of the polystyrene surface and which gave attachment effects in all cases, was from 7.6 x 10^19 electrons/m^2 to 1.5 x 10^21 electrons/m^2. This is greater than the surface charge density of 5 x 10^15 electrons/m^2 which will give the typical trans-membrane potential used for an electrical model of a biological cell [13], although the depth profiles of the charge distributions will be different in the two cases.

Clearly, the Leishmania cells have decided that the electron charged surface is a good place to stick; presumably in some important

respect, it simulates their normal habitat on cuticular surfaces in the gut of their sandfly host. However, one is reluctant to suggest a purely electrostatic explanation because of the likely screening effects of counterions, even if the parasite's vibrating flagellum could act as a vibrating probe electrometer. The provision of the promastigotes with a flagellum is more reminiscent of the possible role of insect antennae as infrared detectors, as discussed by Callahan [14]. Furthermore, Fröhlich predicts coherent electrical oscillations in living biological systems and estimates that they may occur in the sub-millimetre part of the electromagnetic spectrum [15]. It should be realised that although water absorbs electromagnetic radiation strongly from the microwave to the infrared, the absorption is not infinite; the half-value-layer absorption in this region is of the same order as the dimensions of a biological cell [13].

REFERENCES

1) STOKER, M.G.P., O'NEILL, G., BERRYMAN, S. and WAXMAN, V. Int. J. Cancer, 1968, 3, p.683.

2) GRINNELL, F. "Cellular Adhesiveness and Extracellular Substrata", Int. Rev. Cytology, 1978, 53, p.65.

3) KLEMPERRE, H.G. and KNOX, P. "Attachment and Growth of BHK and Liver Cells on Polystyrene: Effect of Surface Groups Introduced by Treatment With Chromic Acid", Lab. Pract., 1977, 26, p.179.

4) AMSTEIN, C F. and HARTMAN, P.A. "Adaptation on Plastic Surface For Tissue Culture by Glow Discharge", J. Clin. Microbiol., 1975, 2. p.46.

5) MARTIN, G.R., and RUNNIN, H. "Effect of Cell Adhesion to the Substratum on the Growth of Chich Embryo Fribroblasts", Exp. Cel. Res., 1974, 85, p.319.

6) MAROUDAS, N.G. "Sulphonated Polystyrene As An Optical Substratum for the Adhesion and Spreading of Mesenchymal Cells In Monvalent and Divalent Saline Solutions", J.Cell Physiol., 1977, 90, p.511.

7) CURTIS, A.S.G. "Cell Adhesion", Prog. Biophys. Mol. Biol., 1973, 27, p.317.

8) GINGELL, D. and TODD, I. "Red Blood Cell Adhesion, II. Interferometric Examination of the Internation with Hydrocarbon Oil and Glass", J. Cell. Sci., 1980, 41, p.135.

9) WEISS, L. and SUBJECK, J.R. J Cell Sci., 1974, 14, p.215.

10) PERRONE, J.B., DE MAIC, I. and SPIELMAN, A. "Regions of Mosquito Salivary Glands Distinguished by Surface Lectin-binding Characteristics, Insect Biochem., 1986, 16, p.313-318.

11) WATSON, P.K. "The Thermalization and Trapping of Electrons", IEEE, Transactions on Electrical Insulation, 1987, E1-22(2), p.129.

12) MOLYNEUX, D.H., WALLBANK, K.R. and INGRAM, G.A. "Trypanosomatid-vector interfaces - In-vitro studies on parasite substrate interactions", NATO ASI Series, Vol. H11, 1987, p.387

13) SMITH, C.W. "High Sensitivity Biosensors and Weak Environmental Stimuli", Industrial Biotechnology, Wales, 1986, 6.

13) CALLAHAN, P.S. "Tuning in to Nature", London: Routledge & Kegan Paul, 1977.

14) FRÖHLICH, H. "The Biological Effect of Microwaves and Related Questions". Advances in Electronics & Electron Physics, 1980, 53. p.85.

CHAPTER (10)

THE EFFECTS OF MAGNETIC FIELDS ON WATER AND ICE FORMATION

10.1 INTRODUCTION

Water is both vital and fundamental for all living organisms in order for them to live, reproduce, and evolve. The existence of water has not been discovered anywhere other than on earth, and over 80% of any individual cell consists of water. In fact, water is the probably source for all living things and some researchers into water are now giving priority to the possibility that water may be the solution to many medical problems.

Jhon [1] discusses the most important sources for the cause of human cancers. It appears that less than 5% have a physical origin, such as radiation damage etc., that less than 5% are caused by external viruses, and that more than 90% may come from our environment, and this includes our water. His research reports that an attempt to overcome the AIDS disease must maintain or promote the body's immune potential, this might be done by changing the water environment. On the other hand, shortages of vitamin C or mineral ions also bring about a decrease of the immune powers in which the role of water is, again, important. In an experiment concerning the examination of the effects of "healers" on water described by Fenwick et al [2], all the healers co-operating in the experiment and "healed" the samples of water as they were directed. They said that they felt that the healing had been successful and they expected a change in the water.

Hayashi [3] states that the role of water in cells or tissues is a key mechanism for every disease, and changes in the properties of water in the organs could be a mark of the beginning of disease. However, these changes are considered to be inducers, or triggers of disease rather than origins or causes.

Pohl [4] has shown the presence of the small A.C. electric fields produced by living cells. There are also reports by Frohlich [5] about the effects of electric and magnetic fields on biological systems which are of course "wet". An article by Smith et al entitled "Water: Friend or Foe?" [6] noted that when materials are wet, or have absorbed moisture, they have different electric and magnetic properties.

There are also further reports by Smith and co-workers [7] indicating that water may have different dielectric properties when exposed to alternating magnetic fields. They report [8] that drinking water can cause a problem for many multiple-allergy patients. Some patients can only tolerate bottled spring water, triple distilled water, or water as fruit juice. In some cases even bottled spring water needs to be buried in the garden for a few days before it can be tolerated. Because of the body's great need for a regular supply of water, water intolerance becomes a severe and acute survival problem. These important observations give us an opportunity to develop this study and to investigate the possible effect of magnetic fields (A.C. and D.C.) on the different states of water.

10.2 Experiments on ice formation

Initially, water was frozen into ice cubes with one electrode on each vertical side of the cube. There were 4 electrodes made of aluminium foil and each electrode had an area of 4 sq. cm. They were arranged vertically on opposite sides of the dish used to freeze the water giving two parallel pairs of electrodes. Once the electrodes were prepared and arranged, they were placed inside the dish touching the sides. The dish was then filled with double distilled water. It is most important to fill the dish very slowly, preferably by using a

pipette, otherwise the electrodes could float away from the sides of the dish. The sample was then placed inside the centre of a prepared solenoid. The solenoid was made of 22 SWG copper wire wound to give 220 turns around an insulated cylinder of diameter of 10 cm and a length of 30 cm. The dish was placed in the centre of the solenoid, so that the resulting magnetic field was perpendicular to one pair of the aluminium foil electrodes and parallel to the other pair. The whole assembly was placed inside a freezer. A sinusoidal waveform was supplied by a signal generator (General Radio type), which drove the coil directly through two wires, trapped in the freezer door seal. The oscillator was switched on for 24 hours at a voltage of 3 volts and set to a frequency of 15 kHz. The freezer temperature was kept constant at -20° C. The water and the resulting ice cube was exposed to a magnetic field for 24 hours and then the capacitance and loss for different frequencies was measured whilst still leaving the sample in the freezer, the oscillator having been switched off. Capacitance and loss were measured by an impedance bridge (General Radio) around the radiated frequency of the sinusoidal waveform (14-16 kHz). This measurement was repeated for a few experiments for both parallel and perpendicular arrangements of the electrodes, to the axis of the applied magnetic field. Graphs (10.1)-(10.4) show examples of the results obtained when loss and capacitance were measured for these electrodes.

Obviously, any effect of magnetic field should be at, or very near to, the radiation magnetic frequency (15 kHz in this case). Unfortunately none of these results gave any clear effect. Therefore, this had to be regarded as a negative result. If there was any effect it was much too small to detect and hence, the experimental method should be made to a

GRAPH (10.1), Electrodes are parallel to the magn etic field

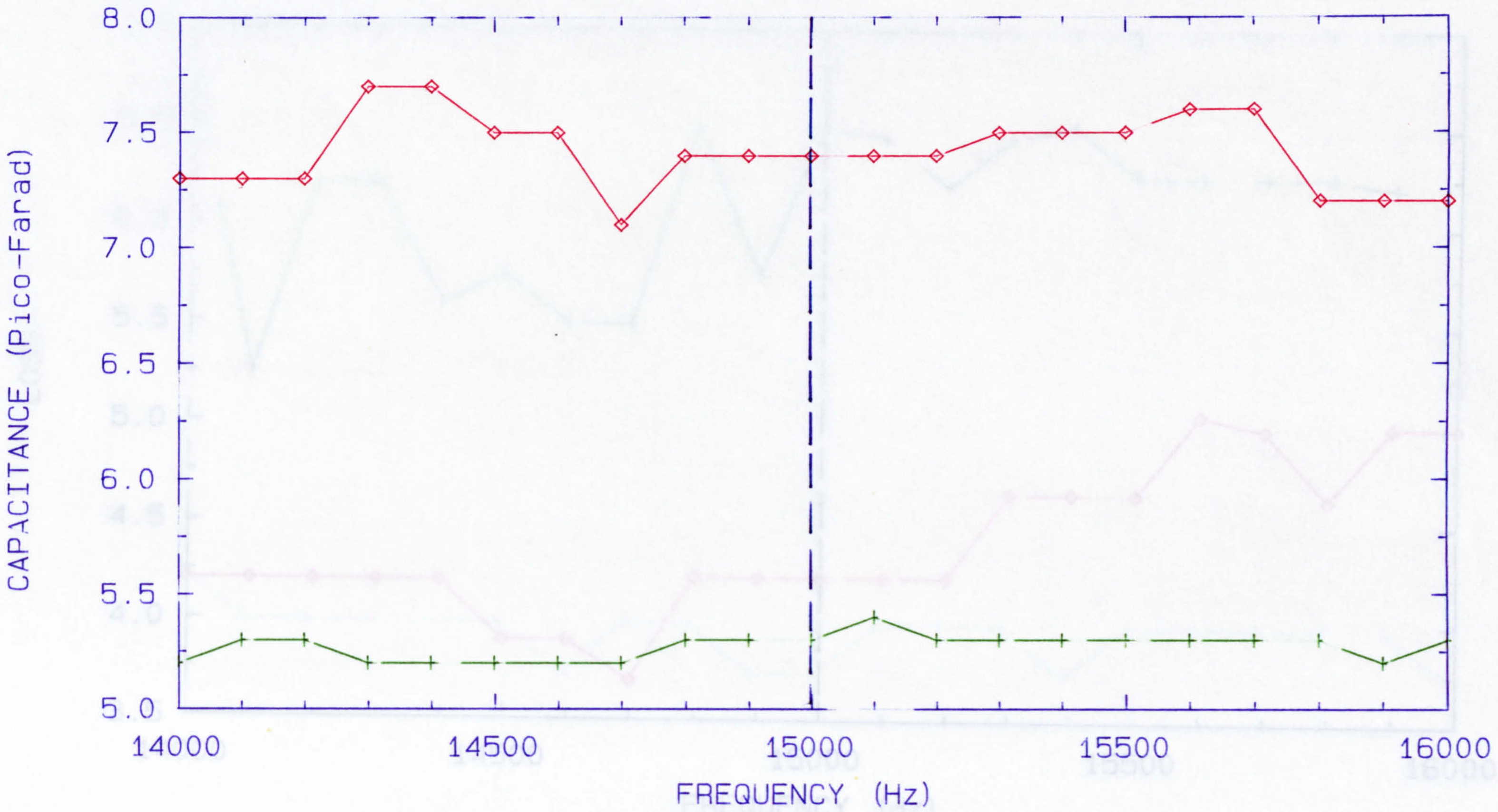

GRAPH(10.2), Electrodes are parallel to the magnetic field

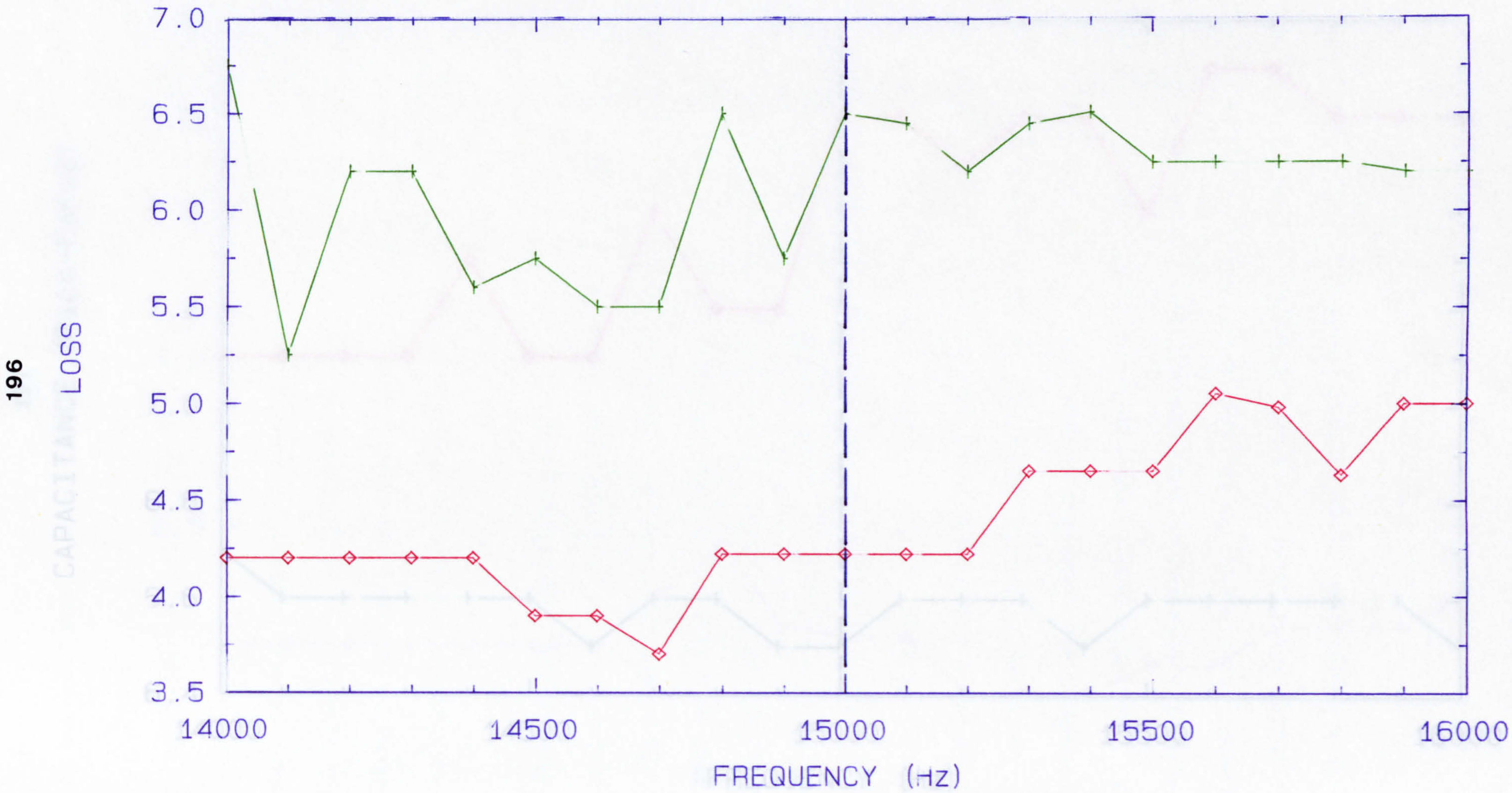

GRAPH (10.3), Electrodes are perpe ndicular to the magnetic field

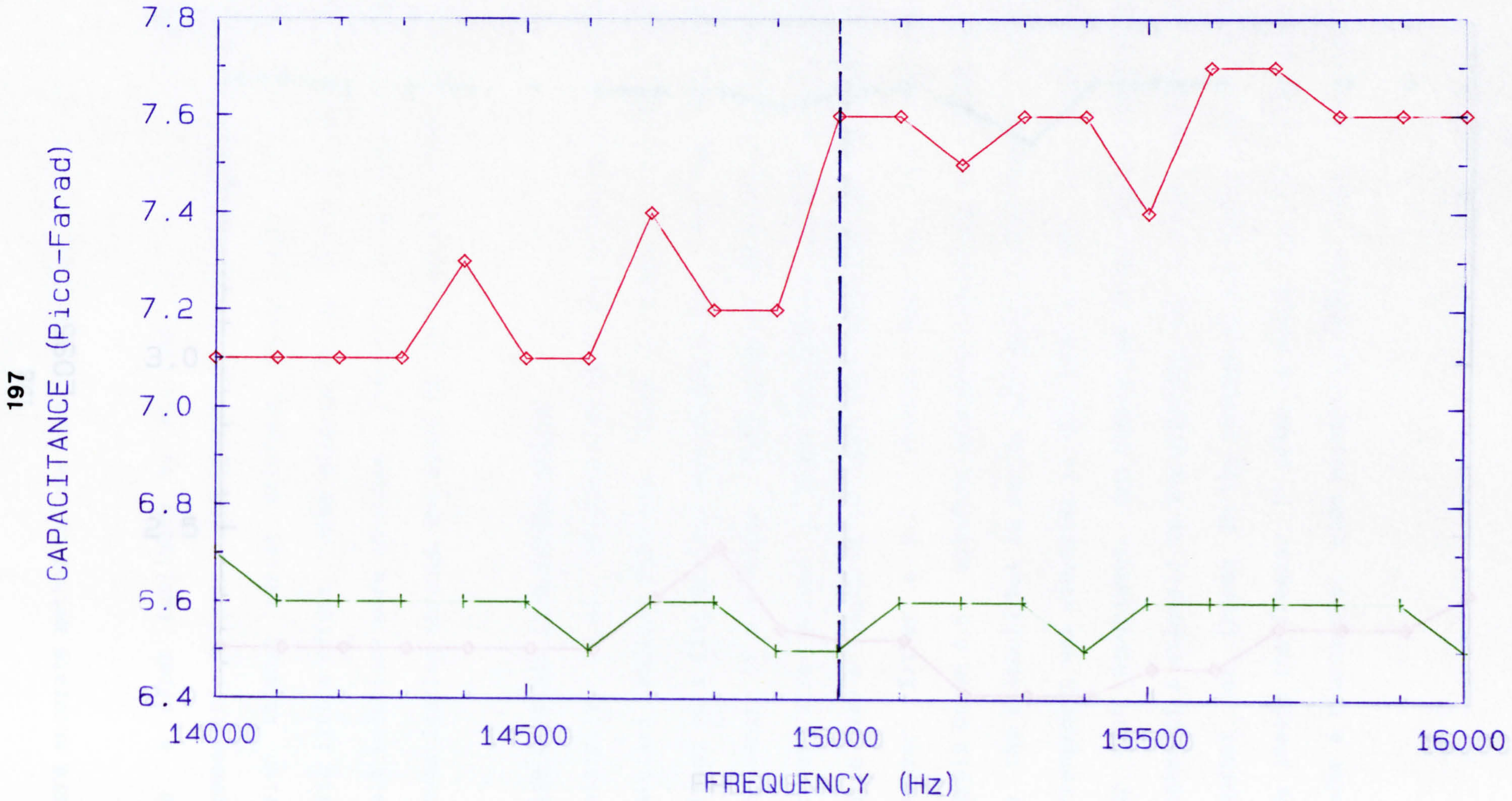

GRAPH (10.4), Electrodes are perpendicular to the magnetic field

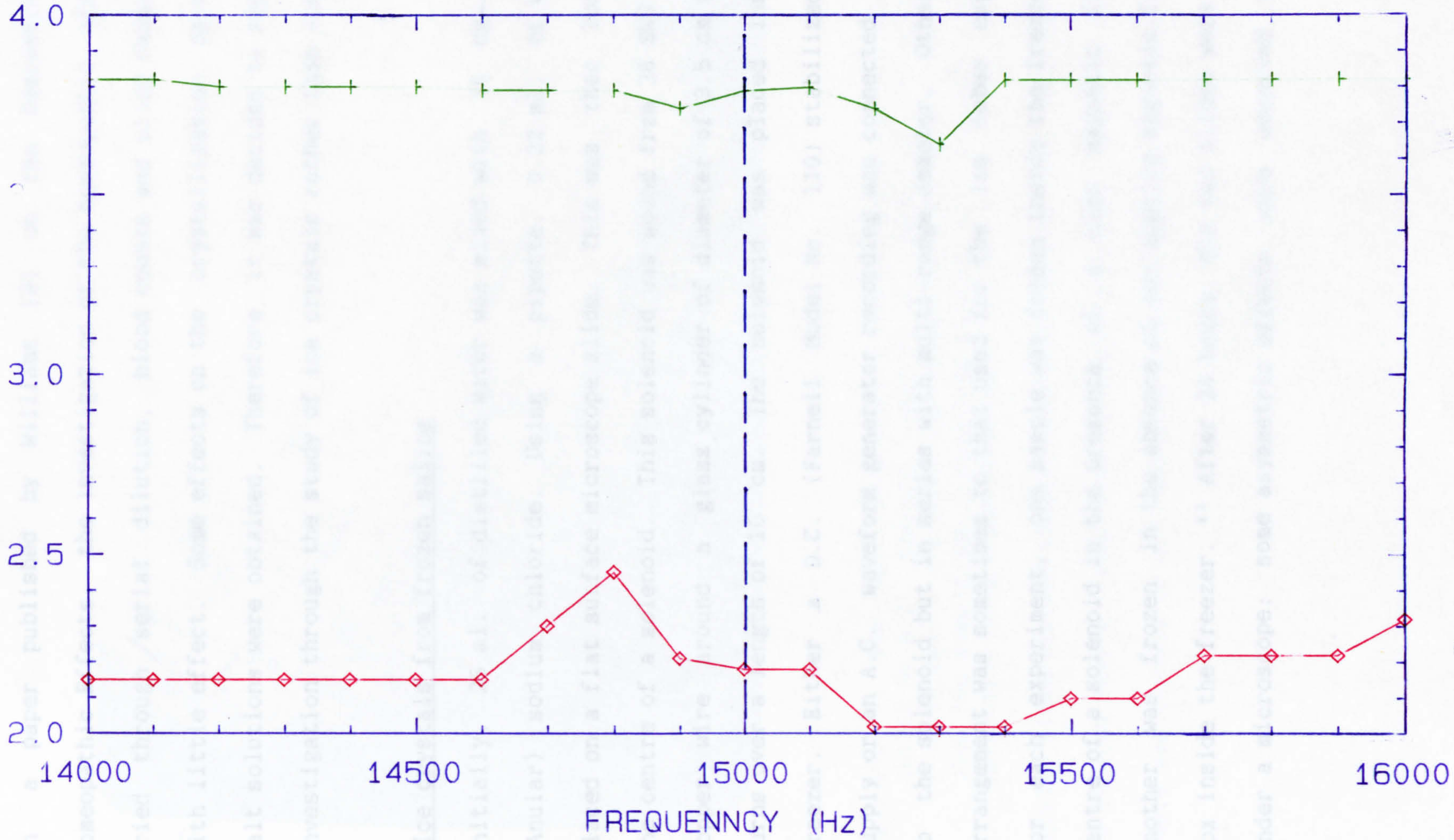

more accurate method before further studies are carried out.

In a paper published by Williams [9] on the Demonstration of Homeopathic Effects, the investigation of the homeopathic effect was tried through serial dilution, blood counts and blood chemistry but with little effect. Some effects on the crystallization patterns of salt solutions were obtained. Therefore, it was decided to repeat this investigation through the study of ice crystals rather than ice cubes.

10.3 Ice crystals from frozen saline

Initially, 25 ml. of distilled water was mixed with 35 mg of pure (Anular) sodium chloride. Using a pipette, 0.22 ml. of water was placed on a flat surface microscope slide. This was then located in the centre of a solenoid. This solenoid was wound from 36 SWG standard copper wire around a glass cylinder of diameter of 3.5 cm for 2,000 turns over a length of 10 cm. The solenoid was placed inside the freezer. Either a D.C. (Farnell Model No. 110) stabilized voltage supply or an A.C. waveform generator recording was connected directly to the solenoid but in series with multi-range ammeter. Otherwise the arrangement was sometimes to that used for the ice cubes experiment. For each experiment, one sample was frozen inside the freezer in the centre of a solenoid in the presence of a high magnetic field and another was frozen in the absence of any applied magnetic field in a box inside the freezer. ** After 24 hours, the two slides were compared under a microscope: some asymmetric effects were observed with the

** Geomagnetic field was not taken into account

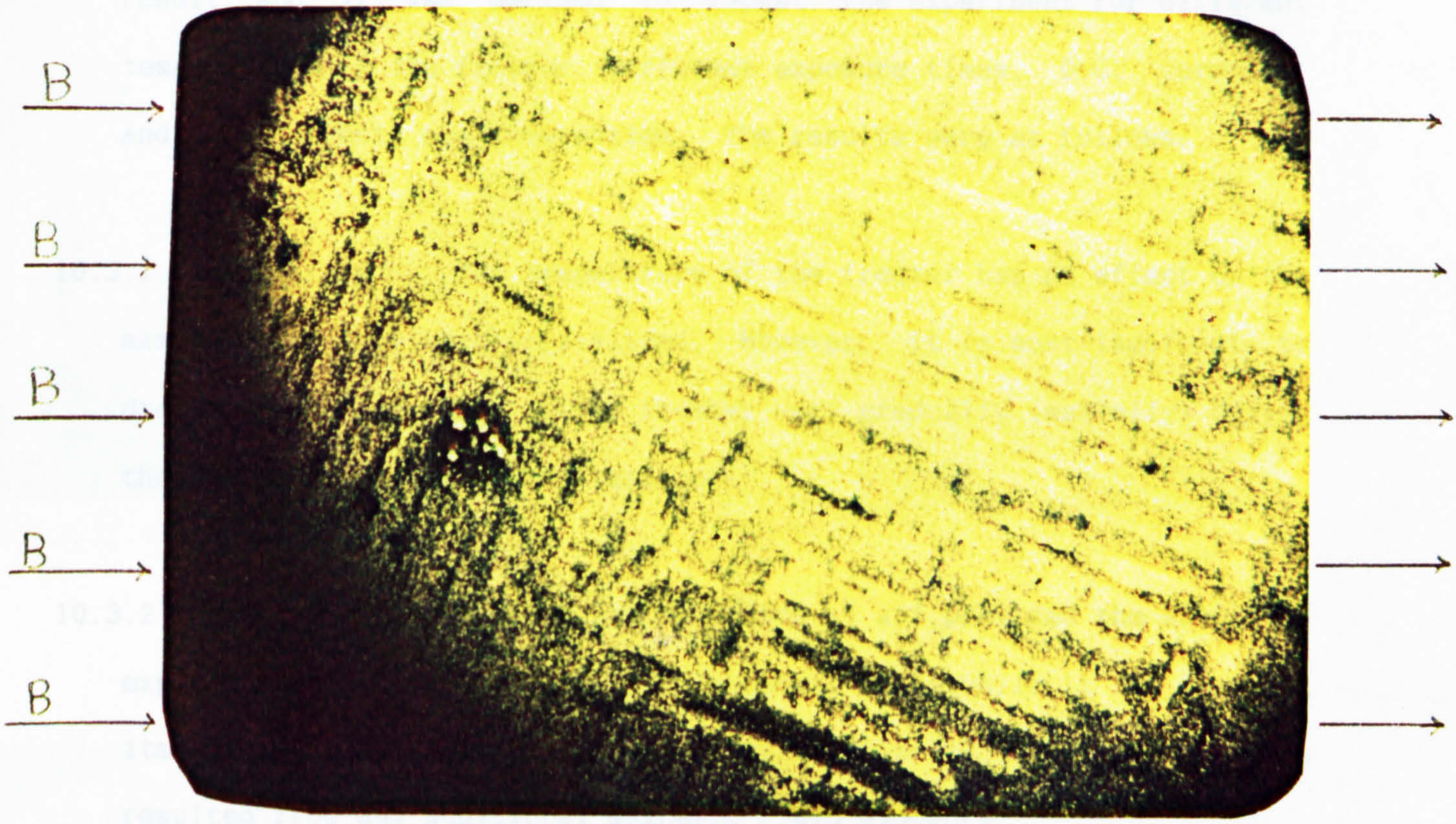

Fig. (10.1). The Nacl dissolved in distilled water was crystalized whilst an A.C. magnetic field of 12.5 gauss (I = 50 mA N = 2000, l = 10 cm, f = 14 kHz) was passed through the sample. However, when the sample was crystalized without any magnetic field, no asymmetric effect was obtained.

magnetic field exposed sample, whilst no effects were observed with the non-treated sample. Fig. (10.1) shows the effect obtained when the sample was exposed to A.C. magnetic field of frequency 14 kHz.

* For D.C. magnetic field the Nacl aligned at 90° to the direction of magnetic field.

It is very clear from the picture that sodium chloride dissolved in water is aligned in a uniform manner, all in the same direction, at an angle to the direction of magnetic field.* This was an encouraging result and it was decided to repeat the experiment for different temperatures of the freezer, different exposure times, D.C. currents, and A.C. currents and frequencies. The results were as follows:

10.3.1 Temperature - The temperature of the freezer has no effect on the samples once they were crystalized. However, it is most important to drop the temperature of the freezer very gradually (manually) during the intial stages of crystalization.

10.3.2 Exposure time - This has no effect at all provided the sample is exposed either to a D.C. or A.C. magnetic field while it is changing its state from liquid to solid (crystalized). No further effects resulted from any additional magnetic field exposure.

10.3.3 Current - This is the current passing though the solenoid and it is this which defines the magnitude of the magnetic field. This plays an important role, the higher the current (A.C. or D.C.) the greater the observed effect, zero current gave no effect. This is true for both A.C. and D.C. currents as the following 8 pictures illustrate. Figures (10.2) and (10.3) show the effects obtained for various magnitudes of magnetic field given by A.C. and superimposed D.C. currents passing through the solenoid. These pictures show that as magnetic field strength is increased, a greater effect is obtained, this is in direct proportion to current or resulting magnetic field.

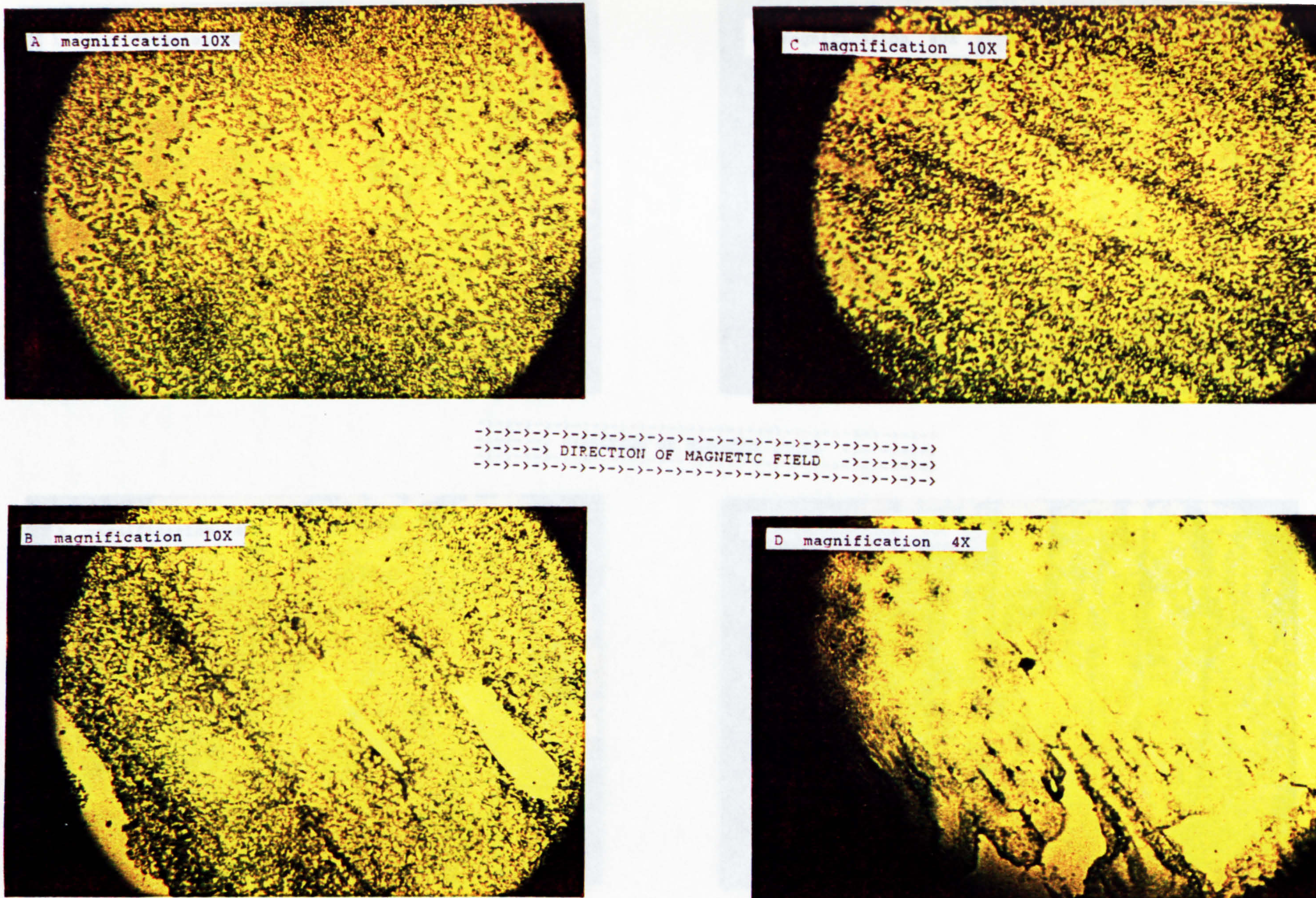

Figure (10.20), An A.C. magnetic field was applied to a coil 10 cm long (N=2000). Notice as current is increasing from 24 mA to 40 mA (A -> B -> C -> D) the effect is getting stronger.

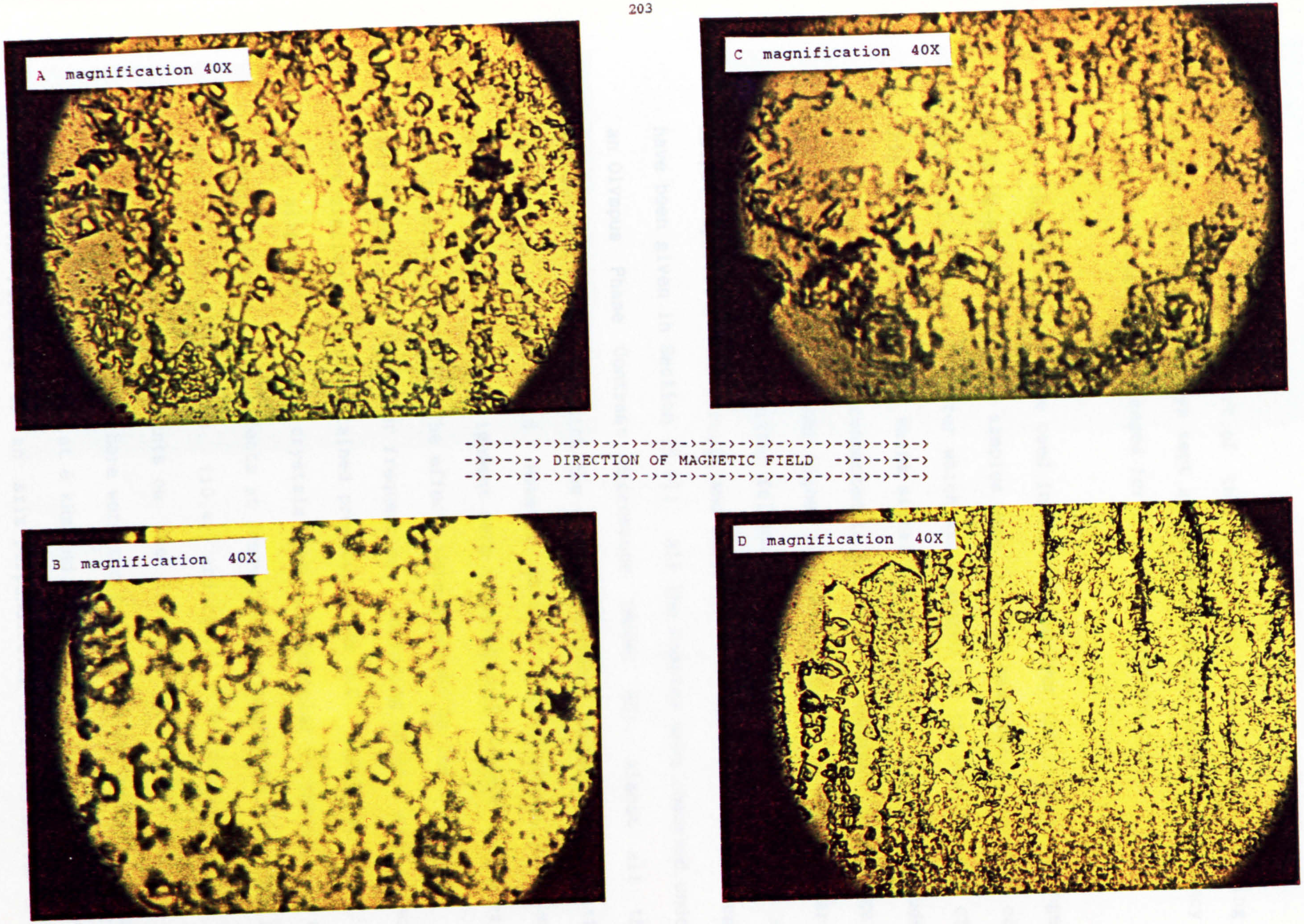

Figure (10.3), Various D.C. current of 0.2 A -> 1 A (A -> B -> C -> D) were passed through a D.C. solenoid with 220 turns and 30 Cm long. It is obvious that as current is increasing, a bigger effect can be obtained.

203

10.3.4 Frequency - In this part of the experiment, the current passing through the coil was always kept steady at 50 mA and only the frequency of the A.C. signal was changed for a 24 hour exposure time.

More than 50 samples were used in experiments over the frequency range of 50 Hz-60 kHz. All the samples were from the same saline solution of pure NaCl in distilled water which was prepared for the earlier part of this experiment. A 50 Hz mains signal was driven by a Variac (Claude Lyons Ltd.) which was connected in series to a rehostat (6 kW range) and an ammeter. For further higher frequency signals, a complementary Darlington Class - AB emitter follower was constructed. This had a 3A output capability (the circuit and description of this emitter follower have been given in Section (5.8)). All the samples were observed under an Olympus Phase Contrast Microscope (Model BH). Almost all the samples had crystalized with the crystal alignment perpendicular to the axis of the magnetic field. However, at certain frequencies, different angles of the crystal alignment were observed with respect to the axis of the magnetic field. The effects were greatest in the 6 kHz and 14 kHz ranges. All the other frequencies, including 50 Hz, gave effects very similar to those obtained previously for D.C. currents; that is the alignment of the crystals was perpendicular to the axis of the magnetic fields. The effects at frequencies around 6 kHz and 14 kHz were as shown in Figs. (10.4) and (10.5). The conclusions of the results of these experiments on the freezing of saline samples in magnetic fields is that there were two frequencies at which the crystal alignments were rotated; at 6 kHz and the alignment was - 62° clockwise direction relative to an axis perpendicular to the direction of the A.C. magnetic field. The D.C. alignment was also perpendicular to the direction of the magnetic field. At a frequency of 14 kHz alignment

205

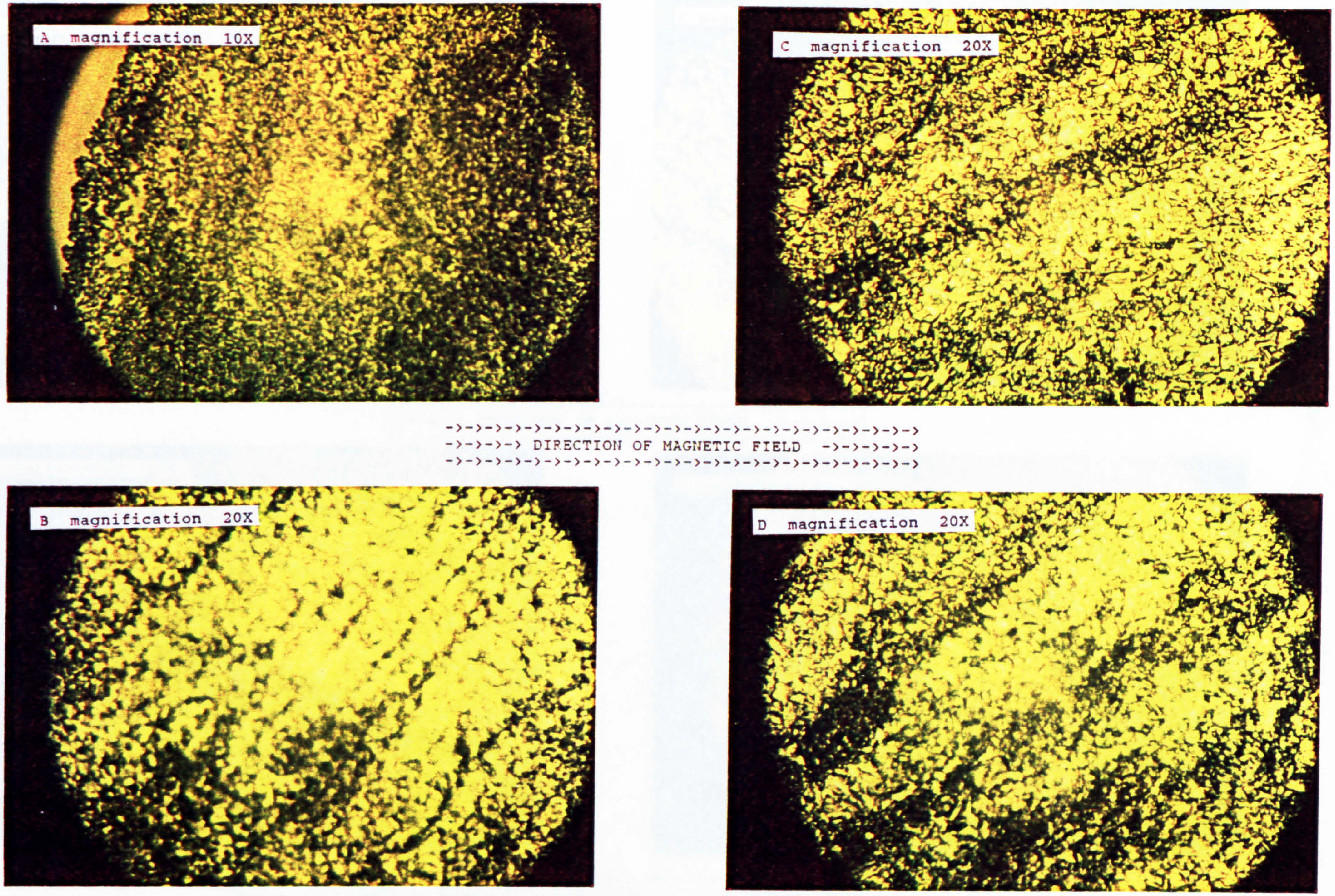

Figure (10.4). An A.C. current of 50 mA was passed through a coil (N=2000) and 10 Cm long. As the frequency was increased from 5.7 kHz(A) to 5.9 kHz(B) the alignment rotated clockwise until at 6 kHz(C) the crystals made an angle of 28 degree to direction of magnetic field. Any further increase in frequency of the field beyound 6 kHz (D 6.2 kHz) would direct the alignment back to perpendicular alignment anticlockwise in which the crystals make an angle of 90 degree to direction of magnetic field.

PAGE NUMBERING AS ORIGINAL

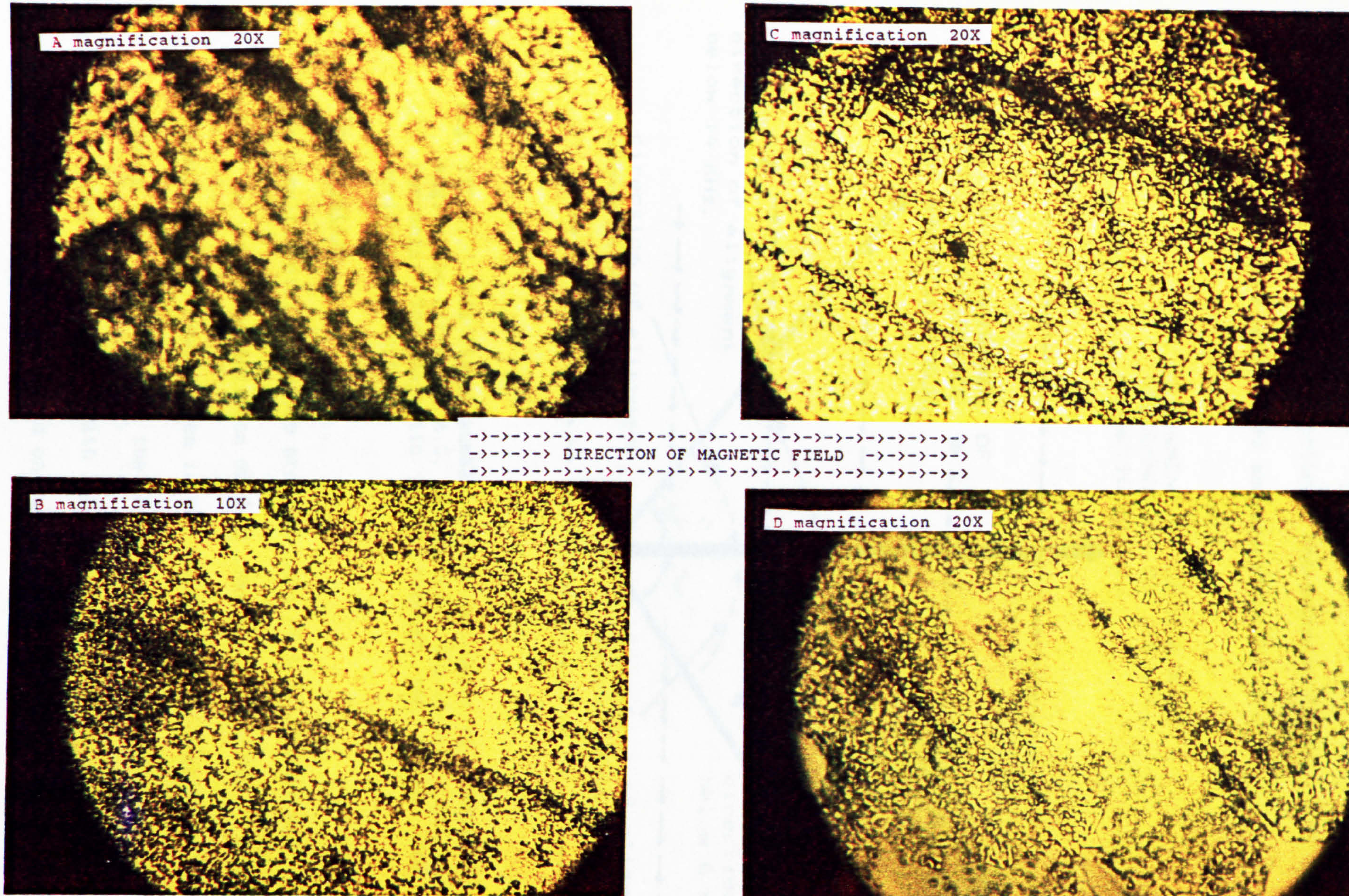

FIGURE (10.5) Nacl and distilled water were crystalized at -20 degree while an A.C. magnetic field (I=50 mA) were passed through the solenoid. As the A.C. frequency was increased to 13.8 kHz the alignment rotated anticlockwise from perpendicular direction (A). When frequency was increased to 14.5 kHz the crystals turned more anticlockwise (B). At this frequency the alignment was 30 degree to direction of magnetic field (Horizontal). Any further increase in A.C. frequency of the magnetic field would rotate the alignment back to perpendicular direction (C,D).

was - 60° in an anti-clockwise direction relative to an axis perpendicular to the direction of the magnetic field, or to the D.C. alignment. These results are summarised in Fig. (10.6).

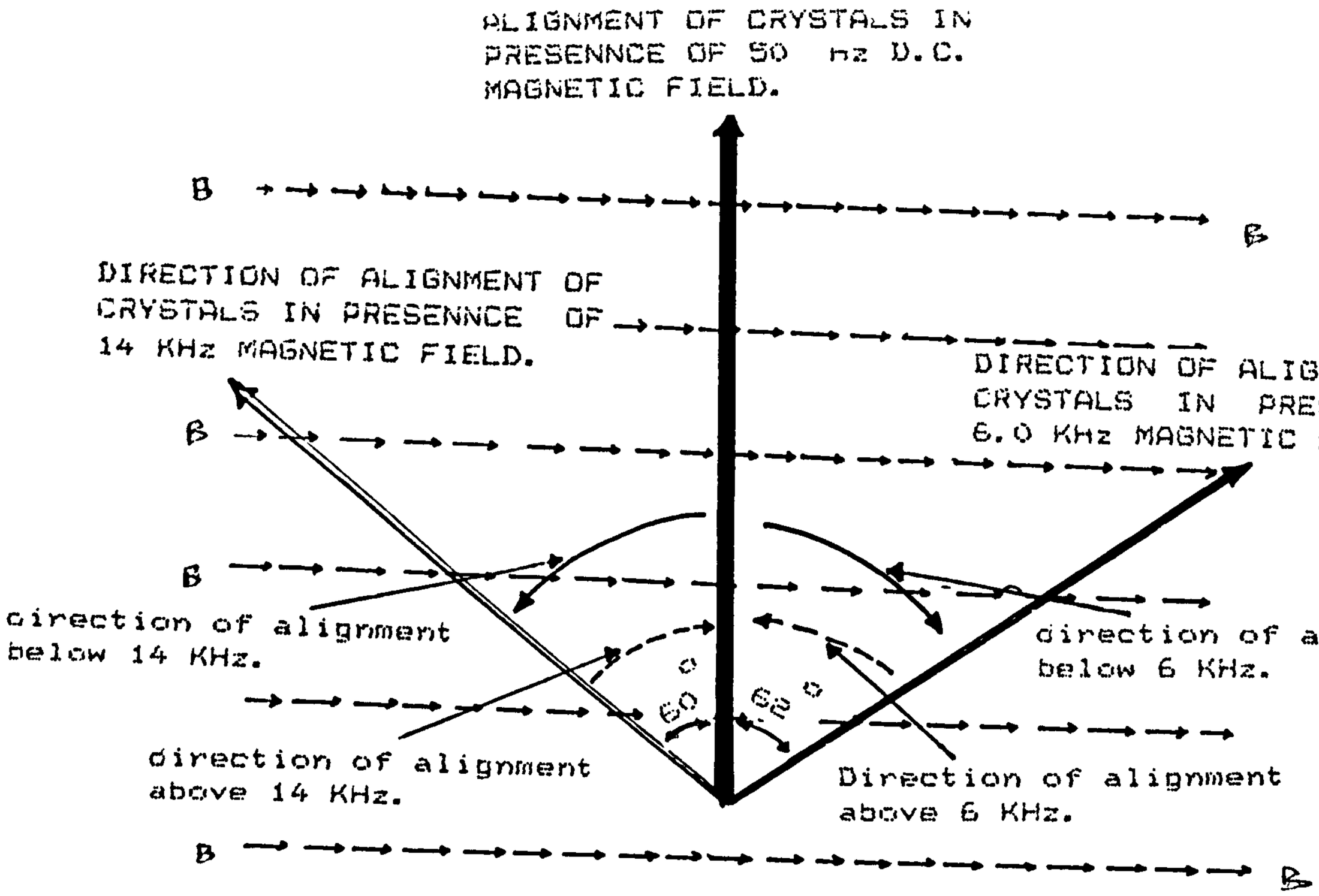

Fig. (10.6). This figure summarises the variation of crystal alignment angles for different A.C. frequencies and in D.C. and 50 Hz main currents. The magnetic field through the sample was always horizontal direction.

10.4 Ice Crystals

The results detailed in the previous part of this chapter have clearly shown a small orientation of NaCl crystals (dissolved in water) when the saline sample was frozen in the presence of a magnetic field. No effects were obtained when the magnetic field was absent. This part of the chapter continues with the investigation of the corresponding effects of a magnetic field on pure water (not saline) where impurities have been minimised.

The research was carried out by forming ice crystals in different strengths of A.C. or D.C. magnetic fields. The magnetic field treated samples were then subjected to X-ray. Both transmission and back scatter X-ray patterns from the samples were studied.

Before describing the effects of magnetic fields on the formation of ice crystals as observed by X-rays, a short review of the basic principles of X-rays is given, followed by an outline of Bragg's Law; the reflection, and transmission of X-rays. The review relates specifically to the possible structures of ice crystals.

10.4.1 Braggs Law

Before the discovery of X-ray diffraction which enabled the arrangements of atoms in a crystal to be determined experimentally, crystallographers had simply assumed that the regular external shapes of crystals were due to the atoms being arranged in regular, repeating patterns

In 1912 three German physicists, Max Von Laue, W Friedrich and P Knipping, found that an X-ray beam, often passing through a crystal, formed a pattern of spots on a photographic plate. Shortly afterwards, W L Bragg and Sir William Bragg showed how the pattern could be used to reveal the positions of the atoms in a crystal. Together they proceeded to unravel the atomic structure of many substances. This has been extended to include the molecules like DNA, that play a vital part in the processes of life largely through the work of D.C. Phillips and his group

10.4.2 Scattering of X-rays

When X-rays fall on a single plane of atoms (as in an ice crystal),

each atom scatters a small fraction of the incident beam and may be regarded as the source of a weak secondary wavelet of X-rays. In most directions, destructive interference of the wavelet occurs but in the direction for which the angle of incidence equals the angle of 'reflection'there is reinforcement and a weak reflected beam is obtained. The X-rays thus behave as if they are weakly 'reflected' by the layer of atoms, as shown in Fig. (10.7)

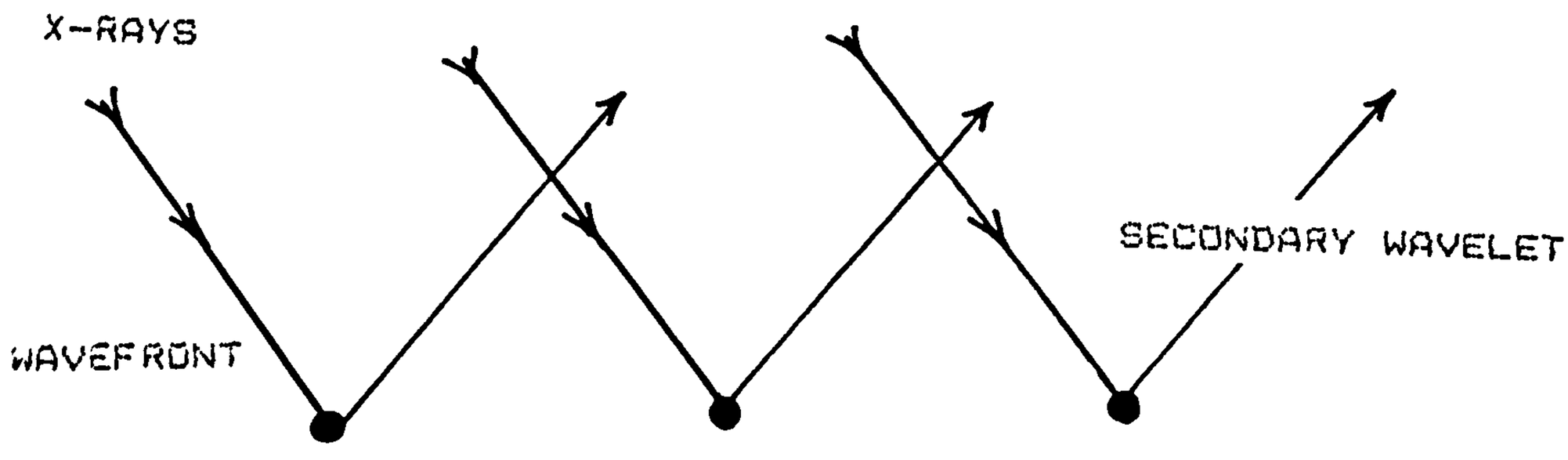

Fig. (10.7) Crystal X-rays are diffracted from crystals

Other planes of atoms to which the X-rays penetrate behave similarly. The reflected beams from all the planes involved interfere and the resultant reflected beam is only strong if the path differs between successive planes is an integer number (n) of wavelengths (λ) of the incident X-radiation.

$$AB + BC = n\lambda$$

If d is the distance between planes of atoms and θ is the glancing angle, then the reflected beam has maximum intensity when

$$2d \sin \theta = n\lambda$$

Hence, as the crystal is rotated so that the glancing angle is increased from zero, and the beam reflected at an angle equal to the incident angle is observed each time, an increase beam is suddenly produced for a glancing angle θ_1, such that $2d\sin\theta_1 = \lambda$. When the

crystal is rotated further, an intense reflected beam is next obtained for an angle θ_2 when $2d\sin\theta_2 = 2/\backslash$. Thus several orders of diffraction images may be observed. Many orders are obtained if $/\backslash$ is small compared with 2d. Conversely, no images are obtained if $/\backslash$ is greater than 2d.

10.4.3 Diffraction of X-rays

As previously explained (section 10.4.2) regular small spacing of atoms in an ice crystal might provide a natural diffraction grating if the wave length of the rays were too short to be used with an optical line grating. X-ray beams may be reflected by an ice crystal, Bragg-fashion, as discussed earlier. Nevertheless, when they strike a photographic film they give a characteristic diffraction pattern.

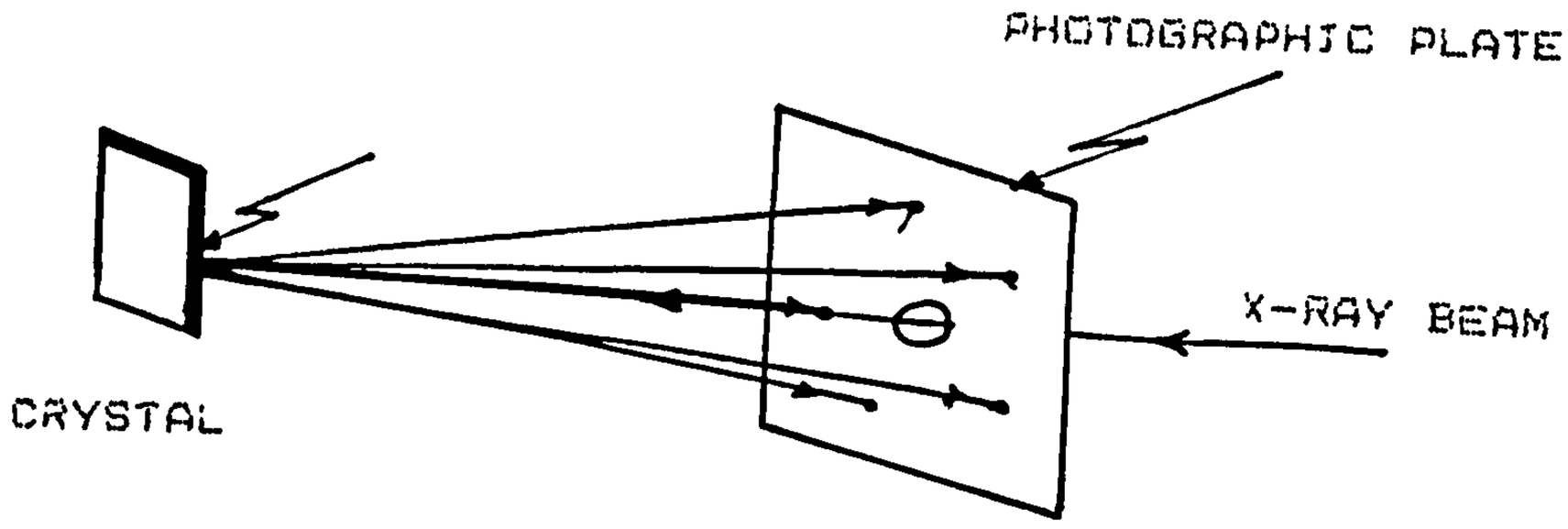

Fig. (10.8) Diffraction of X-rays from a crystal to a photographic film

Figs. (10.9) and (10.10) show a diffraction pattern of an ice crystal made from tap water and clean water. The clean water is de-ionized water which has been double distilled. This was performed in the Chemistry Department of the University where the Laboratory water was obtained by twice distilling de-ionized water in a hard glass, and the water was stored in a hard glass vessel. The tap water is taken from the laboratory sink; this water is not recommended for drinking so the tap water is expected to contain both impurities and ions.

During the experimental work on crystalizing either tap water or clean water, the samples were kept away from environmental magnetic fields (other than the geomagnetic field); they were kept in a metal box inside the freezer whilst the experiment was in progress, and were contained in centrifuge plastic tubes (10 ml) prior to being transferred for experiment.

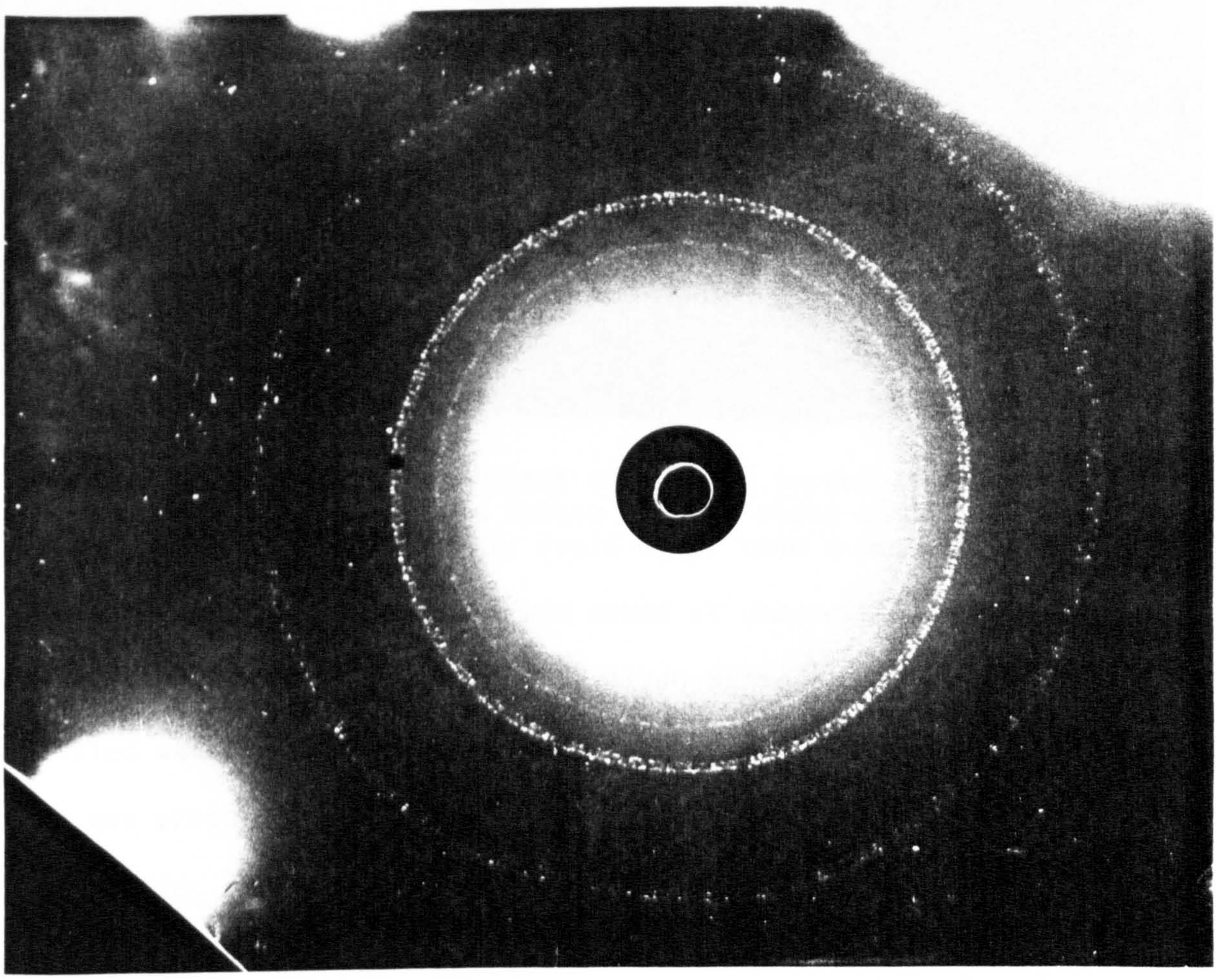

Fig. (10.9) shows random orientation of ice crystals from tap water in the absence of any magnetic field (other than the geomagnetic fields). These rings are probably due to ions and impurities which exist in the tap water and look like the diffraction pattern of powder particles.

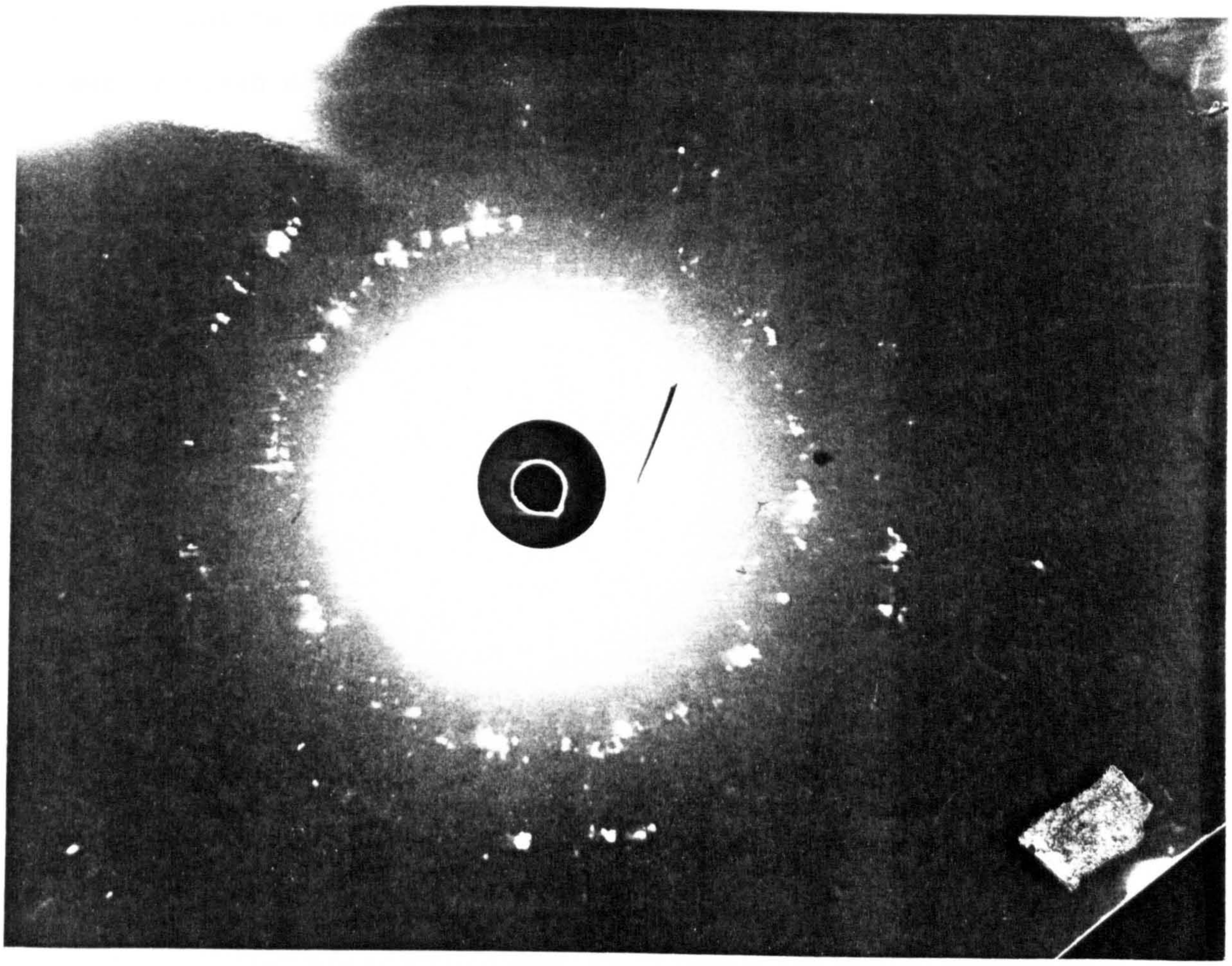

Fig. (10.10) shows broken rings which have larger crystalization of random orientations. The sample is from clean water purified in the absence of any magnetic field other than a geomagnetic field.

This section of the project was aimed at observing any effects of a magnetic field (D.C.) on a sample of clean water (double de-ionized and distilled water) when it had been frozen in the field. The magnetic field was produced by a D.C. Newport Electromagnet Instrument (Type C) which could generate a high D.C. magnetic field (<1K gauss). This magnet had a solenoid with an inner diameter of 3 cm on which the sample could be placed, as shown in Fig. (10.11).

Each sample was exposed to a D.C. magnetic field for at least 24 hours. The freezer had a temperature control and this was dropped manually to 0°C very slowly with the magnetic field passing through the sample

resting inside the solenoid. The samples were prepared as before by freezing clean water in 10 ml plastic centrifuge tubes. Once the sample was crystalized to an ice structure, it was transferred to the Crystallography Laboratory for further experiment.

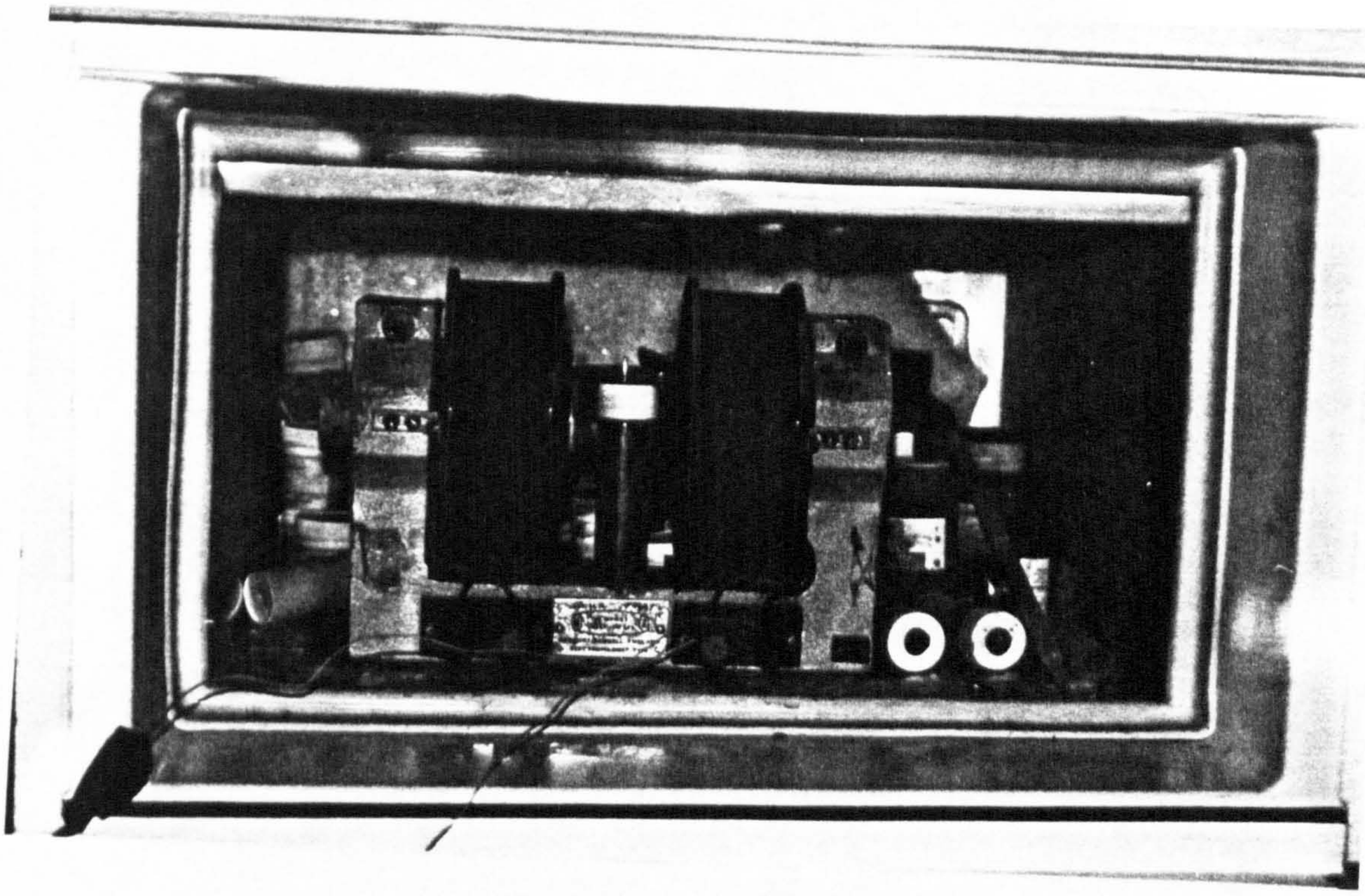

Fig. (10.11) Magnetic field and freezer

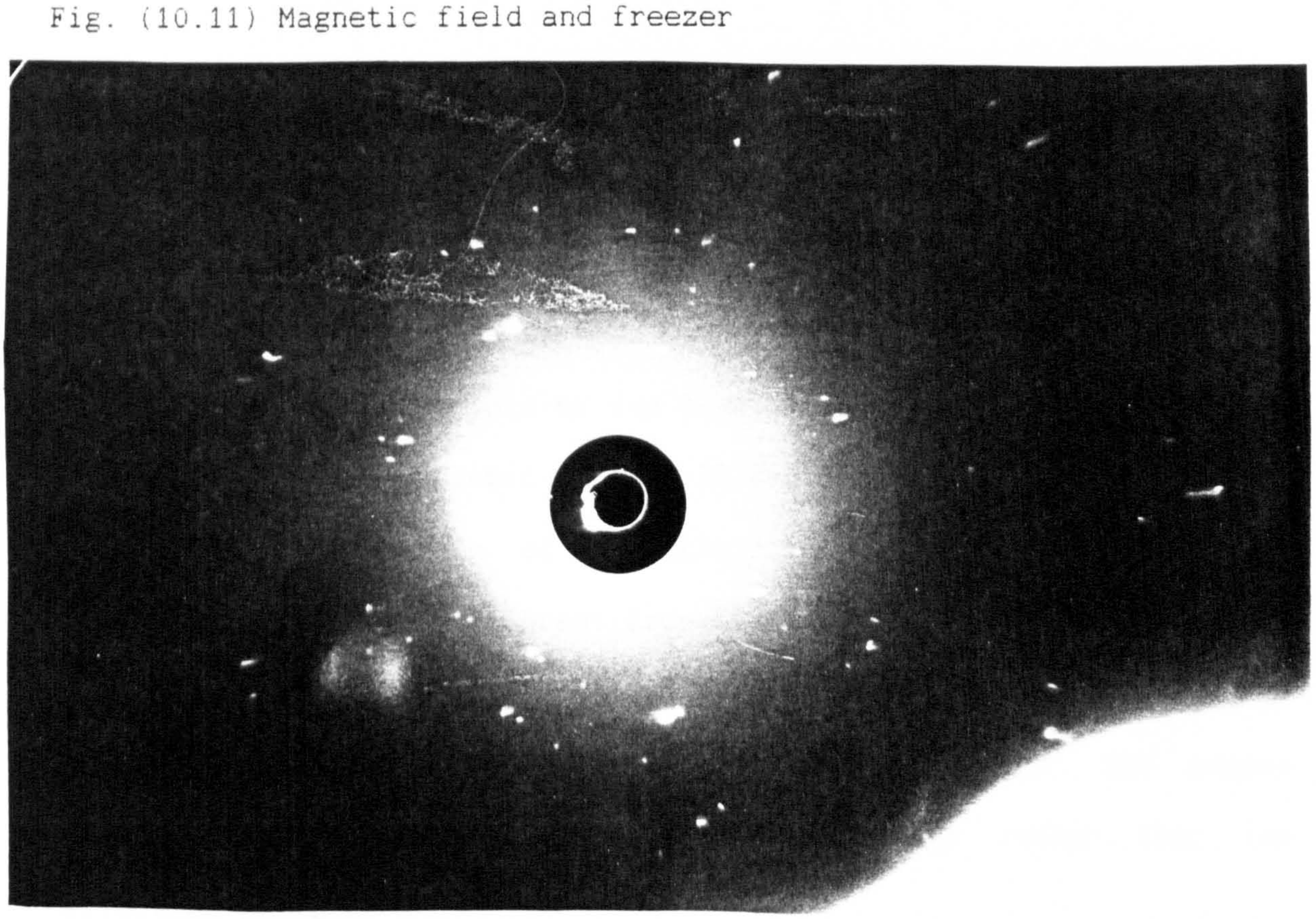

Fig. (10.12) X-ray diffraction pattern of clean water which has been exposed to a D.C. magnetic field. (Magnetic field = 120 gauss/D.C. current = 0.15A

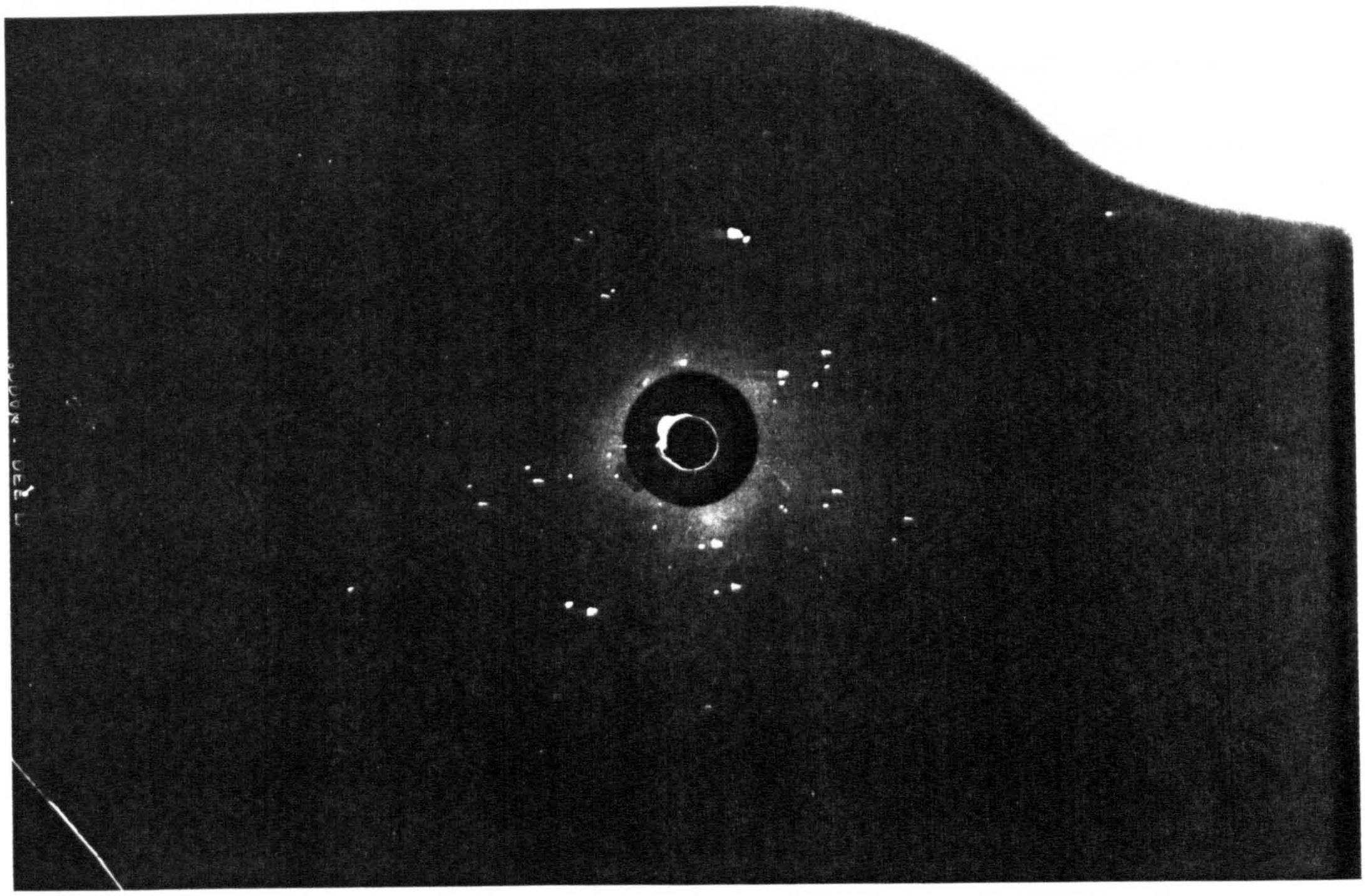

Fig. (10.13) X-ray diffraction pattern of clean water. (Magnetic field = 120 gauss/D.C. current =0.15 A)

The small variations among the X-ray diffraction pattern of the samples show the difficulty of repeating this experiment. This is probably due to the melting ice surface during the X-ray diffraction experiment. The melting of the surface of ice crystals may cause the X-rays to be diffracted from a new atomic plane. It is, however, clear that the X-ray diffraction pattern of magnetic field treated clean water (Fig. (10.12)) is completely different from the X-ray diffraction pattern of clean water which has not been treated by a magnetic field (Fig. (10.10). As the difference clearly needs more research, the author decided to look at the transmission of X-rays rather than the reflection pattern.

10.4.4 Transmission of x-rays

X-rays may be refracted (or transmitted) in passing through a crystal. However, this is not possible for all crystals, but is possible for our experiments, since the crystal is ice and is transparent. X-ray transmission diffraction too, is governed by Bragg's law.

Imagine the X-ray beam strikes an extremely thin transparent ice crystal forming a pattern of spots on a photographic film as placed behind the crystal in the other side of the X-ray beam as shown in Figure (10.14).

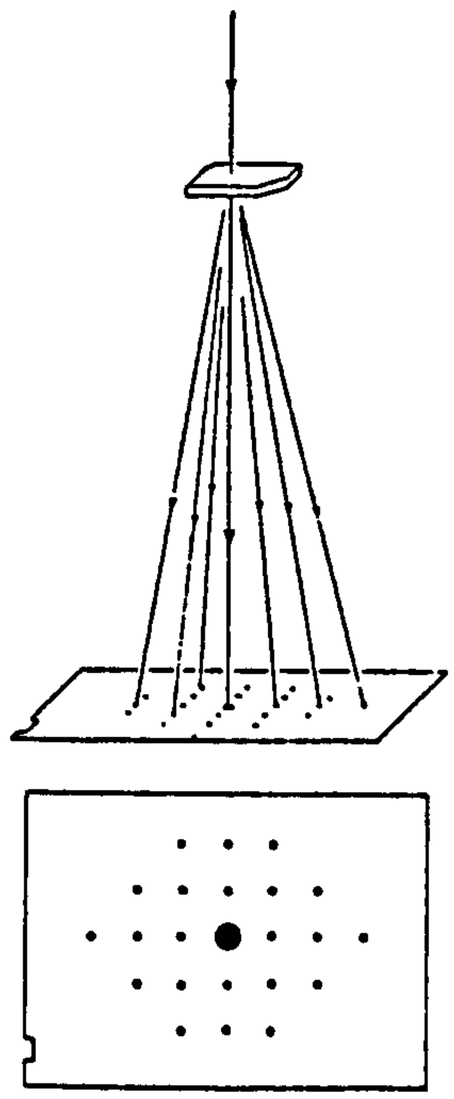

Fig. (10.14) Transmission of X-rays from a crystal to a photographic film.

It is important for the ice crystal to be as thin as possible; this simplifies the X-ray pattern analysis. It was especially important during our investigation as the ice crystals and the crystal pattern needed to be studied carefully. The thin ice crystals were formed by freezing clean water in fine tubes (the non-crystalline tubes were kindly loaned to the author by the Crystallography Laboratory). The objective of the experiment was to observe and study the effect of magnetic fields on water in its solid state (ice). More than 12 samples were exposed to D.C. magnetic fields. The D.C. magnetic field was produced by passing a D.C. current through a Newport electromagnetic Instrument (Type C) coil. The samples were exposed over the range 100 to 300 gauss magnetic field strength. Each time

samples were prepared, one of these (water filled tubes) was subjected to a the magnetic field parallel to the axis of the tube, and the other was subjected to the magnetic field perpendicular to the axis of the tube. The samples were then taken to the Crystallography Laboratory where the their X-ray transmission pattern could be obtained. The samples were always placed in a cold flask before being transported to prevent the sample melting. Fig. (10.15) shows the position of the sample in parallel and perpendicular to the axis of the field.

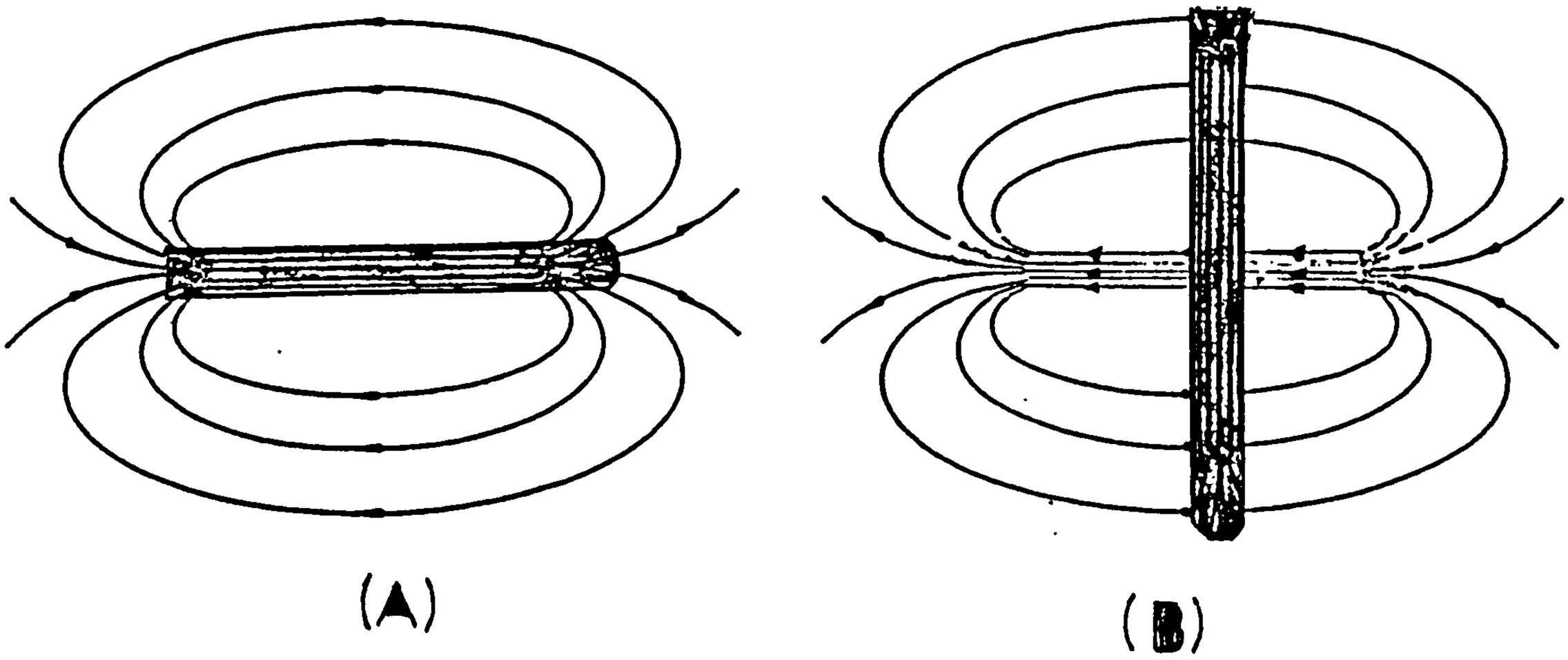

Fig. (10.15) A fine ice tube placed in a) parallel; b) perpendicular to the axis of the field

Fig. (10.16) shows the effect of the magnetic field on the ice tube which has been placed in parallel and perpendicular to the axis of a magnetic field. It can be noticed that the ice crystals have formed in a series of peaks within the ice tube (Fig. (10.16a)), pointing at right angles along the ice tube, when the sample was placed in parallel to the direction of the magnetic field. This is clearly a different

picture compared to the sample which had been placed in a magnetic field perpendicular to the direction of the field. (Fig. 10.16b)).

It would be possible to obtain the X-ray transmission pattern of the sample if it could be kept in its solid state whilst being exposed to X-rays.

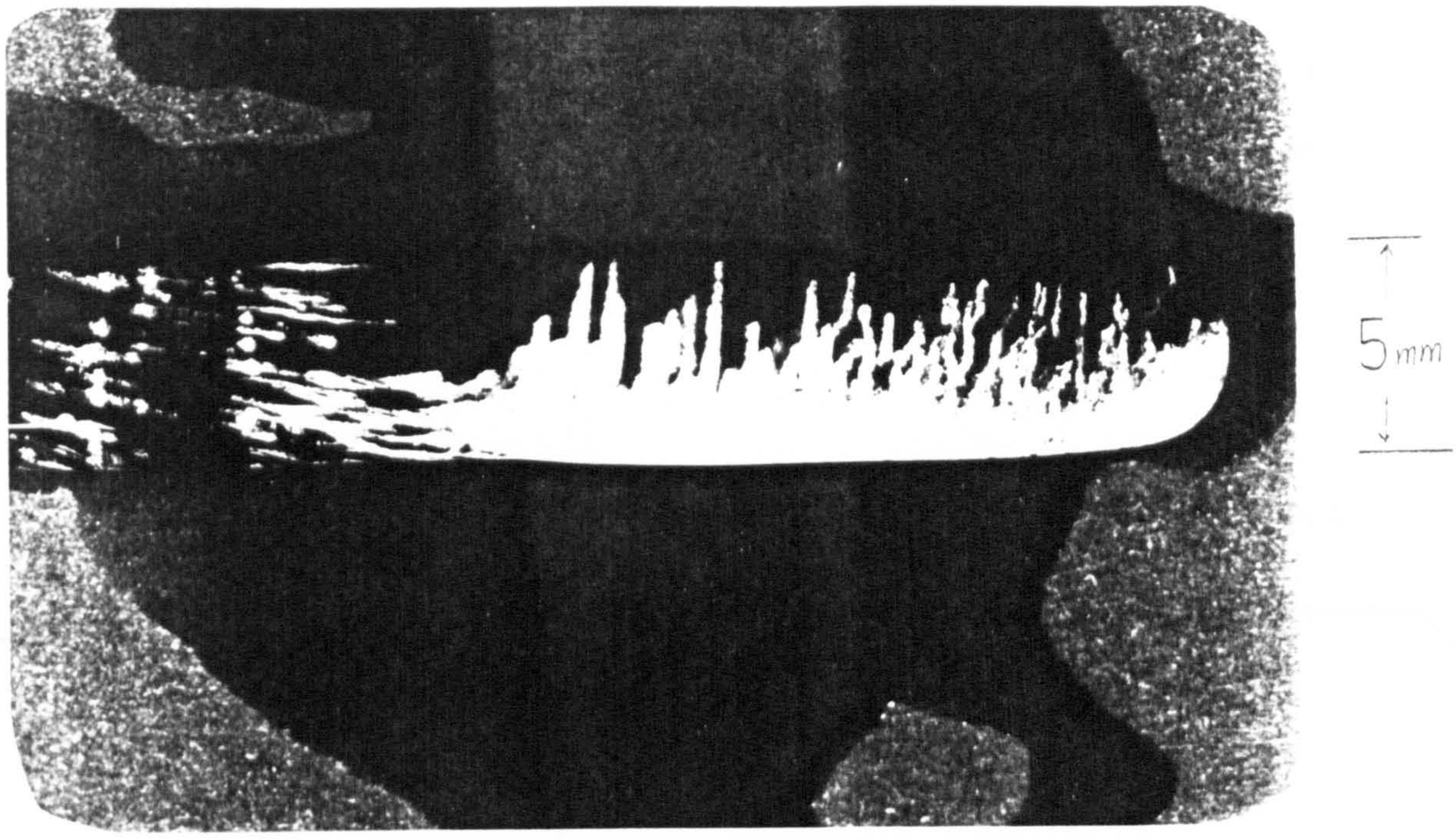

a) Direction of magnetic field is along the axis of the tube.
The crystals have been formed at right angles to the direction of the field.

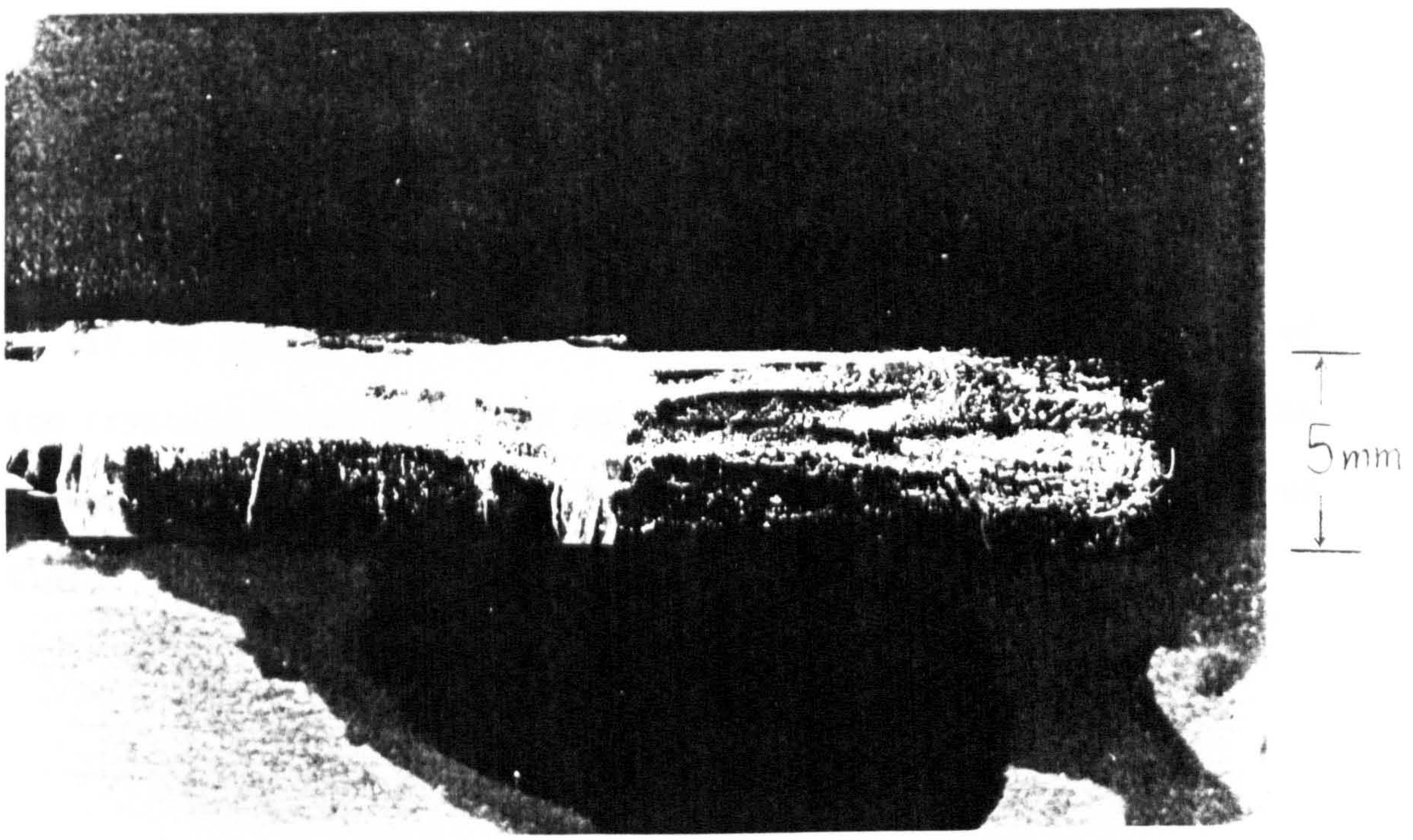

b) Direction of magnetic field is at right angles to the axis of the tube.

Fig. (10.16) The effect of a magnetic field on ice tube crystals. The ice crystals were made from clean water and the margetic field was a) in parallel, b) perpendicular along the axis of the ice tube.

This was performed by containing the fine (2mm diameter) tube of ice in a flask filled with "dry-ice". The assembly of this set-up is shown in Fig. (10.17). The "dry-ice" helped to keep the ice tube frozen for at least a 1/2 hour.

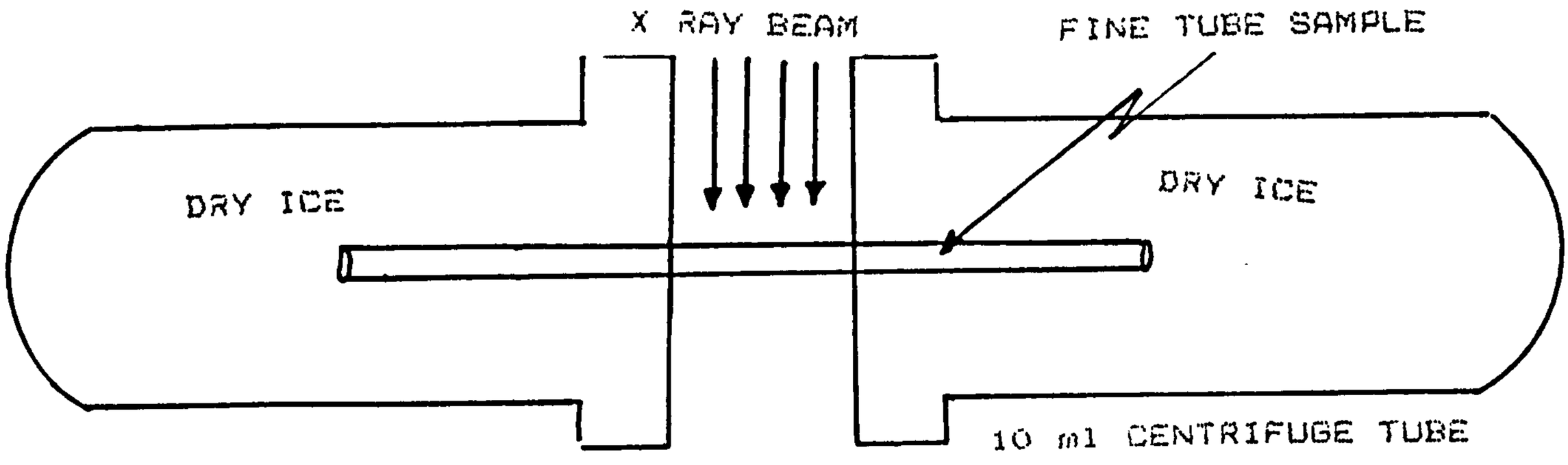

Fig. (10.17) Arrangement used to keep the ice tube sample frozen whilst the X-ray was transmitted through it.

Figs. (10.18) and (10.19) illustrate the X-ray transmission pattern of the ice crystals which have been subjected to a magnetic field. The sample was either placed in parallel or perpendicular along the axis of the field.

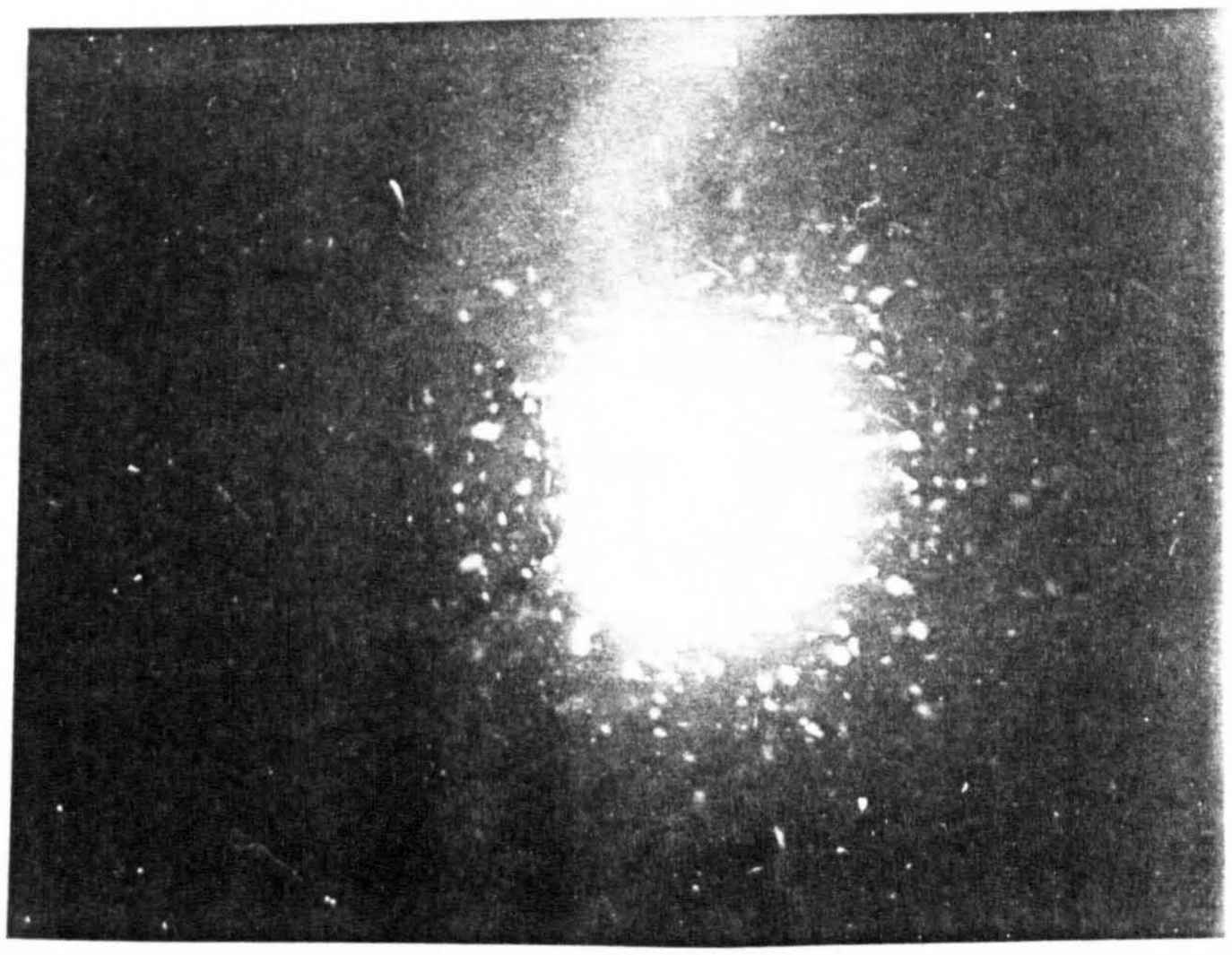

Fig. (10.18) X-ray transmission of a clean water ice crystal which has been exposed to a D.C. magnetic field in parallel to the axis of the ice crystal tube.

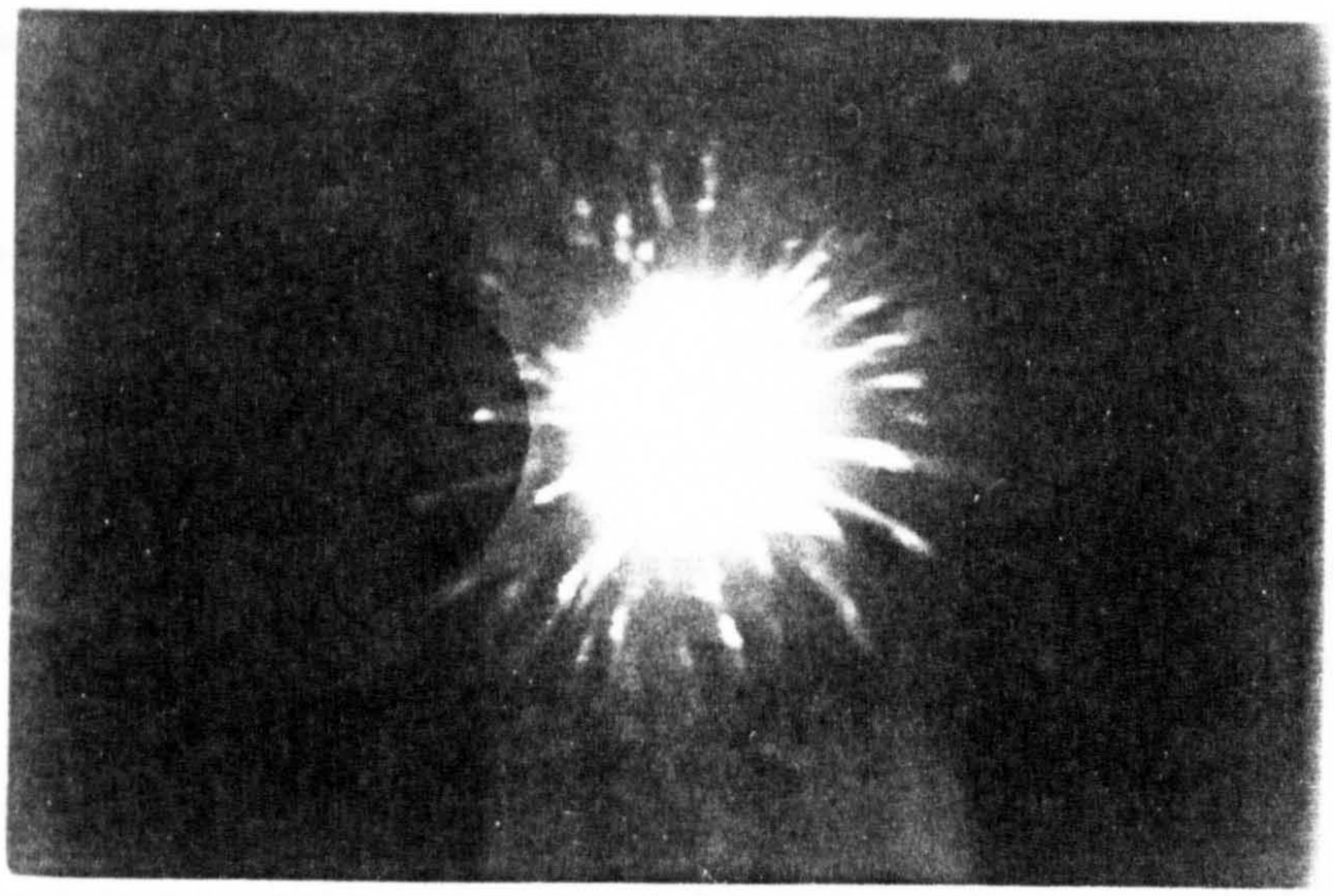

Fig. (10.19) X-ray transmission of a clean water ice crystal which has been exposed to a D.C. magnetic field at right angle to the axis of the ice crystal tube.

The patterns of Fig. (10.16) confirm that a magnetic field has an effect on water if it changes their state whilst the field exists. No such effect could be obtained if the field was absent. The X-ray pictures of Figs. (10.18) and (10.19) clearly show that the direction of the magnetic field on the sample is an important factor in the formation of X-ray patterns on photographic film. The direction of the magnetic field on the sample can change or orient the position of crystals in ice-crystals since they manifest different X-ray transmission pictures.

10.5 Supercooling

When a liquid changes to a solid, it undergoes a change of state or phase. A clean water will freeze sharply at 0°C or below. While the water is freezing, it is evolving its latent heat of fusion, which compensates for the heat lost by cooling, and its temperature does not fall.

The water samples used in this research was double-de-ionized distilled water which was pre-prepared in the Chemistry Department. This water is as free as was possible from impurities and had also very low conductivity (0.5×10^{-6} $\mathcal{S}$ /m).

An experiment was performed to determine the lowest degree of supercooling of the prepared pure clean water before its freezing.

The water was frozen in the freezer with therocouple inserted into the liquid.

The temperature was measured by a digital (co-marked) thermometer. It

was also connected to a plotter (PM 8231 Phillips) so a chart graph record could be obtained of the temperature data as a function of time.

Graph (10.5) shows the results of cooling of the pure clean water in

a) presence

b) absence; of a magnetic field.

Graph (10.5) shows that the water has been cooled to about -7 to -9°C before it is frozen.

This cooling of a liquid below its normal freezing point is called supercooling.

Graph (10.5) shows the chart record of the supercooling of the clean water.

It is interesting to note that once the water changed it's state or phase from a supercooled liquid to ice, the temperature increased by a few (3-4) degrees.

This experiment was repeated 8 times or more and the results are shown in Graph (10.5).

The results in Graph (10.5) do not show any significant differences in supercooling of the clean water between the magnetic field exposed sample and the water which had not been exposed to the magnetic field.

In order to summarise the information regarding the observations

GRAPH (10.5), SUPERCOOL SPECTRUM OF A CLEAN WATER IN PRESEN CE AN D ABSENT OF ANY MAGN ETIC FIELD

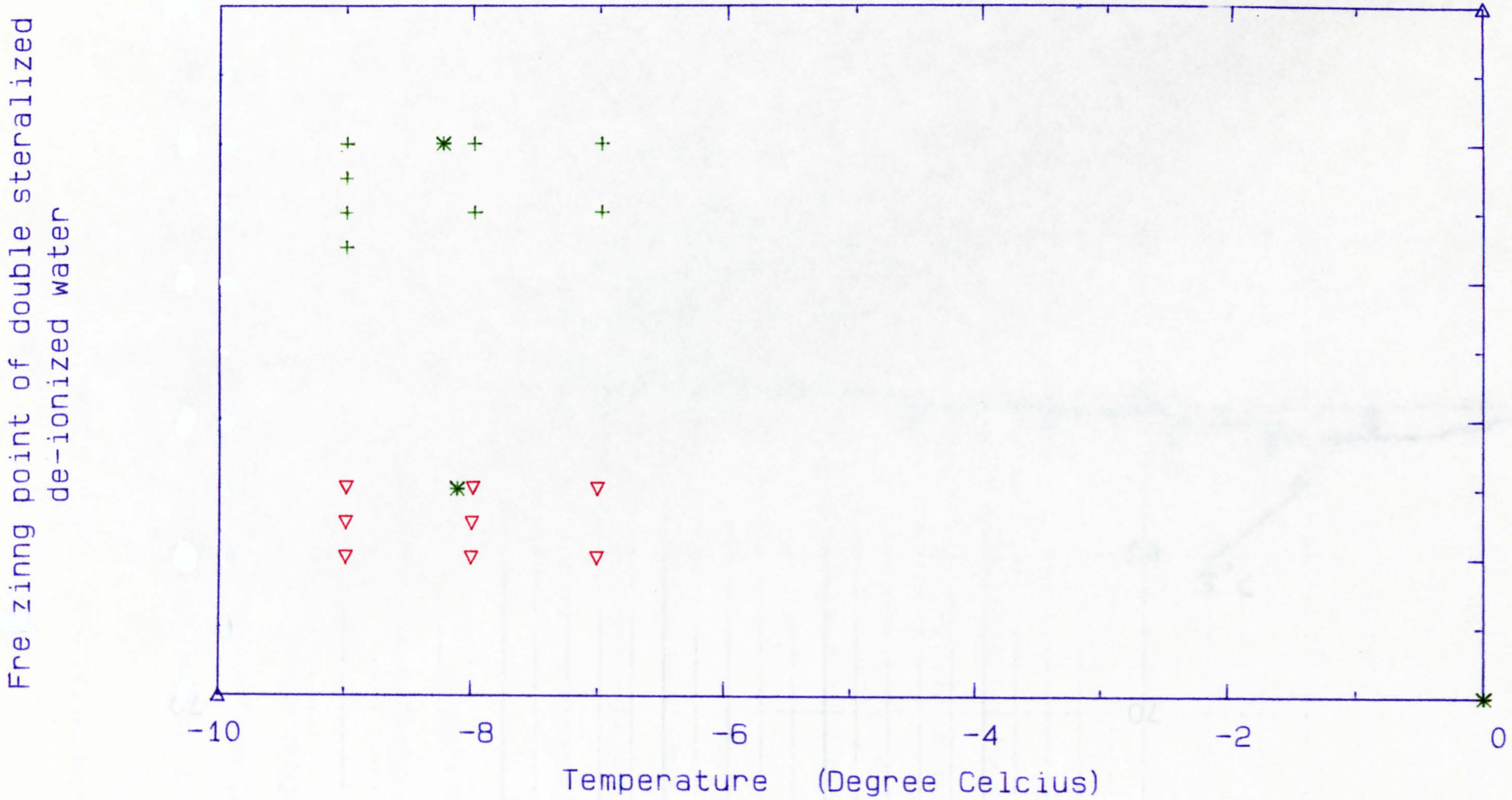

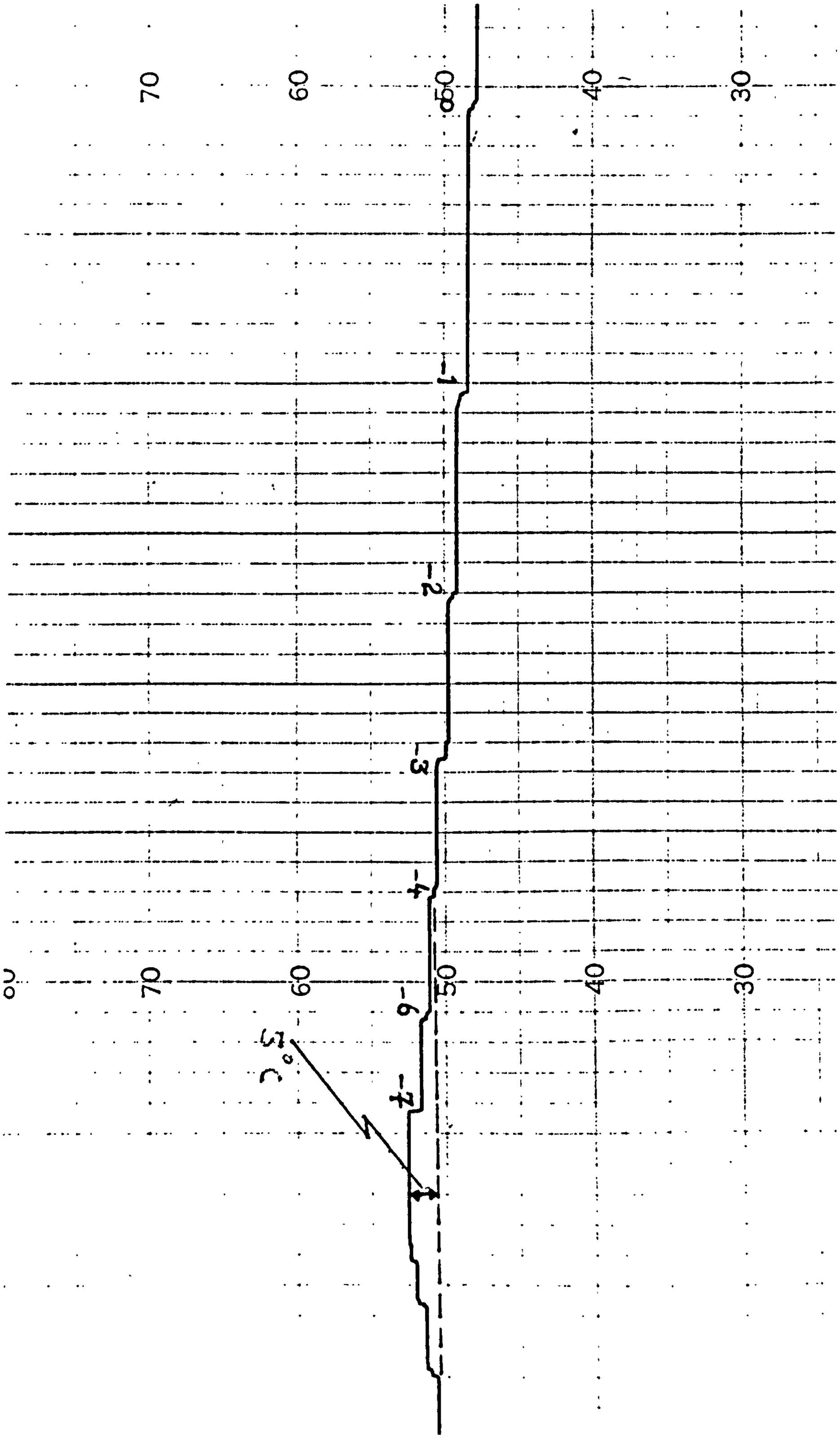

Figure (1.2.2), CHART RECORD COPY OF THE SUPERCOOLING OF THE CLEAN WATER

recorded,the mean and S.D. freeze points have been determined.

This is represented by an "*" in Graph (10.5). Unfortunately they do not tell us anything about the dispersion of the values around the central value.

We therefore need a measure to indicate the spread of the values about the mean.

The standard deviation from the mean is used widely in statistics to indicate the degree of dispersion. It takes into account the deviation of every value from the mean and for our experiment has been found as follows:

Standard deviation of supercooling of magnetic field treated water $[\sigma_{M.F.}] = 0.83$

Standard deviation of supercooling of untreated water which had not been exposed to any magnetic field $[\sigma_{\mathcal{J}}] = 0.78$

10.6 Discussion

In recent times progress has been made in the investigation of the effects of magnetic fields on water. Dielectrophoresis experiments indicate that a magnetic field can affect biological systems (7, 10 11). The result of dielectrophoresis experiments on live cell suspensions have shown anomalies in the region of 2 kHz. The proton magnetic resonance in a geomagnetic field of 0.7 gauss (70 μT) is 2.8 kHz. Effects have also been observed at the electric spin resonance frequency and for the frequencies corresponding to the magnetic movements of the isotopes ^{31}p, ^{23}Na, ^{39}cl and ^{39}K [7]. Because dielectrophoresis experiments readily show up differences between the dielectric properties of the particle and the suspending medium, the effects were easy to investigate initially using this technique. However, the measured magnetic field dependency of the dielectric properties of water showed that there is a drop in capacitance and loss of (spring) water as the proton magnetic field and frequency satisfy proton NMR conditions.

Experiments have shown that the dielectric properties of water can also be changed at other frequencies by exposing water to specific frequencies of magnetic field . The same general pattern of symptoms trapped by electric and magnetic fields is likely to be responsible for the reaction of some patients to magnetic fields [8]. Smith et al [8] have some patients who are hyperallergic to certain chemicals, and also to field-treated water and have subjected that could be due to some resonance structure set up in water. Del Giudice et al [12] have considered quantisation of the electric dipoles of the water molecules and the electromagnetic radiation field.

In the course of the experiment described in this section relating to the effect of a magnetic field on a solid state of water (ice) is observed. The effects described here are based on the information obtained either by looking through a light microscope (when the experimental effects of A.C. and D.C magnetic fields on Nacl dissolved water (brine water)), or X-ray diffraction and transmission patterns of double de-ionized distilled water. Section 10.3 of this chapter shows clearly how the dissolved Nacl in a water solution can be aligned in a uniform manner at an angle to the direction of the magnetic field.

This may be due to the force exerted by water molecules. A change in frequency of A.C. magnetic fields can orient (section 10.3.4.) the crystals in a different direction. Any increase in the strength of a magnetic field would increase the density alignment of the crystals but an increase in temperature of crystallization and magnetic field exposure time did not show any change in the effect. There are particularly interesting X-ray diffraction patterns of the materials which are wet or have absorbed water. A qualitative survey, carried out by Rosalind et al [13], has been made of the types of X-ray diagram given by specimens of sodium thymonucleate (dry NaDNA) at different humidities. The diagrams show that the structure will have different X-ray patterns to the different humidities. Section 10.4 of this chapter has investigated the effect of magnetic fields on ice crystals. The X-ray diffraction pattern of clean water which has not been exposed to a magnetic field (control) was made of multi broken rings. This diffraction pattern was varied as soon as the water was exposed to a D.C. magnetic field (overnight). The sample's diffraction pattern was made up of multi cross lines. Fig. (10.12 shows a six-fold symmetry of clean water which had been exposed to a D.C. magnetic field. In 1985

Smith [6.14] suggested a possible helical structure for water which might have the required electrical properties as shown in Fig. (10.21).

If that is the case then the X-ray diffraction pattern of ice crystals must have 5-fold (and above) symmetry. This experiment has been repeated many times and a multi cross pattern was always visible, however, there was no certain 5-fold symmetry. A continuous helix can be defined in terms of two fundamental quantities: its radius r and its pitch or rise between turns p (Fig. (10.22))

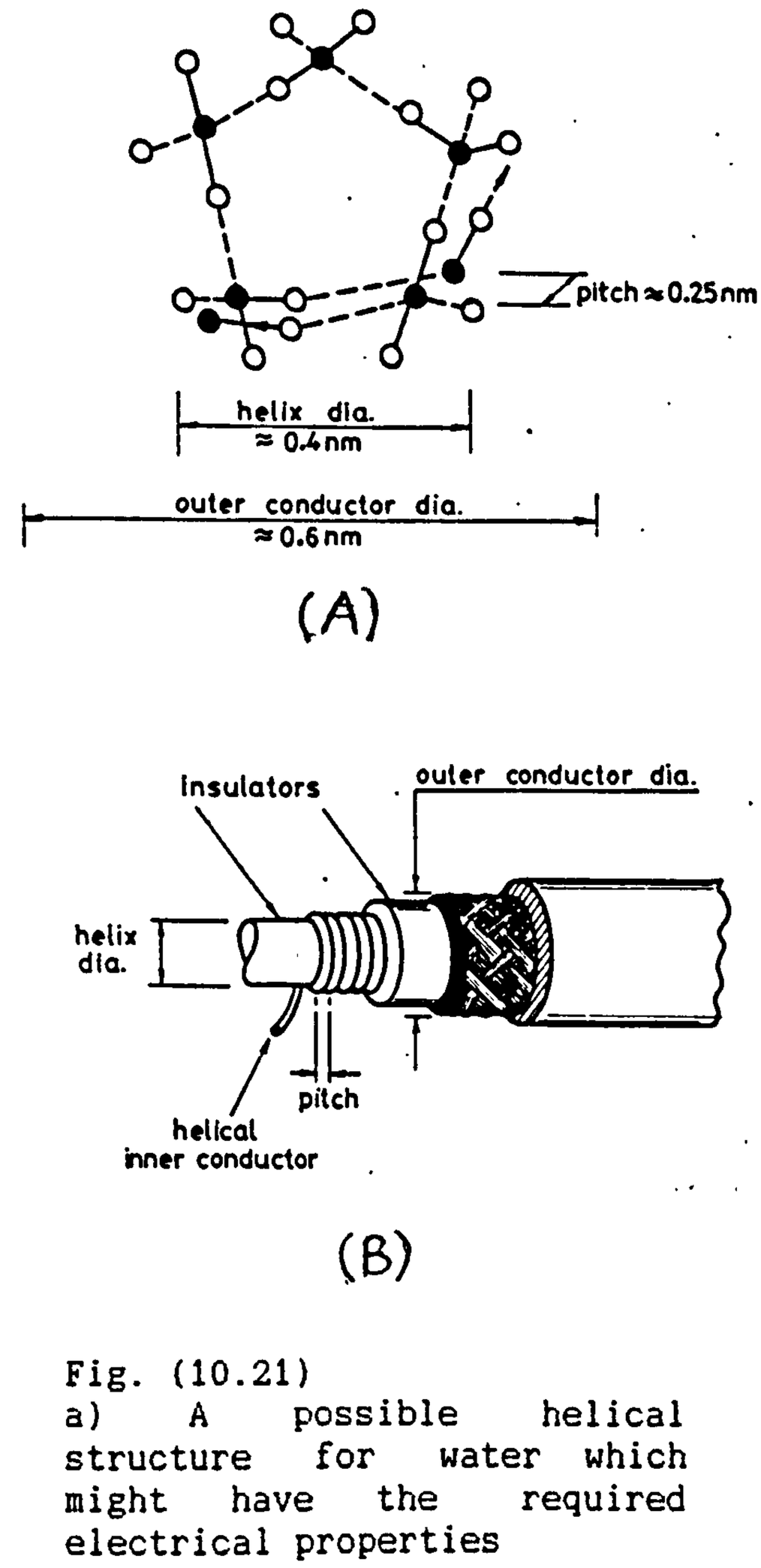

Fig. (10.21)
a) A possible helical structure for water which might have the required electrical properties

b) A typical electrical delay cable having a helical inner conductor.

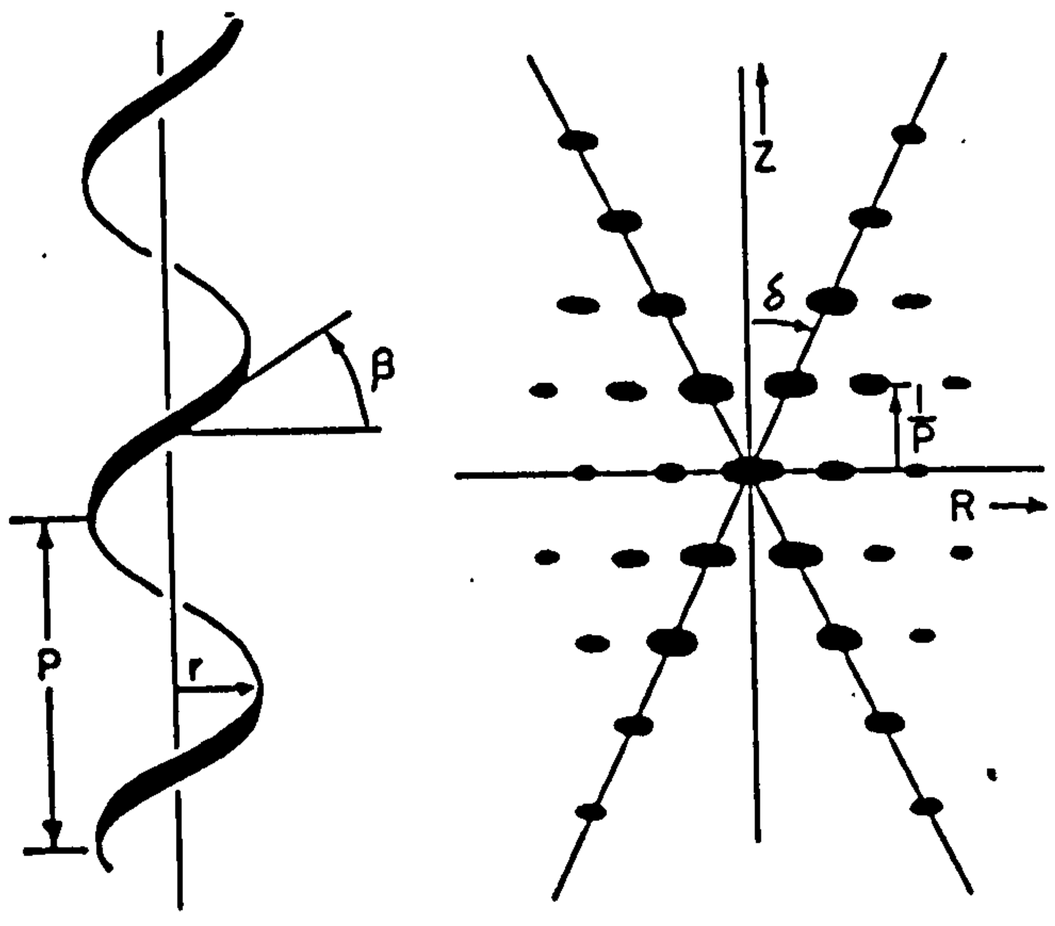

Fig. (10.22) Simple helix (a) and corresponding diffraction pattern, (b) p = pitch, r = radius, and β = pitch angle.

With a true axial repeat of p, the diffraction patterns will be confined to layers of z = $^{L}/_{P}$ L being any positive or negative integer or zero.

According to Amoros et al [14] conventional Laue photographs taken with a flat photographic film perpendicular to the X-ray beam give direct information about the Friedd symmetry of that direction. The entire symmetry of the X-ray beam direction is seen as its projection on the perpendicular photographic film. The symmetry of the photograph is usually obvious.

Thus, we see from Figure (10.13) a clear 6-fold symmetry, and from Figure (10.12) less clear fold symmetries. This is sufficient to decide against the pentagonal helical model and in favour of the dodecahedron model as proposed by Smith Figure (10.23). Both provide the necessary solenoidal symmetry for coupling to a magnetic field. The latter is also the geometry which would result from cavitation in water (Smith, unpublished).

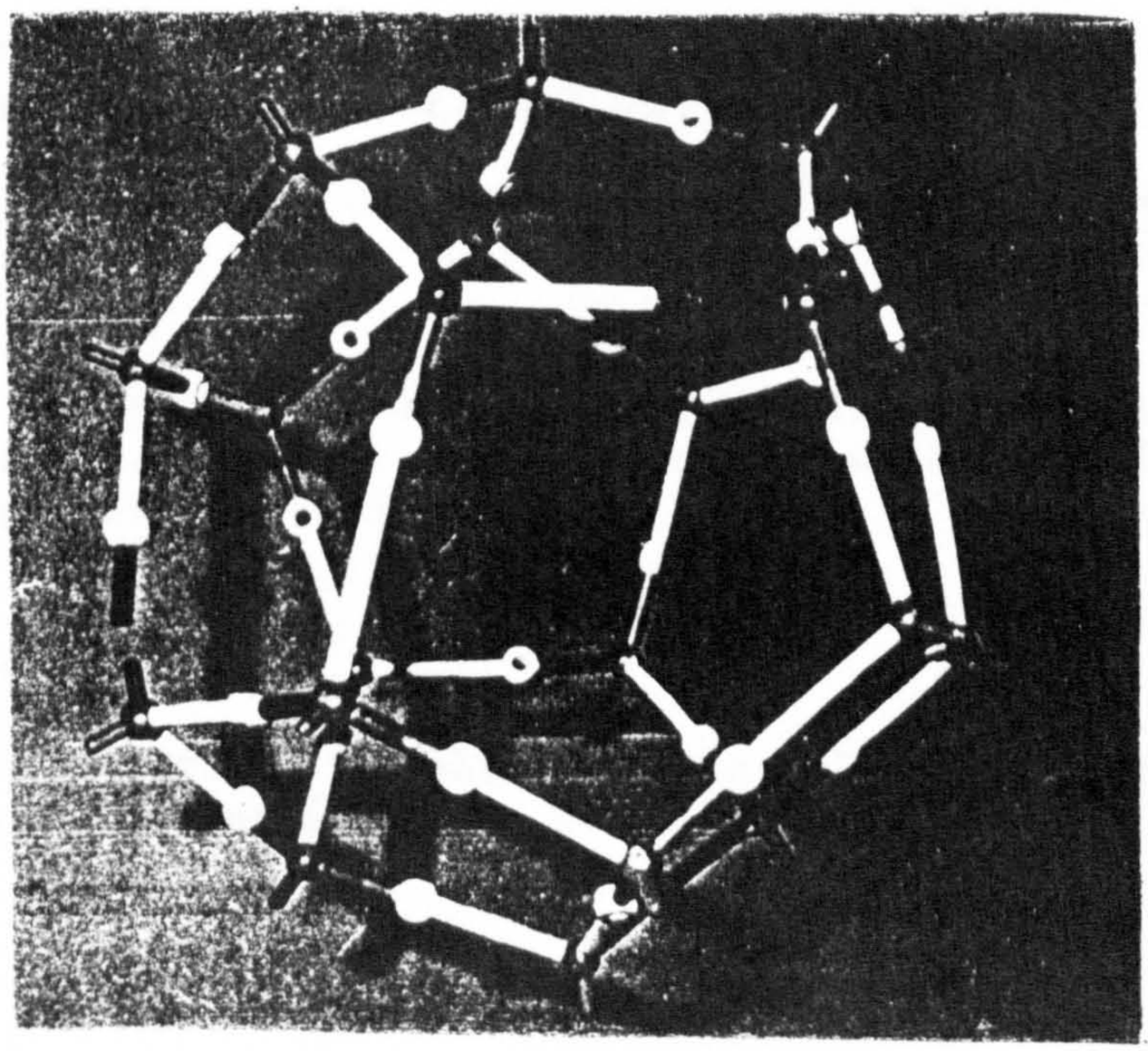

Figure (10.23) A pentagonal dodecahedron model for water (picture prepared by C.W. Smith)

REFERENCES

1) JHON, M.S. "Physico-chemical Approaches to the role of water in modern diseases such as Cancer, Diabetes and AIDS". Speculation Sci. Technol., 1987, 10(3), p.185.

2) FENWICK, P. and HOPKINS, R. "An examination of the effect of healing on water", PhD. Thesis, JSPR 92542, 1987, Israel.

3) HAYASHI, H., JHON, M.S., LOWDIN, P.O. "Some remarks on certain magnetic properties of water in the study of cancer. Int. J. Quant., 1987, 514, p.14.

4) POHL, H.A. "Natural electrical RF oscillation from cells". Journal of Bioenergetics and Biomembranes, 1981, 13, p.314.

5) FRÖHLICH, H. "Coherent Excitation in Active Biological Systems". Modern Biochemistry, Plenum: London, U.K., 1985.

6) SMITH, C.W. "Water Friend or Foe?". Laboratory Practice, 1985, 34(10), p.29.

7) JAFFARY-ASL, A.H., SOLANKI, S.N., AARHOLT, E., SMITH, C.W. "Dielectric Measurements on Live Biological Materials Under Magnetic Resonance Conditions". Journal of Biological Physics, 1983, 11, p.15.

8) SMITH, C.W., CHOY, R., MONRO, J.A. "Man and His Environment in Health and Disease". Proc. 3rd Int. Symp., Dallas, Texas, February 21-24, 1985.

9) WILLIAMS, H., SABARTH, E. "In vitro Demonstration of Homeopathic Effects", in Proc. 42nd Cong. Int. Homeopathic Med. League. Arlington, Am. Inst. Homeopathy, Washington DC, 29 Mar-2 Apr., 1987.

10) JABERANSARI, M. "Dielectrophoresis, Electrodyanmic and Magnetic Resonance Phenomena, MSc. Thesis, Salford University, 1985.

11) POHL, H. Conf. on Organic and Biological Semiconductors, University of Nottingham, 23-25 Sept., 1980.

12) GIUDICE, E.G., PREPARATA, G., VITIELLO, G. "Water as a free dielectric dipole laser". Physical Review Letters, 1988, 6(9), p.1085.

13) ROSALIND, B. FRANKLIN and GOSLING, G. "The structure of sodium thymonvitreate fibres. I. The influence of water content". Acta Crystallographic, 1953, 6, p.673.

14) AMOROS, J.L., BUERGEMM, J. and De AMOROS, M.C. "The Lave Method", London: Academic, 1975.

15) LUDWIG, W. Translation: "Biophysical opinion". Biophysikalisches Labor Diplomphysiker 21, 1988, D7240 Horb a N.1.

CONCLUSION

CONCLUSION

Previous work concerned with dielectric measurements on water and dielectrophoresis measurements on pearl-chain formations of yeast cells (Saccharomyces cerevisiae), showed anomalies when the ambient magnetic field satisfied specific resonance conditions.

The present thesis has described measurements of a cellular-spin-resonance (CSR) in Saccharomyces cerevisiae and Leishmania major cells. The evidence that living cells naturally produce oscillating electric fields in the r.f. region is by now quite strong, and proceeds from a variety of experimental evidence. A spectrum of cell rotation speeds of lone cells with different values of the applied frequency shows the existence of two frequency regions where cellular-spin-resonance occurs. These regions are at 3 kHz and 70 kHz respectively. This experiment predicted a square law dependence of the rotation rate of the lone cells upon the field strength above 20 kHz, however, for frequencies below 20 kHz the rotation rate of the lone cells is found to be linearly dependent on the field strength.

The use of vacuum sputtered thin film metal electrodes allows lone cells to be studied more accurately by using a short working distance objective lens on the microscope. The linear oscillatory motion of lone cells observed at low (sub-Hertz) frequencies implies that there must also be some surface charge phenomena involved. The effect is by way of being electrophoretic, but the collection mechanism of the surface charge may be dielectrophoretic.

Work has been described relating to the Leishmaniae parasite cells which, normally grow only when they are attached to the gut of a living sandfly. During the investigations, the attachment of Leishmania major

cells to scratches made in polystyrene petri dishes, both with a metal stylus and with a diamond stylus were equally effective in causing a localised attachment of parasites to the scratches. The use of a diamond stylus eliminated the possibility of surface contamination with a metal and consequent chemical or ioni c effect. The treatment of polystyrene petri-dishes by electron beam bombardment was found to facilitate the attachment of the parasite cells "in vitro", over the whole area bombarded, thus facilitating their culture. It also became clear that the parasite cells have a preference for a negatively charged surface.

The most effective electron dose range for promoting the attachment of Leishmania major cells to a polystyrene substrate was found to be in the range 10^{17}---› $0.5x10^{20}$ electron/m^2. In this charge density range the parasite's flagellum became modified into an attachment organ as occurs naturally in its sandfly host. Hence there is often expanding of its membrane to increase the area of cell-substrate contact presumably to fasciliate adhesion and nutrition. Treatment of the substrate with positive ion beams did not result in any case of attachment of the parasites.

By way of preliminary experiments into the role of water in the electrical phenomena investigated, ice crystals were formed by the freezing of supercool water in the presence of a magnetic field. The resulting ice crystals were always asymmetric relative to the magnetic field direction. X-ray diffraction photographs of these ice crystals showed distinct patterns of spots if the water used was double distilled, otherwise ring-like powder diffraction patterns were obtained. Possible interpretations of these patterns have been discussed. The author believes this line of investigation warrants

more research; the application of more up-to-date X-ray equipment and computerised analysis is vital. This experiment should be extended to cover the wide range alternating magnetic field known to have biological effects.

A P P E N D IC ES

APPENDIX 1 Savouraud Dextose Agar

Sabouraud dextrose agar (Oxoid Ltd)

Oxoid code powder CM41

Formula

	Grams per litre
mycological peptone (oxoid L40).....	10
dextrose.....	40
agar no.1(oxoid L11).....	15

pH 5.6(approx.)

Description

This modification of Sabouraud agar was made by Carlier in 1948. It is intended for the cultivation and differentiation of fungi. The medium is often used with antibiotics for the isolation of pathogenic fungi from material containing large number of other fungi or bacteria.

Directions

Suspend 65 g powder in 1 litre of distilled water. Bring to the boil to disolve completely. Sterlize by autoclaving at 121 ^{o}C for 15 minutes.

Sabouraud liquid medium

Oxoid code powder *CM147*

Formula

	Grams per litre
pancreatic digest of casein (oxoid L42).....	5
peptic digest of fresh meat (oxoid L49).....	5
dextrose.....	20

pH 5.7(approx.)

Description

Sabouraud liquid medium is a myological sterility test medium conforming with the requirements for the medium described in the United States Pharmacopia (1965) for the determination of pharmaceutical products in order to avoid false sterility tests. The medium may also be recommended for the cultivation of moulds,yeast,and acidophilic bacteria.

Directions

Add 30 g powder in 1 litre of distilled water. Mix well, distribute into final container and sterilize by autoclaving at 121 ^{o}C for 15 minutes.

RS data

Programmable Crystal Oscillators

Stock numbers 301-858, 301-864

Two programmable crystal oscillators which can be used to generate 57 different output frequencies. The broad range of output frequencies is derived from the internal crystal oscillator. Two different base frequency oscillators of 600kHz and 1MHz are available giving output frequencies from 0.005Hz up to 1MHz. The oscillators are housed in standard 16-pin DIL packages.

Features

- Provide 57 different frequencies from a single internal quartz crystal.
- Frequency range from 0.005Hz to 1MHz.
- Laser trimmed for high accuracy.
- Lower power consumption.
- TTL compatible.

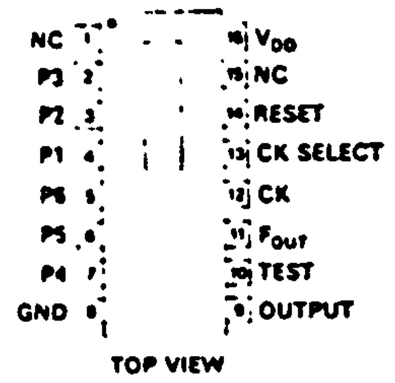

TOP VIEW

Absolute maximum ratings

Supply voltage	−0.3 to +10V
Operating temperature	−10 to +70°C
Storage temperature	−30 to +85°C

Performance specification

Calibration tolerance	±100p.p.m.
Frequency stability	±0.015%
Voltage coefficient	10p.p.m/V typ.
	25p.p.m/V max.
Aging	10p.p.m max.

Electrical characteristics T_a=25°C V_{DD}=5V

Symbol	Parameter	Min	Typ	Max	Unit
V_{DD}	Supply voltage	4.0	5.0	6.0	V
I_{OH}	Output current: Hi[1]			-1.0	mA
I_{OL}	Output current: Lo[2]	1.6			mA
V_{IH}	Input voltage: logic 1	V_{DD}-1.0		V_{DD}	V
V_{IL}	Input voltage: logic 0	0.0		1.0	V
I_{IH}	Input current reset: Hi			0.5	μA
I_{IL}	Input current reset: Lo	-15			μA
I_{IH}	Input current Prog 1-6, CSEL, CK, TEST: Hi			15	μA
I_{IL}	Input current Prog 1-6, CSEL, CK, TEST: Lo	-0.5			μA
I_{DD}	Supply current[3]		0.7	1.0	mA

[1]V_{OH} = 4V [2]V_{OL} =0.4V [3]Crystal: 600kHz, OUT: 60kHz

Switching characteristics

Ta =25°C V_{DD}=5V C_L=15pf

Symbol	Parameter	Typ	Max	Unit
t_R	Reset delay time		1.0	μsec
t_E	Timing error after reset released		1.5	μsec
t_r	Rise time	70		nsec
t_f	Fall time	30		nsec
F_{in}	External oscillator operating frequency		1.25	MHz

WARNING!

CAUTION:

ESD (Electro-Static-Discharge) sensitive device. The digital control inputs are diode protected; however, permanent damage may occur on unconnected devices subject to high energy electrostatic fields. Unused devices must be stored in conductive foam or shunts. The protective foam should be discharged to the destination socket before devices are removed.

Figure 1 **Block diagram**

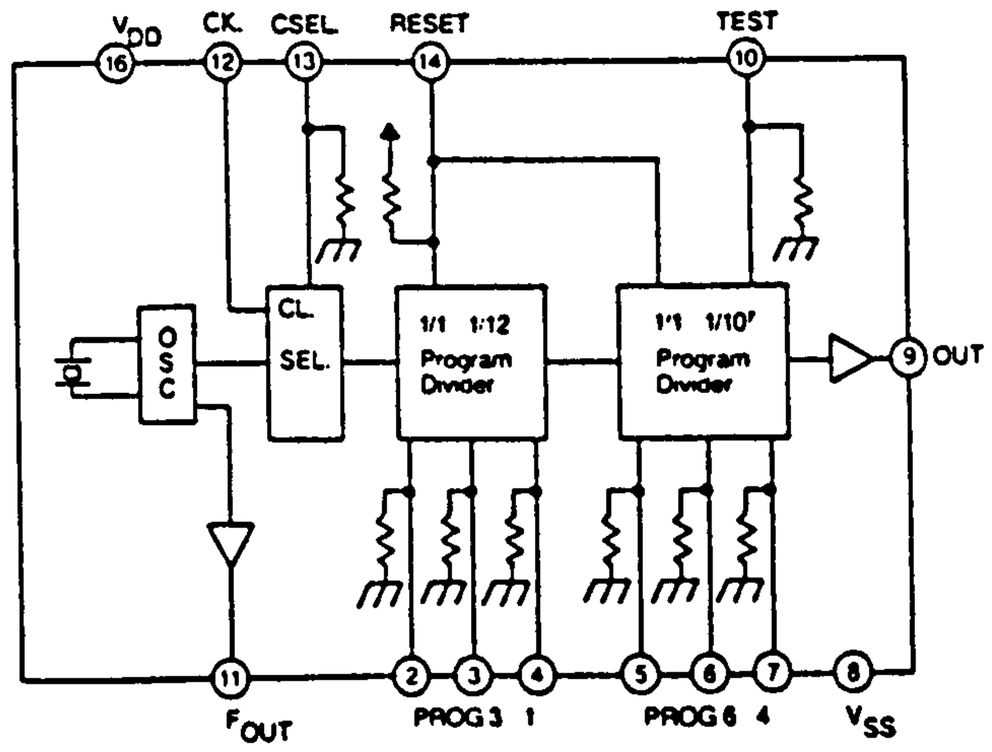

Figure 2 **Timing diagram**

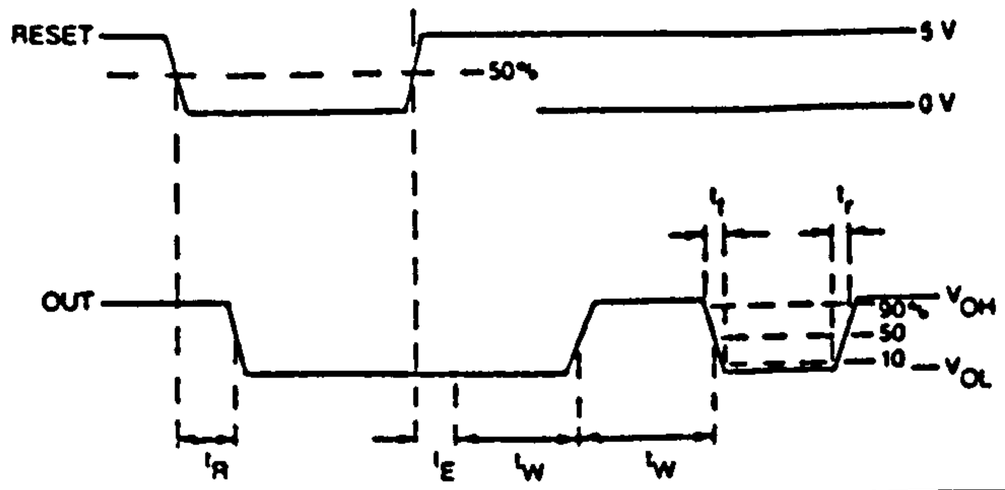

RS data

Pin Functions
Prog 1 through Prog 6 control divide ratio of base frequency.

Prog 1	Prog 2	Prog 3	Dividing ratio	Prog 4	Prog 5	Prog 6	Dividing ratio
0	0	0	1 1	0	0	0	1 1
0	0	1	1 10	0	0	1	1 10
0	1	0	1 2	0	1	0	1 10²
0	1	1	1 3	0	1	1	1 10³
1	0	0	1 4	1	0	0	1 10⁴
1	0	1	1 5	1	0	1	1 10⁵
1	1	0	1 6	1	1	0	1 10⁶
1	1	1	1 12	1	1	1	1 10

OUT: Supplies programmed output frequency with rectangular pulse shape (50% duty cycle, except as noted)

TEST. Setting this terminal Hi multiplies programmed output frequency by 1,000, except when programmed divide ratio is less than 1/1000.

FOUT: Supplies base frequency of internal crystal oscillator.

CK: External clock input.

CSEL. Clock select. Setting this terminal Hi causes the divider to count the frequency of an external clock instead of the internal clock.

RESET: Setting this terminal Lo resets all counters and sets output to Lo.

(All inputs except CK and RESET have internal pull-down resistors. RESET has an internal pull-up resistor.)

Output frequencies of 600kHz unit (301-858)

UNIT: Hz

Program Pin Settings		P4	0	0	0	0	1	1	1	1
		P5	0	0	1	1	0	0	1	1
P1	P2	P6 / P3	0	1	0	1	0	1	0	1
0	0	0	600K	60K	6K	600	60	6	0 6	0 06
0	0	1	60K	6K	600	60	6	0 6	0 06	0 006
0	1	0	300K	30K	3K	300	30	3	0 3	0 03
0	1	1	200K	20K	2K	200	20	2	0 2	0 02
1	0	0	150K	15K	1 5K	150	15	1 5	0 15	0 015
1	0	1	120K	12K	1 2K	120	12	1 2	0 12	0 012
1	1	0	100K	10K	1K	100	10	1	0 1	0 01
1	1	1	50K	5K	500	50	5	0 5	0 05	0 005

*33⅓% duty cycle **40% duty cycle

Output frequencies of 1MHz unit (301-864)

UNIT: Hz

Program Pin Settings		P4	0	0	0	0	1	1	1	1
		P5	0	0	1	1	0	0	1	1
P1	P2	P6 / P3	0	1	0	1	0	1	0	1
0	0	0	1M	100K	10K	1K	100	10	1	0 1
0	0	1	100K	10K	1K	100	10	1	0 1	0 01
0	1	0	500K	50K	5K	500	50	5	0 5	0 05
0	1	1	333 3K*	33 3K*	3 3K*	333 3*	33 3*	3 3*	0 33*	0 033*
1	0	0	250K	25K	2 5K	250	25	2 5	0 25	0 025
1	0	1	200K	20K	2K	200	20	2	0 2	0 02
1	1	0	166 6K*	16 6K*	1 6K*	166 6*	16 6*	1 66*	0 16*	0 016*
1	1	1	83 3K*	8 3K*	833 3*	83 3*	8 3*	0 83*	0 083*	0 0083*

*33⅓% duty cycle **40% duty cycle

Applications

Figure 3 **One shot timer**

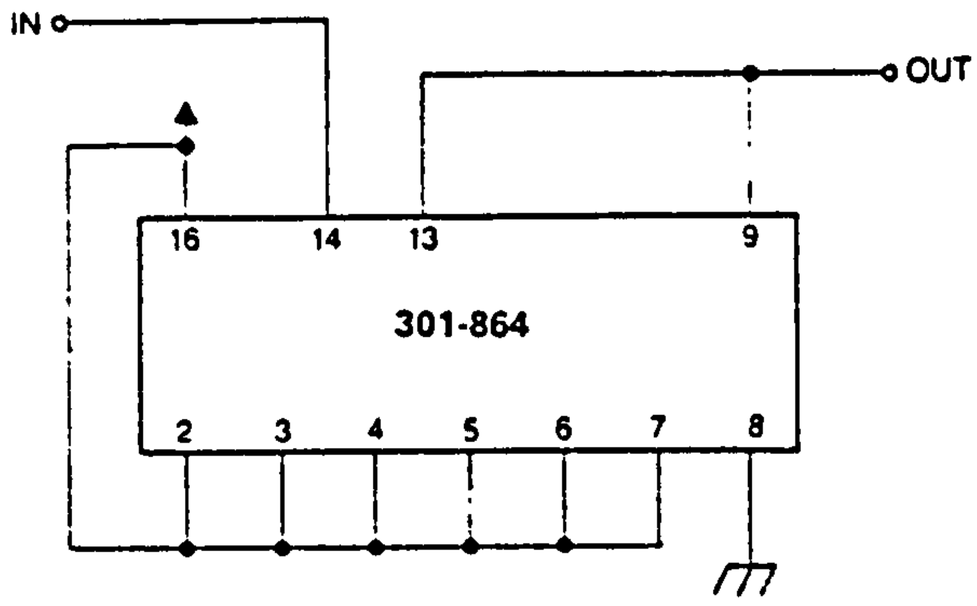

Figure 4 **Square wave generator providing 0.005Hz to 600kHz (for 600kHz oscillator)**

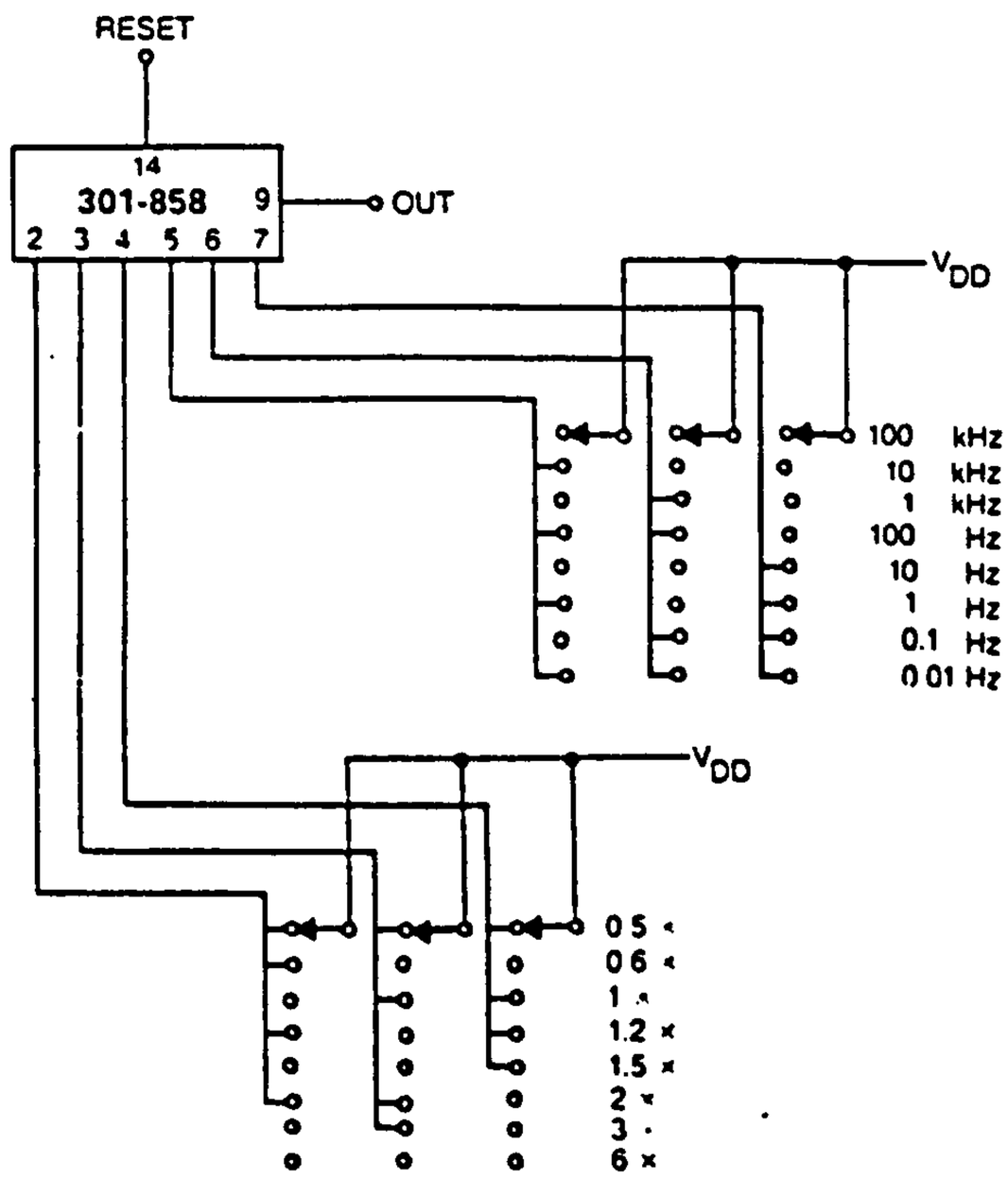

R.S. Components Ltd. PO Box 99, Corby, Northants, NN17 9RS
An Electrocomponents Group Company
Telephone: 0536 201234

typical clear, load, and count sequences

Illustrated below is the following sequence:

1. Clear outputs to zero.
2. Load (preset) to binary thirteen.
3. Count up to fourteen, fifteen, carry, zero, one, and two.
4. Count down to one, zero, borrow, fifteen, fourteen, and thirteen.

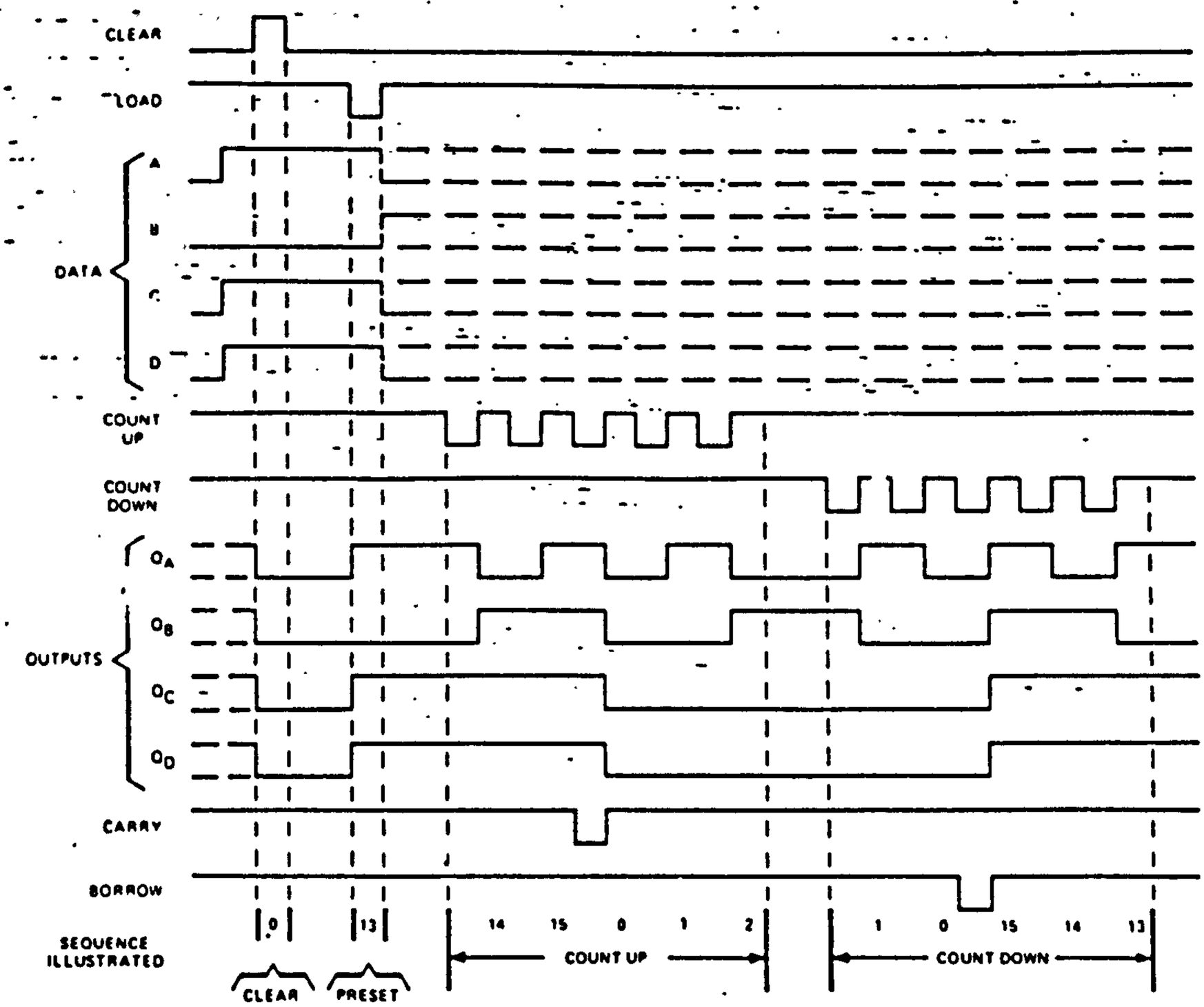

NOTES: A. Clear overrides load, data, and count inputs.

B. When counting up, count-down input must be high; when counting down, count-up input must be high.

switching characteristics, V_{CC} = 5 V, T_A = 25°C

PARAMETER¶	FROM INPUT	TO OUTPUT	TEST CONDITIONS	MIN	TYP	MAX	UNIT
f_{max}			C_L = 15 pF, R_L = 400 Ω, See Figures 1 and 2	25	32		MHz
t_{PLH}	Count-up	Carry			17	26	ns
t_{PHL}					16	24	
t_{PLH}	Count-down	Borrow			16	24	ns
t_{PHL}					16	24	
t_{PLH}	Either Count	Q			25	38	ns
t_{PHL}					31	47	
t_{PLH}	Load	Q			27	40	ns
t_{PHL}					29	40	
t_{PHL}	Clear	Q			22	35	ns

¶ f_{max} = maximum clock frequency
t_{PLH} = propagation delay time, low to high level output
t_{PHL} = propagation delay time, high to low-level output

TYPES SN54192, SN54193, SN54L192, SN54L193, SN54LS192, SN54LS193 SN74192, SN74193, SN74L192, SN74L193, SN74LS192, SN74LS193 SYNCHRONOUS 4-BIT UP/DOWN COUNTERS (DUAL CLOCK WITH CLEAR)

BULLETIN NO. DL-S 7711828, DECEMBER 1972—REVISED AUGUST 1977

- Cascading Circuitry Provided Internally
- Synchronous Operation
- Individual Preset to Each Flip-Flop
- Fully Independent Clear Input

TYPES	TYPICAL MAXIMUM COUNT FREQUENCY	TYPICAL POWER DISSIPATION
'192, '193	32 MHz	325 mW
'L192, 'L193	7 MHz	43 mW
'LS192, 'LS193	32 MHz	95 mW

SN54', SN54LS'... J OR W PACKAGE
SN54L'... J PACKAGE
SN74', SN74L', SN74LS'... J OR N PACKAGE
(TOP VIEW)

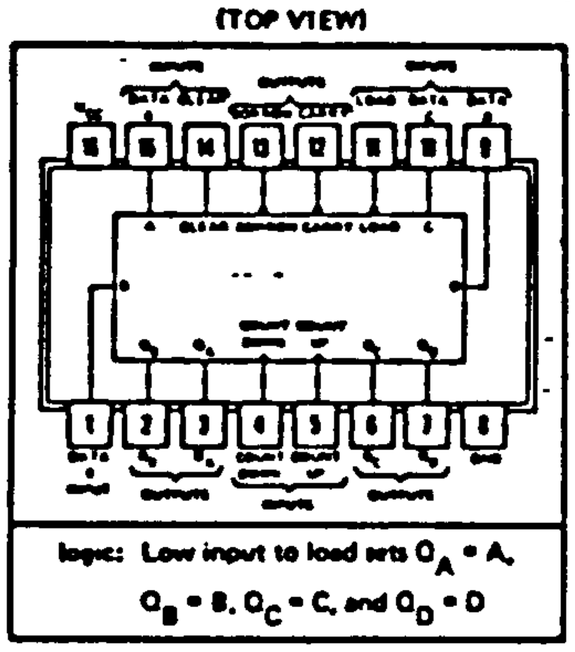

logic: Low input to load sets $Q_A = A$, $Q_B = B$, $Q_C = C$, and $Q_D = D$

description

These monolithic circuits are synchronous reversible (up/down) counters having a complexity of 55 equivalent gates. The '192, 'L192, and 'LS192 circuits are BCD counters and the '193, 'L193 and 'LS193 are 4 bit binary counters. Synchronous operation is provided by having all flip-flops clocked simultaneously so that the outputs change coincidently with each other when so instructed by the steering logic. This mode of operation eliminates the output counting spikes which are normally associated with asynchronous (ripple-clock) counters.

The outputs of the four master-slave flip-flops are triggered by a low-to-high-level transition of either count (clock) input. The direction of counting is determined by which count input is pulsed while the other count input is high.

All four counters are fully programmable; that is, each output may be preset to either level by entering the desired data at the data inputs while the load input is low. The output will change to agree with the data inputs independently of the count pulses. This feature allows the counters to be used as modulo-N dividers by simply modifying the count length with the preset inputs.

A clear input has been provided which forces all outputs to the low level when a high level is applied. The clear function is independent of the count and load inputs. The clear, count, and load inputs are buffered to lower the drive requirements. This reduces the number of clock drivers, etc., required for long words.

These counters were designed to be cascaded without the need for external circuitry. Both borrow and carry outputs are available to cascade both the up- and down-counting functions. The borrow output produces a pulse equal in width to the count-down input when the counter underflows. Similarly, the carry output produces a pulse equal in width to the count-up input when an overflow condition exists. The counters can then be easily cascaded by feeding the borrow and carry outputs to the count-down and count-up inputs respectively of the succeeding counter.

recommended operating conditions

	SN54192 SN54193			SN74192 SN74193			UNIT
	MIN	NOM	MAX	MIN	NOM	MAX	
Supply voltage, V_{CC}	4.5	5	5.5	4.75	5	5.25	V
High-level output current, I_{OH}			−400			−400	μA
Low-level output current, I_{OL}			16			16	mA
Clock frequency, f_{clock}	0		25	0		25	MHz
Width of any input pulse, t_w	20			20			ns
Data setup time, t_{su} (see Figure 1)	20			20			ns
Data hold time, t_h	0			0			ns
Operating free-air temperature, T_A	−55		125	0		70	°C

Courtesy of Texas Instruments Incorporated.

Appendix: Data Sheets

2708/8708*
8K AND 4K UV ERASABLE PROM

	Max. Power	Max. Access	Organization
2708	800 mW	450 ns	1K x 8
2708L	425 mW	450 ns	1K x 8
2708-1	800 mW	350 ns	1K x 8
2704	800 mW	450 ns	512 x 8

- Low Power Dissipation — 425 mW Max. (2708L)
- Fast Access Time — 350 ns Max. (2708-1)
- Pin Compatible to Intel® 2308 ROM
- Static — No Clocks Required
- Data Inputs and Outputs TTL Compatible during both Read and Program Modes
- Three-State Outputs — OR-Tie Capability

The Intel® 2708 is a 8192-bit ultraviolet light erasable and electrically reprogrammable EPROM, ideally suited where fast turnaround and pattern experimentation are important requirements. All data inputs and outputs are TTL compatible during both the read and program modes. The outputs are three-state, allowing direct interface with common system bus structures. A pin-for-pin mask programmed ROM, the Intel® 2308, is available for large volume production runs of systems initially using the 2708.

The 2708L at 425 mW is available for systems requiring lower power dissipation than from the 2708. A power dissipation savings of over 50%, without any sacrifice in speed, is obtained with the 2708L. The 2708L has high input noise immunity and is specified at 10% power supply tolerance. A high-speed 2708-1 is also available at 350 ns for microprocessors requiring fast access times. For smaller size systems there is the 4096-bit 2704 which is organized as 512 words by 8 bits. All these devices have the same programming and erasing specifications of the 2708. The 2704 electrical specifications are the same as the 2708.

The 2708 family is fabricated with the N-channel silicon gate FAMOS technology and is available in a 24-pin dual in-line package.

PIN CONFIGURATION

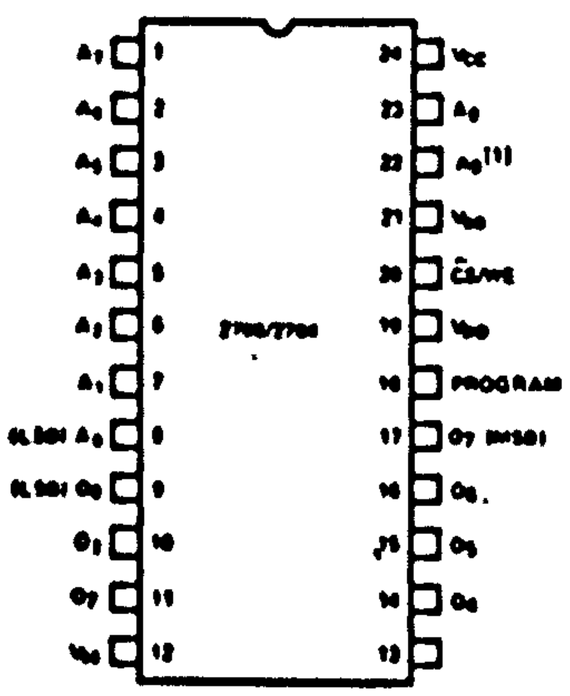

NOTE 1: PIN 22 MUST BE CONNECTED TO V_{BB} FOR THE 2704

BLOCK DIAGRAM

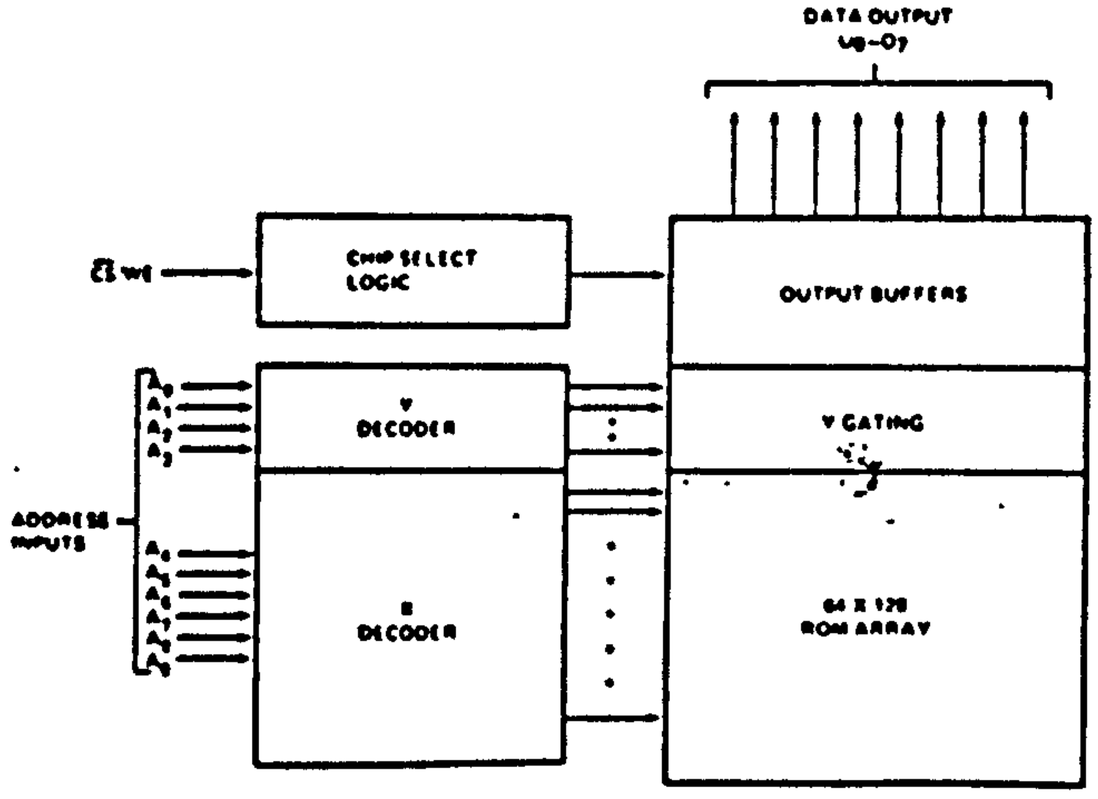

PIN NAMES

A_0–A_{10}	ADDRESS INPUTS
O_0–O_7	DATA OUTPUTS/INPUTS
$\overline{CS}/\overline{WE}$	CHIP SELECT/WRITE ENABLE INPUT

PIN CONNECTION DURING READ OR PROGRAM

	PIN NUMBER							
MODE	DATA I/O 9-11, 13-17	ADDRESS INPUTS 1-8, 22-23	V_{BB} 12	PROGRAM 18	V_{DD} 19	$\overline{CS}/\overline{WE}$ 20	V_{BB} 21	V_{CC} 24
READ	D_{OUT}	A_{IN}	GND	GND	+12	V_{IL}	-5	+5
DESELECT	HIGH IMPEDANCE	DON'T CARE	GND	GND	+12	V_{IH}	-5	+5
PROGRAM	D_{IN}	A_{IN}	GND	PULSED 26V	+12	V_{PROG}	-5	+5

*All 8708 specifications are identical to the 2708 specifications.

Courtesy of Intel Corporation.

PROGRAMMING

The programming specifications are described in the PROM/ROM Programming Instructions on page 4-83.

Absolute Maximum Ratings*

Temperature Under Bias	-25°C to +85°C
Storage Temperature	-65°C to +125°C
V_{DD} With Respect to V_{BB}	+20V to -0.3V
V_{CC} and V_{SS} With Respect to V_{BB}	+15V to -0.3V
All Input or Output Voltages With Respect to V_{BB} During Read	+15V to -0.3V
$\overline{CS}/WE$ Input With Respect to V_{BB} During Programming	+20V to -0.3V
Program Input With Respect to V_{BB}	+35V to -0.3V
Power Dissipation	1.5W

*COMMENT

Stresses above those listed under "Absolute Maximum Ratings" may cause permanent damage to the device. This is a stress rating only and functional operation of the device at these or any other conditions above those indicated in the operational sections of this specification is not implied. Exposure to absolute maximum rating conditions for extended periods may affect device reliability.

DC and AC Operating Conditions During Read

	2708	2708-1	2708L
Temperature Range**	0°C – 70°C	0°C – 70°C	0°C – 70°C
V_{CC} Power Supply	5V ± 5%	5V ± 5%	5V ± 10%
V_{DD} Power Supply	12V ± 5%	12V ± 5%	12V ± 10%
V_{BB} Power Supply	-5V ± 5%	-5V ± 5%	-5V ± 10%

READ OPERATION

D.C. and Operating Characteristics

Symbol	Parameter	2708, 2708-1 Limits Min.	Typ.[2]	Max.	2708L Limits Min.	Typ.[2]	Max.	Units	Test Conditions
I_{LI}	Address and Chip Select Input Load Current		1	10		1	10	µA	V_{IN} 5.25V or V_{IN} V_{IL}
I_{LO}	Output Leakage Current		1	10		1	10	µA	V_{OUT} 5.5V CS/WE 5V
I_{DD}	V_{DD} Supply Current		50	65		21	28	mA	Output Data Switching Current[4]
I_{CC}	V_{CC} Supply Current		6	10		2	4	mA	All Inputs 5V
I_{BB}	V_{BB} Supply Current		30	45		10	14	mA	CS/WE 5V T_A = 0°C
V_{IL}	Input Low Voltage	V_{SS}		0.65	V_{SS}		0.65	V	
V_{IH}	Input High Voltage	3.0		V_{CC}+1	2.2		V_{CC}+1	V	
V_{OL}	Output Low Voltage			0.45			0.4	V	I_{OL} 1.6mA (2708, 2708-1) I_{OL} 2mA (2708L)
V_{OH1}	Output High Voltage	3.7			3.7			V	I_{OH} -100 µA
V_{OH2}	Output High Voltage	2.4			2.4			V	I_{OH} -1 mA
P_D	Power Dissipation		800			325		mW	T_A 70°C
						425		mW	T_A = 0°C

NOTES: 1. V_{BB} must be applied before V_{CC} and V_{DD}. V_{BB} must also be the last power supply switched off.
2. Typical values are for T_A = 25°C and nominal supply voltages.
3. The total power dissipation is not calculated by summing the various currents (I_{DD}, I_{CC}, and I_{BB}) multiplied by their respective voltages since current does not flow between the various power supplies and V_{SS}. The I_{DD}, I_{CC}, and I_{BB} currents should be used to design the power supply capability only.
4. I_{BB} for the 2708L is specified at the programmed level and is 18 mA maximum at the unprogrammed level.

ERASURE CHARACTERISTICS

The erasure characteristics of the 2708 are such that erasure begins to occur when exposed to light with wavelengths shorter than approximately 4000 Angstroms (Å). It should be noted that sunlight and certain types of fluorescent lamps have wavelengths in the 3000–4000Å range. Data show that constant exposure to room level fluorescent lighting could erase the typical 2708 in approximately 3 years, while it would take approximatley 1 week to cause erasure when exposed to direct sunlight. If the 2708 is to be exposed to these types of lighting conditions for extended periods of time, opaque labels are available from Intel which should be placed over the 2708 window to prevent unintentional erasure.

The recommended erasure procedure (see page 3-55) for the 2708 is exposure to shortwave ultraviolet light which has a wavelength of 2537 Angstroms (Å). The integrated dose (i.e., UV intensity X exposure time) for erasure should be a minimum of 15 W-sec/cm^2. The erasure time with this dosage is approximately 15 to 20 minutes using an ultraviolet lamp with a 12000 µW/cm^2 power rating. The 2708 should be placed within 1 inch of the lamp tubes during erasure. Some lamps have a filter on their tubes which should be removed before erasure.

C. 2708/2704 Family Programming

Initially, and after each erasure, all 8192/4096 bits of the 2708/2704 are in the "1" state (output high). Information is introduced by selectively programming "0" into the desired bit locations. A programmed "0" can only be changed to a "1" by UV erasure.

The circuit is set up for programming operation by raising the CS/WE input (pin 20) to +12V. The word address is selected in the same manner as in the read mode. Data to be programmed are presented, 8 bits in parallel, to the data output lines (O_1–O_8). Logic levels for address and data lines and the supply voltages are the same as for the read mode. After address and data set up, one program pulse per address is applied to the program input (pin 18). One pass through all addresses is defined as a program loop. The number of loops (N) required is a function of the program pulse width (t_{PW}) according to N x t_{PW} $\geq$ 100 ms.

The width of the program pulse is from 0.1 to 1 ms. The number of loops (N) is from a minimum of 100 (t_{PW} = 1 ms) to greater than 1000 (t_{PW} = 0.1 ms). There must be N successive loops throuhg all 1024 addresses. *It is not permitted to apply N program pulses to an address and then change to the next address to be programmed.* Caution should be observed regarding the end of a program sequence. The CS/WE falling edge transition must occur before the first address transition when changing from a program to a read cycle. The program pin should also be pulled down to V_{ILP} with an active instead of a passive device. This pin will source a small amount of current (I_{ILL}) when CS/WE is at V_{IHW} (12V) and the program pulse is at V_{ILP}.

Programming Examples (Using N x t_{PW} $\geq$ 100 ms)

Example 1: All 8096 bits are to be programmed with a 0.5 ms program pulse width.

The minimum number of program loops is 200. One program loop consists of words 0 to 1023.

Example 2: Words 0 to 100 and 500 to 600 are to be programmed. All other bits are "don't care". The program pulse width is 0.75 ms.

The minimum number of program loops is 133. One program loop consists of words 0 to 1023. The data entered into the "don't care" bits should be all 1's.

Example 3: Same requirements as example 2, but the PROM is now to be *updated* to include data for words 750 to 770.

The minimum number of program loops is 133. One program loop consists of words 0 to 1023. The data entered into the "don't care" bits should be all 1's. Addresses 0 to 100 and 500 to 600 must be re-programmed with their original data pattern.

2704, 2708 Family
PROGRAM CHARACTERISTICS

T_A = 25°C, V_{CC} = 5V ±5%, V_{DD} = +12V ±5%, V_{BB} = -5V ±5%, V_{SS} = 0V, Unless Otherwise Noted.

D.C. Programming Characteristics

Symbol	Parameter		Min.	Typ.	Max.	Units	Test Conditions
I_{LI}	Address and CS/WE Input Sink Current				10	μA	V_{IN} = 5.25V
I_{IPL}	Program Pulse Source Current				3	mA	
I_{IPH}	Program Pulse Sink Current				20	mA	
I_{DD}	V_{DD} Supply Current	2708, 2704		50	65	mA	Worst Case Supply Currents[1]: All Inputs High CS/WE = 5V; T_A = 0°C
		2708L		21	28	mA	
I_{CC}	V_{CC} Supply Current	2708, 2704		6	10	mA	
		2708L		2	4	mA	
I_{BB}	V_{BB} Supply Current	2708, 2704		30	45	mA	
		2708L		10	14	mA	
V_{IL}	Input Low Level (except Program)		V_{SS}		0.65	V	
V_{IH}	Input High Level For all Addresses and Data	2708, 2704	3.0		V_{CC} + 1	V	
		2708L	2.2		V_{CC} + 1	V	
V_{IHW}	CS/WE Input High Level		11.4		12.6	V	Referenced to V_{SS}
V_{IHP}	Program Pulse High Level		25		27	V	Referenced to V_{SS}
V_{ILP}	Program Pulse Low Level		V_{SS}		1	V	V_{IHP} – V_{ILP} 25V min.

Note 1. I_{BB} for the 2708L is specified in the programmed state and is 18 mA maximum in the unprogrammed state.

A.C. Programming Characteristics

Symbol	Parameter	Min.	Typ.	Max.	Units
t_{AS}	Address Setup Time	10			μs
t_{CSS}	$\overline{CS}$/WE Setup Time	10			μs
t_{DS}	Data Setup Time	10			μs
t_{AH}	Address Hold Time	1			μs
t_{CH}	$\overline{CS}$/WE Hold Time	.5			μs
t_{DH}	Data Hold Time	1			μs
t_{DF}	Chip Deselect to Output Float Delay	0		120	ns
t_{DPR}	Program To Read Delay			10	μs
t_{PW}	Program Pulse Width	.1		1.0	ms
t_{PR}	Program Pulse Rise Time	.5		2.0	μs
t_{PF}	Program Pulse Fall Time	.5		2.0	μs

NOTE: Intel's standard product warranty applies only to devices programmed to specifications described herein.

2704, 2708 Family Programming Waveforms

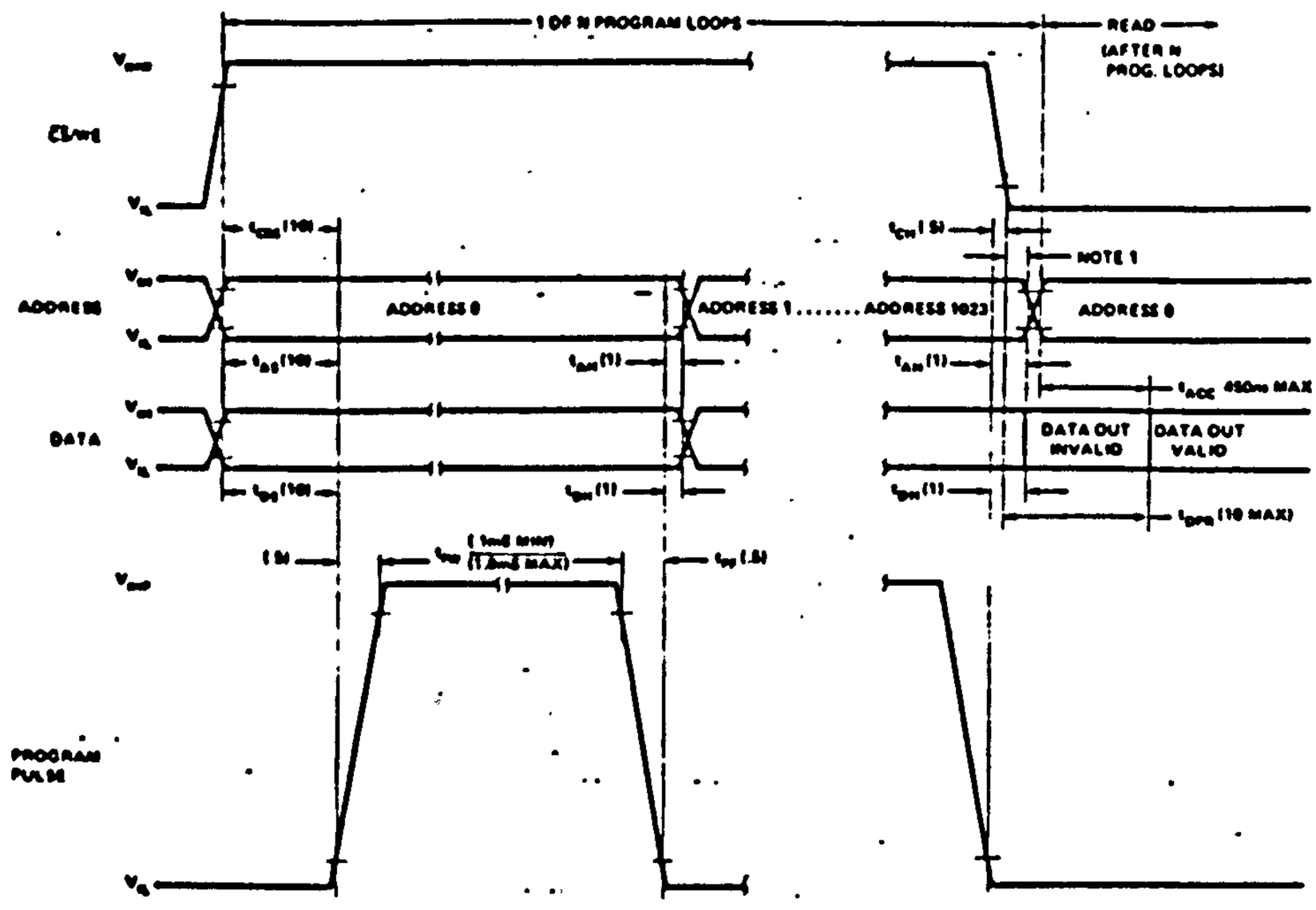

NOTE 1. THE $\overline{CS}$/WE TRANSITION MUST OCCUR AFTER THE PROGRAM PULSE TRANSITION AND BEFORE THE ADDRESS TRANSITION.

NOTE 2. NUMBERS IN ( ) INDICATE MINIMUM TIMING IN μS UNLESS OTHERWISE SPECIFIED.

Appendix: Data Sheets

MOTOROLA

MC1408
MC1508

Specifications and Applications Information

EIGHT-BIT MULTIPLYING DIGITAL-TO-ANALOG CONVERTER

. . . designed for use where the output current is a linear product of an eight-bit digital word and an analog input voltage.

- Eight-Bit Accuracy Available in Both Temperature Ranges
  Relative Accuracy: ±0.19% Error maximum
  (MC1408L8, MC1408P8, MC1508L8)
- Seven and Six-Bit Accuracy Available with MC1408 Designated by 7 or 6 Suffix after Package Suffix
- Fast Settling Time – 300 ns typical
- Noninverting Digital Inputs are MTTL and CMOS Compatible
- Output Voltage Swing – +0.4 V to -5.0 V
- High-Speed Multiplying Input
  Slew Rate 4.0 mA/μs
- Standard Supply Voltages +5.0 V and -5.0 V to -15 V

EIGHT-BIT MULTIPLYING DIGITAL-TO-ANALOG CONVERTER

SILICON MONOLITHIC INTEGRATED CIRCUIT

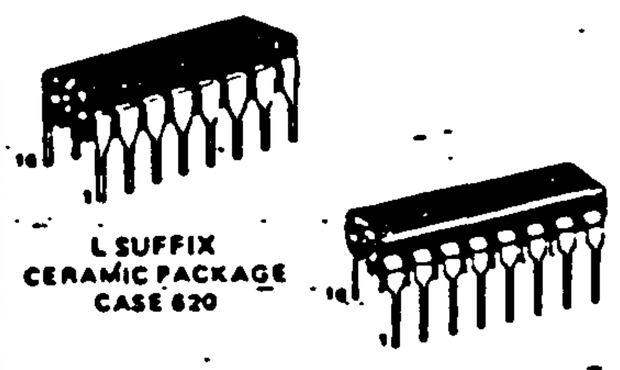

FIGURE 1 – D-to-A TRANSFER CHARACTERISTICS

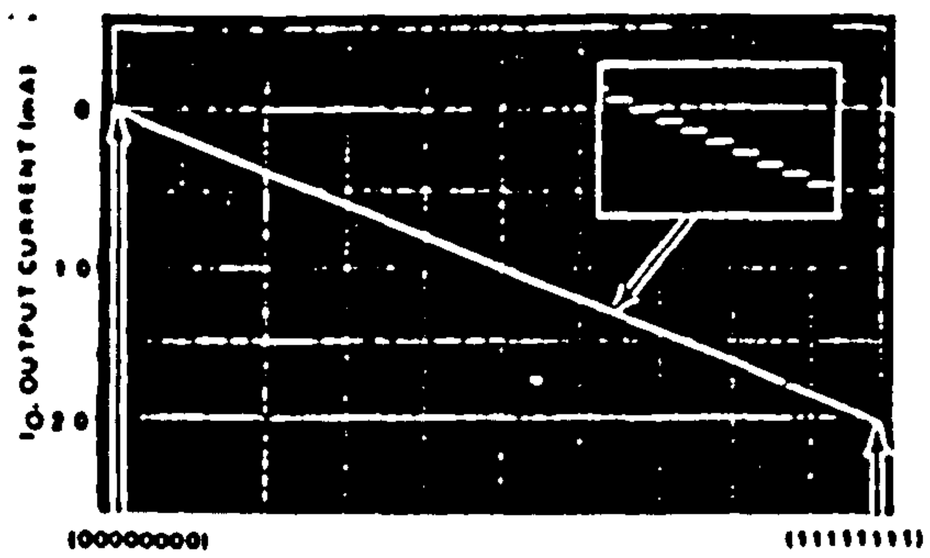

FIGURE 2 – BLOCK DIAGRAM

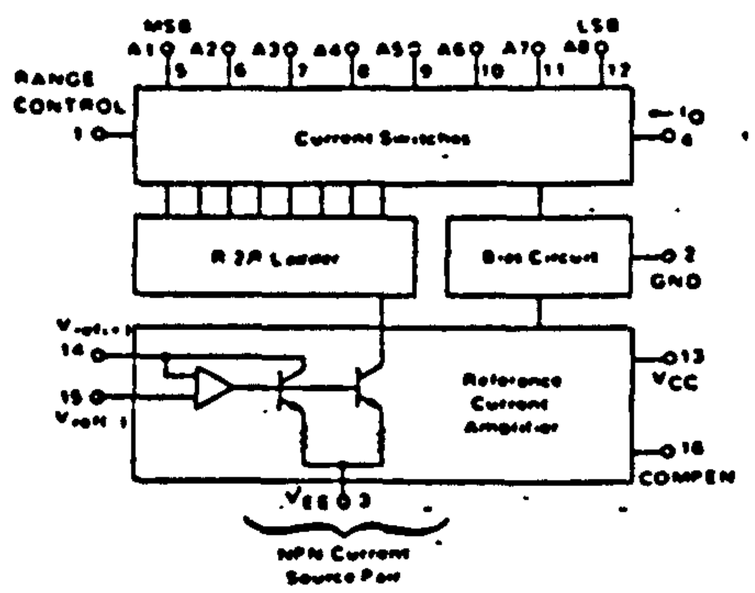

TYPICAL APPLICATIONS

- Tracking A-to-D Converters
- Successive Approximation A-to-D Converters
- *2 1/2 Digit Panel Meters and DVM's*
- Waveform Synthesis
- Sample and Hold
- Peak Detector
- Programmable Gain and Attenuation
- CRT Character Generation
- Audio Digitizing and Decoding
- Programmable Power Supplies
- Analog-Digital Multiplication
- *Digital-Digital Multiplication*
- Analog-Digital Division
- Digital Addition and Subtraction
- Speech Compression and Expansion
- Stepping Motor Drive

MAXIMUM RATINGS (T_A = +25°C unless otherwise noted.)

Rating	Symbol	Value	Unit
Power Supply Voltage	V_{CC} V_{EE}	+5.5 -16.5	Vdc
Digital Input Voltage	V_5 thru V_{12}	0 to +5.5	Vdc
Applied Output Voltage	V_O	+0.5, -5.2	Vdc
Reference Current	I_{14}	5.0	mA
Reference Amplifier Inputs	V_{14}, V_{15}	V_{CC}, V_{EE}	Vdc
Operating Temperature Range MC1508 MC1408 Series	T_A	 -55 to +125 0 to +75	°C
Storage Temperature Range	T_{stg}	-65 to +150	°C

ELECTRICAL CHARACTERISTICS (V_{CC} = +5.0 Vdc, V_{EE} = -15 Vdc, $\frac{V_{ref}}{R14}$ = 2.0 mA, MC1508L8, T_A = -55°C to +125°C, MC1408L Series, T_A = 0 to +75°C unless otherwise noted. All digital inputs at high logic level.)

Characteristic	Figure	Symbol	Min	Typ	Max	Unit
Relative Accuracy (Error relative to full scale I_O) MC1508L8, MC1408L8, MC1408P8 MC1408P7, MC1408L7, See Note 1 MC1408P6, MC1408L6, See Note 1	4	E_r	 - - -	 - - -	 ±0.19 ±0.39 ±0.78	%
Settling Time to within ±1/2 LSB (includes t_{PLH}) (T_A = +25°C) See Note 2	5	t_S	-	300	-	ns
Propagation Delay Time T_A = +25°C	6	t_{PLH}, t_{PHL}	-	30	100	ns
Output Full Scale Current Drift		TCI_O	-	±20	-	PPM/°C
Digital Input Logic Levels (MSB) High Level, Logic "1" Low Level, Logic "0"	3	 V_{IH} V_{IL}	 2.0 -	 - -	 - 0.8	Vdc
Digital Input Current (MSB) High Level, V_{IH} = 5.0 V Low Level, V_{IL} = 0.8 V	3	 I_{IH} I_{IL}	 - -	 0 -0.4	 0.04 -0.8	mA
Reference Input Bias Current (Pin 15)	3	I_{15}	-	-1.0	-5.0	μA
Output Current Range V_{EE} = -5.0 V V_{EE} = -15 V, T_A = 25°C	3	I_{OR}	 0 0	 2.0 2.0	 2.1 4.2	mA
Output Current V_{ref} = 2.000 V, R14 = 1000 Ω	3	I_O	1.9	1.99	2.1	mA
Output Current (All bits low)	3	$I_{O(min)}$	-	0	4.0	μA
Output Voltage Compliance (E, ≤ 0.19% at T_A = +25°C) Pin 1 grounded Pin 1 open, V_{EE} below -10 V	3	V_O	 - -	 - -	 -0.55, +0.4 -5.0, +0.4	Vdc
Reference Current Slew Rate	6	SR I_{ref}	-	4.0	-	mA/μs
Output Current Power Supply Sensitivity		PSRR(-)	-	0.5	2.7	μA/V
Power Supply Current (All bits low)	3	I_{CC} I_{EE}	- -	+13.5 -7.5	+22 -13	mA
Power Supply Voltage Range (T_A = +25°C)	3	V_{CCR} V_{EER}	+4.5 -4.5	+5.0 -15	+5.5 -16.5	Vdc
Power Dissipation All bits low V_{EE} = -5.0 Vdc V_{EE} = -15 Vdc All bits high V_{EE} = -5.0 Vdc V_{EE} = -15 Vdc	3	P_D	 - - - -	 105 190 90 160	 170 305 - -	mW

Note 1. All current switches are tested to guarantee at least 50% of rated output current.

Note 2. All bits switched.

APPENDIX 3 Three dimensional program

ISOPRJ

Example

```
CALL ISOPRJ(NUMX,XLOW,XHIGH,NUMY,YLOW,YHIGH,AZ,IVIEW,NW,W)
```

Arguments

NUMX	Number of points in X- direction.
XLOW,XHIGH	Least and greatest of equally spaced X- values.
NUMY	Number of points in Y- direction.
YLOW,YHIGH	Least and greatest of equally spaced Y- values.
AZ(I,J)	Array of Z values corresponding to the NUMX*NUMY nodes of the grid. AZ must have dimensions (NUMX,NUMY).
IVIEW	Specifies which of 4 alternative directions of view of the surface are to be taken. (IVIEW=0, 1, 2 or 3).
W	Real one-dimensional array of workspace of dimension NW.
NW	NW must be not less than NUMX*NUMY+9*M, where M is the greater of NUMX and NUMY.

Description

ISOPRJ draws an isometric view of the surface defined by the array of heights AZ over the region bounded by XLOW,XHIGH and YLOW,YHIGH. By default a base to the view is drawn at the height of the lowest AZ value, and the base lines are annotated with the appropriate X- and Y- values at suitable intervals. The same physical step size is used in X- and Y- directions so that if identical scaling is required it is important that the user chooses his grid so that $\frac{XHIGH-XLOW}{NUMX-1} = \frac{YHIGH-YLOW}{NUMY-1}$. A reasonable ration between the Z scale and X- and Y- scales is chosen by default to display the surface meaningfully and the overall scaling is such that the plot just fills the users' current plotting area.

If IVIEW=0, the view drawn has the XMIN,YMIN corner at the bottom (nearest) corner. IVIEW=1 gives a view with the surface rotated 90° clockwise about the Z axis, IVIEW=2 a view rotated 180° and IVIEW=3 a view rotated 270°. For any other values of IVIEW the alternative according to IVIEW Mod 4 is chosen.

Note

AZ(I,J) is the Z value corresponding to the point with coordinates

```
C*************************************************************
C                                                            *
C                                                            *
C  THREE DIMENSIONAL PROGRAM BY                              *
C        M.JABERANSARI                                       *
C                                                            *
C*************************************************************

      DIMENSION XX(10,30), YY(10,30), ZARR(10,30)
      REAL WW(2000)
      CHARACTER FILE*80,Q*1
10    PRINT*,'=========================================='
      PRINT*,'WHAT IS NUMBER OF ROWS IN DATA FILE(X S)'
      READ(1,*)M
      PRINT *,'WHAT IS NUMBER OF COLUMBS IN DATA FILE(Y S)'
      READ(1,*)N
      XL=9999999
      XH=0
      YL=9999999
      YH=0
      PRINT*,'SPECIFY WHICH DIRECTION OF VIEW TO BE TAKEN(0,1,2 OR 3)
      READ(1,*)X
CCCC  OPEN THE DATA FILE
      PRINT*,'ENTER NAME OF DATA FILE;'
      READ(1,'(A)')FILE
      OPEN(5,FILE=FILE)
CCCC  READ THE X,Y,Z VALUES
      READ (5,*)M,N
      DO 50 I=1,M
      DO 50 J=1,N
      READ(5,*)XX(I,J),YY(I,J),ZARR(I,J)
CCCC  FIND THE SMALLEST AND LARGEST VALUES OF X
         IF (XX(I,J) .LT.XL) XL=XX(I,J)
         IF (XX(I,J) .GT.XH) XH=XX(I,J)
CCCC  FIND THE SMALLEST AND LARGEST VALUES OF Y
         IF (YY(I,J) .LT.YL) YL=YY(I,J)
 50      IF (YY(I,J) .LT.YH) YH=YY(I,J)
      CALL PLN
      NW=2000
      CALL ISOPRJ (M,XL,XH,N,YL,YH,ZARR,X,NW,WW)
      CALL DEVEND
      CLOSE(5)
      CLOSE(1)
      PRINT*,'DO YOU WISH TO PLOT ANOTHER GRAPH? (Y/N)'
      READ(1,'(A)')Q
      IF (Q.EQ.'Y')THEN
      GOTO 10
      ENDIF
      STOP
      END
```

APPENDIX 4 Least square program

The least squares method was prepared as a program written in Basic language. The program can either read the datapoint (input) from a file which already existing in user's username or the data can be typed in at the terminal real time (That is while the program is running). Having read the data then it will calculate the gradient of the line, error in the gradient, intercept point on y axis and error in intercept. The program listing is as follows:

```
C**************************************************
C                                                  *
C      LEAST SQUARE PROGRAM BY                     *
C           M.JABERANSARI                          *
C                                                  *
C**************************************************

      10 D1=0

      20 D2=0

      24 F=0

      25 X=0

      26 Y=0

      27 X2=0
```

```
28 Y2=0
29 PRINT "DO YOU WISH TO ENTER DATA POINTS AT THIS TERMINAL,"
30 PRINT "OR DO YOU WISH TO READ THE DATA FROM A FILE(T OR F)"
35 INPUT A$
40 IF A$="F" THEN GOTO 330
50 PRINT "PLEASE INPUT THE NUMBER OF DATA POINTS YOU WISH TO CALCULATE"
70 INPUT N
75 REM READ THE DATA FIREST
80 FOR I=1 TO N
90 PRINT "X VALUE OF POINT ",I
100 INPUT X(I)
110 PRINT "Y VALUE OF POINT ",I
120 INPUT Y(I)
130 X=X+X(I)
140 Y=Y+Y(I)
145 X2=X2+X(I)**2
147 Y2=Y2+Y(I)^2
160 NEXT I
161 PRINT
162 PRINT
163 PRINT
165 PRINT N,"DATA POINTS READ"
166 PRINT
167 PRINT
170 PRINT "PLEASE SPECIFY THE SYMBOL TO BE CALCULATED"
171 PRINT "A FOR ALL"
177 PRINT "EM FOR GRADIENT AND ERROR IN GRADIENT"
178 PRINT "EC FOR INTERCEPT AND ERROR IN INTERCEPT"
179 INPUT P$
188 FOR I=1 TO N
```

```
189 D1=D1+(X(I)-X/N)^2
190 D2=D2+((X(I)-X/N)*Y(I))
195 NEXT I
200 LET M=D2/D1
210 LET C=(Y/N-M*X/N)
220 FOR I=1 TO N
230 F2=(Y(I)-M*X(I)-C)^2
235 F=F+F2
240 NEXT I
250 E1=SQR(F/((N-2)*D1))
260 E2=SQR((1+X2/D1)*(F/(N*(N-2))))
265 M=D2/D1
266 IF P$="EC" THEN GOTO 300
270 PRINT" THE GRADIENT M IS ",M
280 PRINT" THE ERROR IN THE GRADIENT IS ",E1
285 IF P$="A" THEN GOTO 300
290 GOTO 330
300 PRINT "THE INTERCEPT ON Y AXIS C IS ",C
310 PRINT" THE ERROR IN THE INTERCEPT IS ",E2
312 GOTO 400
330 PRINT "TYPE THE NAME OF THE FILE WHERE DATA SHOULD BE READ"
340 INPUT F$
350 DEFINE  FILE #1="F$"
360 FOR I=I TO N
370 READ #1,X(I),Y(I)
380 X=X+X(I)
385 Y=Y+Y(I)
387 X2=X2+X(I)^2
389 Y2=Y2+Y(I)^2
390 NEXT I
```

```
395 GOTO 161
400 PRINT "WOULD YOU LIKE TO HAVE ANOTHER TRIAL?"
410 PRINT ".....(Y OR N)....................."
420 INPUT  M$
430 IF M$="Y" THEN GOTO 10
440 END
```

MILLIPORE

APPENDIX 5 Millipore letter

Mr. M Jaberansarz
Researcher
Electronic & Electrical Eng Dept
University of Salford
The Cresent
Salford, Manchester, M5 4QT
United Kingdom

Dear Mr. Jaberansarz,

Thank you for completing and returning the reply-card from the 13th edition of "Millipore News".
Enclosed is the product information you requested.

If after studying this literature you require further assistance, or would like the opportunity of discussing your particular application further, please contact George Kingaby of our Technical Service Department on (01) 864 5499.

Millipore has always been committed to the highest technical support for its products and this tradition will continue.

If you wish to place your order urgently, or obtain specific price information, please use our telephone order service.

Yours sincerely,

MILLIPORE (U.K.) Ltd.

Ian Gallantree
Marketing Manager MPD

Millipore (U.K.) Ltd. 11/15 Peterborough Road Harrow Middlesex HA1 2YH
Telephone : (011 864 5499 Telex No. 24 191 milpor g

MILLIPORE

MILLICELL-HA CULTURE PLATE INSERTS
ORDERING INFORMATION

Description	Quantity/Pk	Catalogue No.	Price (£)*
Millicell-HA culture plate insert, 0,45 um, 12 mm diameter, individually packed, sterile	50	PIHA 012 50	50.00
Millicell-HA culture plate insert, 0,45 um, 30 mm diameter, individually packed, sterile	50	PIHA 030 50	70.00

* Prices do not include V.A.T. at 15% and delivery charge at 3%.
This is not a quotation. List prices are subject to change without notice.

06/1986

UK 13/2345

Millipore (U.K.) Ltd. 11/15 Peterborough Road Harrow Middlesex HA1 2YH
Telephone : (011 864 5499 Telex No. 24 191 milpor g

PUBLICATION

AARHOLT, E., JABERANSARI, M., JAFARY-ASL, A.H., MARSH, P.N., SMITH, C.W. NMR Conditions and biological systems, in: Marino, A.A. (ed). Handbook of bioelectricity. Marcel Dekker, New York, 1988, Chap.26.